Volume 32

Climate change represents a severe global issue also driven by the consumption of fossil fuels, which ultimately release greenhouse gases into the atmosphere. Simultaneously, the rising demand for food, energy, and chemicals requires a shift from fossil to sustainable raw materials. Utilizing renewable carbon sources (i.e., biomass, CO_2, organic waste) ensures a fossil-free future. Over recent years, itaconate has gained increasing interest as a prospective bio-based platform chemical. To replace nowadays petroleum-derived substances like methacrylic acid in industrial applications, enhancing the economic viability of the current biotechnological production processes using the fungus *Aspergillus terreus* is essential.

Ustilaginaceae, a family of smut fungi, display a broad product spectrum featuring organic acids (e.g., itaconate, malate, succinate). These molecules are considered value-added chemicals with potential applications in the pharmaceutical, food, and chemical industry. Importantly, in combination with feeding alternative C-sources as (co-)substrates (e.g., acetate, formate, lignocellulose), these microorganisms offer excellent potential for reducing CO_2 emissions and land use.

This thesis focused on bioprocess optimization and metabolic engineering strategies to establish a sustainable, industrially relevant Ustilaginaceae itaconate production host competitive to *A. terreus*. Concerning the bioprocess optimization aspect, acetate and formate were inverstigated as co-substrates. Investigating the biodiversity using in total 72 Ustilaginaceae, *Ustilago maydis* MB215 and *Ustilago cynodontis* NBRC 9758 were identified as potential production hosts using these co-substrates in combination with glucose.

Formate was supplied from chemical CO_2 hydrogenation reactions using a biphasic Ru-catalyst without any purification, highlighting the many possibilities of combining chemo- and biocatalysis for carbon capture and utilization. Long-term itaconate production during the stationary phase was achieved using an external ceramic membrane avoiding itaconate product inhibition. Thereby, itaconate production was increased 3-fold.

The successful incorporation of CO_2-derived substrate utilization within this work combined with metabolic engineering and bioprocess optimization improved Ustilaginaceae itaconate production. The here presented results contribute to the production of itaconate from sustainable carbon sources, with the overall goal of reducing land use and carbon footprints.

ISBN 978-3-98555-176-7

Toward a CO_2-neutral biotechnology: itaconate production using CO_2 derived co-substrates

Lena Ullmann

Lena Ullmann

Toward a CO_2-neutral biotechnology: itaconate production using CO_2 derived co-substrates

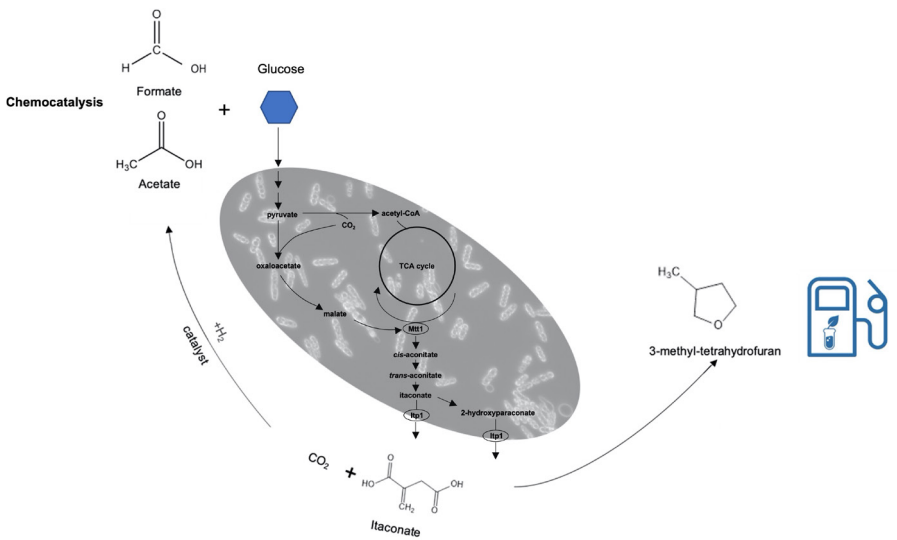

iAMB Institute of Applied Microbiology | ABBt Aachen Biology and Biotechnology | RWTH AACHEN UNIVERSITY

Edition Wissenschaft Apprimus

Toward a CO_2-neutral biotechnology: itaconate production using CO_2 derived co-substrates

Von der Fakultät für Mathematik, Informatik und Naturwissenschaften der RWTH Aachen University zur Erlangung des akademischen Grades einer Doktorin der Naturwissenschaften genehmigte Dissertation

vorgelegt von

Lena Ullmann,

M. Sc. Molekulare und Angewandte Biotechnologie

aus

Elmshorn, Schleswig-Holstein, Deutschland

Berichter: Univ.-Prof. Dr.-Ing. Lars Mathias Blank

Univ.-Prof. Dr.-Ing. Andreas Jupke

Tag der mündlichen Prüfung: 29.08.2023

Diese Dissertation ist auf den Internetseiten der Universitätsbibliothek verfügbar.

Bibliografische Information der Deutschen Nationalbibliothek
Die Deutsche Nationalbibliothek verzeichnet diese Publikation in der Deutschen Nationalbibliografie; detaillierte bibliografische Daten sind im Internet über https://portal.dnb.de abrufbar.

Lena Ullmann:

Toward a CO_2-neutral biotechnology: itaconate production using CO_2 derived co-substrates

1. Auflage, 2023

Gedruckt auf holz- und säurefreiem Papier, 100% chlorfrei gebleicht.

Wissenschaftsverlag des Instituts für Industriekommunikation und Fachmedien
an der RWTH Aachen
Steinbachstr. 25, 52074 Aachen
Internet: www.apprimus-verlag.de, E-Mail: info@apprimus-verlag.de

Printed in Germany

ISBN 978-3-98555-176-7

D 82 (Diss. RWTH Aachen University, 2023)

Eidesstattliche Erklärung

Ich, Lena Ullmann, erkläre hiermit, dass diese Dissertation und die darin dargelegten Inhalte die eigenen sind und selbstständig, als Ergebnis der eigenen originären Forschung, generiert wurden.

Hiermit erkläre ich an Eides statt

1. Diese Arbeit wurde vollständig oder größtenteils in der Phase als Doktorand dieser Fakultät und Universität angefertigt;
2. Sofern irgendein Bestandteil dieser Dissertation zuvor für einen akademischen Abschluss oder eine andere Qualifikation an dieser oder einer anderen Institution verwendet wurde, wurde dies klar angezeigt;
3. Wenn immer andere eigene- oder Veröffentlichungen Dritter herangezogen wurden, wurden diese klar benannt;
4. Wenn aus anderen eigenen- oder Veröffentlichungen Dritter zitiert wurde, wurde stets die Quelle hierfür angegeben. Diese Dissertation ist vollständig meine eigene Arbeit, mit der Ausnahme solcher Zitate;
5. Alle wesentlichen Quellen von Unterstützung wurden benannt;
6. Wenn immer ein Teil dieser Dissertation auf der Zusammenarbeit mit anderen basiert, wurde von mir klar gekennzeichnet, was von anderen und was von mir selbst erarbeitet wurde;
7. Ein Teil oder Teile dieser Arbeit wurden zuvor veröffentlicht, und zwar in:
   https://doi.org/10.3390/jof7020098
   https://doi.org/10.3390/jof8030269
   https://doi.org/10.3390/jof8121277

Aachen, 17.01.2023

Lena Ullmann

Funding

This work was funded by the Deutsche Forschungsgemeinschaft (DFG, German Research Foundation) under Germany´s Excellence Strategy within the Cluster of Excellence „The Fuel Science Center“ 2186.

Danksagung

Ich möchte mich ganz besonders bei meinem Doktorvater Prof. Dr.-Ing. Lars M. Blank bedanken – für die Möglichkeit, am iAMB meine Doktorarbeit durchführen zu dürfen, für die Übernahme der Erstkorrektur und für die Unterstützung, die ich während meiner Promotion von dir erhalten habe. Dein Rat in wissenschaftlichen, aber auch persönlichen Dingen, deine Denkanstöße und deine Offenheit für jegliche Ideen schätze ich sehr und haben maßgeblich zu den Ergebnissen des Projekts beigetragen. Besonders möchte ich dabei betonen, dass dir neben der wissenschaftlichen Arbeit, die Gemeinschaft und Kollegialität und nicht zuletzt der Spaßfaktor am iAMB ebenso wichtig waren. Weiterhin danke ich dir dafür, dass du es mir ermöglicht hast, in einem so gut ausgestatteten und modernen Labor zu arbeiten. Es hat dem Projekt an nichts gefehlt und falls doch, hast du versucht, es dennoch mögich zu machen. Ganz besonders möchte ich dir dafür danken, dass du dir immer Zeit genommen hast und immer versucht hast mir zu helfen.

Ein weiteres Dankeschön gilt Prof. Dr.-Ing. Andreas Jupke, der die Zweitkorrektur für meine Dissertation übernommen hat.

Vielen Dank auch an alle FSC-Projektpartner, Melanie, Carina, Hendrik und Carolin. Mit euch hat die Arbeit im FSC Cluster super viel Spaß gemacht. Vielen Dank auch an Till Tiso, für die Koordination und Hilfestellung im FSC Projekt.

Außerdem möchte ich mich bei meinen Kooperationspartnern Nils Guntermann (ITMC Aachen) und Daniel Wibberg (CeBiTec Bielefeld) bedanken. Es war mir immer eine Freude mit euch zusammenzuarbeiten.

Auch meinen Studierenden Daniel, Karla, Andreas, Tristan, Gereon, Hannah, Philipp, Laura, Tim und Annto möchte ich ganz herzlich danken. Vielen lieben dank für eure Zeit, Ausdauer, Motivation und euren Ehrgeiz. Ihr wart alle ein großer Bestandteil dieses Projektes und habt sehr zu seinem Erfolg beigetragen. Umso mehr freue ich mich, dass einige von euch nun selbst ihre wissenschaftliche Karriere am iAMB weiterführen.

Ein großer Dank gilt zudem dem gesamten iAMB. Es war eine wunderschöne, einzigartige und vor allem erlebnisreiche Zeit mit euch. Ich habe mich immer wohl gefühlt und ich hoffe das wir uns das ein oder andere Mal noch sehen. Ein ganz spezieller Dank geht an die Hühner-Truppe Melanie, Marie, Karla, Marielle, Carina und Gina. Des Weiteren möchte ich mich bei Melanie und Alexander für ihre vielen und stundenlangen Korrekturbemühungen bedanken. Meiner ehemaligen Betreuerin Simone möchte ich für ihre Unterstützung während und nach meiner Masterarbeit danken. Außerdem danke ich dir dafür, dass du dich immer für mich eingesetzt hast und mich in meinen Plänen für ein Doktorstudium stets bestärkt hast.

Ich möchte mich außerdem bei meiner Familie - besonders bei meiner Mutter und meinem Bruder - bedanken. Danke, dass ihr immer hinter mir steht, dass ihr mich immer wieder ermutigt habt meinen Weg zu gehen und dass ihr nie an mir gezweifelt habt.

Meinem Freund Henning möchte ich dafür danken, dass du immer für mich da bist. Meine Zeit als Doktorandin war oft stressig, du hattest aber immer offenes Ohr und großes Verständnis. Danke für deinen Rückhalt und deine Motivation, ohne dich hätte ich es nicht geschafft. Danke für die schöne gemeinsame Zeit bisher und alles, was noch auf uns wartet.

Contents

Summary

Today's (chemical) industry is founded on fossil-based raw materials (i.e., coal, gas, and oil), despite their negative impacts on our all future, including global warming. A change from fossil to sustainable raw materials is required since the demand for food, energy, and chemicals will keep increasing for the next decades. Using renewable carbon sources (i.e., biomass, CO_2, organic waste) will allow a future independent of fossil carbon.

Ustilaginaceae, a family of smut fungi, displays a broad product spectrum featuring organic acids (e.g., itaconate, malate, succinate), polyols (e.g., erythritol, mannitol), and extracellular glycolipids (ustilagic acid, mannosylerythritol lipids). These molecules are considered value-added chemicals with potential applications in the pharmaceutical, food, and chemical industry. Importantly, in combination with feeding alternative C-sources as (co-)substrates (e.g., acetate, formate, glycerol, lignocellulose), these microorganisms offer excellent potential for reducing CO_2 emissions and land use. Organic acids, such as itaconic acid, can function as sustainable alternatives to fossil-based chemicals, since their functional groups enable their use as building blocks. This work focused on bioprocess optimization and metabolic engineering strategies to establish a sustainable, industrially relevant Ustilaginaceae itaconate production host competitive to *Aspergillus terreus*. Concerning the bioprocess optimization aspect, acetate and formate were presented Investigating the biodiversity using 72 Ustilaginaceae, *Ustilago maydis* MB215 and *Ustilago cynodontis* NBRC 9758 were identified as potential production hosts using the displayed co-substrates. Metabolic engineering was performed using CRISPR/Cas9 genome editing and the FLP/FRT system with marker recycling. This way, a novel itaconate-producing chassis strain was designed characterized by a reduced by-product spectrum (ΔUA, ΔMEL) and the insertion of an overexpressed *mttA* gene of *A. terreus*. The wildtype and metabolically engineered strains of *U. maydis* and *U. cynodontis* were further optimized by applying the Design of Experiment (DoE) methodology. The established empirical models were used for predicting itaconate production (titer, yield), focusing on the glucose/co-substrate ratio. Acetate assimilation in *U. maydis* was investigated using off-gas analysis and a ^{13}C-labeling approach. While acetate was not incorporated into itaconate when glucose was present, the induction of the glyoxylate shunt for increased acetate utilization seemed promissing. Extra electrons from formate were supplied from biphasic Ru-catalysed CO_2 hydrogenation reactions without any purification, highlighting the many possibilities of chemo- and biocatalysis for carbon capture and utilization. Long-term itaconate production during the stationary phase (weeks rather than days) was achieved using an external ceramic membrane to avoid product inhibition. The here presented results contribute to the production of itaconate from sustainable carbon sources, with the overall goal of reducing land use and carbon footprints.

Zusammenfassung

Die heutige (chemische) Industrie wird von fossilen Rohstoffen dominiert, obwohl diese endlich und zudem umweltschädlich sind. Eine Umstellung von Erdöl-basierten auf nachhaltige und bio-basierte Rohstoffe ist daher zwingend erforderlich, da der Bedarf an Nahrungsmitteln, Energie und Chemikalien weltweit jährlich steigt. Die Nutzung erneuerbarer Kohlenstoffquellen (z.B. Biomasse, CO_2, organische Abfälle) ist eine Vorraussetzung für eine Zukunft, die unabhängig von fossilem Kohlenstoff ist.

Die Familie der Ustilaginaceae (Brandpilzverwandte) weisen ein vielseitiges Produktspektrum, von beispielsweise organischen Säuren, Polyolen (z. B. Erythrit, Mannit) und extrazellulären Glykolipiden auf, die als Plattformchemikalien mit potenziellen Anwendungen in der Pharma-, Lebensmittel- und chemischen Industrie bekannt sind. Diese Mikroorganismen bieten in Kombination mit der Verwendung alternativer C-Quellen als (Co-) Substrate (z.B. Acetat, Formiat, Glycerin, Lignocellulose) ein hervorragendes Potenzial für die industrielle Biotechnologie und tragen damit potenziell zu den zentralen Herausforderungen der heutigen Zeit bei, einschließlich der CO_2-Freisetzung sowie der Landnutzung.

Organische Säuren, wie beispielsweise Itaconsäure, können als nachhaltige Alternative zu fossilen Chemikalien fungieren, da ihre funktionellen Gruppen den Einsatz als Baustein in der chemischen Industrie ermöglichen. Ziel dieser Arbeit war es einen effizienten Biokatalysator zu entwickeln, der konkurrenzfähig zu dem derzeitigen Produktionsstamm *A. terreus* ist.

Zur Bioprozessoptimierung wurde der Einsatz von CO_2-basierten Co-Substraten, wie Acetat und Formiat, ermöglicht, um das Ziel einer potenziell CO_2-neutralen Itaconsäureproduktion zu erreichen. Während der Kultivierungsexperimente wurden 72 Ustilaginaceae für die Verstoffwechselung der Co-Substrate sowie der Itaconsäureproduktion getestet. Dabei stachen zwei Pilze besonders heraus: *U. maydis* MB215 und *U. cynodontis* NBRC 9758, welche unter Verwendung der genannten Co-Substrate eine vebesserte Produktion aufwiesen. Mittels *Metabolic Engineering* unter Verwendung von CRISPR/Cas9- und dem FLP/FRT System wurde ein neuer ITA *U. maydis* Produktionsstamm entwickelt, welcher ein reduiertes Nebenproduktspektrum (ΔUA, ΔMEL) und eine erhöhte Itaconsäureproduktion aufwies (P_{etef}mttA). Wildtyp- und metabolisch veränderte Stämme (*U. maydis* und *U. cynodontis*) wurden daraufhin unter Anwendung der DoE-Methode (Design of Experiment) weiter charakterisiert und optimiert. Die etablierten empirischen Modelle wurden daraufhin verwendet, um die Itaconatproduktion innerhalb des gegebenen Designraums vorherzusagen und das Glukose-zu-Co-Substrat-Verhältnis zu optimieren.

Proof-of-Principle-Bioreaktorexperimente demonstrierten das Potential der Verwendung einer externen Keramikmembran, wodurch eine Produktinhibierung von Itaconat vermieden wurde. Die im Rahmen dieser Arbeit vorgestellten Ergebnisse tragen zur nachhaltigen Produktion von Itaconsäure mit dem übergeordneten Ziel einer reduzierten Klimabilanz bei.

List of abbreviations

List of units

%	percent
#	number
Ø	diameter
°C	degree Celsius
Ω	ohm
cm	centimeter
d	day
g	gram
g	gravitational-force
h	hour
kb	kilo basepairs
kg	kilogram
L	liter
m	meter
M	molar
min	minute
mL	milliliter
mM	millimolar
nm	nanometer
RIU	refractive index units
rpm	revolutions per minute
v/v	volume per volume
vpm	volume flow per unit of liquid volume per minute
µ	growth rate
µg	microgram
µL	microliter
µm	micrometer

List of microorganisms

A. itaconicus	*Aspergillus itaconicus*
A. terreus	*Aspergillus terreus*
A. bothriochloae	*Anthracocystis bothriochloae*
A. heteropogonicola	*Anthracocystis heteropogonicola*
E. coli	*Escherichia coli*
M. eriachnes	*Macalpinomyces eriachnes*
M. mackinlayi	*Macalpinomyces mackinlayi*
M. ordensis	*Macalpinomyces ordensis*
M. spermophorus	*Macalpinomyces spermophorus*
M. tubiformis	*Macalpinomyces tubiformis*
P. antartica	*Pseudozyma antartica*
P. hubeiensis	*Pseudozyma hubeiensis*
P. tsukubaensis	*Pseudozyma tsukubaensis*
S. bothriochloae	*Sporisorium bothriochloae*
S. caledonicum	*Sporisorium caledonicum*

S. cenchri-elymoidis	*Sporisorium cenchri-elymoidis*
S. cerevisiae	*Saccharomyces cerevisiae*
S. consanguineum	*Sporisorium consanguineum*
S. scitamineum	*Sporisorium scitamineum*
S. cruentum	*Sporisorium cruentum*
S. exsertum	*Sporisorium exsertum*
S. iseilematis-ciliati	*Sporisorium iseilematis-ciliati*
S. lanigeri	*Sporisorium lanigeri*
S. scitamineum	*Sporisorium scitamineum*
S. setariae	*Sporisorium setariae*
S. themedae	*Sporisorium themedae*
S. tumiforme	*Sporisorium tumiforme*
S. walkeri	*Sporisorium walkeri*
U. gigantosporum	*Ustanciosporium gigantosporum*
U. curta	*Ustilago curta*
U. cynodontis	*Ustilago cynodontis*
U. egenula	*Ustilago egenula*
U. filiformis	*Ustilago filiformis*
U. lituana	*Ustilago lituana*
U. maydis	*Ustilago maydis*
U. rabenhorstiana	*Ustilago rabenhorstiana*
U. schmidtiae	*Ustilago schmidtiae*
U. trichophora	*Ustilago trichophora*
U. triodiae	*Ustilago triodiae*
U. vetiveriae	*Ustilago vetiveriae*
U. xerochloae	*Ustilago xerochloae*

General abbreviations

AAI	average amino acid identity
Ace	acetate
ACK-PTA	acetate kinase – phosphotransacetylase
ACS	acetyl-CoA synthetase
adi1	aconitate-delta-isomerase 1
ADP	adenosine diphosphate
ANI	average nucleotide identity
ANOVA	analysis of variance
ATP	adenosine triphosphate
BES	bio-electrochemical systems
BLAST	basic local alignment search tool
bp	base pairs
Ca	calcium
$CaCl_2$	calcium chloride
$CaCO_3$	calcium carbonate
Cas	CRISPR protein
CCD	central composite design
CDW	cell dry weight
cm	centimeter
Cmol	carbon mole
CO	carbon monoxide
CO_2	carbon dioxide

CoA	coenzyme A
CRISPR	clustered regularly interspaced short palindromic repeats
C-source	Carbon source
dgat	diacylglycerol lipids
DIC	dicarboxylate carrier
DoE	U.S. Department of Energy
DOE	Design of Experiments
DOT	dissolved oxygen tension
DNA	deoxyribonucleic acid
DNAse	deoxyribonuclease
DO	dissolved oxygen
DSP	downstream processing
3D	3-dimensional
e.g.	exempli gratia
et al.	et alii or et aliae
EDTA	ethylenediaminetetraacetic acid
emt1	erythritol/mannose transferase
EtOH	ethanol
eV	electron volt
FBA	flux balance analysis
$FeSO_4$	iron(II) sulfate
g	g-force
GC	gas chromatography
GC-content	guanine-cytosine content
Glc	glucose
H_2	hydrogen
H_2O	water
H_2SO_4	sulfuric acid
HPLC	High performance liquid chromatography
i.e.	id est
iAMB	Institute of Applied Microbiology
ITA	itaconate
itp1	itaconate transport protein
kb	kilobase pairs
KEGG	Kyoto encyclopedia of genes and genomes
KH_2PO_4	potassium dihydrogen phosphate
kV	kilovolt
L	liter
LB	lysogeny broth
LCA	life-cycle assessment
LPS	lipopolysaccharides
Mb	megabase
MEL	mannosylerythritol lipids
MES	2-(N-morpholino)ethanesulfonic acid
$MgSO_4$	magensium sulfate
$MnCl_2$	manganese(II) chloride
MS	mass spectrometry
3-MTHF	3-methyl-tetrahydrofuran
MTM	modified tabuchi medium

mtt1	mitochondrial tricarboxylate transporter 1
n.d.	not determined
Na_2EDTA	ethylenediaminetetraacetic acid disodium salt
Na_2HPO_4	disodium hydrogen phosphate
Na_2MoO_4	sodium molybdate
NaCl	sodium chloride
$NAD(P)^+$	nicotinamide adenine dinucleotide (phosphate)
NAD(P)H	reduced nicotinamide adenine dinucleotide (phosphate)
NH_4Cl	ammonium chloride
nm	nanometer
NRPS	nonribosomal peptides
OD_{600}	optical density at 600 nm
OFAT	one-factor-at-a-time
orf	open reading frame
PCR	polymerase chain reaction
pH	potentia hydrogenii
POCP	percentage of conserved proteins
q	production rate
rdo1	glyoxalase domain-containing protein RDO1
RI	refractive index
ria1	regulator of itaconic acid biosynthesis
RIPP	ribosomally synthesized and post-translationally modified peptides
RNA	ribonucleic acid
RSD	response surface design
Ru	ruthenium
RWTH	Rheinisch-Westfälische Technische Hochschule
S	substrate
sp.	species
SRVs	score ratio values
syngas	synthesis gas
tad1	trans-aconitate decarboxylase 1
TAG	triacylglycerol
TCA cycle	tricarboxylic acid cycle
tRNA	transfer RNA
TRY	titer, rate, and yield
UA	ustilagic acid
US	United States
USD	United States dollar
USP	upstream processing
UV	ultraviolet
v/v	volume per volume
vvm	volume flow per unit of liquid volume per minute
w/v	weight per volume
wt	wildtype
YEP	yeast extract peptone
Y	yield
$ZnSO_4$	zinc sulfate
μ	growth rate

List of figures

List of tables

Chapter 1

General introduction

Contributions:

This chapter was written by Lena Ullmann and reviewed by Lars M. Blank.

1 General introduction

1.1 Bioeconomy – a sustainable bio-based production of chemicals

The world population is constantly growing and exceeded 7.9 billion in 2022, increasing the demand for food, fuels, chemicals, and electricity [1]. Most of the manufacturing processes for goods of everyday life rely on fossil resources [2]. With the incessant growth of the world's population, the already high dependency on coal, petroleum, and natural gas will further increase [3]. However, fossil resources are limited and unequally distributed on earth, resulting in price volatility and political turmoil, as we experience especially in the current year 2022.

However, the main drawback of a fossil-based industry is the high emission of greenhouse gases, which contributes to global warming [2], [4]. Global warming is by far the most significant threat humankind is currently facing. According to recent data, an average increase in the global temperature of 2 °C will lead to the death of one hundred million people and the extinction of millions of faunal and floral species [2]. Consequently, the Paris Climate Agreement asserted that the participating countries should limit global warming to less than 2 °C over the next 15 years, achieving net-zero emissions by 2050. Thus, the transition from a fossil-based to a sustainable bio-based economy is inevitable and the major challenge of today's times [5].

The envisaged circular bioeconomy is a relatively new economic growth model, that aims to decouple economical growth from fossil fuel dependency, using renewable carbon sources (i.e., biomass, CO_2, waste) instead [5]. Such renewable biological resources from land and sea are for example crops, forests, fish, animals and microorganisms to produce food, chemicals, energy, and fuels [6]. Waste is also considered a valuable source of energy and resources [5]. The overall goal is to create a circular bioeconomy, wherein the emitted CO_2 is fixed by plants and – in the future – also by microbes to produce biomass, and chemocatalysis, which can be used as a feedstock for the production of platform chemicals such as displayed **Figure 1** [5], [7]. Thus, renewable or bio-based resources have a closed carbon cycle addressing sustainability compared to fossil resources [5].

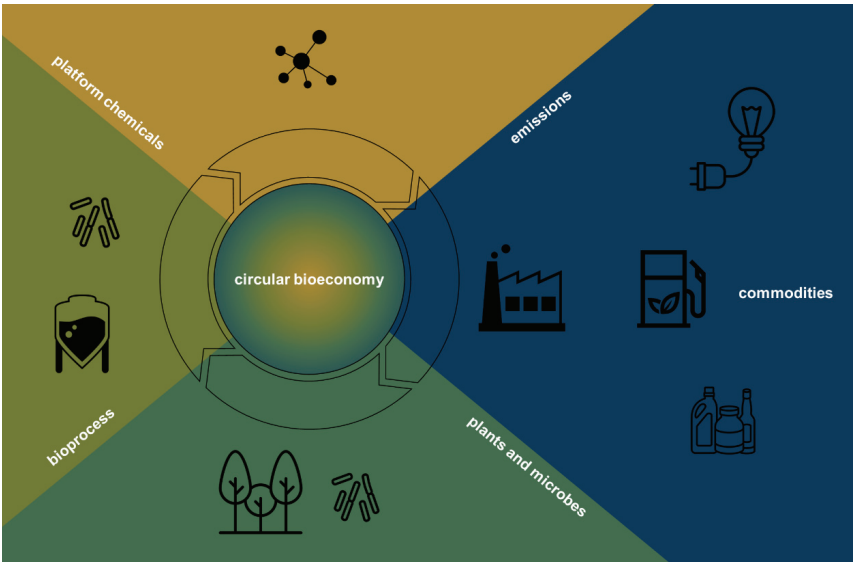

Figure 1: Circular bioeconomy. Modified from [8].
CO_2-emissions are fixed by plants, trees, and microbes, which are converted into usable substrates for microorganisms. The microorganisms produce platform chemicals in bioreactors, which can then be used as building blocks for commodities (energy, fuels, chemicals, goods), resulting in new emissions at the end-of-life of the commodities.

1.1.1 Production of fuels from bio-based feedstocks

In Biotechnology, microorganisms are applied to produce platform and bulk chemicals, as well as biofuels, from bio-based resources. Biomass is defined as “all non-fossil-based living or dead organisms and organic material that have an intrinsic chemical energy content” [9]. A summary of alternative bio-based feedstocks for a circular bioeconomy is listed in **Table 1**.

Table 1: Overview of alternative bio-based feedstocks [5].

Feedstock category	Feedstock
Animal-based	Manure
Plant-based biomass/ lignocellulosic biomass	*Virgin biomass* 1. forest-based biomass (wood) 2. crops (corn, sugar beet, …) *Waste biomass* 3. agricultural waste (bagasse, straw) 4. wood processing waste
Aquatic biomass	Micro- and macroalgae, small aquatic plants
Food waste	Inedible parts of food (husks, peels), materials after use (cobs, coffee/tea grounds), restaurant and domestic food waste, waste cooking oil

Waste	Solid municipal waste, biodiesel-derived glycerol, municipal wastewater, wasterwater (food industry, animal husbandry)
Sources of CO_2-waste	Anaerobic digesters, ethanol fermenting plants, syngas, CO_2-rich exhaust gases

Regarding biofuel production, biomass is categorized into first-, second-, and third-generation feedstocks [10]. First-generation feedstocks include vegetable oil, corn, sugarcane, as well as starch and sucrose fractions of plant carbohydrates [10]. Ethanol and biodiesel produced from these first-generation feedstocks are considered as first-generation biofuels [10]. First-generation biofuels are directly related to generally edible biomass [10]. Bioethanol is commonly produced in fermentation processes using C6 sugars (mainly glucose) as substrates and yeast strains such as *Saccharomyces cerevisiae* as biocatalysts [10]. One major drawback of using first-generation feedstocks in bioprocesses is the competition with the food and feed industry. This provokes the food-versus-fuel debate and may lead to increasing prices or a shortage in the availability of these resources [11]. Further, the yields are lowered by exclusively using the readily fermentable fractions of plants while neglecting the remaining fractions, which does not contribute to a sustainable bioeconomy. However, many biotechnological production processes still rely primarily on glucose as a carbon source [12].

The food-versus-fuel debate drove the development of second-generation or advanced biofuels, such as cellulosic ethanol and Fischer-Tropsch liquids. Non-edible lignocellulosic biomass, such as agricultural residues, wood and forest residues, and grasses, belongs to second-generation feedstocks [10]. The price for this biomass is significantly lower than edible biomass making its use attractive. In general, second-generation feedstocks are more complex and not accessible in their untreated form, which makes their application dependent on new technologies [10]. Before use, such biomass must be pretreated and hydrolyzed (enzymatically and/or chemically) before use [12]. Before sugar monomer fermentation, e.g., to ethanol, the fibrous matrix structure of lignocellulose must be broken up into hemicellulose, cellulose chains, and lignin, hexose and pentose sugars have to be hydrolyzed from the separation products [10]. Many microbes commonly used in bioprocesses cannot even utilize the monomers of the hydrolysates resulting from second-generation feedstocks [13]. Hence, these microbes must either be engineered to use the carbon sources or new microbes have to be selected for bioprocesses. Most processes using second-generation feedstocks are still on an experimental scale. In contrast, bioethanol from lignocellulosic biomass is a prominent example of a bio-based process applicable at the industrial scale with various plants already in operation [14].

Since many microbes can utilize alcohols, ethanol can be used not only as a biofuel or platform chemical but also as a carbon source for producing valuable products. Further,

microorganisms are able to use the displayed feedstocks (**Table 1**) and other non-conventional ones from industrial production and societal consumption, such as CO_2 and plastic waste [15]. One advantage is, e.g., minimizing land use by using CO_2 directly as a carbon source for microbes. This concept contributes to a circular bioeconomy. Feedstocks formed by aquatic autotrophic organisms (e.g., algae) are termed third-generation feedstocks, whereas algae have a distinctive growth yield compared with classical lignocellulosic biomass [16]. Due to their high lipid and biomass productivity, microalgae are an attractive alternative to vegetable oils and, therefore, a resource for biodiesel production [17]. Thereby, high lipid productivity displays a key characteristic of a species used for biodiesel production [17]. Despite these significant advantages, biodiesel production from algae has not been economically profitable [17].

1.2 Itaconic acid as a platform chemical

Platform chemicals are small molecules that can be utilized as building blocks for producing chemicals and materials of higher value [18]. In 2004, the U.S. Department of Energy (DoE) tested more than 300 chemicals with great biotechnological potential and identified twelve building block chemicals that could potentially be produced competitively from biomass which are displayed in **Table 2**. The twelve building blocks can be subsequently converted to high-value bio-based chemicals or materials. Thereby, building block chemicals as considered for this analysis are molecules with multiple functional groups that possess the potential to be transformed into new families of useful molecules. The criteria for selection was based on the market potential for the building blocks and their derivatives and the technical complexity of their synthesis pathways [13].

Table 2: Top 12 sugar-derived building block chemicals assigned in 2004 by the U.S. Department of Energy (DoE) [13].

Building block chemicals
1,4-succinic, fumaric, and malic acid
2,5-furan dicarboxylic acid
3-hydroxy propionic acid
aspartic acid
glucaric acid
glutamic acid
itaconic acid
levulinic acid
3-hydroxybutyrolactone
glycerol
sorbitol
xylitol / arabinitol

One of the listed promising candidates is itaconic acid, also known as 2-methylidenebutanedioic acid (CAS 97-65-4), an unsaturated, non-toxic C5 dicarboxylic organic acid (**Figure 2**). It has a molecular weight of 130.1 g mol^{-1}. The molecule contains one carboxyl group linked to the methylene group. Further, it is a white crystalline acid with a solubility in water of 83.1 g L^{-1} at 20 °C with a pH of 2. The pK_a values are 3.84 (pK_{a1}) and 5.55 (pK_{a2}) [19]

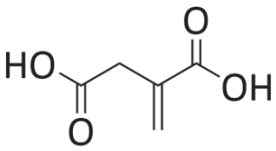

Figure 2: Chemical structure of itaconic acid [19].

The first documentation about itaconate and its production was in 1837 when it was discovered by Baup [20]. Itaconic acid was first described as a product of the pyrolytic distillation of citric acid [21]. Itaconic acid was also produced by the decarboxylation of aconitic acid [19]. Other chemical syntheses are known, such as the distillation of citric acid, followed by the treatment of the yielded anhydrides, oxidation of mesityl oxides with the subsequent isomerization of the formed citraconic acid, or oxidation of isoprene [22]. Subsequently, the first production methods were based on chemical synthesis procedures [20], [22]. Due to the high production costs caused by chemical synthesis, it was not possible to establish a foothold in the market [23]. The first report about the microbial production of itaconic acid was published in 1931 with a filamentous fungus named *Aspergillus itaconicus*, followed by the first patent filed by Charles Pfizer Co. for itaconic acid production with *Aspergillus terreus* [21], [24]. Over time, the

fermentation process with *A. terreus* was optimized, finally outcompeting the chemical process [19]. Thus, *A. terreus* has been used for industrial itaconate production since 1950 [19].

1.2.1 Application fields of itaconate

The chemical structure of itaconic acid with a number of functional groups allows a variety of chemical reactions, like salt formations, polymerization, or esterifications with alcohols and therefore a broad spectrum of applications [13], [25]. Important derivatives are itaconic diamide, 2-methyl-1,4-butanediamin, 3-methylpyrrolidine, 3- and 4-methyl-N-methylpyrrolidinone, 2-methyl-1,4-butanediol, 3-methyl-tetrahydrofuran, and 3- and 4-methyl-γ-butyrolactone (**Figure 3**) [13].

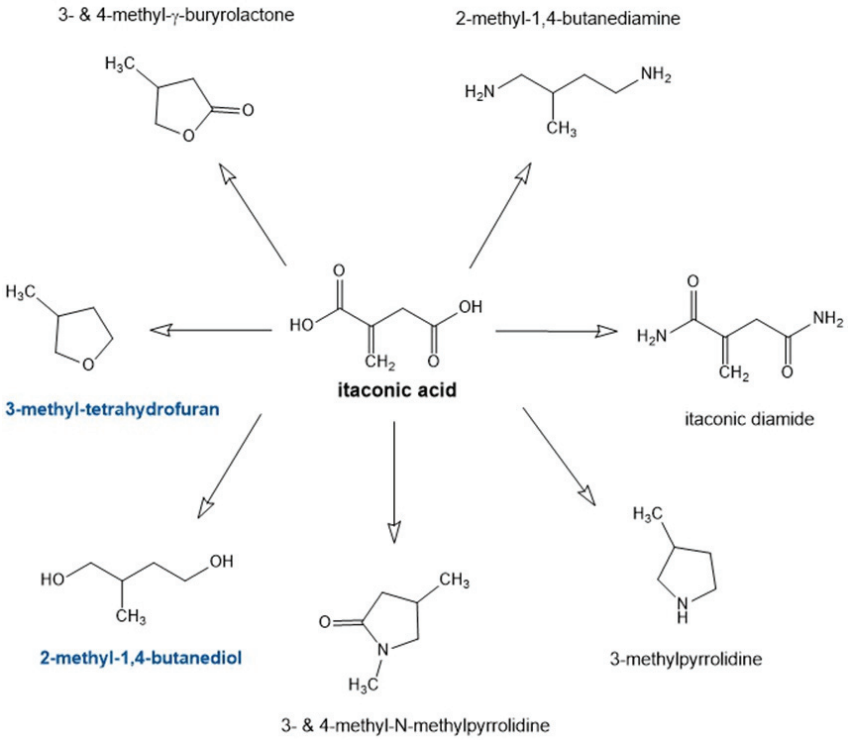

Figure 3: Itaconic acid and its derivates [13].

Radical polymerization and/or esterification with a wide range of co-monomers further expands the application range of itaconic acid [26]. As co-monomers, itaconic acid derivates are applied in the industrial production of polymers, surfactants and fibers. The alkali salt or sulfonated form of self-polymerized itaconate, polyitaconate, is used as a detergent and in shampoos [27].

Further polymerizations with acrylamide or methyl-methacrylate generate superabsorbent hydrogels for pharmaceutical applications [28]. Itaconate and its derivatives are also used in the production of resins, as building blocks for acrylic plastics, acrylate latexes, and anti-scaling agents, as well as in the synthesis of artificial glass and bioactive compounds in the agricultural, pharmaceutical, and medical sector [24], [27]. Additionally, derivatives such as 3-methyl-tetrahydrofuran or 2-methyl-1,4-butanediol may function as biofuels [29], [30]. Besides the application fields mentioned, itaconate may function as a therapeutic agent for autoimmune diseases since mammalian macrophages produce it. It subsequently plays a crucial role in the human immune response against microbial pathogens [31]–[33]. In contrast to this detailed knowledge of the biological role of itaconate production in higher eukaryotes, little is known about the ecological reason why fungi, like *Ustilago* and *Aspergillus*, produce itaconate.

1.2.2 Market potential of itaconate

Although itaconate has numerous potential applications, its market size and value were only 41,400 t in 2011, corresponding to 74.5 million USD [34], [35]. This is caused by the high price of around 2.0 USD per kilogram and is an exclusive criterion for further market penetration. In 2022, the size and share of the itaconic acid market were determined to increase from 98.4 to 110.4 USD in 2027 [36]. Production costs need to be further reduced to be competitive with petroleum-based products like acrylic acid and potentially replace them in industrial processes. With the assumption of a future price decrease, itaconate has the potential to replace polyacrylic acid, which is petroleum-based, with a market worth of 11 billion USD [23], [27], [34]. Nevertheless, easy biodegradability in soil and non-toxicity are critical factors in the growth of the itaconic acid business [36]. Favorable government regulations to promote bio-based production processes due to environmental safety can further boost growth. For example, the size of the Chinese itaconic acid market is expected to exceed 21 USD by 2025 [36]. Asia-Pacific countries (APAC) are the leading producers and consumers of itaconic acid, supplying over 54 % of the global demand [36]. Germany's market size of itaconic acid was 3.9 million USD in 2020 [36].

More improvements are necessary to reduce the price of itaconate for further market growth. Certainly, fermentation conditions, especially the downstream process, significantly influence the product's price [37]. The selected microorganisms and C-sources also influence the production process, in turn impacting the price. Unquestionably, many other factors, such as production location and energy costs, also affect the price. However, the following sections will discuss only the influence of the microorganisms used for itaconic acid production, the bioprocess itself, and the downstream process.

1.2.3 Industrial production of itaconate

Currently, itaconic acid can be produced biologically or chemically [38]. The filamentous fungus *A. terreus* still represents the state-of-the-art production process. *A. terreus* stands out with an excellent tolerance to low pH values combined with high product yields and titers. So far, the highest reported itaconate titer for *A. terreus* is 160 g L^{-1}, obtained on a laboratory scale [39]. The highest reported productivity reached 1.15 g L h^{-1} [40] and the highest yield 0.72 $g_{itaconate}$ $g_{C\text{-}source}^{-1}$ equaling the theoretical maximum yield [41].

Nevertheless, the use of *A. terreus* as a production host remains challenging. *A. terreus* can grow in a pellet or filamentous form, while high itaconate production can only be achieved during growth in pellet form [42]. When filamentous growth occurs, itaconic acid productivity decreases. Thus, a cost-extensive morphology control is essential to reach high productivity [39]. The morphology mainly depends on the medium composition. Impurities like manganese, e.g., were shown to induce mycelium formation [25]. This growth behavior leads to a cost¬intensive pretreatment of the fermentation medium, intensive monitoring during the production process, and high purification costs [22], [25]. Consequently, alternative production hosts are required to create a more economical production process. Besides *A. terreus*, the Ustilaginaceae family, including *Pseudozyma* and *Ustilago* species [43],[44], as well as *Candida* [45], and *Helicobasidium* species [46] are known itaconate producers. An overview of performance parameters such as itaconate titer, productivity, and yield of the different microorganisms is given in **Table 3** [47], [48].

Table 3: Selection of itaconate producing microorganisms and the characteristics of the corresponding fermentative processes (modified from [47], [48]**).**

strain	substrate	working volume, fermentation type	itaconate titer [g L^{-1}]	itaconate yield [g_{ITA} g^{-1}]	reference
A. terreus DSM 23081	glucose	1.5 L, submerged fermentation	160	0.46 g_{ITA} g_S^{-1}	[39]
	glucose	15 L, submerged fermentation	86	0.62 g_{ITA} g_S^{-1}	[25]
	glucose	1.5 L, submerged fermentation	146	0.59 g_{ITA} g_S^{-1}	[40]
A. terreus NRRL 265	sucrose	50 mL, submerged fermentation	49	-	[49]
mutant of *A. terreus* NRRL 265 and 1960	beet and sugarcane molasses	2 L, submerged fermentation	50	-	[50]
A. terreus NRRL 1960	xylose and glucose	14 L, immobilized MO in submerged fermentation	30	0.54 g_{ITA} g_S^{-1}	[51]
A. terreus NRRL 1960	glucose	6 L, submerged fermentation	130	0.9 g_{ITA} g_S^{-1}	[52]
A. terreus SKR10 N45	corn starch	100 mL, submerged fermentation	50	0.25 g_{ITA} g_S^{-1}	[53]
A. terreus TN484-M1	corn sorghum	3 L submerged fermentation	48	0.34 g_{ITA} g_S^{-1}	[54]

A. terreus CECT 20365	sugar beet press-mud, dry olive residues, glycerol	10 g solid-state fermentation	-	0.44 g_{ITA} kg^{-1}	[55]
mutant of *A. terreus* ATCC 10020	glucose, sucrose, fructose, mannose, starch hydrolysate, molasse	45 mL, semi-solid-state fermentation	-	0.55 g_{ITA} g_s^{-1}	[56]
mutant of *Aspergillus niger* ATCC 1015	glucose	100 mL, submerged fermentation	1.2	-	[57]
Candida sp.	glucose	25 mL, submerged fermentation	35	-	[45]
mutant of *Escherichia coli*	glucose	1 L, submerged fermentation	32	0.49 g_{ITA} g_s^{-1}	[58]
Helicobasidium mompa TANAKA	sweet potato	14 mm of the feedstock, solid-state fermentation	0.5	-	[59]
P. antarctica Y-7808	glucose	1 L, submerged fermentation	30	0.38 g_{ITA} g_s^{-1}	[44]
mutant of *U. cynodontis*	glucose	1.3 L, submerged fermentation	22	0.42 g_{ITA} g_s^{-}	[60]
mutant of *U. cynodontis*	glucose	1.3 L, submerged fermentation	83	0.30 g_{ITA} g_s^{-1}	[61]
U. maydis MB215	glucose	2 or 6 L, submerged fermentation	44.5	0.24 g_{ITA} g_s^{-1}	[62]
mutant of *U. maydis* MB215	glucose	1.3 L, submerged fermentation	63	0.26 g_{ITA} g_s^{-1}	[63]
mutant of *U. maydis* MB215	glucose	1.3 L, submerged fermentation	220	0.33 g_{ITA} g_s^{-1}	[64]
mutant of *U. maydis* MB215	glucose	1.3 L, submerged fermentation	75.7	0.66 g_{ITA} g_s^{-1}	[65]
U. rabenhorstiana	glucose	1 L, submerged fermentation	50	0.27 g_{ITA} g_s^{-1}	[66]
mutant of *Yarrowia lipolytica*	glucose	1.5 L, submerged fermentation	1.2	0.058 g_{ITA} g_s^{-1}	[67]

A. terreus and *U. maydis*, the itaconic acid biosynthesis pathways have been characterized, and the associated gene clusters have recently been identified [63], [68], [69]. Interestingly, the metabolic steps involved in these pathways differ in the two fungi (**Figure 4**) [69], [70]. In the case of *A. terreus*, pyruvate is generated from glucose *via* glycolysis taking place in the cytosol and subsequently enters the mitochondria [71]. It is converted to acetyl-coenzyme A (CoA), a central metabolism intermediate and an activated form of acetate. Together with oxaloacetate, acetyl-CoA forms citrate within the tricarboxylic acid cycle (TCA) [71]. Citrate is then dehydrated to *cis*-aconitate, which is transported from the mitochondria back into the cytosol *via* the putative mitochondrial tricarboxylic transporter MttA and converted to itaconate in a *cis*-aconitate decarboxylase (CadA)-mediated reaction. Itaconate is finally exported out of the cell by a protein of the major facilitator superfamily (MFS) [70].

Differences between the both fungi relate to the first conversion of citrate to cis-aconitate. Whereas *A. terreus* expresses a *cis*-aconitate decarboxylase, *U. maydis* utilizes an aconitate-delta-isomerase in conjunction with a specific *trans*-aconitate decarboxylase [69]. The involved transport steps, however, are comparable inboth fungi: a mitochondrial carrier family (MCF) protein (MttA in *A. terreus* and Mtt1 in *U. maydis*) and a major facilitator superfamily (MFS) protein (MfsA in *A. terreus* and Itp1 in *U. maydis*) are encoded in the respective itaconate gene clusters [70].

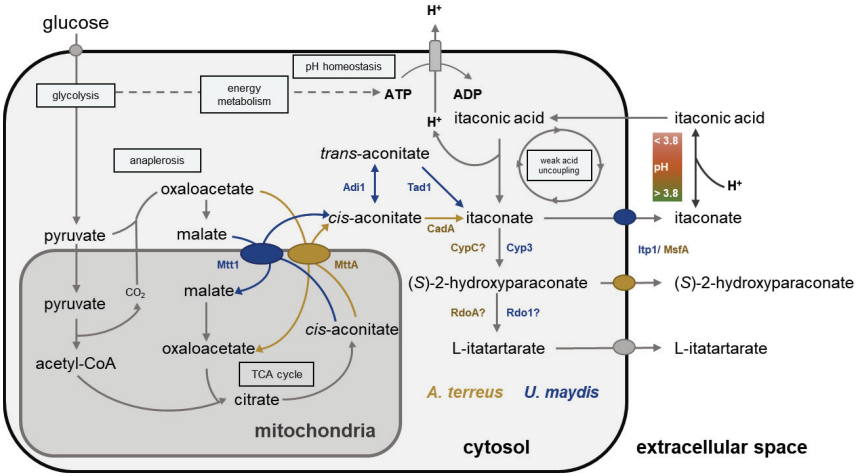

Figure 4: Overview of metabolic and (sub)cellular aspects of fungal itaconic acid production.
Enzymes specific to *A. terreus* are indicated in orange, *U. maydis* in blue (adapted from [70].

In *U. maydis*, it was demonstrated that a deletion of either of the transporter genes results in a significant reduction of the secreted itaconate level [63]. In contrast, in the related species *U. cynodontis*, the deletion of *mtt1* completely abolishes itaconate production [72]. These observations highlight the metabolic importance of the transporters. So far, no equivalent knockout studies have been reported for *A. terreus*.

For a long time, the performance of *A. terreus* dwarfed all other (engineered) itaconate-producing strains [42]. However, after strain engineering and fermentation process optimization, a maximum titer of 220 g L^{-1} was lately achieved using *U. maydis* as a production host [64]. To improve the performance of strains naturally producing itaconate or to enable other strains to synthesize itaconate as a new product *via* metabolic engineering, adequate knowledge about the underlying biosynthesis pathway is demanded.

1.3 Ustilaginaceae as alternative productions hosts

The industrial itaconate production process with *A. terreus* faces specific challenges, such as sensitivity to hydromechanical stress, increased viscosity of the fermentation broth, and sensitivity toward an interruption of oxygen supply [19], [42]. Further, itaconic acid production in *A. terreus* strongly depends on its morphology [42]. Thereby, morphology control is a significant challenge that hinders cultivations' reproducibility [42]. Thus, the current research focused on finding alternative natural itaconate-producing organisms which are more robust and less sensitive against impurities [19]. In the past decade, the Ustilaginaceae family attracted special attention including the model organism *U. maydis* [48], [73]. The advantages of *U. maydis* are its haploid yeast-like growth and insensitivity to shear forces [48]. Further, high cell density fermentations are feasible using *U. maydis*, showing a relatively short doubling time with high productivities, yields and titers [48], [64].

Ustilaginaceae belong to the basidiomycete fungi and comprise a family of mostly plant pathogenic microorganisms that infect various crops and grasses, causing smut disease [74]. The Ustilaginaceae family consists of 14 genera, including *Ustilago*, *Sporisorium*, and *Macalpinomyces* [75]. Despite their pathogenicity and capability to infect economically relevant crops, such as barley, sugarcane, wheat, and oats [76], smut fungi attracted particular attention in industrial biotechnology.

Ustilaginaceae exhibit a versatile product spectrum, including organic acids (e.g., itaconate, malate, succinate) [22], [77]–[79], polyols (e.g., erythritol, mannitol) [80], [81], and extracellular glycolipids [73], which are considered value-added chemicals with potential applications in pharmaceutical, food, and chemical industries [82], [83]. For instance, mannosylerythritol lipids (MELs) are surface-active glycolipids secreted by various fungi, including *U. maydis*. MELs can be used as biosurfactants, displaying the much-demanded biodegradable resource for producing detergents or pharmaceuticals [84]–[86]. With this manifold production spectrum, Ustilaginaceae represent promising cell factories in the field of biotechnology, which have the potential to contribute to the transition from a fossil- to a bio-based economy [48]. **Figure 5** summarizes the biochemical pathways of Ustilaginaceae's main biotechnologically usable products.

The Ustilaginaceae family includes the well-established model organism *U. maydis* with a fully sequenced genome and highly developed genetic tools, enabling further research on improving the itaconate production parameters and thereby realizing the full potential of this production host [87]. Its yeast-like growth during fermentation processes is advantageous since less intensive morphology control is required compared to *A. terreus* [19]. Moreover, *U. maydis* is more robust toward varying impurities, particularly relevant to reducing production costs and using alternative feedstocks [48], [62].

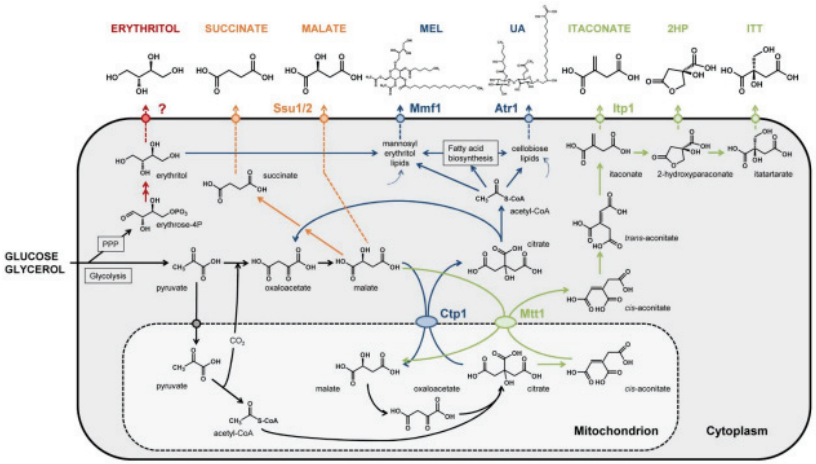

Figure 5: Interconnection between biochemical pathways for the main biotechnological products of Ustilaginaceae (adapted from [88]).
Mitochondrial antiporters and plasma membrane exporters are indicated in bold colors as stated in the following: red, erythritol; green, itaconate; orange, C4 dicarboxylates; blue, glycolipids. Abbreviations: ITT, itatartarate; PPP, pentose phosphate pathway; 2HP, 2-hydroxyparaconate.

Significant improvements in the efficiency of itaconate production have been made by metabolic engineering and process development, increasing the yield, titer, and rate of itaconate production in *U. maydis* and related species [64], [65], [73]. For itaconate production from glucose, a maximal theoretical yield of 0.72 $gi_{taconate}\ g_{glucose}^{-1}$, which equals 1 mol itaconate per mol glucose, is reported [65]. The latest study focused on an integrated process design that resulted in a maximum itaconate titer of 220 g L^{-1}, with a total acid titer of 248 g L^{-1}, representing a significant improvement compared to the best-published itaconate titers of *U. maydis* and *A. terreus* [64].

1.4 Alternative feedstocks for itaconic acid production

The competitiveness of bio against petro-based products displays a first step toward the vision of a circular economy. To achieve economic production and to compete with fossil fuels, it is necessary to use low-cost feedstocks. Furthermore, utilization of every production side stream to minimize waste and, ultimately, CO_2 formation [26]. Current biotechnological processes for itaconate production with *A. terreus* and *U. maydis* are based on carbohydrates, such as molasses, xylose, arabinose, and glucose [10, 27]. Recent studies approach the use of alternative substrates. Thus, glycerol, the main by-product in biodiesel production, is applied as an alternative feedstock for the itaconate production process with *U. vetiveriae* [18, 28]. Schlembach *et al.* (2020) presented a consolidated bioprocess approach for converting

cellulose waste streams into itaconic acid by the co-cultivation of Trichoderma reesei as cellulase producer and *U. maydis* as itaconate producer [89]. Another study by Regestein *et al.* (2018) focused on designing a complete process from beech wood to itaconate suitable for *U. maydis* and *A. terreus* [90].

A new approach to produce itaconate by Ustilaginaceae is based on the upcycling of abundant CO_2 to a feedstock and the subsequent use of CO_2-derived C1- and C2-compounds like formate and acetate as co-substrates [91]. The retention of one carbon atom during itaconate production means that they could consist of up to 50% carbon derived from CO_2 as schematically shown in **Figure 6**.

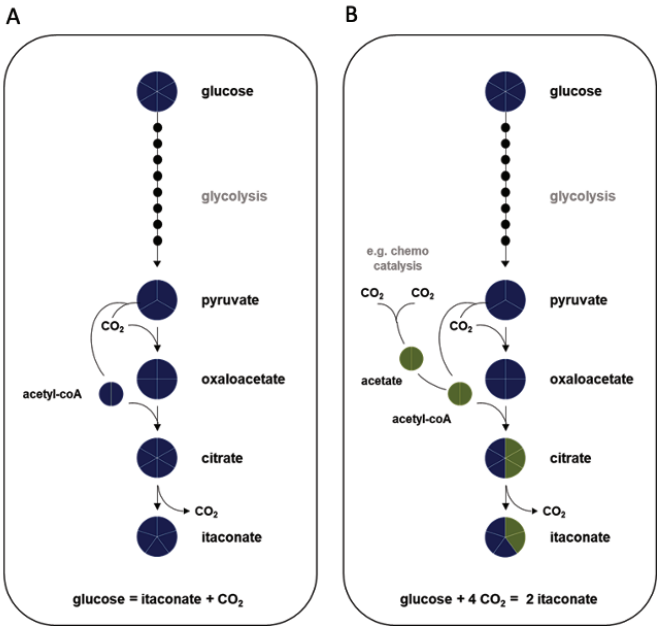

Figure 6: Simplified itaconate production pathway in Ustilaginaceae.
A: Established itaconate production pathway [63], [92] vs. B: proposed pathway incorporating CO_2. CO_2 could be incorporated either directly or *via* chemo catalytic C2-intermediates (e.g., acetate).

By combining chemistry (CO_2-fixation) and biology, up to 50% of the final product could be derived from CO_2, thereby aiming for a carbon-negative or neutral footprint of itaconate.

1.4.1 Acetate

1.4.1.1 Acetate production

Acetic acid is a two-carbon monocarboxylic acid (CH_3COOH) with a molecular mass of 60 g mol^{-1} and shows a pK_a value of 4.75; thus, acetic acid is predominantly dissociated as acetate (CH_3COO^-) at physiological pH [93]. The global demand for acetic acid is growing as

it produces various chemicals with potential applications in the textile, food, construction, and automobile industry [94].

Acetate is conventionally produced synthetically *via* chemical synthesis and biotechnologically *via* fermentation [93], [94]. *Via* the chemical production route, acetate is produced fossil-based by carbonylation of methanol, ethylene oxidation, or alkane oxidation. Chemical synthesis accounts for about 75 % of the total acetate production [93]. Chemical production covers most of the industrial acetate production, whereas biotechnological production covers about 10 % of the total acetate production, especially for the production of vinegar [95]. In aerobic fermentation, acetic acid bacteria like *Acetobacter* produce acetate through the respiration of ethanol [95]. Hence, it can be formed from sugars, glycerol, lignocellulosic biomass, or waste materials [94], [96]–[98]. Furthermore, acetate can empower the development of low-cost, sustainable bioprocesses without causing conflicts with arable land and the food chain [99].

Next to conventional production, there are also attempts to produce acetate from CO_2 as a waste stream, thereby contributing to a circular bioeconomy approach. One approach is converting synthesis gas (syngas) into acetic acid [94]. Anaerobic bacteria can grow on syngas, a mixture of inorganic waste gases containing primarily CO, H_2, and CO_2. Species like *Clostridium* or *Acetobacterium* are able to anaerobically produce acetate from this inorganic waste gas mixture [100]–[102]. A promising development in the field of gas fermentation is the successful commercialized operation of the first ethanol-production plant operating since 2018 [103].

Another promising approach is microbial electrosynthesis (MES) [104]. MES, based on bioelectrochemical systems (BESs), offer a potentially sustainable route for producing useful platform and commodity chemicals [104]. Thereby, MES does not use fossil-based substrates but uses microorganisms' metabolism to reduce CO_2 to valuable chemicals [86].

Microbial electrosynthesis shows the advantages of low operational costs, no land requirements, and a process that can operate sustainably. The versatility of the microbial culture that can be applied in MES allows its use for the bioproduction of a wide range of chemicals, such as different acids, alcohols, and fuels, among others [104]. The current acetate production approaches reach titers of 12.4 g L^{-1} [104]. These titers are low compared to other processes but increased from 0.6 g L^{-1} in the last decade [104]. This improvement excellently demonstrates the ongoing progress in the field of microbial electrosynthesis. Nevertheless, the low product yield, the product purification, and the problematic scale-up show the limitations that need to be addressed in research [104], [105].

Recent work in the broad context of green chemistry focused on a new catalytic system for the formal isomerization of methyl formate to acetic acid and methyl acetate, opening a possible route for a "defossilized" production of acetic acid ultimately based on CO_2 and H_2 as primary feedstocks [106].

1.4.1.2 Acetate assimilation

Using acetate as a carbon feedstock requires understanding its metabolism, including the enzymes involved, namely their gene expression and and regulation. Generally, acetate is directed to major metabolic pathways through acetyl-CoA [93]. The acetate assimilation for *U. maydis* has yet to bewell researched. However, the assimilation in yeasts may give a similar overview since an acetyl-CoA synthase (ACS) also exists in *U. maydis* [95] [107]. In yeast, acetate can enter the cell *via* passive diffusion of the undissociated acid and *via* the Fps1 channel in the plasma membrane [108]. According to Kretschmer *et al.* (2018), different acetate uptake mechanisms occur depending on the extracellular pH in *U. maydis* [109]. Subsequently, acetate serves as a substrate for the ACS enzyme, which converts acetate to acetyl-CoA in the cytosol [110]. Regarding the use of acetate as a carbon source, it was shown for *U. maydis* to be utilized in peroxisomal β-oxidation resulting in the production of acetyl-CoA [98]. In contrast, in yeast, the glyoxylate shunt or the carnitine shuttle mediates acetate transport to the mitochondria [111].

Nevertheless, high acetate levels of acetate were found to induce increased cellular stress levels, especially regarding mitochondrial dysfunction in *U. maydis* [109], whereby using acetate as a sole carbon source is possible but remains challenging. A combination of glucose and acetate as carbon sources resulted in higher cell numbers compared to growth on an individual carbon source, suggesting a possible use of acetate as a co-substrate next to glucose [109].

1.4.2 Formate

1.4.2.1 Formate production

With the vision of a truly circular bioeconomy, C1 compounds gain attention as biotechnological substrates, because they can be produced efficiently and almost infinitely from widely available resources, utilizing excess energy [112].

Compared to other C1 compounds like methane, carbon monoxide, and methanol, formate is particularly interesting because it is non-explosive, non-toxic, easily storable, and highly soluble in water [113]. In contrast to methanol, formate has mainly been neglected as a potential industrial feedstock due to its relatively high price. The only exceptions were proposals to use formate as an auxiliary substrate to supplement the cell with reducing power and thus boost bioproduction [114], [115]. With developments in electrochemical, photochemical, and catalytic methods of generating formate, interest in its use as a microbial feedstock is rising [116]–[118]. Thus, promising methods for sustainable production of formate include the electrochemical reduction of carbon dioxide [119], [120], CO_2 hydrogenation [121], [122], photoreduction of CO_2 [123], oxidation of natural gas [124], oxidation of biomass [125], and hydration of syngas [126].

The electrochemical reduction of CO_2 is one of the most effective ways to synthesize formate [106]. The use of inexpensive electric energy during off-peak hours would be ideal. Faradaic efficiencies exceed 90 % [108], whereas the electrodes' durability remains a challenge [115]. Hydrogenation of CO_2 uses transition metal complexes to catalyze the reaction of CO_2 and H_2 to formate [110].

The vision of utilizing formate as a sole feedstock for the industrial production of feed, fuels, food, value-added chemicals, or other products, as proclaimed by Yishai *et al.* (2016), is not an option for itaconic acid production with native strains of either *A. terreus*, *U. maydis* or *U. cynodontis* since these organisms do not grow solely on formate [118]. Nevertheless, there have been attempts to implement synthetic pathways for formate assimilation in *S. cerevisiae* [127]. The so-called reductive glycine pathway was most efficient for aerobic growth on formate [113]. In *S. cerevisiae*, this pathway could be triggered simply by overexpressing native enzymes. However, downstream assimilation of the obtained glycine has yet to be shown, and this new strain could only grow without glycine supplementation [127]. While being an attractive long-term ambition, there is much work to do till the implementation of such synthetic pathways could lead to itaconic acid production being able to compete with the highly efficient itaconic acid production based on carbohydrates.

With developments in electrochemical, photochemical, and catalytic methods of generating formate, interest in its use as a microbial feedstock is rising [113], [118]. For starters, the consumption of formate as a secondary substrate would already be an accomplishment [91], [114]. With methods like CO_2 hydrogenation, producing formate directly from the CO_2 accumulation as an unused by-product during itaconic acid production is theoretically possible.

1.4.2.2 Formate assimilation

The utilization of formate needs to be better described for *Ustilago*. Formate enters the cell as formic acid *via* passive transport through the membrane or *via* transporters, though the definite mechanisms remain unknown. Formate degradation *via* formate dehydrogenases (FDHs) is present in all methylotrophic microorganisms, which can perform oxidations of formate to CO_2 as one of the primary sources of electrons in the form of NADH. NAD^+-dependent FDHs were found in all yeasts of the genera *Candida*, *Pichia*, and *Hansenula* using methanol and were isolated and characterized from different strains [128]. Even though it is not a methylotrophic organism, these enzymes are also present in *U. maydis*. We proposed that the FDH activity in *U. maydis'* cytosol is similar to the mechanism in *S. cerevisiae* described by Overkamp *et al.* (2002) [129].

1.5 Scope and outline of this thesis

This thesis was written as part of the Cluster of Excellence “Fuel Science Center” (FSC). This thesis’s overall aim was to develop an Ustilaginaceae biocatalyst for the co-metabolization of CO_2-derived substrates, i.e., acetate and formate, to enable a carbon-neutral or even negative itaconate production, which is a candidate for bio(-hybrid) fuel synthesis.

Chapter 1 provides a general introduction to the topic. The necessary switch from a fossil- to a bio-based economy using renewable substrates is outlined. In particular, the use of microbial cell factories, especially *U. maydis*, for biotechnological production of platform chemicals is stated. As itaconic acid is the product of choice in this study, an overview of its production, market potential, applications, alternative feedstocks, and challenges to overcome are given.

Chapter 2 describes the materials and methods used in this thesis.

Chapter 3 1 deals with the co-metabolism of acetate and formate as alternative CO_2-derived feedstocks, testing 72 Ustilaginaceae strains from 36 species. The fungal growth and product spectrum with a particular interest in itaconate are characterized. Evaluating growth and itaconate production, *U. maydis* MB215 and *Ustilago rabenhorstiana* NBRC 8995 are applicable as promising candidates for acetate co-metabolization, while *U. cynodontis* NBRC 7530 is identified as a potential production host applying formate as co-substrate for enhanced itaconate production. The selected strains with the best itaconate production are characterized in more detail in controlled-batch bioreactor experiments to confirm the co-substrate utilization. Further, the optimum glucose and acetate feeding ratio were examined *via* the design of experiments (DoE) methodology for *U. maydis* and *U. rabenhorstiana.*

In **Chapter 3.2**, using acetate as a feedstock for *U. maydis’* itaconate production is further investigated. Within this work, a new chassis strain, *U. maydis* Δ*fuz7* Δ*cyp3* ΔMEL ΔUA P_{etef}mttA ΔP_{ria1}::P_{etef} is engineered and tested for acetate co-substrate metabolization. Further, acetate co-metabolization is investigated *via* offgas analysis and ^{13}C-labeling methodology. By applying the DoE methodology, cultivation parameters (glucose, acetate, and ammonium chloride concentrations) are optimized. Product inhibition of itaconate and the toxic effects of acetate are addressed by implementing an external membrane module enabling cell retention and simultaneous product removal into the existing process. The potential of continuous cultures with *U. maydis* is demonstrated during proof-of-principle bioreactor cultivations.

Chapter 3.3 describes the implementation of a CO_2-derived substrate for itaconate production using metabolically engineered *U. cynodontis* strains. By applying the DoE methodology, cultivation parameters are optimized resulting in two empirical models predicting itaconate titer and yield for *U. cynodontis* Δ*fuz7* Δ*cyp3* P_{etef}mttA ΔP_{ria1}::P_{etef} . Further, utilizing a solution of sodium formate obtained from biphasic Ru-catalysed CO_2 hydrogenation approach within a

fully integrated biocompatible process as co-substrate is examined, e.g., by testing different solvents required for the hydrogenation process.

Chapter 3.4 presents 17 high-quality draft genome sequences (N50 > 1 Mb) obtained by combining third-generation nanopore and second-generation Illumina sequencing. The obtained data are analyzed with taxonomical genome-based bioinformatics methods, such as Percentage of Conserved Proteins (POCP), Average Nucleotide Identity (ANI), and Average Amino Acid Identity (AAI) analyses. Further, conserved core genes are determined to calculate a phylogenomic core genome tree of the Ustilaginaceae that supported the results of the other phylogenomic analysis. Besides genomic comparisons, secondary metabolite clusters (i.e., itaconic acid, mannosylerythritol lipids, and ustilagic acid) of biotechnological interest are also analyzed.

In **Chapter 4**, all results and achievements are discussed and placed in a larger context. Improvements and research ideas for even more efficient and sustainable itaconate production are elucidated with a particular focus on the overall goal of industrial production.

In general, this thesis confirms the potential of Ustilaginaceae, especially *U. maydis* and *U. cynodontis*, as alternative hosts for the industrial production of itaconate. Strain optimization and process development further enlarge this potential and ensure that this microorganism significantly contributes to the required change from petroleum-derived to sustainable, economically bio-based production process.

Chapter 2

Material and methods

Partially published as:

Ullmann, L., Phan, A. N. T., Kaplan, D. K. P., Blank, L. M. Ustilaginaceae Biocatalyst for Co-Metabolism of CO_2-Derived Substrates toward Carbon-Neutral Itaconate Production. *J. Fungi* 2021, 7, 98. https://doi.org/10.3390/jof7020098

Ullmann, L., Wibberg, D., Busche, T., Rückert, C., Müsgens, A., Kalinowski, J., Blank, L. M. Seventeen Ustilaginaceae High-Quality Genome Sequences Allow Phylogenomic Analysis and Provide Insights into Secondary Metabolite Synthesis. *J. Fungi* 2022, 8, 269. https://doi.org/10.3390/jof8030269

Ullmann, L., Guntermann, N., Kohl, P., Müsgens, A., Schröders, G., Franciò, G., Leitner, W., Blank, L. M. Improved Itaconate Production with *U. cynodontis* via Co-Metabolism of CO_2-Derived Formate. *J. Fungi* 2022, 8, 12. https://doi.org/10.3390/jof8121277

Contributions:

This chapter was written by Lena Ullmann and reviewed Lars M. Blank.

2 Material and methods

2.1 Chemicals

The chemicals used in this study were obtained from Sigma-Aldrich (St. Louis, MO, USA), Carl Roth (Karlsruhe, Germany), or Merck (Darmstadt, Germany) unless stated otherwise.

2.2 Strains, media, and culture conditions

All Ustilaginaceae wildtype strains used in this work are listed in **Table 4.** Metabolically engineered *Ustilago* strains generated and used in this work are listed in **Table 5**.

Table 4: Wildtype strains used within this study.

No. (iAMB strain collection)	Strain	Origin
#2841	*Anthracocystis bothriochloae* BRIP 60896 a	Queensland Plant Pathology Herbarium, Australia
#2842	*Anthracocystis heteropogonicola* BRIP 60901 a	
#2209	*Macalpinomyces eriachnes* RK 028	CBS 131454
#2814	*Macalpinomyces mackinlayi* BRIP 52549 a	Queensland Plant Pathology Herbarium, Australia
#2816	*Macalpinomyces ordensis* BRIP 26904 a	
#2833	*Macalpinomyces spermophorus* BRIP 60430 a	
#2835	*Macalpinomyces spermophorus* BRIP 60448 a	
#2834	*Macalpinomyces tubiformis* BRIP 60434 a	
#1946	*Pseudozyma antartica*	NRRL Y - 7808
#1947	*Pseudozyma antartica*	NRRL Y - 8295
#2696	*Pseudozyma hubeiensis*	NBRC 105053
#2697	*Pseudozyma hubeiensis*	NBRC 105054
#2698	*Pseudozyma hubeiensis*	NBRC 105055
#2710	*Pseudozyma tsukubaensis*	NBRC 1940
#2818	*Sporisorium bothriochloae* BRIP 26908 a	Queensland Plant Pathology Herbarium, Australia
#2835	*Sporisorium caledonicum* BRIP 28043 a	
#2815	*Sporisorium cenchri-elymoidis* BRIP 26491 a	
#2210	*Sporisorium consanguineum* RK133	CBS 131454
#2211	*Sporisorium cruentum*	CBS 131456
#2212	*Sporisorium exsertum*	RK033
#2832	*Sporisorium iseilematis-ciliati* BRIP 60429 a	Queensland Plant Pathology Herbarium, Australia
#2838	*Sporisorium iseilematis-ciliati* BRIP 60887 a	
#2813	*Sporisorium lanigeri* BRIP 27609 a	
#2213	*Sporisorium scitamineum*	CBS 131457
#2823	*Sporisorium setariae* BRIP 26910 a	Queensland Plant Pathology Herbarium, Australia
#2819	*Sporisorium themedae* BRIP 26917 a	
#2820	*Sporisorium tumiforme* BRIP 26919 a	
#2214	*Sporisorium walkeri* RK031	CBS 131462
#2215	*Ustanciosporium gigantosporum* UMa706	CBS 131464

#2821	*Ustilago curta* BRIP 26929 a	Queensland Plant Pathology Herbarium, Australia
#2705	*Ustilago cynodontis*	NBRC 7530
#2706	*Ustilago cynodontis*	NBRC 9727
#2707	*Ustilago cynodontis*	NBRC 9758
#2824	*Ustilago cynodontis* BRIP 28040 a	Queensland Plant Pathology
#2850	*Ustilago egenula* BRIP 60884 a	Herbarium, Australia
#2218	*Ustilago filiformis* UMa701	CBS 131469
#2826	*Ustilago lituana* BRIP 46795 a	Queensland Plant Pathology Herbarium, Australia
#1951	*Ustilago maydis*	DSM 14603
#1949	*Ustilago maydis*	DSM 3121
#2229	*Ustilago maydis* MB215	DSM 17144
#2134	*Ustilago maydis* No. 196	
#2135	*Ustilago maydis* No. 197	
#2136	*Ustilago maydis* No. 198	
#2144	*Ustilago maydis* No. 206	
#2152	*Ustilago maydis* No. 215	
#2158	*Ustilago maydis* No. 469	Prof. M. Bölker, Philipps University Marburg, Germany
#2162	*Ustilago maydis* No. 474	
#2167	*Ustilago maydis* No. 480	
#2169	*Ustilago maydis* No. 482	
#2172	*Ustilago maydis* No. 485	
#2177	*Ustilago maydis* No. 491	
#2178	*Ustilago maydis* No. 492	
#2179	*Ustilago maydis* No. 495	
#2196	*Ustilago maydis* FB1 Mating type a1b1	Banuett & Herskowitz, 1989,
#2197	*Ustilago maydis* FB2 Mating type a2b2	Minnesoty USA
#3600	*Ustilago maydis*	Bernd Leuchtle [130]
#2199	*Ustilago maydis*	RK 123 [131]
#2105	*Ustilago maydis*	RK 212 [131]
#2108	*Ustilago maydis*	RK 215 [131]
#2708	*Ustilago rabenhorstiana*	NBRC 8995
#2817	*Ustilago schmidtiae* BRIP 26906 a	Queensland Plant Pathology Herbarium, Australia
#2219	*Ustilago trichophora* RK 089	CBS 131473
#2699	*Ustilago trichophora*	NBRC 100155
#2700	*Ustilago trichophora*	NBRC 100156
#2701	*Ustilago trichophora*	NBRC 100157
#2702	*Ustilago trichophora*	NBRC 100158
#2703	*Ustilago trichophora*	NBRC 100159
#2704	*Ustilago trichophora*	NBRC 100160
#2822	*Ustilago triodiae* BRIP 26907 a	Queensland Plant Pathology Herbarium, Australia
#2220	*Ustilago vetiveriae* RK 075	CBS 131474

#2836	*Ustilago xerochloae* BRIP 60876 a	Queensland Plant Pathology Herbarium, Australia
#2221	*Ustilago xerochloae* UMa702	CBS 131476

Table 5: Metabolically engineered Ustilaginaceae strains used within this study with description and reference.

No. (iAMB strain collection)	Description	Reference
#4856	*U. maydis* MB215 Δ*cyp3* ΔMEL ΔUA Δdgat ΔP_{ria1}::P_{etef} Δ*fuz7* P_{etef}mttA_K14	Johanna Becker [73]
#4186	*U. maydis* MB215 Δ*cyp3* Δ*fuz7* $\Delta P_{ria}1$::P_{etef}	Hamed Tehrani
#6188	*U. maydis* MB215 Δ*cyp3* Δ*fuz7* ΔUA ΔP_{ria1}::P_{etef}	this study
#6754	*U. maydis* MB215 Δ*cyp3* Δ*fuz7* ΔUA ΔMEL ΔP_{ria1}::P_{etef}	this study
#7072	*U. maydis* MB215 Δ*fuz7* Δ*cyp3* ΔUA ΔMEL P_{etef}mttA ΔP_{ria1}::P_{etef}_K1	this study
#7073	*U. maydis* MB215 Δ*fuz7* Δ*cyp3* ΔUA ΔMEL P_{etef}mttA ΔP_{ria1}::P_{etef}_K2	this study
#7074	*U. maydis* MB215 Δ*fuz7* Δ*cyp3* ΔUA ΔMEL P_{etef}mttA ΔP_{ria1}::P_{etef}_K3	this study
#7075	*U. maydis* MB215 Δ*fuz7* Δ*cyp3* ΔUA ΔMEL P_{etef}mttA ΔP_{ria1}::P_{etef}_K4	this study
#7076	*U. maydis* MB215 Δ*fuz7* Δ*cyp3* ΔUA ΔMEL P_{etef}mttA ΔP_{ria1}::P_{etef}_K5	this study
#7077	*U. maydis* MB215 Δ*fuz7* Δ*cyp3* ΔUA ΔMEL P_{etef}mttA ΔP_{ria1}::P_{etef}_K6	this study
#7078	*U. maydis* MB215 Δ*fuz7* Δ*cyp3* ΔUA ΔMEL P_{etef}mttA ΔP_{ria1}::P_{etef}_K7	this study
#4852	*U. cynodontis* Δ*fuz7* Δ*cyp3* ΔP_{ria1}::P_{etef}	Hamed Tehrani [72]
#4853	*U. cynodontis* Δ*fuz7* Δ*cyp3* ΔP_{ria1}::P_{etef} ::P_{etef}mttA	Hamed Tehrani [72]

Growth and production experiments using Ustilaginaceae strains were performed using modified Tabuchi medium according to Geiser *et al.* (2016) [63], containing 0.2 g L^{-1} $MgSO_4$ $7H_2O$, 0.01 g L^{-1} $FeSO_4$ $7H_2O$, 0.5 g L^{-1} KH_2PO_4, 1 mL L^{-1} vitamin solution, 1 mL L^{-1} trace element solution, and as buffer 19.5 g L^{-1} 2-(N-morpholino) ethanesulfonic acid (MES). Different carbon sources such as glucose, sodium acetate, and sodium formate were used as well as different c-source concentrations as indicated. NH_4Cl was added in indicated concentrations. The vitamin solution contained (per liter) 0.05 g D-biotin, 1 g D-calcium pantothenate, 1 g nicotinic acid, 25 g myo-inositol, 1 g thiamine hydrochloride, 1 g pyridoxol hydrochloride, and 0.2 g para-aminobenzoic acid. The trace element solution contained (per liter) 1.5 g EDTA, 0.45 g $ZnSO_4$ $7H_2O$, 0.10 g $MnCl_2$ $4H_2O$, 0.03 g $CoCl_2$ $6H_2O$, 0.03 g $CuSO_4$ $5H_2O$, 0.04 g Na_2MoO_4 $2H_2O$, 0.45 g $CaCl_2$ $2H_2O$, 0.3 g $FeSO_4$ $7H_2O$, 0.10 g H_3BO_3, and 0.01 g KI. Cultivation experiments were performed at 30 °C.

Shaking cultures of Ustilaginaceae and mutants strains were performed in System Duetz® (24 well plates, Enzyscreen, Heemstede, Netherlands) with a filling volume of 1.5 mL (d = 50 mm, n = 300 rpm, T = 30 °C and Φ = 80 %, Infors HT Multitron Pro shaker, Bottmingen, Switzerland) or in 500 mL shaking flasks with a filling volume of 50 mL (d = 25 mm, n = 200 rpm, T = 30 °C and Φ = 80 %, Infors HT Multitron Pro shaker, Bottmingen, Switzerland) as indicated. Experiments for biomass formation were performed using the Growth Profiler GP960 (EnzyScreen, Heemstede, Netherlands). Strains were cultivated in polystyrene grey square 24-deep-well microplates (CR1424d) with transparent bottom and a filling volume of 1.5 mL (225 rpm, d = 50 mm). Cultures were inoculated to a final OD_{600} of 0.5 with cells from an overnight culture in MTM medium. For System Duetz cultivation experiments, for each sample point, a complete plate was taken as a sacrificial sample to ensure continuous oxygenation.

For cultivation measuring off-gas BlueSens sensors (BlueSens gas sensor GmbH, Herten, Germany) and simultaniously cell growth the Cell Growth Quantifier (CGQ) system (aquila biolabs GmbH, Baesweiler, Germany) were used. Shaking conditions were 30 °C and 150 rpm in an Eppendorf Shaker (Eppendorf AG, Hamburg, Germany). 1L BlueSens shake flasks were used with a filing volume of 50 ml MTM medium using a maximum of 4 g L^{-1} carbon source. Main cultures were inoculated to a final OD_{600} of 0.1.

The cultivation for the ^{13}C-labeling experiment was divided into two phases. The first phase determines the growth phase for biomass formation. Thereby, 250 mL shake flasks were used containing 25 mL Modified Tabuchi Medium with MES buffer. 50 g L^{-1} glucose, 3 g L^{-1} acetate with 0.8 g L^{-1} NH_4CL were added to the medium and strains were cultured for 48 h. The second phase was used for cultivation with fully labeled acetate under nitrogen limitation condition. After 48 h, (OD 10-12) 20 mL of each flask was transferred to a 50 mL Falcon, washed with 0.9 % NaCl solution and the supernatant was discarded. Cells were centrifuged at 1,473 g using a Heraeus Megafuge 16R (ThermoFisher Scientific, Schwerte, Germany) and a a TX-400 rotor (Thermo Scietific, Schwerte, Germany) for washing for 3 min. For subsequent second cultivation phase, the cells were re-suspended in 10 ml MTM containing 2 g L^{-1} glucose and 2 g L^{-1} $^{13}C_2$-acetate as substrates whereas no nitrogen source was added. Cultivation was performed in 100 mL shake flasks whereas samples were taken every 4 h for the 24 h cultivation period.

Controlled batch cultivations were performed in a BioFlo® 120 bioreactor with a total volume of 1.3 L and a working volume of 0.5 L in combination with DASware Control Software 5.3.1 (Eppendorf, Hamburg, Germany). All cultivations were performed in batch medium containing varying substrate and ammonium chloride concentrations, 0.2 g L^{-1} $MgSO_4 \cdot 7H_2O$, 0.01 g L^{-1} $FeSO_4 \cdot 7H_2O$, 0.5 g L^{-1} KH_2PO_4, 1 g L^{-1} yeast extract, 1 mL L^{-1} vitamin solution, 1 mL L^{-1} trace element solution, and 19.5 g L^{-1} MES as buffer. During cultivation, pH was monitored *via* online pH probes (phferm, Hamilton, Bonaduz, Switzerland) and maintained at pH 6.5 by automatic

addition of 10 M NaOH and 1 M HCl. Dissolved oxygen tension (DOT) was kept constant at approximately 80 % saturation by automatic adjustment of the stirring rate (800 – 1200 rpm). The bioreactor was aerated with an aeration rate of 1 L min^{-1} (2 vvm), while evaporation was limited by sparging the air through a water bottle. The temperature was set at 30 °C. The bioreactor was inoculated to a final OD_{600} of 0.5 with cells from an overnight culture in 50 mL MTM containing 50 g L^{-1} glucose and 5 g L^{1} of respective co-substrate (sodium acetate, sodium formate).

2.3 Membrane set-up

A 250 mm long ceramic microfiltration membrane with 0.2 µm pore size and 7 mm channel diameter (SCHUMASIV™ 01/7 by Pall Filtersystems GmbH, Crailsheim, Germany) was used for cell-retention and product removal during itaconate production process. Additional technical information is provided in the following **Table 6.**

Table 6: Technical information of SCHUMASIV™ 01/7 microfiltration membrane

	Parameter	Values
Material	Module housing	1.4404/1.4571
	Support material	α-Al_2O_3
	Membrane material	α-Al_2O_3
	O-ring	VITON
Module idenitification	Title	D10x01 – 0250 KS DN10
	Item number	89581910-01-a
	Ceramic element	01/7
	Ordering number	MF 1200 Z 01 070 0250 T
Size	Inner diameter	0.7 cm
	Amount of elements	1
	Channel lenght	25 cm
	Module diameter	1 cm
	Pore size	1.2 µm
	Max. pressure	10 bar
Additionals	Min./max. temperature	-10/100 °C
	Total volume	50 mL
	Pore size	1200 nm
	Vol. (inner channel)	9.62 cm^3
	Vol. (outer tube)	40.38 cm^3
	Filtration area	54.98 cm^3

The fermentation broth flows through the inside of a ceramic tube (**Figure 7**). The membrane is housed by a steel module. Small metabolites and substrates like itaconic acid can permeate the ceramic membrane module and can be separated though side outlets.

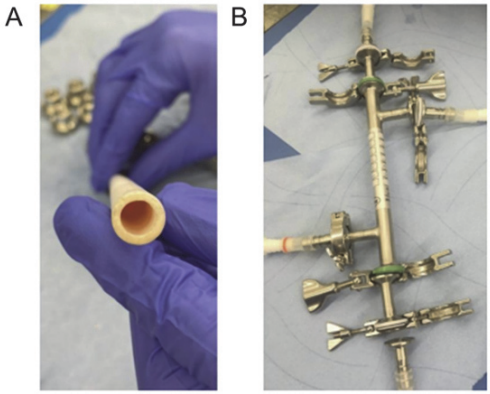

Figure 7: Membrane channel and housing module.
The ceramic filtration membrane is shown in A. The channel sits in the middle of the steal housing shown in B, together forming a two-channel system

Figure 7 shows the ceramic tube used. Fermentation broth flows through the inside, while small molecules like itaconic acid can permeate the membrane. The membrane is housed by the steel module shown in **Figure 7 B**. The experimental setup is schematically shown in **Figure 8.**

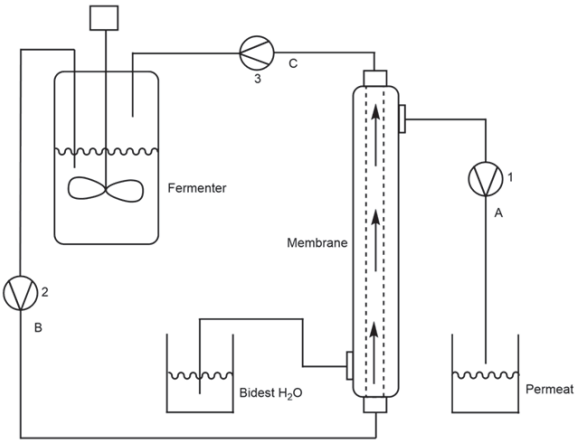

Figure 8: Schematic set-up for itaconic acid recovery using a microfiltration crossflow membrane module.
1-3: Pump number, A = Permeat flow, B = Feed flow, C = Retentat flow

Three peristaltic pumps were used. Two in the recirculation loop with up to 60 mL min^{-1} flow rates (101U, Watson and Marlow, Rommerskirchen, Germany) and one on the filtrate side (Ismatec ip-12, Cole-Parmer GmbH, Wertheim am Main, Germany). The latter supports

multiple tubes and can therefore be used to feed with the same rate as filtrate is drained. Each individual pump showed setpoint from 0.1 - 9.9. In all characterization and filtration processes, the setting of the feed and retentate pumps was set as identical.

Three glycerine manometers (MS 1,663 GLY CR, Wilka, Velbert, Germany) with a pressure indication from 0 to 4 bar were used to control pressure changes upstream and downstream of the membrane (**Figure 8**).

To prevent contamination and fouling, the membrane was subjected to a cleaning process before and after the membrane setup for filtration with cell retention was applied according to manufacturer's instructions. For this purpose, the system was first rinsed with bidest H_2O until the retentate appeared clear. Then followed by cleaning with 1 % w/w sodium hydroxide solution (NaOH) for 15 min at 50 °C with subsequent use of bleach (NaOCl, 400 ppm free chlorine) for 15 min at 50 °C. The permeate valve was kept closed during this process. Then the retentate side was drained. A following cleaning step by filling and pumping with a 2 % w/w NaOH solution for 30 min at 60 – 80 °C with closed permeate valve was performed. The process was continued for another 30 min with open permeate valve. Then the retentate and permeate sides of the membrane were emptied. The system was rinsed with bidest H_2O until a pH value of 7 - 8 was reached. A 0.5 - 1% w/w nitric acid solution (HNO_3) was used for 15 min at 60 – 70 °C with closed permeate valve. This step was continued for another 15 min with open permeate valve. The system was drained and then rinsed with bidest H_2O until a neutral pH value was obtained.

2.4 Analytical methods

2.4.1 Cell growth measurement

Cell growth was determined by measuring the optical density at 600 nm (OD_{600}) with an Ultrospec 10 Cell Density Meter (Amersham Biosciences, Freiburg, Germany). For microscopy the OD_{600} of the culture was adjusted to 5 with 0.9 % NaCl. Differential interference contrast (DIC) or dark field (DF) microscopy was performed with a Leica DM1000 light microscope (Leica Microsystems, Wetzlar, Germany). Images were recorded with a Leica MC190 digital microscope camera (Leica Microsystems, Wetzlar, Germany). Images were taken at 63-fold magnification. The cell morphology was analyzed by microscopy at different time points in all cultivations. The ammonium concentration in the culture supernatant was measured by a colorimetric method, according to Willis *et al.* (1996) [132] using salicylate and nitroprusside. For CDW determination 1 mL culture broth was centrifuged at maximum speed (Heraeus Pico 17 centrifuge, ThermoFisher Scientific, Schwerte, Germany) and the pellet was dried (Scan Speed 40 lyophilizer, Labogene ApS, Allerød, Denmark) for 24 h at 38 °C.

Carbon sources and metabolites such as glucose, acetate, formate, itaconate, malate, succinate, erythritol, and (S)-2-hydroxyparaconate in the supernatant were analyzed *via* high-

performance liquid chromatography (HPLC). All samples were filtered with Rotilabo® syringe filters (CA, 0.20 µm) and afterward diluted in a range of 1:5 – 1:50 with 5 mM H_2SO_4. Supernatants were analyzed in a DIONEX UltiMate 3000 HPLC System (Thermo Scientific, Schwerte, Germany) with a Metab-AAC column (300 x 7.8 mm column, ISERA, Düren, Germany). Elution was performed with 5 mM H_2SO_4. at a flow rate of 0.6 ml, $min^{-1,}$ and a temperature of 40 °C. For detection, a SHODEX RI-101 detector (Showa Denko Europe GmbH, Munich, Germany) and a a DIONEX UltiMate 3000 Variable Wavelength Detector (Thermo Scientific, Schwerte, Germany) set to 210 nm were used.

2.4.2 LC-RI/UV-MS/MS

The identification of extracellular metabolites was performed on a Nexera UHPLC system (Shimadzu Corporation, Duisburg, Germany) with 0.2 % formic acid as eluent. After the samples were separated on an Isera Metab-AAC 300 × 7.8 mm column (ISERA, Düren, Germany), the flow was divided into 2 directions with the split ratio of 1 to 10. The major part of the samples was measured with a RID-20A Refractive Index detector and an SPD-40 UV detector at 210 nm (Shimadzu Corporation, Duisburg, Germany). The rest were analyzed with a triple quadrupoles mass spectrometry 8060 (Shimadzu Corporation, Duisburg, Germany). The retention time from all detectors and the MS/MS mass spectrums of samples were compared directly to authentic standards. As the standard was not available for ITT, the structure prediction was performed with the software CFM-ID 3.0 [133].

2.4.3 ^{13}C-labeling *via* GC-MS

Strains for the isotope labeling experiments were grown under the conditions stated in **section 2.2**. For analysis an ISQ GC/MS instrument (Thermo Scientific, Schwerte, Germany) was used operating in selected ion monitoring mode (SIM) a VF-5ms capillary column (30 m × 250 µm i.d., 0.25 µm film thickness, Agilent, Santa Clara, CA, United States) together with 10 m EZGuard using a ramp profile of 100 °C for 2 min, then 100 – 200 °C at 15 °C min^{-1}, and then 200 - 325 °C at 20 °C min^{-1} with a helium carrier gas flow rate of 1.0 mL min^{-1}. Injection, mass spectrometer transfer line, and ion source temperatures were 250, 280, and 300 °C, respectively. Samples were run in triplicate.

Samples and standards (itaconate, succinate, α-keto-glutarate, citrate und malate) were prepared as stated in the following. 100 µL of the respective sample was transferred into GC-glass vials and was dried using a lyophilizer (Scan Speed 40 lyophilizer, Labogene ApS, Allerød, Denmark). 50 µL of methoxyamine hydrochloride (MeOX) (20 mg mL^{-1} in pyridine) were added to each dried sample for methoximation. Samples were incubated at 37 °C for 90 min. Then, silylation has been performed by adding 50 µL of N-methyl-N-(trimethylsilyl) trifluoroacetamide (MSTFA) at 37 °C for 30 min. Samples were analyzed within 24 h.

2.4.4 Design of Experiment (DoE) approach

The software Design Expert 11 (Stat-Ease, Minneapolis, MN, United States) was used to set up and evaluate Design of Experiments (DoE) approaches. A response surface 3-factor central composite design (CCD) was chosen to simultaneously evaluate the influence of varying concentrations of glucose, co-substrate, and ammonium chloride on itaconic acid production. To enhance the significance of the model, each condition was tested in replicates. Factors showing a significant influence (p-value ≤ 0.05) were incorporated into the model. If a factor with a non-significant influence was substantial for maintaining the model hierarchy, exceptions were made. The input data were transformed, if necessary, according to the recommendations of the software. To prove the predicted conditions and confirm the design, validation in 24-deep-well plates and up-scaling shaking flasks were performed.

2.4.4.1 Acetate co-metabolizatíon

DoE using Ustilaginaceae wildtype strains

Models predicting itaconate production during acetate co-metabolization cultivations were set up as stated in the following. Glucose (30 - 100 g L^{-1}) and acetate (2 - 12 g L^{-1}) were used as numerical factors and the buffer system (19.5 g L^{-1} MES or 33g L^{-1} $CaCO_3$) was set as a categorical factor. The software Design Expert® generated testing conditions for the design points of the central composite design (**Table 9**). The buffer system as a categoric factor duplicates the test conditions. To increase the significance of the model, each condition was tested in replicates. In total, the number of all replicates was defined to 24 for each buffer system to fill one 24-deep-well plate for each buffer. As the central point is most important for the model the number of replicates was set to 4. Each cube point was tested in 3 replicates and the star points were tested in duplicates, as they are less important for the model significance.

DoE using metabolically engineered strains

Models predicting itaconate production during acetate co-metabolization cultivations were set up as stated in the following. Glucose (13.65 – 165 g L^{-1}), sodium acetate (3 – 18 g L^{-1}) and ammonium chloride (0.8 – 4 g L^{-1}) were set as numerical factors (**Table 16**). Thereby, 10 different conditions were tested, whereas the approaches with the lowest (13.65 g L^{-1}) and highest (316.4 g L^{-1}) glucose concentration were carried out as triplicates. All medium level (165 g L^{-1}) glucose conditions were implemented as triplicates as well, except the central condition (165 g L^{-1} glucose, 10.5 g L^{-1} sodium acetate, 2,4 g L^{-1} ammonium chloride) as a sextuplet. The approaches with 50 and 280 g L^{-1} glucose were carried out as triplets. To enhance the significance of the model, each condition was tested in replicates. Factors showing a significant influence (p-value ≤ 0.05) were incorporated into the model. If a factor with a non-significant influence was substantial for maintaining the model hierarchy, exceptions were made. The input data were transformed, if necessary, according to the recommendations

of the software. To prove the predicted conditions and confirm the design, validation in 24-deep-well plates and up-scaling to shakeing flask levels were performed.

2.4.4.2 Formate

Models predicting itaconate production during formate co-metabolization cultivations were set up as stated in the following. 15 different conditions were tested, whereas the approaches with the lowest (13.65 g L^{-1}) and highest (316.4 g L^{-1}) glucose concentration were carried out as quadruplets. All medium level (165 g L^{-1}) glucose conditions were implemented as quadruplets too, except the central condition (165 g L^{-1} glucose, 8,75 g L^{-1} formate, 2,4 g L^{-1} ammonium chloride) as an octuplet. The approaches with 50 and 280 g L^{-1} glucose were carried out as quintuplets (**Table 35**). The resulting 72 replicas were split up onto three 24-deep-well plates (System Duetz). The first plate (A) was made up of conditions expected to reach maximum titers within approximately two weeks and the other two plates (B and C) were made up of conditions expected to reach maximum titers within five weeks. The range of factor settings were based primarily on the investigation of single factors during previous studies [91].

2.5 Statistical analysis

All values are the arithmetic mean of at least two biological replicates. Error bars indicate the deviation from the mean for n = 2, if n > 2 error bars indicate the standard error of the mean. Hierarchical Cluster Analysis (HCA) was performed using the MultiExperiment Viewer (MeV). Due to the high number of 1296 growth curves obtained during this study (**section 3.1**), a MatLab function modified from [134] was used for standardized maximum growth rate calculation.

2.6 Genome sequencing

2.6.1 Genomic DNA isolation

For genome sequencing, 17 strains of the Ustilaginaceae family were chosen. Eleven representatives of the *Ustilago* genus (*U. curta, U. cynodontis, U. lituana, four U. maydis strains, U. trichophora, U. vetiveriae, and U. xerochloae*), and species of three other genera *(Sporisorium, Pseudozyma, Macalpinomyces*) were chosen. *Ustanciosporium gigantosporium* of the order of Ustilaginales represents the taxonomic outgroup.

Cells from frozen glycerol stocks were grown on YEP agar plates at 30 °C for 24 – 48 h. Single colonies of the fungal strains were grown in modified Tabuchi medium according to Geiser *et al.* (2016) [63] at 30 °C for 24 h (300 rpm, 80 % humidity, d = 50 mm, Infors HT Multitron Pro shaker, Bottmingen, Switzerland). Cells were disrupted using type C bead tubes (Macherey-Nagel, Düren, Germany) for 25 min at full speed horizontally on a flat-bed vortexer (Vortex-Genie 2, Scientific Industries, New York, NY, USA). Genomic DNA was isolated by

NucleoBond High molecular weight DNA Kit (Macherey-Nagel, Düren, Germany) according to the manufacturer's instructions.

2.6.2 Nanopore library preparation and GridION® sequencing

A sequencing library with genomic DNA from the different fungal strains was prepared using the Nanopore Rapid DNA Sequencing kit (SQK-RAD04, Oxford Nanopore Technologies, Oxford, UK) according to the manufacturer's instructions. Sequencing was performed on an Oxford Nanopore GridION Mk1 sequencer using an R9.4.1 flow cell, which was prepared according to the manufacturer's instructions.

2.6.3 Illumina library preparation and MiSeq sequencing

Whole-genome-shotgun PCR-free libraries were constructed from 5 µg of gDNA with the Nextera XT DNA Sample Preparation Kit (Illumina, San Diego, CA, USA) according to the manufacturer's protocol. Quality of the resulting libraries was controlled by using an Agilent 2000 Bioanalyzer with an Agilent High Sensitivity DNA Kit (Agilent Technologies, Santa Clara, CA, USA) for fragment sizes of 500 – 1000 bp. Paired-end sequencing was performed on the Illumina MiSeq platform (2 × 300 bp, v3 chemistry). Adapters and low-quality reads were removed by an in-house software pipeline prior to polishing as recently described [135].

2.6.4 Base calling, reads processing, and assembly

MinKNOW (Oxford Nanopore Technologies) was used to control the run using the 48 h sequencing run protocol; base calling was performed offline using Bonito. The assembly was performed using canu v2.1.1 [136]. The resulting contigs were polished with Illumina short-read data using Pilon [137] run for ten iterative cycles. BWA-MEM [138] was used for read mapping in the first five iterations and Bowtie2 v2.3.2 [139] in the second set of five iterations.

2.6.5 Gene prediction and genome annotation

Gene prediction was performed by applying GeneMark-ES 4.6.2 [140] using default settings. Predicted genes were functionally annotated using a modified version of the genome annotation platform GenDB 2.0 [141] for eukaryotic genomes as previously described [142]. For automatic annotation within the platform, similarity searches against different databases, including COG [143], KEGG [144], and SWISS-PROT [145], were performed.

In addition to genes, putative tRNA genes were identified with tRNAscan-SE [146]. Completeness, contamination, and strain heterogeneity were estimated with BUSCO (v3.0.2 [147]), using the fungi-specific single-copy marker genes database (odb9). The obtained genome sequences were deposit **Table 7.**

Table 7: DDBJ/EMBL/GenBank database accession numbers.

Strain No.	Assembly Name	Assembly ACC	Study ID	Sample ID	Contig ACC
#2169	Umay_482_v1	GCA_928722285	PRJEB50355	ERS10392836	CAKMXG010000001-CAKMXG010000046
#2169	Umay_482_v2	GCA_928722265	PRJEB50355	ERS10392837	CAKMXF010000001-CAKMXF010000068
#2172	Umay_485	GCA_928722245	PRJEB50356	ERS10381369	CAKMXD010000001-CAKMXD010000043
#2136	Umay_198	GCA_928743665	PRJEB50359	ERS10419843	CAKMXO010000001-CAKMXO010000107
#2816	BRIP_26904_a	GCA_928724745	PRJEB50498	ERS10395116	CAKMXJ010000001-CAKMXJ010000042
#2701	NBRC_100157	GCA_928724775	PRJEB50365	ERS10395119	CAKMXL010000001-CAKMXL010000048
#2212	RK_033	GCA_928724755	PRJEB50360	ERS10395351	CAKMXK010000001-CAKMXK010000041
#2215	UMa706_1	GCA_928724875	PRJEB50363	ERS10395376	CAKMXN010000001-CAKMXN010000086
#2215	UMa706_2	GCA_928724795	PRJEB50363	ERS10395377	CAKMXM010000001-CAKMXM010000036
#2814	BRIP_52549_a	GCA_928852645	PRJEB50497	ERS10422304	CAKMXS010000001-CAKMXS010000079
#2821	BRIP_26929_a	GCA_928722295	PRJEB50499	ERS10393563	CAKMXH010000001-CAKMXH010000039
#2214	RK031	GCA_928858565	PRJEB50362	ERS10422305	CAKMXV010000001-CAKMXV010000022
#1946	NRRL_Y-7808	GCA_928872045	PRJEB50496	ERS10422313	CAKMYB010000001-CAKMYB010000027
#2706	NBRC_9727	GCA_928865425	PRJEB50366	ERS10422385	CAKMXY010000001-CAKMXY010000048
#2826	BRIP_46795_a	GCA_928869825	PRJEB50500	ERS10422474	CAKMYA010000001-CAKMYA010000069
#2836	BRIP_60876_a	GCA_928856705	RJEB50501	ERS10422499	CAKMXT010000001-CAKMXT010000026
#2836*	-	ERZ4998446	PRJEB50495	ERS10422500	ERZ4998446.1-ERZ4998446.260
#2213	UMa698	GCA_928991175	PRJEB50361	ERS10422257	CAKMYD010000001-CAKMYD010000051
#2220	RK_075	GCA_928722275	PRJEB50364	ERS10392838	CAKMXE010000001-CAKMXE010000037

2.6.6 Comparative genome analyses and phylogenetic analyses

The genomes of the sequenced and annotated fungal strains were used for comparative genome analyses. Comparative analyses between fungal genomes were accomplished using a modified version of the comparative genomics program EDGAR designed to handle eukaryotic genomes and their multi-exon genes [148], [149] as described recently [150]. Within the EDGAR workflow, classification of genes as core genes (genes shared in all genomes within a tested set) or singletons was performed based on BLAST Score Ratio Values (SRVs) and visualized in a Venn diagram. In addition, Average Nucleotide Identity (ANI) and Average Amino Acid Identity analyses (AAI) were performed based on the GeneMark prediction similarly to previously described methods [150] to determine the relationship between the different species. Multiple alignments for all core protein sequences were created using MUSCLE [151]. Pairwise Percentage of Conserved Proteins (POCP) analysis was performed according to [152] and as previously described [153]–[155].

For the AAI method, the percent identity values between amino acid sequences of orthologous genes as computed by the BLAST algorithm are analyzed [156]. In comparison, ANI values are computed based on an all-against-all BLAST comparison of 1020-bp pieces of the nucleotide sequences of the selected genomes as described by Goris *et al.* (2007) [157]. An ANI or AAI of 97 % for a pairwise genome comparison is the currently recommended replacement for the 70 % DDH values for species delineation of fungi [158]. The average nucleotide and amino acid identity between two genomes can be used for fungal species delineation, but it is not suitable for genus demarcation. We used the Percentage of Conserved Proteins (POCP) between two strains to estimate their evolutionary and phenotypic distance. A comprehensive genomic survey indicated that the POCP could serve as a robust genomic index for establishing the genus boundary [152], [159].

2.6.7 CO_2 hydrogenation in presence of NaOH and cis-[$RuCl_2(C_{12}$-dppm$)_2$]in apolar solvent/ H_2O

The reagents and solvents were obtained from commercial suppliers. Schlenk-Technique was applied for air sensitive compounds with an inert argon atmosphere (argon 4.8). The chemicals were degassed, and solvents were additionally dried over 3 Å molecular sieves before use for synthesis. For catalytic reactions, the solvents were degassed *via* a glass frit by bubbling with Argon for 30 minutes before use. Reaction gases hydrogen 5.0 and carbon dioxide 4.6 were used without further purification.

High pressure reactions were carried out in stainless steel window autoclaves built and maintained by the mechanical workshop of the Institute for technical and macromolecular chemistry of RWTH Aachen University see **Figure 9.** The autoclaves were equipped with a magnetic stir bar and a digital pressure gauge.

To exclude oxygen from the system, vacuum was applied (< 1 × 10 - 2 mbar) in preparation for the experiments followed by flushing with argon. This procedure was repeated at least three times.

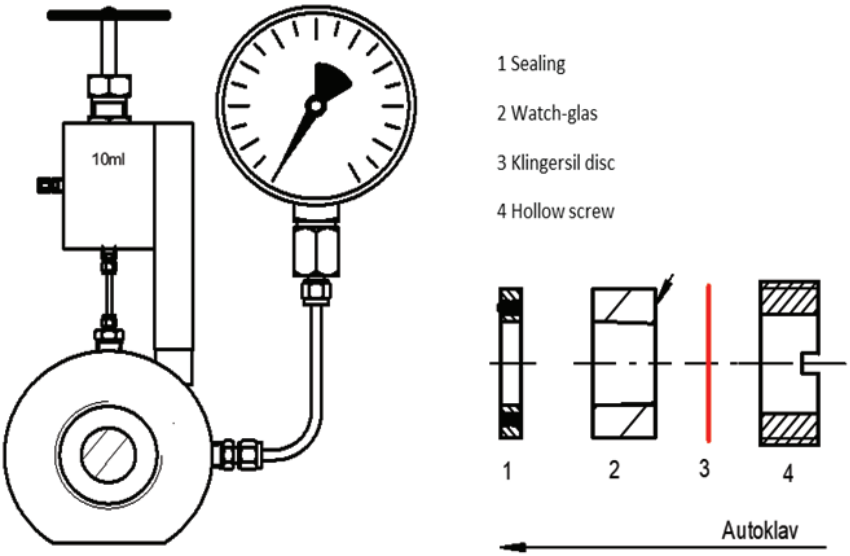

Figure 9: Schematics of the used 10 mL window autoclave.

An aqueous solution of NaOH (1 M, 3 mL) was introduced in argon counterflow. The catalyst cis-[$RuCl_2(C_{12}$-dppm$)_2$] [160] (2.29 mg, 1 µmol) was dissolved in octylacetate, anisole or tetradecane (2 mL), respectively, and added into the autoclave. The autoclave was sealed and pressurized with CO_2 (30 bar) and H_2 (60 bar) at r.t. (total pressure 90 bar). CO_2 pressurization

took about 5 minutes under stirring to saturate the solution verified by closing the valve from time to time and observing whether the pressure remained constant. When the set pressure remained constant, stirring was stopped, the CO_2-pressure was carefully released and H_2 was added rapidly reaching saturation. The autoclave was then heated to 70 °C and the pressure monitored with digital pressure gauges connected to a PC. The pressure increases upon heating, and it was waited till constant value before the reaction was started by switching on the stirring. Completion of the reaction was indicated by constant pressure after the pressure drop (within 0.5 h with anisole, 2 h with octyl acetate and 25 h with tetradecane). The autoclave was then cooled to r.t. and the pressure was released carefully. For catalyst recycling, the aqueous phase was removed carefully in argon counterflow to be analyzed by ^{1}H-NMR as described to determine the formate concentration. To the catalyst phase still residing in the reactor, fresh NaOH-solution was added in argon counterflow. The procedure was then two times repeated as described. The removed aqueous product phases were used in fermentation experiments without any further treatment. The obtained concentration of sodium formate was 0.78 - 0.81 mol L^{-1}, corresponding to 53 - 55 g L^{-1}.

Chapter 3

Results

Chapter 3.1

Ustilaginaceae biocatalyst for co-metabolism of CO_2-derived substrates toward carbon-neutral itaconate production

Partially published as:
Ullmann, L., Phan, A. N. T., Kaplan, D. K. P., Blank, L. M. Ustilaginaceae Biocatalyst for Co-Metabolism of CO_2-Derived Substrates toward Carbon-Neutral Itaconate Production. *J. Fungi* 2021, 7, 98. https://doi.org/10.3390/jof7020098

Contributions:
Lena Ullmann performed all experiments, analyzed the data, prepared figures, and wrote this chapter. Daniel Kaplan performed biodiversity screening experiments. An N. T. Phan performed extracellular metabolite identification via LC-UV/RI-MS/MS and analyzed the results. Lars M. Blank advised on all experiments, analyzed and discussed data, and reviewed the chapter.

We thank Michael Bölker and Ronny Kellner for providing many of the strains used in the screening. The LC-UV/RI-MS/MS use as a courtesy of Shimadzu Corporation.

3 Results

3.1 Ustilaginaceae biocatalyst for co-metabolism of CO_2-derived substrates toward carbon-neutral itaconate production

3.1.1 Summary

The family Ustilaginaceae (belonging to the smut fungi) are known for their plant pathogenicity. Despite the fact that these plant diseases cause agricultural yield reduction, smut fungi attracted special attention in the field of industrial biotechnology. Ustilaginaceae show a versatile product spectrum such as organic acids (e.g., itaconate, malate, succinate), polyols (e.g., erythritol, mannitol), and extracellular glycolipids, which are considered value-added chemicals with potential applications in the pharmaceutical, food, and chemical industries. This study focused on itaconate as a platform chemical for the production of resins, plastics, adhesives, and biofuels. During this work, 72 different Ustilaginaceae strains from 36 species were investigated for their ability to (co-) consume the CO_2-derived substrates acetate and formate, potentially contributing toward a carbon-neutral itaconate production. The fungal growth and product spectrum with special interest in itaconate was characterized. *Ustilago maydis* MB215 and *Ustilago rabenhorstiana* NBRC 8995 were identified as promising candidates for acetate metabolization whereas *Ustilago cynodontis* NBRC 7530 was identified as a potential production host using formate as a co-substrate enhancing the itaconate production. Selected strains with the best itaconate production were characterized in more detail in controlled-batch bioreactor experiments confirming the co-substrate utilization. Thus, a proof-of-principle study was performed resulting in the identification and characterization of three promising Ustilaginaceae biocatalyst candidates for carbon-neutral itaconate production contributing to the biotechnological relevance of Ustilaginaceae.

3.1.2 Introduction

Itaconic acid is an unsaturated dicarboxylic acid that shows a broad application spectrum due to its two functional groups. It is considered a versatile platform chemical since its derivatives, itaconic acid diamide, 2-methyl-1,4-butanediamine, 2-methyl-1,4-butanediol,3-methyl-pyrrolidin, 3-methyl-tetrahydrofuran, or unsaturated esters, show potential applications as styrene-butadiene rubbers, synthetic latexes, superabsorbents, unsaturated polyester resins, plastics, coatings, chemical fibers, biofuels, and detergents [22], [23], [27], [29], [64], [83], [161], [162].

Since the 1950s, industrial biotechnological production of itaconate has been performed by the filamentous fungus *Aspergillus terreus*. This long production and optimization history have enabled titers in a range of 85 – 100 g L^{-1} and yields near the theoretical maximum at low pH,

making *A. terreus*, so far, the best industrial production host for itaconate [19], [39], [52]. On a laboratory scale, final titers of 160 g L^{-1} were recently described for *A. terreus* [39]. However, microbial itaconate production using this fungus remains challenging. It shows a production dependent on a certain morphology which is required for its high productivity leading to an increase of the production costs [34], [163]. Thus, alternative production hosts are searched. Besides *A. terreus*, other microorganisms have been reported as natural itaconate producers such as yeasts belonging to *Candida* species, smut fungi belonging to the family of Ustilaginaceae such as the pH tolerant *U. cynodontis*, and the yeast-like *U. maydis*, which have recently been engineered to higher efficiency [43], [72], [164], [165]. *U. maydis* itself is a well-studied model organism in biotechnology, plant pathogenicity, and cell biology [63], [166]–[168]. Significant improvements on the efficiency of itaconate production in *Ustilago* have been made increasing the yield, titer, and rate of itaconate production in *U. maydis* and related species by metabolic engineering and process development [64], [72], [73]. For itaconate production from glucose, a maximal theoretical yield of 0.72 g itaconate g $glucose^{-1}$, which equals 1 mol itaconate mol $glucose^{-1}$ is reported [63]. Thereby, the latest study focused on an integrated process design that resulted in a maximum itaconate titer of 220 g L^{-1}, with a total acid titer of 248 g L^{-1}, which displayed a significant improvement compared to the best-published itaconate titers reached with *U. maydis* and with *A. terreus* [64].

Nevertheless, progress in biotechnology and microbial itaconic acid production is required to further replace petroleum-based products. In 2011, the market size of itaconic acid was relatively small, with 41,400 tons and a market value of USD 74.5 million [35]. This was caused by the relatively high price of approximately two dollars per kg and the availability of cheaper petro-based alternatives such as acrylic acid. To be competitive against petro-based products and access further markets, costs need to reduce to around USD 0.5 per kg [169]. Assuming a price decrease, itaconic acid could replace acrylic acid in the production of poly(methyl methacrylate), the production of which is petroleum-based with a market worth USD 11 billion [23], [27], [34].

The competition against petro-based products displays a first step toward the vision of a circular economy. Furthermore, utilization of every production side stream to minimize waste and ultimately CO_2 formation is required [15]. To achieve economic production and to compete with fossil fuels, it is necessary to use low-cost feedstocks. Current biotechnological processes for itaconic acid production with *A. terreus* and *U. maydis* are based on carbohydrates, such as molasses, xylose, arabinose, and glucose [19], [170] Furthermore, glycerol from biodiesel is an alternative feedstock for the itaconate production process using *U. vetiveriae* [165], [171]. To improve the sustainability of the itaconate production process, a new approach with potential CO_2-derived C1 and C2 compounds (formate and acetate) as co-substrates is needed to reduce the carbon footprint, potentially toward the overall goal of a carbon-neutral itaconic acid production process.

Formate recently gained interest as a carbon source that can be readily synthesized from CO_2 *via* (electro-)chemical catalysis [172]. In contrast, acetate can be synthesized by acetogens from CO_2 and H_2, in combination with glucose at rates of about 30 mmol gCDW $^{-1}$ h $^{-1}$ [173], [174]. Furthermore, research on energy storage producing chemically stable and valuable products using CO_2 feedstocks was carried out focusing on microbial electrosynthesis (MES). Thereby, acetate was produced at 61% Coulombic efficiency and fully recovered as an acidified stream containing up to 13.5 g L^{-1} (225 mM) acetic acid [175].

The acetate assimilation mechanisms in yeasts were already identified [107]. Acetate can enter the cell through passive diffusion, although several transporters are implicated in the uptake of acetate into the cell [176], [177]. It serves as a substrate for the enzyme acetyl-CoA synthase (ACS), which converts acetate to acetyl-CoA in the cytosol [107]. The acetate assimilation for *U. maydis* has not been well researched yet, but the assimilation in yeasts may give a similar overview since acetyl-CoA synthase (ACS) exists in *U. maydis* as well [110]. According to Kretschmer *et al.* (2018), different acetate uptake mechanisms occur depending on extracellular pH [109]. This study observed that activation of long-chain fatty acids and acetate as a growth-dependent carbon source depends on peroxisomal activation to short acyl-CoAs. This includes acetyl-CoA and its shuttling to the mitochondria *via* carnitine [109]. Furthermore, growth on acetate as a sole carbon source was shown [109]. Demonstrating the connection between acetate and β-oxidation in *U. maydis*, it was observed that certain deletion mutants, e.g., defective in had1 gene, encoding the mitochondrial β-oxidation enzyme hydroxyacyl coenzyme A dehydrogenase, were unable to grow on acetate [109].

A proposed pathway for acetate and formate assimilation in *U. maydis* -incorporating itaconic acid production is shown in **Figure 10.** Thereby, the itaconate biosynthesis pathway in *U. maydis* and the corresponding genes are identified and well-characterized [63], [92]. Pyruvate is generated from glucose through glycolysis taking place in the cytoplasm. It enters the mitochondria, where it is converted to acetyl-CoA and forms citrate together with oxaloacetate in the TCA cycle. Citrate is dehydrated to *cis*-aconitate which is transported from the mitochondria into the cytosol *via* the mitochondrial tricarboxylate transporter Mtt1. In the cytosol, cis-aconitate is converted into itaconate *via* the intermediate *trans*-aconitate. Itaconate can be further converted to 2-hydroxyparaconate by Cyp3. Secretion of itaconate and possibly 2-hydroxyparaconate and itatartarate (ITT) into the medium is mediated by the major facilitator Itp1 [63], [92]. During the conventional itaconate production process using glucose, the theoretical stoichiometry is glucose equals itaconate plus CO_2. In contrast, the theoretical stoichiometry of the acetate co-feeding process is glucose plus four CO_2 equals two molecules of itaconate.

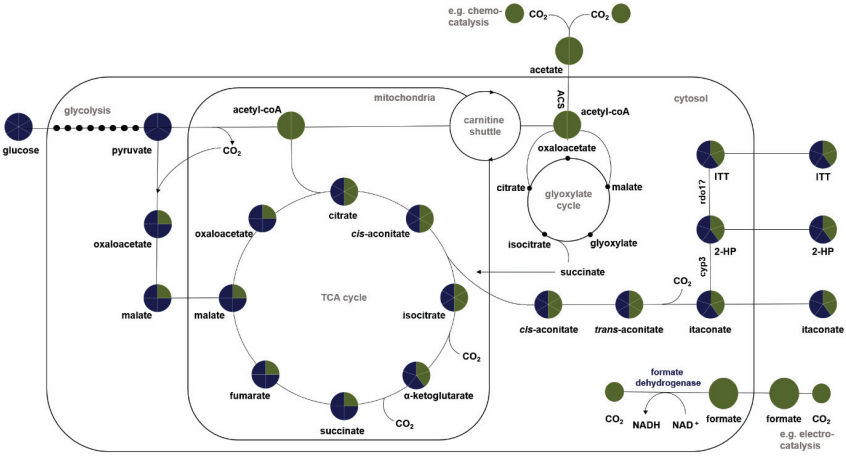

Figure 10: Itaconate biosynthesis pathway in *U. maydis* with a proposed acetate and formate assimilation. Pyruvate is generated from glucose through glycolysis taking place in the cytoplasm. It enters the mitochondria, where it is converted to acetyl-CoA and forms citrate together with oxaloacetate during the TCA cycle. Citrate is dehydrated to *cis*-aconitate which is transported from the mitochondria into the cytosol *via* the mitochondrial tricarboxylate transporter Mtt1. In the cytosol, *cis*-aconitate is converted into itaconate *via* the intermediate *trans*-aconitate. Itaconate can be further converted to 2-hydroxyparaconate (2-HP) by Cyp3. 2-hydroxyparaconate might be converted to itatartarate (ITT) by Rdo1. Secretion of itaconate and possibly 2-hydroxyparaconate and itartarate into the medium is mediated by the major facilitator Itp1. Modified from [63], [92]. Proposed acetate assimilation modified from [107], [109]. Acetate enters the cell *via* passive diffusion and/or *via* putative acetate transporters [109], [176], [177]. It serves as a substrate for the enzyme acetyl-CoA synthase (ACS) [110], which converts acetate to acetyl-CoA in the cytosol [33]. Growth on acetate depends on peroxisomal activation to short acyl-CoAs including acetyl-CoA and its shuttling to the mitochondria *via* carnitine [109]. Proposed formate assimilation *via* formate dehydrogenases is known for methylotrophic microorganisms [128]. These enzymes are also present in *U. maydis* [40]. Indicated circle segments represent the number of carbon atoms per molecule. Blue circles indicate carbon derived from conventional glucose whereas green color indicates carbon possibly derived from CO_2.

Formate degradation *via* formate dehydrogenases (FDHs) is present in all methylotrophic microorganisms, which can perform oxidations of formate to CO_2 as one of the main sources of energy in the form of NADH. NAD+ -dependent FDHs were found in all yeasts of the genera *Candida*, *Pichia*, and *Hansenula* using methanol and were isolated and characterized from different strains [128]. Even though it is not a methylotrophic organism, these enzymes are also present in *U. maydis*. So far, formate degradation *via* formate dehydrogenases (FDHs) is not characterized in such detail for *U. maydis*. Nevertheless, we proposed that the FDH activity in the cytosol is similar to the mechanism in Saccharomyces cerevisiae described by Overkamp *et al.* (2002) [129]. Besides native metabolic routes, synthetic pathways display a valuable tool such as Gonzalez de la Crus *et al.* (2019) previously identified the synthetic reductive glycine pathway as the most efficient route for aerobic growth on formate [178].

The goal of this study was to develop Ustilaginaceae biocatalysts for co-metabolism of CO_2-derived substrates toward carbon-neutral itaconate production. Acetate and formate as carbon sources recently gained interest but their utilization remains challenging [118], [179]. Acetate shows toxicity and inhibitory effects on many microorganisms whereas even co-utilization with glucose challenges the underlying regulatory networks of metabolism favoring glucose

utilization [180]–[182]. Here, to exploit nature's biodiversity, 72 different Ustilaginaceae of 36 species were tested for acetate and formate use. Growth on substrate mixtures and product spectrum with special interest in itaconate was characterized. Thereby, *U. maydis* and *U. rabenhorstiana* were identified as promising candidates for acetate metabolization whereas *U. cynodontis* was identified as a potential production host enhancing its itaconate production by the use of formate as a co-substrate. Selected strains with the highest itaconate production were further characterized in controlled-batch cultivation experiments confirming the trends observed in small scale cultivations. Furthermore, extracellular metabolites were identified enabling future metabolic engineering strategies. Thus, a proof-of-principle study was performed resulting in the identification and characterization of three promising Ustilaginaceae biocatalyst candidates for carbon-neutral itaconate production contributing to the biotechnological relevance of Ustilaginaceae.

3.1.3 Results and discussion

3.1.3.1 Biodiversity screening for growth on acetate and formate in combination with glucose

For the identification of promising biocatalysts contributing to a CO_2-neutral synthesis of itaconic acid, 72 different Ustilaginaceae strains of 36 species in total were cultivated and screened for growth on acetate and formate as potential co-substrates derived from CO_2. Strains were cultivated on different concentrations of both co-substrates (2.5, 5.0, and 10.0 g L^{-1}) in combination with 20.0 g L^{-1} glucose. Promising candidates were considered as those growing under a desirably high concentration of either of these co-substrates while achieving a higher maximal biomass concentration compared to their growth on glucose only (**Figure 11**).

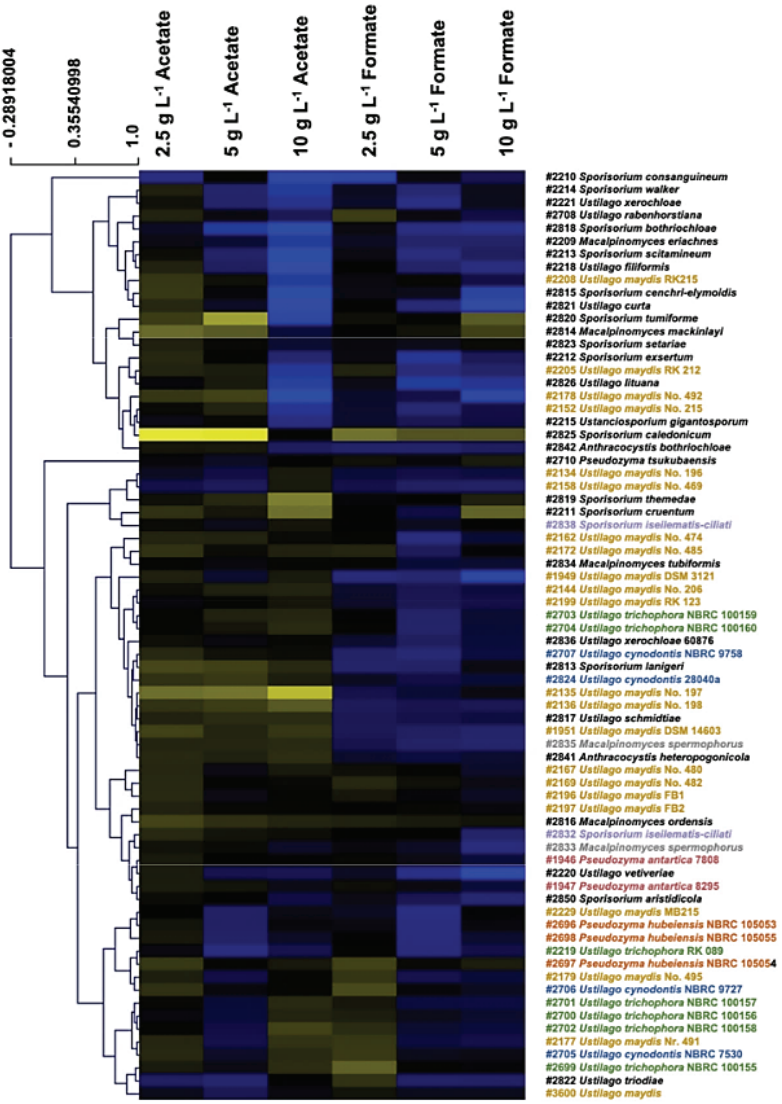

Figure 11: Overview of biodiversity screening results.
Hierarchical cluster analysis (HCA) heatmap showing whole set growth screening results obtained during 24-deep-well plate cultivation in MTM medium with 4 g L^{-1} NH_4Cl using the Growth Profiler system by EnzyScreen. Strains were cultivated for growth on both co-substrates under various conditions of 2.5, 5.0, and 10.0 g L^{-1} in combination with 20.0 g L^{-1} glucose. Maximum optical density (OD600) was normalized to the growth of the respective glucose reference and visualized *via* color scales in the HCA heatmap indicating relative growth [%] Blue color indicates a lower growth, black a comparable growth behavior, and yellow a higher growth compared to the respective glucose reference. Strains belonging to one species were colored accordingly in the displayed rows. Experiments were performed with two biological duplicates. Raw data are provided in appendix section **Table 21** and **Table 22**. Data associated to this figure were taken from Daniel Kaplan's Bachelor Thesis [183].

Via HCA, distinct co-substrate effects on the different Ustilaginaceae strains were revealed. Higher co-substrate concentrations entailed a decrease of the maximum OD_{600} and the growth rates for most of the tested strains (appendix, **Table 21** and **Table 22**), whereas formate, in general, showed a stronger inhibitory effect on microbial growth compared to acetate. While the addition of 2.5 g L^{-1} acetate led to reduced biomass concentrations in one-third of the tested Ustilaginaceae, the addition of the same concentration of formate reduced the maximal OD_{600} in 75% of the strains. The highest co-substrate concentration of 10 g L^{-1} led to a decrease of 69% of all strains with acetate and 97% using formate as a co-substrate. These results confirm previous studies where acetate showed toxicity and inhibitory effects on many microorganisms [180], [182] [134], [184]. One factor impacting cell growth of the tested Ustilaginaceae might be the pH shift during cultivation starting from pH 6.5 shifting up to a maximum pH of 8.6 when acetate or formate are metabolized. pH values were determined at the end of the cultivation experiments, and raw values are provided in the Supplementary Materials section (appendix, **Table 23**). Calculating the average pH values of all 72 strains for each tested condition resulted in 5.7 ± 0.2 (glucose reference), 6.3 ± 0.3 (2.5 g L^{-1} acetate), 7.0 ± 0.4 (5 g L^{-1} acetate), 8.3 ± 0.7 (10 g L^{-1} acetate), 6.5 ± 0.2 (2.5 g L^{-1} formate), 7.4 ± 0.7 (5 g L^{-1} formate), and 7.9 ± 0.8 (10 g L^{-1} formate). Usually, microorganisms prefer a limited and specific pH range. Furthermore, smut fungi are known to grow filamentous under non-optimal growth conditions [72].

Nevertheless, acetate and formate are known to have the following effects on microorganisms. According to Kretschmer *et al.* (2018), acetate provokes mitochondrial stress in *U. maydis*. Higher concentrations of acetate not only cause acidification of the cytosol, leading to impaired enzyme activity, initiation of programmed cell death, and increased levels of reactive oxygen species (ROS), but also reduce the expression of ROS detoxification mechanisms, boosting oxidative stress further [109].The insights of Lastauskiene *et al.* (2014) are comparable in terms of the effects of formate on Candida species. Formate inhibits the cytochrome-coxidase, which is responsible for maintaining a proton gradient by oxidizing cytochrome-c and by reducing oxygen to water. Protons resulting from the formate catalyzation are transferred into the mitochondrial intermembrane space ensuring ATP synthesis through ATP-synthase [185]. The described issues could be tackled with specific feeding strategies such as fed-batch or with a pH-control during bioreactor fermentations. Thus, the decreasing trend in the maximum optical density (OD_{600}) and growth rate could be explained by the previously described inhibiting effects of acetate and formate, especially with higher co-substrate concentrations.

Further observations during HCA analysis could be made concerning the biodiversity among the tested smut fungi of 36 different species in total. Twenty-two *U. maydis* strains were tested for growth on acetate and formate whereas no clear trend was observed for all strains as they are distributed all over the clusters (**Figure 11**). This finding is encouraged by a previous study from Geiser *et al.* (2014) that showed a high variation in the itaconate production of 52 different

U. maydis strains [43]. In contrast, certain strains showed a similar trend, and therefore they were clustered close to each other on the HCA plot. *U. maydis* #1951, #2135, and #2136 showed a higher growth on acetate but, in contrast, did not grow well on formate compared to their respective glucose reference. Four other *U. maydis* strains, #2167, #2169, #2196, and #2197, were grouped close together. Those strains showed better performance on formate compared to the previously discussed group. In addition, seven different *U. trichophora* strains were tested during this study which showed a less broad distribution compared to the *U. maydis* strains. Except for the two strains *U. trichophora* #2703 and #2704, the remaining five strains were clustered relatively close to each other on the plot. Furthermore, the tested *U. cynodontis* strains #2705 and #2706 were clustered relatively close to each other indicating a similar co-substrate utilization pattern. Both strains were later picked as candidates for best formate utilization (**Figure 13**). In total, three different *Pseudozyma hubeiensis* strains #2696, #2696, and #2698 were tested, showing a close clustering in the plot. Nevertheless, due to the broad biodiversity and different tested co-substrate conditions, the interpretation of clearly differentiated clusters and their trends 7.6 g L^{-1} itaconate was obtained. The increased carbon source concentrations resulted in up to 2-fold higher product yields. Thereby, the maximum obtained yield among the strains was 0.07 ± 0.0 $Y_{P/S}$ [g_{ITA} $g_{C\text{-}source}^{-1}$] corresponding to the low carbon source concentration vs. 0.15 ± 0.0 in the presence of the higher carbon source concentration. Nevertheless, the same trends were observed regarding the co-substrate utilization and itaconate production, i.e., strains that perform well at low carbon source concentrations also perform well at high carbon source concentrations. Thus, testing for best itaconate producers was continued with the high carbon source concentration.

An overview of the itaconic acid production screening results of the most promising Ustilaginaceae strains is displayed in **Figure 12** and **Figure 13**. The utilization of acetate and formate will be discussed separately. Detailed production parameters are listed in appendix **Table 24** - **Table 30.**

3.1.3.2 Itaconate production using acetate

An overview of the itaconic acid production screening results of the most promising Ustilaginaceae strains for acetate co-metabolization is displayed in **Figure 12**. Compared to biodiversity screening results, itaconic acid production experiments resulted in a different outcome. *U. maydis* #1946, which obtained the highest growth using acetate as a co-substrate, did not produce a significant amount of itaconate. Furthermore, 0.1 ± 0.0 g L^{-1} itaconate was produced using 50 g L^{-1} glucose, while cultivation with acetate resulted in a decrease toward 0.01 ± 0.0 g L^{-1}. In contrast, max. OD_{600} increased from 60 ± 5 to 69 ± 7. Thus, this strain might use the co-substrate for biomass formation rather than for itaconate production.

The two strains *U. maydis* #2229 and *U. rabenhorstiana* #2708 performed best in System Duetz cultivation, reaching itaconate titers of 7.4 ± 0.3 g L^{-1} and 6.8 ± 0.1 g L^{1}, respectively, which corresponds to a 2.2-fold and 1.6-fold increase of the production. *U. maydis* #2229

showed a 2.3-fold increase based on $Y_{P/S}$ [g_{ITA} $g_{C\text{-}source}^{-1}$] and a 2.1-fold increase based on $Y_{P/S}$ [C-mol$_{ITA}$ C-mol$_{C\text{-}source}^{-1}$]. Total itaconate production of *U. cynodontis* #2707, *U. maydis* #2135, and *U maydis* #2136 was observed in a range between 2 and 3 g L^{-1} itaconate in the presence of acetate: 2.9 ± 0.0 g L^{-1}, 3.3 ± 0.4 g L^{-1}, and 2.3 ± 0.1 g L^{-1}. The itaconate titer reached by *U. maydis* #2136 decreased compared to the cultivation on glucose only (2.8 ± 0.6 g L^{-1}). Nevertheless, two promising strains were identified which reached higher product titers using acetate as a co-substrate - *U. maydis* #2229 and *U. rabenhorstiana* #2708 - which were further characterized during controlled-batch fermentations.

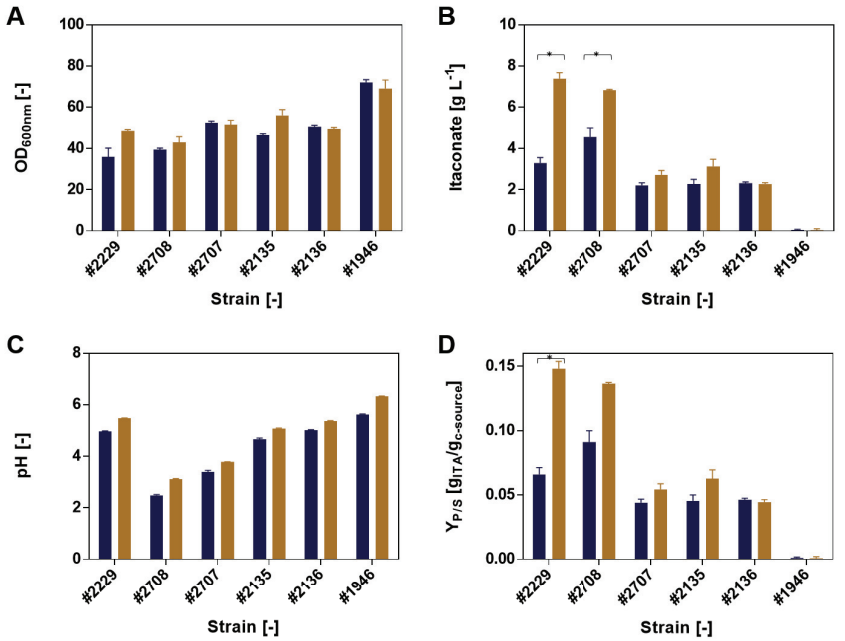

Figure 12: Itaconic acid production of selected Ustilaginaceae strains.
(A) Maximum optical density (OD_{600} [-]), (B) maximum itaconic acid production [g L^{-1}], (C) minimum pH [-], (D) $Y_{P/S}$ [g_{ITA} $g_{C\text{-}source}^{-1}$] during System Duetz® 24-deep-well plate cultivation experiments with 1.5 mL MTM medium and 0.8 g L^{-1} NH_4Cl. Ustilaginaceae candidates using acetate as a co-substrate are shown in orange (6.25 g L^{-1}). Respective glucose references (50 g L^{-1}) are shown in blue. Error bars indicate the deviation from the mean for n = 2. Statistically significant differences in itaconic acid production ($p \leq 0.05$) are indicated as *.

3.1.3.3 Itaconate production using formate

Comparing formate conditions of the biodiversity screening and itaconate production results, differences can be drawn among the tested strains (**Figure 13**). Except for *U. cynodontis* #2705, the tested strains reached lower itaconate titers when formate was present during cultivation. Formate was not only not used for itaconate production, but it interfered with the production. The reference strain *U. maydis* #2229 exhibited a reduced itaconate titer of 0.3 ±

0.0 g L^{-1} (7.4-fold decrease). *U. maydis* #2177 and #2196 did show a drastic decrease in itaconate production as well. A shifting pH effect toward alkaline values during formate cultivations was observed, probably contributing to reduced itaconate titers (**Table 30,** appendix).

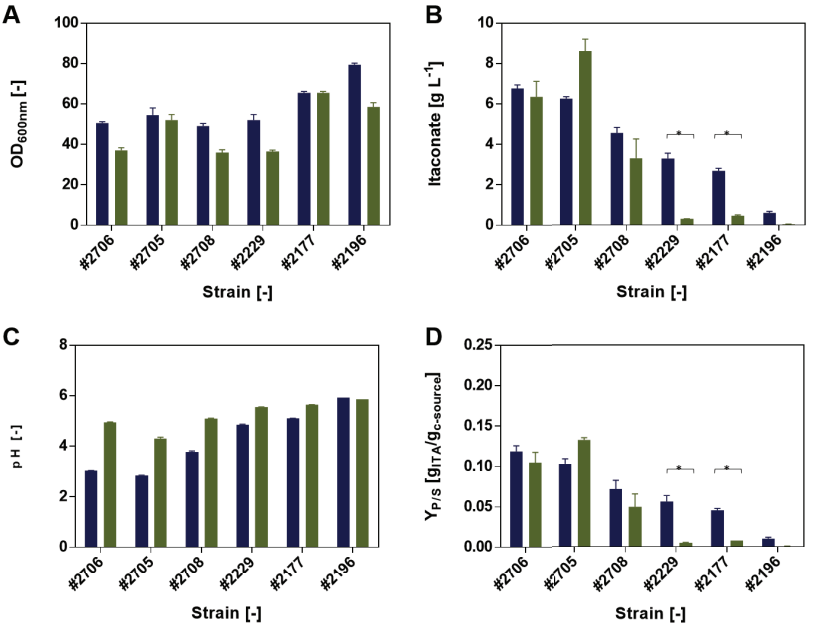

Figure 13: Itaconic acid production of selected Ustilaginaceae strains.
(A) Maximum optical density (OD_{600} [-]), (B) maximum itaconic acid production [g L^{-1}], (C) minimum pH [-], (D) $Y_{P/S}$ [g_{ITA} $g_{C\text{-}source}^{-1}$] during System Duetz® 24-deep-well plate cultivation experiments with 1.5 mL MTM medium and 0.8 g L^{-1} NH_4Cl. Ustilaginaceae candidates using formate as a co-substrate are shown in green (6.25 g L^{-1}). Respective glucose references (50 g L^{-1}) are shown in blue. Error bars indicate the deviation from the mean for n = 2. Statistically significant differences in itaconic acid production ($p \leq 0.05$) are indicated as *.

During the performed screening for the best itaconate producers using acetate or formate as co-substrates, the following strains were considered as promising candidates and were used for subsequent experiments: *U. maydis* #2229 and *U. rabenhorstiana* #2708 for acetate co-metabolism and *U. cynodontis* #2705 for formate co-metabolism.

3.1.3.4 Controlled-batch fermentation of the best itaconate producers

To further investigate and confirm itaconic acid production of the three most promising Ustilaginaceae candidates, *U. maydis* #2229, *U. rabenhorstiana* #2708, and *U. cynodontis* #2705 were cultivated in controlled-batch fermentation (**Figure 14** and **Table 8**). Thereby, cultivation conditions remained similar to small-scale production experiments.

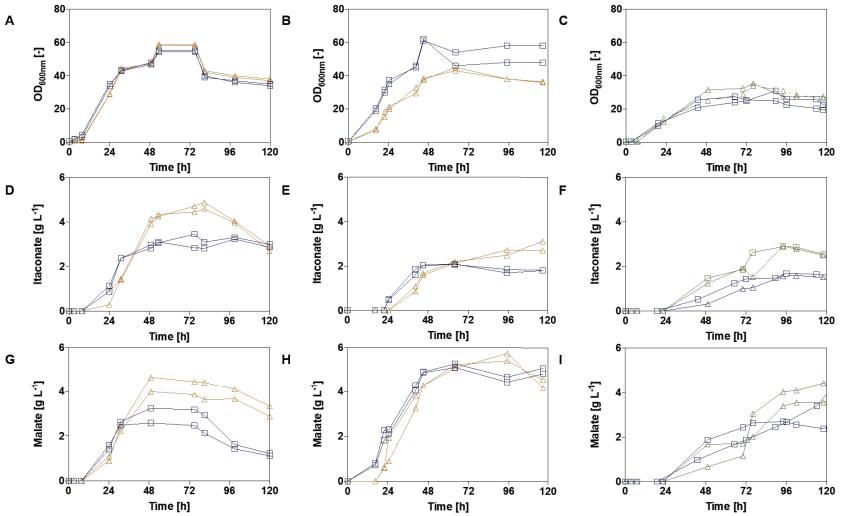

Figure 14: Controlled-batch fermentations of selected Ustilaginaceae candidates.
OD_{600} of (A) *U. maydis* #2229, (B) *U. rabenhorstiana* #2708, and (C) *U. cynodontis* #2705. Itaconate production is shown for (D) *U. maydis* #2229, (E) *U. rabenhorstiana* #2708, and (F) *U. cynodontis* #2705. Malate production is visualized for (G) *U. maydis* #2229, (H) *U. rabenhorstiana* #2708 and (I) *U. cynodontis* #2705 during fermentation in a bioreactor containing MTM medium (0.8 g L^{-1} NH_4Cl, 30 °C, 80% DOT, at pH 6.5). Ustilaginaceae candidates using acetate as a co-substrate are shown in orange, and formate co-substrate cultivations are shown in green (6.25 g L^{-1}). Respective glucose references (50 g L^{-1}) are shown in blue.

By comparing the controlled-batch cultivation differences in growth, phases of the tested organisms appear. Substrate consumptions are displayed in **Figure 15**.

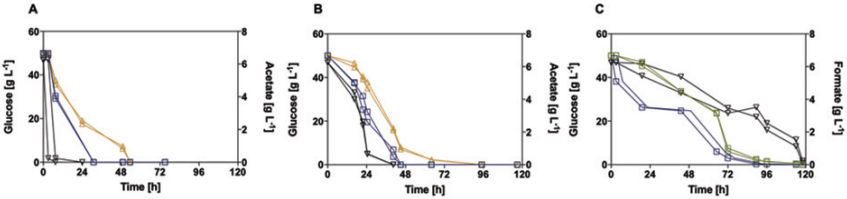

Figure 15: C-source consumption during controlled batch fermentations of promising Ustilaginaceae candidates.
U. maydis #2229 (A), *U. rabenhorstiana* #2708 (B) and *U. cynodontis* #2705 (C) fermentation in a bioreactor containing MTM medium (0.8 g L^{-1} NH_4Cl, 19.5 g L^{-1} MES, 30°C, 80% DOT, at pH 6.5). Glucose consumptions using acetate as a co-substrate are shown in orange, formate co-substrate cultivations are shown in green. Respective glucose references (50 g L^{-1}) are shown in blue. Black indicates co-substrate consumption (6.25 g L^{-1}).

In general, additional acetate and formate were consumed simultaneously with glucose, and no diauxic growth or metabolic adaption was observed. Nevertheless, the glucose consumption was prolonged with the addition of a co-substrate. *U. maydis* #2229 consumed glucose within 31 h compared to 53 h in the presence of acetate. *U. rabenhorstiana* #2708 depleted glucose within 48 h compared to doubling consumption times of 95 h under co-substrate conditions. *U. cynodontis* #2705 showed a longer growth phase in comparison to the

acetate cultivations of 92 h compared to 100 h using formate as a co-substrate. In contrast, 6.25 g L^{-1} acetate was consumed within 24 h by *U. maydis* and 40 h by *U. rabenhorstiana*. Formate depletion was observed after 118 h for *U. cynodontis*.

During bioreactor experiments, the strains produced metabolites such as itaconate, malate, erythritol, and succinate under nitrogen limitation. Total itaconic acid concentrations are displayed in **Table 8** and were observed as the following: 4.7 ± 0.2 g L^{-1} for *U. maydis* #2229 using acetate compared to 3.3 ± 0.1 g L^{-1} for its glucose reference, 2.9 ± 0.1 g L^{-1}, vs. 2.1 ± 0.0 g L^{-1} for *U. rabenhorstiana* #2708, and 2.9 ± 0.0 g L^{-1} vs. 1.7 ± 0.1 g L^{-1} for *U. cynodontis* #2705.

Table 8: Production parameters of controlled-batch fermentations of *U. maydis* #2229, *U. rabenhorstiana* #2708, and *U. cynodontis* #2705.
Fermentation experiments were performed in a bioreactor containing MTM medium with 50 g L^{-1} glucose, 0.8 g L^{-1} NH_4Cl, at 30 °C, 80% DOT, and pH 6.5. Co-substrates (acetate, formate) were added with 6.25 g L^{-1}. Statistically significant differences in itaconic acid production ($p \leq 0.05$) are indicated as *.

Strain	C-source	$Titer_{max}$ [g L^{-1}]	$Y_{P/S}$ [$g_{ITA}/g_{C\text{-}source}$]	$Y_{P/S}$ [C-mol_{ITA}/C-$mol_{C\text{-}source}$]
U. maydis #2229	Glucose	3.2	0.07	0.08
		3.3	0.07	0.08
	Glucose + Acetate	4.9	0.09	0.10
		4.6	0.08	0.10
U. rabenhorstiana #2708	Glucose	2.1	0.04	0.05
		2.1	0.04	0.05
	Glucose + Acetate	2.7	0.05	0.06
		3.1	0.06	0.07
U. cynodontis #2705*	Glucose	1.7	0.03	0.04
		1.6	0.03	0.04
	Glucose + Formate	2.9	0.05	0.06
		2.9	0.05	0.06

Obtained itaconate concentrations were lower compared to production screening experiments in small-scale 24-deep-well plates which might be explained by process changes due to the upscaling procedure and/or non-optimized process parameters. Compared to the small-scale screening experiments, higher biomass formation was observed during controlled batch fermentation for *U. maydis* #2229 and *U. rabenhorstiana* #2708. *U. maydis* #2229 obtained an OD_{600} of 49 ± 1 in a small scale compared to 59 ± 1 during batch cultivation experiments in addition to acetate. Therefore, decreased itaconate titers could be explained by a higher biomass formation due to, e.g., pH control and better oxygen supply. Three different strains were tested during batch cultivations, and their optimum as far as pH, air supply, buffer system, and carbon source ratio might be different among the strains.

As far as *U. rabenhorstiana* #2708 is concerned, itaconate production was lower compared to published data [66]The highest itaconate titer of 31.7 g L^{-1} glucose at pH 6.0, corresponding to a yield of 0.34 (w/w) [66]. Comparing the process parameter, oxygen supply is a critical factor. During this study, DOT was kept constant at 80% (aeration cascade 800 - 1200 rpm, 2 vvm). In contrast, Krull *et al.* (2020) observed that the best results were achieved for itaconic acid

production with *U. rabenhorstiana* at the lowest aeration rate of 0.1 vvm and a constant stirring rate of 500 rpm regarding titer, productivity, and yield [66]. Furthermore, they observed that the increase in aeration and stirring rate was related to the formation of 36% more biomass at higher aeration rates because of a better supply of oxygen. Furthermore, several pH values were tested during a study performed by Krull *et al.* (2020) Increasing the pH to 6.5 leads to a decrease in itaconate production [66]. Thus, bioprocess development should be proceeded to enhance itaconate production of the respective Ustilaginaceae candidates during subsequent experiments.

The batch fermentations of *U. maydis* #2229 confirmed the product range found in the screening approaches for glucose, although published itaconate concentrations produced under similar conditions could not be reached [62]. Therefore, additional bioreactor experiments were performed with *U. maydis* #2229, increasing the glucose concentration to 200 g L^{-1} and 25 g L^{-1} acetate accordingly (**Figure 16**).

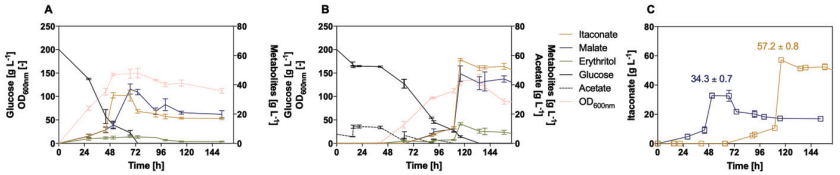

Figure 16: Controlled-batch fermentations of *U. maydis* MB215 increasing glucose concentration to 200 g L^{-1}.
(A) Bioreactor experiments using 200 g L^{-1} glucose, (B) with 200 g L^{-1} glucose and 25 g L^{-1} acetate. Cultivations were performed in MTM medium (0.8 g L^{-1} NH_4Cl, 30 °C, 80% DOT, at pH 6.5). (C) Overview of itaconate production of both experiments. Cultivations using acetate as a co-substrate are shown in orange ($Y_{P/S}$ = 0.25 ± 0.00 [$g_{ITA}/g_{C\text{-}source}$]), and respective glucose references are shown in blue ($Y_{P/S}$ = 0.17 ± 0.00 [$g_{ITA}/g_{C\text{-}source}$]). Error bars indicate the standard error of the mean (n = 3).

Those cultivations led to an itaconate titer of 57.2 ± 0.8 g L^{-1} in the presence of the co-substrate compared to 34.3 ± 0.7 g L^{-1} itaconate of the glucose reference. The yield was improved to 0.25 ± 0.00 [$Y_{P/S} = g_{ITA}\ g_{C\text{-}source}^{-1}$]. Maassen *et al.* (2014) obtained a similar itaconate titer of 32.6 ± 0.8 g L^{-1} using 200 g L^{-1} glucose [62]. The *U. cynodontis* #2705 wildtype can only be compared to previous studies with *U. cynodontis* #2706 reaching titers around 5 g L^{-1} itaconate using 50 g L^{-1} glucose [72].

3.1.3.5 Extracellular metabolite identification *via* LC-UV/RI-MS/MS

A recent study from Becker *et al.* (2020) showed that *U. maydis* chassis strain development leads to an increased itaconate titer due to a reduced by-product spectrum [73]. Ustilaginaceae are known to show a versatile product spectrum including organic acids (e.g., itaconate, malate, succinate), polyols (e.g., erythritol, mannitol), and extracellular glycolipids [43], [164], [186]–[188]. Thus, metabolic engineering and by-product reduction display a promising strategy for chassis strain development. To identify interesting targets for metabolic

engineering, extracellular metabolites of the three selected strains were analyzed during this study. Extracellular metabolites were identified *via* LC-UV/RI-MS/MS while MS/MS mass spectrums of samples were compared directly to authentic standards and are displayed in **Figure 17** and **Figure 18**.

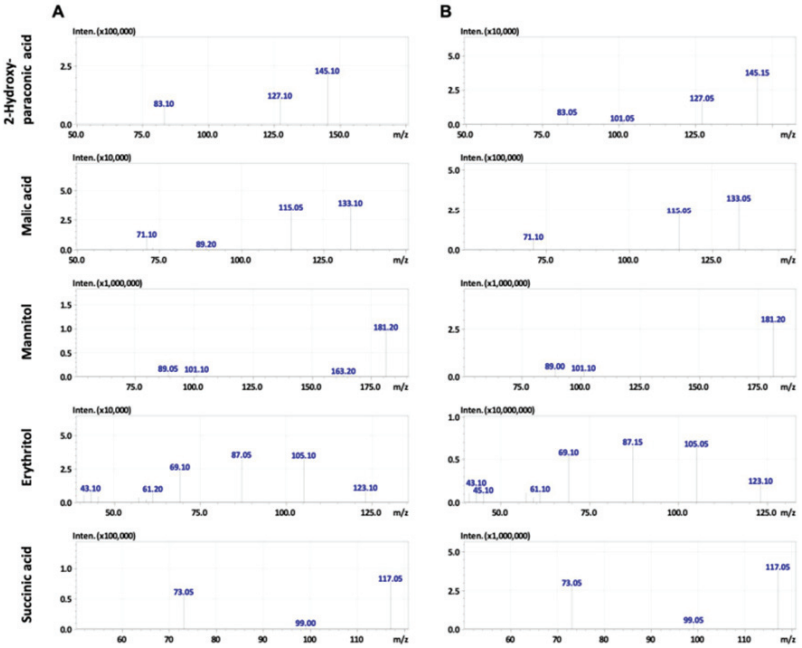

Figure 17: Extracellular metabolite identification *via* LC-UV/RI-MS/MS.
(A) Product ion scan for extracellular metabolite samples and (B) their corresponding standards. Extracellular metabolites in the supernatant formed by *U. maydis* #2229, *U. rabenhorstiana* #2708, and *U. cynodontis* #2705. Samples were taken after 75, 64, and 114 h during fermentation in a bioreactor containing MTM medium (0.8 g L^{-1} NH_4Cl, 19.5 g L^{-1} MES, 30°C, 80% DOT, at pH 6.5).

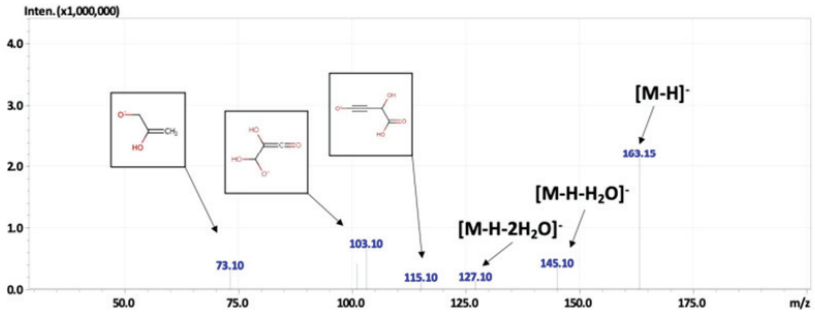

Figure 18: MS/MS spectrum of ITT.
Structure prediction of itatartarate (ITT) was performed *via* CFM-ID 3.0 [133].

Identification of metabolites such as malate, itatartarate, 2-hydroxyparaconic acid, mannitol, erythritol, succinate, and itaconic acid was carried out and implemented in the established HPLC method. **Figure 19** displays an HPLC chromatogram overlay incorporating the identified metabolites obtained during controlled batch fermentations. Thereby, the diversity in extracellular metabolites between the different tested strains *U. maydis* #2229, *U. rabenhorstiana* #2708, and *U. cynodontis* #2705 was observed. Representative time points were chosen for each strain and condition where the highest number of peaks was detected. Thus, analyzed samples were taken after 75, 64, and 114 h during the fermentation of *U. maydis* #2229, *U. rabenhorstiana* #2708, and *U. cynodontis* #2705, respectively.

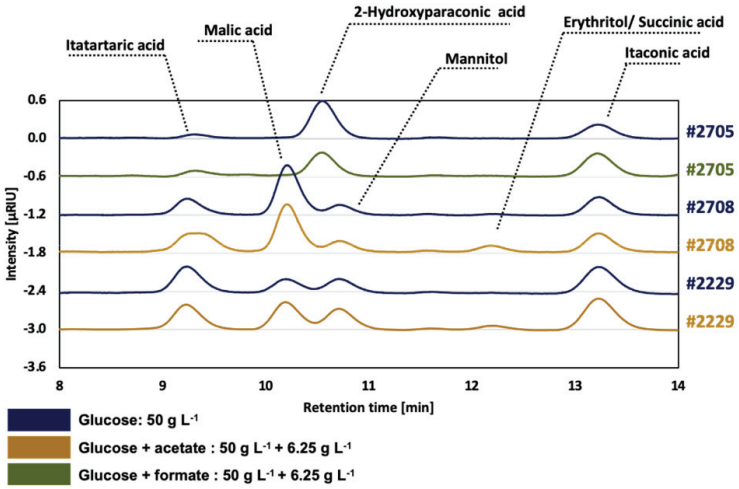

Figure 19: HPLC chromatogram overlay (RI detector).
Extracellular metabolites in the supernatant formed by selected Ustilaginaceae candidates. Samples were taken after 75, 64, and 114 h of *U. maydis* #2229, *U. rabenhorstiana* #2708, and *U. cynodontis* #2705, respectively, during fermentation in a bioreactor containing MTM medium (0.8 g L^{-1} NH_4Cl, 30 °C, 80% DOT, at pH 6.5). Ustilaginaceae using acetate as a co-substrate are shown in orange; formate co-substrate cultivations are shown in green (6.25 g L^{-1}). Respective glucose references (50 g L^{-1}) are shown in blue.

Thereby, differences between the tested strains and each condition were observed. Besides itaconic acid, the major extracellular metabolite produced by *U. cynodontis* #2705 was 2-hydroxyparaconic acid. In contrast, *U. maydis* and *U. rabenhorstiana* showed quite different extracellular metabolic profiles as significant mannitol as well as malic acid production was observed (**Figure 20**). When acetate was added to the medium, these strains exhibited higher erythritol production comparing to the control condition without acetate. Itatartarate and itaconate were identified in all of the displayed samples.

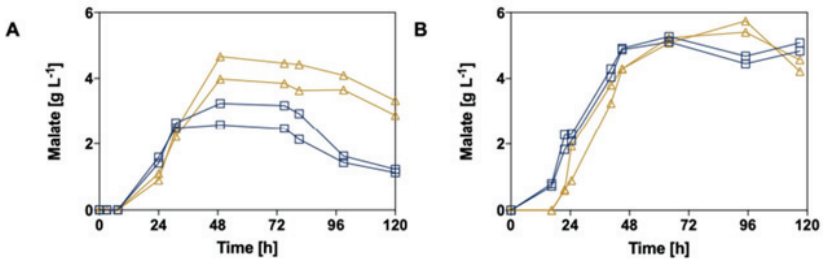

Figure 20: Malate production during controlled batch fermentations of selected Ustilaginaceae.
(A) *U. maydis* #2229 and (B) *U. rabenhorstiana* #2708 fermentation in a bioreactor containing MTM medium (0.8 g L^{-1} NH_4Cl, 30°C, 80% DOT, at pH 6.5). Malate production using acetate as a co-substrate are shown in orange. Respective glucose references (50 g L^{-1}) are shown in blue.

Based on the shown extracellular metabolites results as well as recent studies, several options for metabolic engineering can be employed to alter the metabolic flux distribution to maximize product synthesis. Potential targets are, e.g., overexpression of the mitochondrial transporter Mtt1 [73], the overexpression of the cluster-associated regulator Ria1, disrupting the itaconate oxidase encoding gene *cyp3*, reducing by-product spectrum of extracellular glycolipids as well as heterologous expression of the mitochondrial transporter MttA from *A. terreus* [64], [73]. Furthermore, deletion of *fuz7* enables a stable yeast-like growth [72]. Moreover, a metabolomics method focusing on the central carbon metabolism has recently been developed for *U. maydis*, which can be applied to investigate the cellular metabolic network and support metabolic engineering strategy [189].

3.1.3.6 Design of Experiments approach: investigating the optimum conditions for an acetate co-feeding strategy in promising Ustilaginaceae candidates

Within this work, *U. maydis* MB215 (#2229) and *U. rabenhorstiana* NBRC 8995 (#2708) were identified as promising candidates for acetate co-metabolization. In order to investigate those strains, the respective optimum of glucose to co-substrate ratio was determined using the Design of Experiment (DoE) approach enabling the development of a suitable co-feeding strategy. The response surface methodology was chosen for the investigation, as it is suitable for modeling and analyzing a process statistically where the response is influenced by several variables while the objective is the optimization of the response. As the itaconic acid production from glucose and acetate is the aim of this work, glucose and acetate concentrations were set as two numerical factors for the design (**Table 9**). The respective buffer system (19.5 g L^{-1} MES or 33 g L^{-1} $CaCO_3$) was set as a categorical factor. Thereby, 18 different conditions were tested in total 48 experimental runs.

Table 9: Factor levels for CCD modelling acetate co-metabolization of Ustilaginaceae wild-type strains during this study.
The respective buffer system (19.5 g L^{-1} MES or 33 g L^{-1} $CaCO_3$) was set as a categorical factor. Thereby, 18 different conditions were tested in in total 48 experimental runs.

Factor	-1	0	+1
Glucose [g L^{-1}]	30	65	100
Sodium acetate [g L^{-1}]	2	7	12
Buffer	19.5 g L^{-1} MES		33 g L^{-1} $CaCO_3$

Model design for U. maydis MB215

For each tested condition, the highest itaconate titer and yield were compared for the two buffer systems (**Figure 21**). Considering each condition individually, the cultivation in $CaCO_3$ buffer showed higher values for yield and titer compared to MES buffer. The titer increased for both buffer systems with increasing glucose concentration and for increasing acetate concentration when considering the equally high glucose concentrations. The maximum titer was reached for both MES with 7.8 ± 0.3 g L^{-1} and $CaCO_3$ buffer with 12.9 ± 0.5 g L^{-1} for the condition with the highest total amount of carbon with 100 g L^{-1} glucose and 12 g L^{-1} acetate. Regarding the cultivation with $CaCO_3$ as a buffer, the yield shows similar results. Also, the highest yield was reached for 100 g L^{-1} glucose and 12 g L^{-1} acetate with 0.14 ± 0.00 c-mol_{ITA} c-$mol_{C\text{-}source}^{-1}$. For MES buffer the maximum yield of 0.09 ± 0.00 c-mol_{ITA} c-$mol_{C\text{-}source}^{-1}$ was reached for the condition 65 g L^{-1} glucose and 12 g L^{-1} acetate.

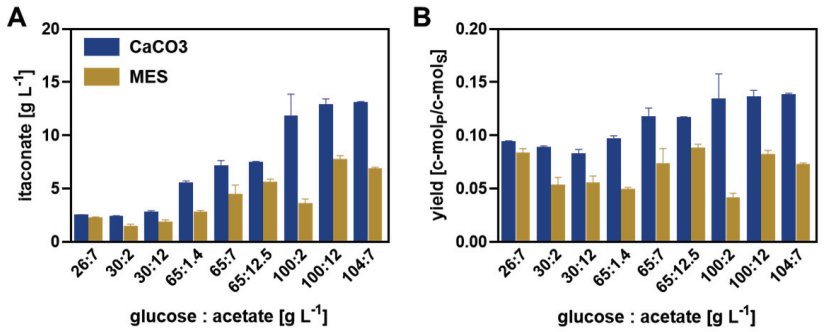

Figure 21: Itaconate production during DoE cultivation experiments of *U. maydis* MB215.
Maximum itaconate titer (a) and yield (b) are compared for each model condition containing defined combinations of glucose and acetate and for both buffer systems MES buffer (orange) and $CaCO_3$ buffer (blue). System Duetz® 24-deep-well plate cultivations were performed with MTM medium containing 0.8 g L^{-1} NH_4Cl (1.5 mL culture volume, 300 rpm, 30 °C). Error bars indicate the deviation from the mean for n ≥ 3. Data associated to this figure were taken from Karla Stein's MasterThesis [190].

U. maydis MB215 (#2229) was able to consume acetate as a cosubstrate in each tested model condition and also showed production of itaconate. Interestingly, the itaconate production was higher for every model condition when cultivated with $CaCO_3$ as a buffer, compared to cultivation with MES buffer. When comparing the pH course during cultivation, the pH was observed to stay more stable for $CaCO_3$ buffer remaining in the neutral range compared to MES buffer shifting to acidic conditions.

The highest values regarding itaconate c-mol yield and titer shown before (**Figure 21**) were used as response values to generate Response surface models using the software Design Expert®. Regarding the model for the titer a quadratic model was chosen based on the software suggestions for deeper analysis. ANOVA was performed to evaluate the model and showed mainly significant model terms and non-significant lack of fit, leading in total to a significant model with a coefficient of determination of $R^2 = 0.98$ for titer model and $R^2 = 0.92$ for yield model (appendix, **Figure 70** and **Figure 71**).

After fitting the model to the data 3D surface graphs modelling itaconate titer (**Figure 22**) and yield (**Figure 23**) by the software, which cover the entire model range by predicting responses for every possible combination of both cosubstrates inside their respective design space.

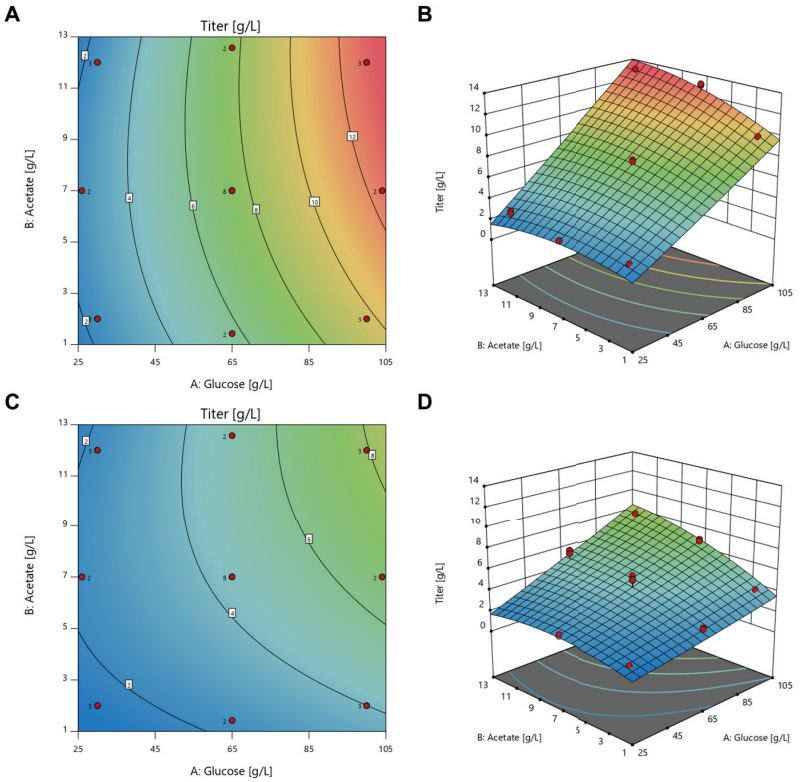

Figure 22: 3D surface models and heatmap diagrams for itaconate titer in *U. maydis* MB215.
Models were generated with Design Expert® software showing the predicted titer response for different concentrations of glucose and acetate as cosubstrates. Two models were generated, one for $CaCO_3$ as a buffer (A - B) and one for MES buffer (C - D). Colored spheres in the graphs represent the measured model conditions. Red spheres indicate model values above the prediction, while light pink spheres refer to model values below the predicted values. Color of the diagrams indicate predicted itaconate titer (1.28146 13.4507 g L^{-1} itaconate). Data associated to this figure were taken from Karla Stein's MasterThesis [190].

The model also predicts that cultivation with $CaCO_3$ buffer lead over the whole model area to higher titers compared to MES buffer.

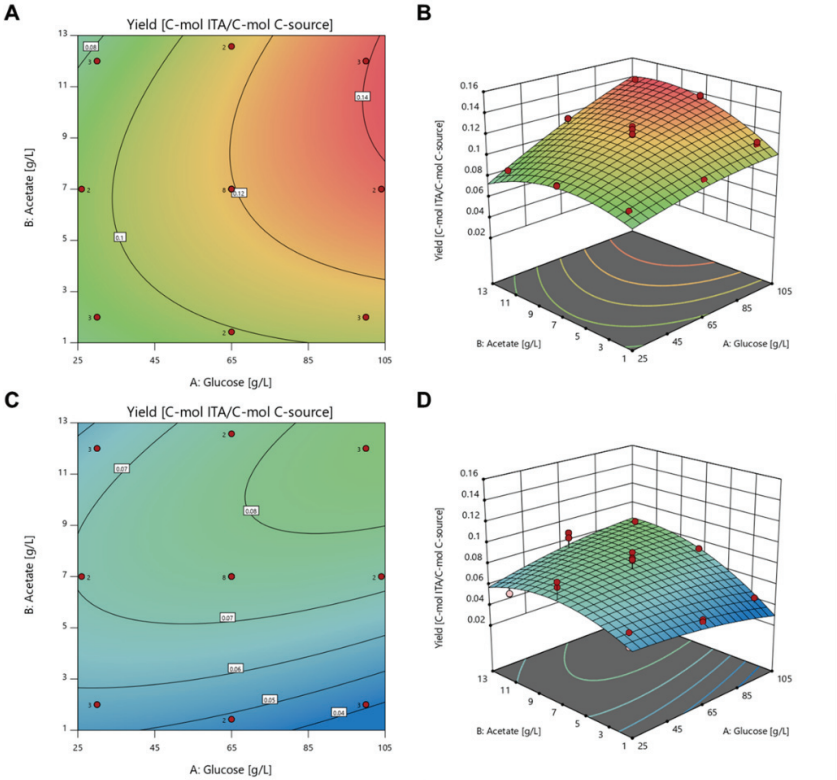

Figure 23: 3D surface models and heatmap diagrams for itaconate yield in *U. maydis* MB215.
Models were generated with Design Expert® software showing the predicted titer response for different concentrations of glucose and acetate as cosubstrates. Two models were generated, one for $CaCO_3$ as a buffer (A - B) and one for MES buffer (C - D). Colored spheres in the graphs represent the measured model conditions. Red spheres indicate model values above the prediction, while light pink spheres refer to model values below the predicted values. Color of the diagrams indicate predicted itaconate yield (0.0389135 0.142683 c-mol c-mol^{-1}). Data associated to this figure were taken from Karla Stein's MasterThesis [190].

In summary, *U. maydis* MB215 utilized acetate as a co-substrate for every tested model condition. The model also predicts the highest itaconate production *via* numerical optimization for high glucose (100 g L^{-1}) and high acetate concentrations (12 g L^{-1}). Concluded regarding this experiment, *U. maydis* MB215 seems to be a promising candidate for itaconate production with a glucose and acetate co-feed.

Model design for U. rabenhorstiana NBRC 8995

U. rabenhorstiana NBRC 8995 was determined as the second most promising candidate in previous investigations regarding itaconate production with acetate as a cosubstrate. It was further investigated concerning the optimum glucose and acetate ratios during this experiment. To maximize the itaconate production, *U. rabenhorstiana* was cultivated with the DoE model conditions to generate a response surface model (**Figure 25**). For each tested condition, the highest itaconate titer and yield were compared for the two buffer systems (**Figure 24**).

Altough in MES buffer cultivations the initial glucose amount was not completely consumed for three tested conditions maximum titer and yield were compared for each condition in MES buffer and $CaCO_3$ see **Figure 24**. The highest total itaconate titer with 10.5 ± 0.3 g L^{-1} was reached for the model condition containing 104 g L^{-1} glucose and 7 g L^{-1} acetate cultivated in $CaCO_3$ buffer. For MES buffer the highest titer was observed for the model condition with 100 g L^{-1} glucose and 2 g L^{-1} acetate reaching 10.1 ± 0.1 g L^{-1}. The maximum yield was reached with 0.12 ± 0.00 c-mol c-mol^{-1} for cultivation with 100 g L^{-1} glucose and 2 g L^{-1} acetate in MES buffer and 0.11 ± 0.01 c-mol c-mol^{-1} for the same condition in $CaCO_3$ buffer.

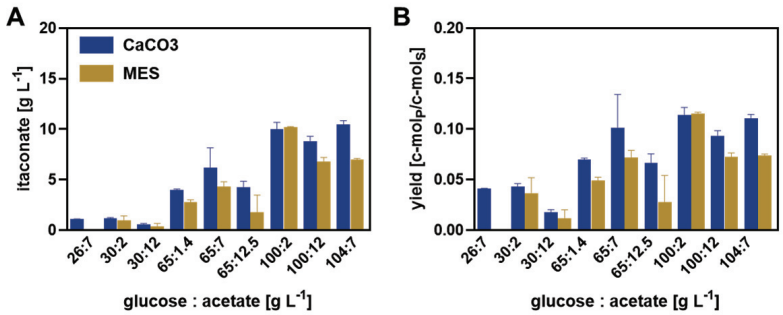

Figure 24: Itaconate production during DoE cultivation experiments of *U. rabenhorstiana* NBRC 8995.
Maximum itaconate titer (a) and yield (b) are compared for each model condition containing defined combinations of glucose and acetate and for both buffer systems MES buffer (orange) and $CaCO_3$ buffer (blue). System Duetz® 24-deep-well plate cultivations were performed with MTM medium containing 0.8 g L^{-1} NH_4Cl (1.5 mL culture volume, 300 rpm, 30 °C). Error bars indicate the deviation from the mean for n ≥ 3: Data associated to this figure were taken from Karla Stein's MasterThesis [190].

Due to the remaining glucose in several MES cultivation conditions, it was not possible to generate significant models including both buffer systems. Therefore, and since CaC_{O3} showed higher yields and titers MES buffer was excluded for the model analysis and models were generated for $CaCO_3$ only. To establish a model regarding the titer, a quadratic model was chosen and transformed logarithmic based on the software options. The ANOVA analysis (appendix, **Figure 72** and **Figure 73**) showed mainly significant model terms, since insignificant model terms were kept only when the hirachy required it, and nonsignificant lack of fit leading in total to a significant model with a coefficient of determination of R^2 = 0.96

(itaconate titer) and $R^2 = 0.87$ (itaconate yield). The generated 3D surface graphs and heatmap diagrams (**Figure 25**) cover the whole model range for both substrates inside their ranges and thereby predict responses for every co-substrate combination inside the model ranges. The model predicts the highest itaconate titer *via* numerical optimization as expected for high glucose concentrations (100 g L^{-1}) since it is used as a main carbon source. Regarding the acetate concentration the highest itaconate production was predicted for 7 g L^{-1} with itaconate titer of 11.8 g L^{-1} and a yield of 0.13 c-mol c-mol^{-1}. For higher and lower acetate concentrations, the titer decreases in the model prediction.

During the experiment's low nitrogen concentration of 0.8 g L^{-1} were used for optimum itaconate production since a nitrogen limitation is known to increase the itaconate production [62]. Nevertheless, the amount might be to low at some point of cultivation to further consume the substrates if high initial substrate concentrations were used. Therefore, increasing the nitrogen concentration might help to avoid leftover of substrates enabling the set up of an MES based model.

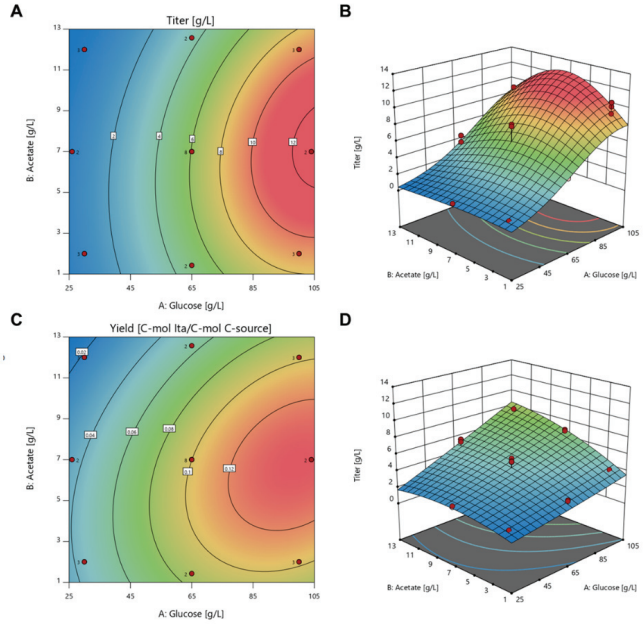

Figure 25: 3D surface models and heatmap diagrams for itaconate production in *U. rabenhorstiana* NBRC 8995.
Models were generated with Design Expert® software showing the predicted titer response for different concentrations of glucose and acetate as cosubstrates. One model was established for $CaCO_3$ as a buffer predicting itaconate titer (A – B) and itaconate yield (C – D). Colored spheres in the graphs represent the measured model conditions. Red spheres indicate model values above the prediction, while light pink spheres refer to model values below the predicted values. Color of the diagrams indicate predicted itaconate titer (0.519065 10.7316 g L^{-1} itaconate) and yield (0.0154439 0.133468 c-mol c-mol^{-1}). Data associated to this figure were taken from Karla Stein's MasterThesis [190].

Model validation

Response surface models were successfully established for the two Ustilaginaceae strains *U. maydis* MB215 (#2229) and *U. rabenhorstiana* NBRC 8995 (#2708) to predict the optimum glucose and acetate combination for a maximum itaconate production.

The investigated strains showed different optimum of substrate combinations, especially regarding the acetate concentration, emphasizing the biodiversity among the family of Ustilaginaceae. To examine how accurate the predictive power of the models actually is, one condition was chosen for each strain close to their respective optimum itaconate production, testing conditions that weren't already covered in the model conditions (**Figure 26**). Since *U. maydis* MB215 #2229 showed optimum itaconate production for high glucose and acetate concentration with 100 g L^{-1} and 12 g L^{-1} respectively, 10 g L^{-1} acetate in combination with 90 g L^{-1} glucose were selected as substrate concentrations for the confirmation run. For *U. rabenhorstiana* #2708 an acetate concentration of 6 g L^{-1} was combined with 90 g L^{-1} glucose, since the maximum production was predicted for 7 g L^{-1} acetate.

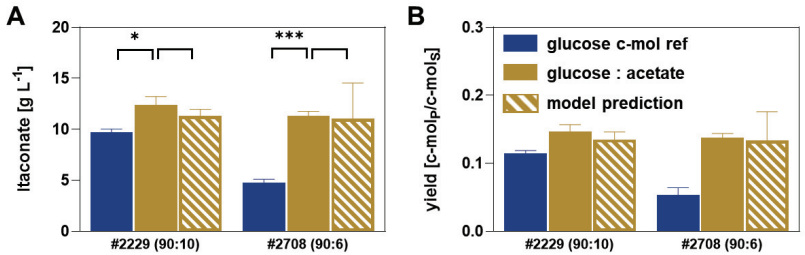

Figure 26: Validation of the generated response surface models.
The generated models with $CaCO_3$ buffer for the two strains *U. maydis* MB215 #2229 and *U. rabenhorstiana* NBRC 8995 #2708 were validated with one confirmation run for each strain. 90 g L^{-1} glucose were used as a main carbon source, combined with 10 g L^{-1} acetate for *U. maydis* and 6 g L^{-1} for *U. rabenhorstiana*. The measured values for titer (A) and yield (B) (filled bar - orange) were compared to the respective model prediction (shaded orange) and a glucose reference containing the same amount of total carbon (blue). System Duetz® 24deepwell plate cultivations were performed at 30°C with MTM medium containing 0.8 g L^{-1} NH_4Cl and 33 g L^{-1} $CaCO_3$. Error bars indicate the deviation from the mean for n=3. Statistically significant differences in itaconic acid production ($0.01 < p < 0.05$) are indicated as *. A strong evidence for statistically differences ($0.001 < p < 0.01$) is indicated as ** and *** refer to a very strong evidence ($p < 0.001$). Data associated to this figure were taken from Karla Stein's MasterThesis [190].

For this experiment a reference cultivation without acetate was performed for every strain with the same carbon amount of glucose compared to the carbon in the selected conditions for both glucose and acetate. Since the DoE cultivations did not include cultivations with glucose only, this experiment also aimed to confirm whether co-feeding of acetate independent of the concentration leads to increased itaconate production in Ustilaginaceae.

Firstly, for *U. maydis* the cultivation with the acetate condition reached a titer of 12.3 ± 0.7 g L^{-1} with a corresponding yield of 0.15 ± 0.01 c-mol c-mol^{-1}. Compared with the model prediction of 11.2 ± 0.5 g L^{-1} and 0.14 ± 0.01 c-mol c-mol^{-1} the values do not differ significantly. The

respective glucose reference cultivation reached a titer of 9.8 ± 0.3 g L^{-1} and a yield of 0.11 ± 0.00 c-mol c-mol^{-1} which are significantly lower compared to cultivation with acetate. With 11.3 ± 0.4 g L^{-1} and 0.14 ± 0.00 c-mol c-mol^{-1} the cultivation of *U. rabenhorstiana* confirmed the model prediction, while the glucose reference reached a titer of 4.8 ± 0.2 g L^{-1} and a yield of 0.05 ± 0.01 c-mol c-mol^{-1}, which is significantly lower compared to the cultivation with acetate. During this experiment the response surface models for three different Ustilaginaceae strains were validated. Since the reached titers and yield did not differ significantly from the model prediction, the validation was considered as successful for all three strains, indicating that the models have an accurate predictive power regarding the yield or titer response for a defined substrate combination within the model ranges.

To find the most suitable strain for upscaling experiments various factors are involved and each of the tested strains provides advantages for a further investigation. Unfortunately, little research focused on itaconate production with *U. rabenhorstiana*, wherefore no engineered strains are available for further investigations [66]. *U. maydis* MB215 showed the highest itaconate production for the highest fed acetate level. Thus, it is considered as a promising candidate, since the overall goal of a carbon-neutral itaconate production is based on co-feeding acetate during the production process. Another advantage is, that research focused on *U. maydis* as a production host and through morphological and metabolic engineering strains are available to operate close to the theoretical yield with reduced formation of side products [64], [65], [73].

3.1.4 Conclusion

Here, the co-utilization of acetate and formate by strains of the genus Ustilaginaceae was reported. From 72 different Ustilaginaceae strains of 36 species, *U. maydis* MB215 (#2229) and *U. rabenhorstiana* NBRC 8995 (#2708) were identified as promising candidates for acetate co-metabolization while *U. cynodontis* NBRC 7530 (#2705) was identified as a potential production host using formate as a co-substrate for the production of itaconate, a platform chemical for polymer and biofuel production. The current industrial production of plastic monomers and fuels from fossil resources has to be reduced and in the long-run stopped, requiring alternative technologies. Itaconate is promising, as it has been, for the last 70 years, produced in fermentations using sugars as substrate. However, with a shift of the carbon source in the chemical industry, land-use for sugar production for biotechnology would be skyrocketing, a scenario that will come fast to a maximum, although most agricultural land is still used for meat production, and only about 25% of all grains are used for human consumption. Still, the use of carbon sources that are derived from CO_2 and green hydrogen opens possibilities for the carbon-neutral production of chemicals and fuels and, most importantly, scales without a proportional land-use.

While acetate can be directly used as a carbon and energy source, formate co-consumption only delivers extra electrons to the fungal metabolism. The co-substrate strategies presented here indeed highlighted single strains of the Ustilaginaceae that could not only utilize simultaneously both substrates but also produce more itaconate. Nevertheless, individual bioprocess development is essential to further improve itaconate production and evaluate their capabilities. During this study, the tested wildtype strains produced a broad range of extracellular products, emphasizing the biodiversity of this microbial family. Based on the shown data on extracellular metabolites and previous results, several options for metabolic engineering were displayed to alter the metabolic flux distribution to maximize product synthesis. As far as co-substrate utilization is concerned, an adaptive laboratory is a valuable tool potentially enhancing co-substrate tolerance and utilization. Furthermore, the optimum glucose co-substrate ratio will be determined during subsequent Design of Experiment (DoE) approaches enabling the development of a suitable co-feeding strategy. Specifically, ^{13}C-labeling experiments can lead to a better understanding of acetate and formate assimilation pathways in Ustilaginaceae contributing toward a carbon-neutral itaconate production in the future. These efforts will showcase the reduction of the carbon footprint of biotechnology, without increasing land-use. The latter not only is, in the authors' opinion, a major driver for the acceptance of the transition in the chemical industry from fossil to renewable carbon sources but also opens up opportunities for stabilizing soil and water health and thereby biodiversity

Chapter 3.2

Acetate co-feeding toward carbon-neutral itaconate production by *Ustilago maydis*

Contributions:

Lena Ullmann performed cultivation and bioreactor experiments of *U. maydis*, analyzed the data, prepared figures, and wrote this chapter. DoE cultivation experiments were carried out by Philipp Kohl and Gereon Schröders coordinated by Lena Ullmann. Philipp Kohl performed ^{13}C-labeling experiments. Metabolically engineered *U. maydis* strains were constructed by Lena Ullmann, Andreas Müsgens and Hannah Kahlen. Lars M. Blank advised on all experiments, analyzed and discussed data, and reviewed this chapter.

3.2 Acetate co-feeding toward carbon-neutral itaconate production by *Ustilago maydis*

3.2.1 Summary

Within the last decade, Ustilaginaceae have shown a rising potential for industrial exploitation as novel biocatalysts. *Ustilago maydis*, a member of the Ustilaginaceae family, is a promising host for the production of a range of metabolites including itaconic acid. Itaconic acid is a bio-based building block in the polymer and pharmaceutical industry. Recently, this dicarboxylic acid was produced from glucose with metabolically and morphology engineered *U. maydis* strains at up to maximum theoretical yield. The use of acetate derived from CO_2 as co-feed can further increase the efficiency of itaconate production with Ustilaginaceae wildtype strains by reducing the demand of glucose and thus the agricultural land required. Acetate is regarded as a promising carbon feedstock in biological production owing to its possible from the C1 carbon sources CO_2, CO, and methane. Here, we investigated acetate as carbon feedstock for itaconate production using a new chassis strain *U. maydis* Δ*fuz7* Δ*cyp3* ΔMEL ΔUA P_{etef}mttA $\Delta P_{ria1}::P_{etef}$. By applying a design-of-experiment (DoE) methodology, cultivation parameters (glucose, sodium acetate, and ammonium chloride concentrations) were optimized resulting in two empirical models predicting itaconate titer and yield by establishing a suitable feeding strategy. Further, the metabolic role of acetate was investigated for *U. maydis via* off-gas analysis and a ^{13}C-labeling approach. Product inhibition by itaconate and toxic effects of acetate were addressed by implementing an external membrane module into the existing cultivation enabling cell retention and simultaneous product removal. During bioreactor cultivations, the potential of continuous cultures with *U. maydis* was demonstrated displaying constant production rates for 500 h. In summary, *U. maydis* is well suited for itaconate production from alternative substrates and allows efficient bioprocess development beyond a traditional fed-batch.

3.2.2 Introduction

The non-renewable nature of fossil resources and the environmental concerns about global warming have encouraged the use of carbon-neutral substrates for biofuel and bulk chemical production. In order to achieve such independence from fossil resources, a sustainable bio economy is needed, with materials of biological origin and their incorporation into resource-protecting processes [191]. The success of this sustainable production technology largely depends on the efficiency of microbial cell factories and the cost of carbon feedstocks. Microbial production of organic acids are examples for a chemical industry aiming for sustainability [37].

Here, a promising building block - itaconic acid – is presented, which is a natural product of microorganisms and versatile due to its functional groups [13]. Itaconic acid was ranked as

one of the top 12 bio-based platform chemicals with high biotechnological potential in 2004 by the Department of Energy [13].

Ustilago maydis belongs to the Ustilaginaceae family and is a natural itaconate producer. This smut fungus naturally produces a versatile spectrum of valuable products, such as other organic acids (succinic acid, malic acid), polyols, glycolipids, and neutral lipids, with a broad application spectrum in the pharmaceutical, chemical, and food industry [187], [192]–[194]. Further, it represents a well-established model organism, e.g. for biotechnology [70], [88], [195], plant pathology [196], [197], cell biology [198], protein secretion [199], and even for the elucidation of basic principles of primary metabolism [200].

Regarding industrial use as a production host, *U. maydis* implicates crucial advantages. When compared to the currently used filamentous fungi *A. terreus*. *U. maydis* shows unicellular growth in its haploid form, simplifying handling and fermentation processes tremendously, thereby reducing costs. *U. maydis* grows at high cell densities, is osmotolerant, and handles high substrate and product titers. Further, the fungi is tolerant toward impurities present in the growth medium and industrial feedstocks, and handles hydromechanical stress well. Nevertheless, until now *A. terreus* remains the industrial production host to its prominent tolerance to low pH values combined with high product titers and yields. On a laboratory scale, titers of 160 g L^{-1} were recently reported [19], [34]. For a long time, the performance of *A. terreus* outcompeted all other (engineered) itaconate-producing strains. However, after strain engineering and fermentation optimization, a maximum titer of 220 g L^{-1} was lately achieved using *U. maydis*. Becker *et al.* (2019) focused on increasing the metabolic flux into the itaconate biosynthesis pathway by overexpressing the itaconate gene cluster regulator *ria1* and preventing side product formation ((*S*)-2-hydroxyparaconate, ustilagic acid (UA), mannosylerythritol (MEL), and diacylglycerol lipids (dgat)) [64], [65].

However, the Δ*dgat* mutation decreased the fitness of the engineered strain. Therefore, in this study a new chassis strain was established following the cloning strategy of Becker et. al (2019) combining a reduced by-product spectrum and itaconic acid overexpression while keeping TAG biosynthesis resulting in strain *U. maydis* Δ*fuz7* Δ*cyp3* ΔMEL ΔUA P_{etef}mttA $_{\Delta P_{ria1}::P_{etef}}$ [65]. Using CRISPR/Cas 9 for genome editing a marker-free chassis strain was generated. This chassis strain was used ifor mixed substrate use. Acetate can empower the development of low-cost, sustainable bioprocesses, without any conflicts with arable land and the food chain [93], [99], [201].

The global acetate production is approximately 13 million metric tons, priced at USD 350–450 per ton, which is slightly cheaper than conventional glucose, which is priced at USD 500 per ton [202], [203]. However, acetate can be produced from C1 carbon sources using both chemical and biological methods. Chemical synthesis covers about 75% of the total acetate production. The biotechnological production covers about 10 percent of the total acetate production, especially for the production of vinegar [95]. In aerobic fermentation, acetate is

produced through the respiration of ethanol by acetic acid bacteria like *Acetobacter* [95]. Thereby, acetate can be produced from various feedstocks such as sugars, glycerol, lignocellulosic biomass, or even waste materials, mainly by *Acetobacter* species.

Next to the conventional production, there are also approaches for acetate production from CO_2, which are of special interest regarding the use as a co-substrate for a sustainable production of itaconate. One approach is the conversion of synthesis gas (syngas) into acetic acid [204]. Species like *Clostridium* or *Acetobacterium* were reported to be suitable for the anaerobic conversion of syngas to acetate [102], [205]. The technology of gas fermentation has recently been commercialized with the first production plant for ethanol operating since 2018 [103], which is a promising development in this field of research. Another promising approach is the microbial electrosynthesis (MES). MES based on bio-electrochemical systems (BESs), offers a potentially sustainable route of producing useful platform and commodity chemicals [104]. Thereby, MES does not involve the use of fossil-based substrates, but instead uses microorganisms' metabolism to reduce CO_2 to valuable chemicals [104]. Recent work in the broad context of green chemistry focused on a new catalytic system for the formal isomerization of methyl formate to acetic acid and methyl acetate. This approach opens a possible route for a defossilized production of acetic acid based ultimately on CO_2 and H_2 as primary feedstocks [206].

Within this work the potential of acetate as carbon feedstock for itaconate production was investigated using the new modified chassis *U. maydis* Δ*fuz7* Δ*cyp3* ΔMEL ΔUA P_{etef}mttA ΔP_{ria1}::P_{etef}. The metabolic consequences of acetate were investigated in *U. maydis via* off-gas analysis and by a ^{13}C-labeling approach. By applying a design-of-experiments (DoE) methodology, cultivation parameters (glucose, acetate, and ammonium chloride concentrations) were optimized resulting in two empirical models predicting itaconate titer and yield. The insights were used to establish a feeding strategy, which was applied in subsequent experiments using an external ceramic membrane enabling cell retention with simultaneous product removal. This strategy allowed bioprocess intensification by avoiding itaconate product inhibition.

3.2.3 Results and discussion

3.2.3.1 *U. maydis* chassis strain development

To generate an *U. maydis* chassis with reduced by-product formation, multiple knockouts were successively performed in a single strain. The strain *U. maydis* Δ*fuz7* Δ*cyp3* ΔP_{ria1}::P_{etef} engineered by Hosseinpour Tehrani et. al (2019) was used as a starting point [68]. To overcome limitations by available selection markers suitable for *U. maydis*, a CRISPR/Cas9 system was used [73], [207]. The cloning strategy was based on Becker *et al.* (2019) [208].

The additional modifications were performed consecutively in the order ΔUA, ΔMEL *via* CRISPR/Cas9 and insertion of P_{etef}mttA to the *ip*-locus using the FRT/FLP-mediated approach

[65], [68], [208]. Modifications were successfully verified by PCR resulting in 7 clones of the strain *U. maydis* Δ*fuz7* Δ*cyp3* ΔMEL ΔUA P_{etef}mttA ΔP_{ria1}::P_{etef}. The obtained strains within this study are displayed in **Table 10.**

Table 10: Summary of metabolically engineered *U. maydis* MB215 strains.

Strain	No. iAMB strain collection
U. maydis MB215 Δ*fuz7* Δ*cyp3* ΔMEL ΔUA P_{etef}mttA ΔP_{ria1}::P_{etef}_K1	#7072
U. maydis MB215 Δ*fuz7* Δ*cyp3* ΔMEL ΔUA P_{etef}mttA ΔP_{ria1}::P_{etef}_K2	#7073
U. maydis MB215 Δ*fuz7* Δ*cyp3* ΔMEL ΔUA P_{etef}mttA ΔP_{ria1}::P_{etef}_K3	#7074
U. maydis MB215 Δ*fuz7* Δ*cyp3* ΔMEL ΔUA P_{etef}mttA ΔP_{ria1}::P_{etef}_K4	#7075
U. maydis MB215 Δ*fuz7* Δ*cyp3* ΔMEL ΔUA P_{etef}mttA ΔP_{ria1}::P_{etef}_K5	#7076
U. maydis MB215 Δ*fuz7* Δ*cyp3* ΔMEL ΔUA P_{etef}mttA ΔP_{ria1}::P_{etef}_K6	#7077
U. maydis MB215 Δ*fuz7* Δ*cyp3* ΔMEL ΔUA P_{etef}mttA ΔP_{ria1}::P_{etef}_K7	#7078
U. maydis MB215 Δ*fuz7* Δ*cyp3* ΔP_{ria1}::P_{etef}	#6188
U. maydis MB215 Δ*fuz7* Δ*cyp3* ΔMEL ΔUA ΔP_{ria1}::P_{etef}	#6754
U. maydis MB215 Δ*fuz7* Δ*cyp3* ΔMEL ΔUA Δ*dgat* P_{etef}mttA ΔP_{ria1}::P_{etef}_K14	#4856 [208]

3.2.3.2 Acetate co-metabolization

Investigating of acetate co-metabolization via CO_2 off-gas analysis

Previously acetate was used as a co-substrate. Thereby, lower growth rates and lower optical densities were obtained, when compared to glucose only. During this work, acetate was further examined as a sole carbon source. Here, the CO_2 concentration in the headspace was monitored as a measure for growth (**Figure 27**).

Cultivation conditions using acetate as a sole carbon source (**Figure 27 A, B**) result in a significantly lower CO_2 production compared to cultivations on glucose (**Figure 27 C**). The minor increase in the CO_2 might be from the pre-culture, as no difference is observed between cultivations with 2 or 4 g L^{-1} acetate.

The results suggest that acetate could not be metabolized for growth by *U. maydis* as a sole carbon source. Acetate assimilation by *U. maydis* has not been well researched yet, but the assimilation in yeasts may give a hint. In yeasts, acetate is passively transported into the cell by a monocarboxylate permease. This permease is a proton symporter, which is responsible for acetate and format transport in *Saccharomyces cerevisiae*, for example [209], [210]. Intracellularly, acetate is converted into acetyl-CoA in the cytosol by an *acetyl-CoA synthetase* (ACS) driven by ATP consumption. In *U. maydis*, the enzyme acetyl-CoA synthetase is present and no other pathways for the consumption of acetate were reported for *Ustilago*. In bacteria such as *E. coli*, different enzymes besides ACS, i.e. ACK-PTA (acetate kinase – phosphotransacetylase), are known to enable growth on acetate as the sole carbon source [203].

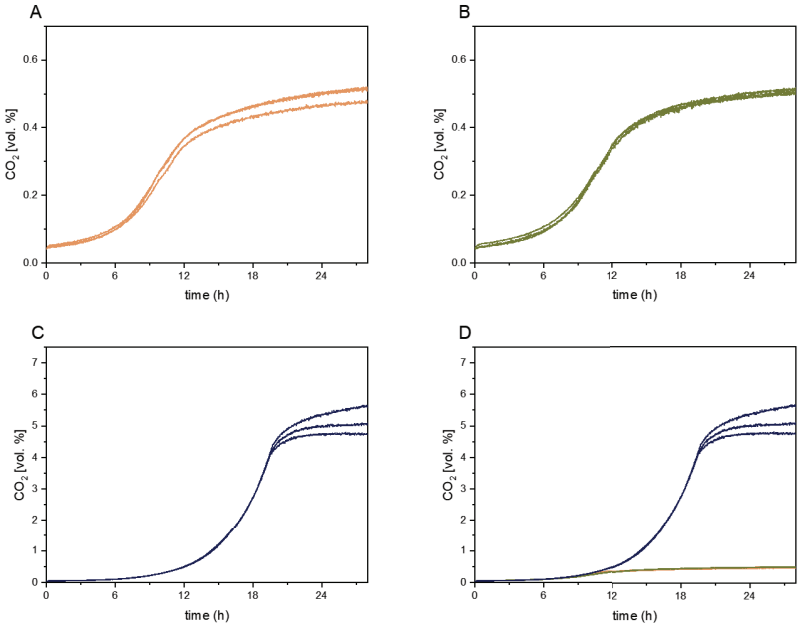

Figure 27: CO_2 volume concentration in the headspace of shake flask cultivations of *U. maydis* MB215 Δ*cyp3* Δ*fuz7* ΔUA ΔMEL $\Delta P_{ria1}::P_{etef}$ P_{etef}mttA during acetate cultivation experiments.
Cultivations were performed with (A) 2 g L^{-1} acetate (orange), (B) 4 g L^{-1} acetate (green), (C) 4 g L^{-1} glucose (blue) as C-source in MTM using 0.8 g L^{-1} NH_4Cl and 19.5 g L^{-1} MES. Diagram D shows comparison of A, B and C. 1 L shaking flasks were filled with 50 mL medium (30 °C, 150 rpm, n=3). Data associated to this figure were taken from Philipp Kohl's Master Thesis [211].

Acetate assimilation takes place primarily through the glyoxylate shunt in various microorganisms [93]. Further, in yeast and fungi the pathways are compartmentalized and hence transporters are required. A study conducted by Palmieri *et al.* (2002) observed that yeast mutants lacking the gene for a dicarboxylate carrier (DIC) failed to grow on acetate or ethanol as sole carbon source whereas they were able to grow on glucose [212]. DIC is an integral membrane protein that catalyzes a dicarboxylate–phosphate exchange across the inner mitochondrial membrane in yeast [212].

Acetate as sole carbon source for *U. maydis* did not support growth (**Figure 27**). Potentially, the glyoxylate shunt is just not activated under these conditions. Due to the fact that, growth on ethanol of fatty acids were reported for substrates that are also using the glyoxylate shunt as anaplerotic. To test if a regulatory reason exists for the non-growth phenotype of *U. maydis*, glyoxylate was used a co-substrate. First, growth on glyoxylate as a sole carbon source compared to the combination with glucose was examined (**Figure 28 A**). Secondly, co-

metabolization of glyoxylate and acetate was tested (**Figure 28 B**). Thirdly, a combination of all three substrates was used (**Figure 28 B**).

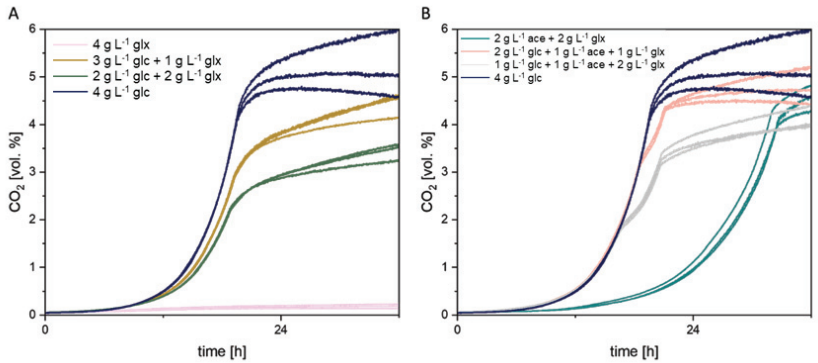

Figure 28: CO_2 volume concentration in the headspace of shake flask cultivations of *U. maydis* MB215 Δ*cyp3* Δ*fuz7* ΔUA ΔMEL $\Delta P_{ria1}::P_{etef}$ P_{etef}mttA during glyoxylate cultivation experiments.
Cultivations were performed with varying C-sources in MTM using 0.8 g L^{-1} NH_4Cl and 19.5 g L^{-1} MES. 1 L shaking flasks were filled with 50 mL medium (30 °C, 150 rpm, n=3). (A) summarized cultivation conditions of 4 g L^{-1} glyoxylate (pink), 2 g L^{-1} glucose and 2 g L^{-1} glyoxylate (green), 3 g L^{-1} glucose and 1 g L^{-1} glyoxylate (yellow) and 4 g L^{-1} glucose (dark blue). (B) showed cultivation conditions of 2 g L^{-1} glucose and 2 g L^{-1} acetate (light blue), 4 g L^{1} glucose (dark blue), 2 g L^{-1} glucose, 1 g L^{-1} acetate and 1 g L^{-1} glyoxylate (orange) as well as 1 g L^{-1} glucose, 1 g L^{-1} acetate and 2 g L^{-1} glyoxylate (grey). Substrate abbreviation: glc for glucose, ace for acetate, and glx for glyoxylate. Data associated to this figure were taken from Philipp Kohl's Master Thesis [211].

With glyoxylate as a sole carbon source a maximum CO_2 value in the headspace of 0.28 vol.% was observed, indicating that minimal or no glyoxylate was metabolized. In contrast, glyoxylate consumption was observed in cultivations with glucose, although glyoxylate was not fully consumed, whereas glucose and acetate were fully consumed within 36 h (**Table 11**).

Table 11: Glyoxylate consumption during *U. maydis* MB215 Δ*cyp3* Δ*fuz7* ΔUA ΔMEL $\Delta P_{ria1}::P_{etef}$ P_{etef}mttA cultivation experiment.
Cultivations were performed with varying C-sources in MTM using 0.8 g L^{-1} NH4Cl and 19.5 g L^{-1} MES. 1 L shaking flasks were filled with 50 mL medium (30 °C, 150 rpm, n=3). Data were obtained *via* HPLC analysis were obtained from Philipp Kohl's Master Thesis [211].

Condition	Consumed glyoxylate [g L^{-1}]
4 g L^{-1} glyoxylate	0
3 g L^{-1} glucose + 1 g L^{-1} glyoxylate	0.33 ± 0.02
2 g L^{-1} glucose + 2 g L^{-1} glyoxylate	0.27 ± 0.03
2 g L^{-1} acetate + 2 g L^{-1} glyoxylate	0.47 ± 0.02
2 g L^{-1} glucose +1 g L^{-1} acetate + 1 g L^{-1} glyoxylate	0.42 ± 0.04
1 g L^{-1} glucose + 1 g L^{-1} acetate + 2 g L^{-1} glyoxylate	0.16 ± 0.07

Interestingly, a combination of 2 g L^{-1} acetate and 2 g L^{-1} glyoxylate lead to growth and a CO_2 production of 5.3 ± 0.6 vol. % in the headspace. In contrast glucose co-metabolization (2 g L^{-1} glucose + 2 g L^{-1} glyoxylate) resulted in a lower CO_2 production of 3.1 ± 0.2 vol. %. The combination of glucose, glyoxylate, and acetate did not result in a higher CO_2 production compared to the 4 g L^{-1} glucose reference condition. To conclude, glyoxylate was beneficial for

acetate co-metabolization. Whereas acetate did not function as a sole carbon source for *U. maydis*, addition of glyoxylate resulted in cell growth and CO_2 production.

To verify whether the glyoxylate not only boosts acetate consumption but also results in an increased biomass and itaconate production, cultivations were carried out using the Growth Profiler system by Enzyscreen. In total 16 different approaches with varying substrate concentrations were tested (**Figure 29**).

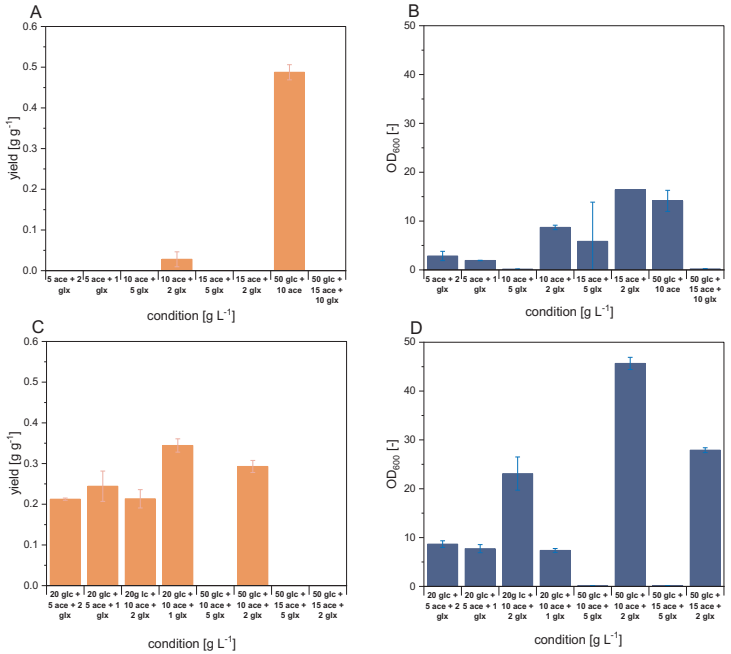

Figure 29: Cultivation experiments investigating the influence of glyoxylate on itaconate yield and biomass production.
Cultivations were performed with varying glucose, acetate, and glyoxylate concentrations using the Growth Profiler device by Enzyscreen. *U. maydis* MB215 Δ*cyp3* Δ*fuz7* ΔUA ΔMEL ΔP_{ria1}::P_{etef} P_{etef}mttA was cultivated in MTM 0.8 g L^{-1} NH_4Cl, 19.5 g L^{-1} MES in 24-well microtiterplates (grey) with a filling volume of 1.5 mL (30 °C, 225 rpm). Itaconate yield determination was shown in (A) and (C), biomass determination in (B) and (D). Substrate abbreviation: glc for glucose, ace for acetate, and glx for glyoxylate. Error bars indicate the deviation from the mean (n= 3). Data associated to this figure were taken from Philipp Kohl's Master Thesis [211].

The results show no increase in itaconate production due to the addition of glyoxylate in the medium for *U. maydis* MB215 Δ*cyp3* Δ*fuz7* ΔUA ΔMEL ΔP_{ria1}::P_{etef} P_{etef}mttA. Cultivation conditions using acetate and glyoxylate without glucose present in the medium lead to biomass formation but no itaconate production was observed. Thereby, one exeption was observed for condition 10 g L^{-1} acetate and 2 g L^{-1} glyoxylate resulting in an itaconate production of 0.15 ± 0,10 g L^{-1}. In general, obtained OD_{600} values were low in a range of max. 10 - 15. Thus, it can be hypothized that the nitrogen was not fully completed and the absence of itaconate

production might result from the lack of nitrogen limitation during cultivation experiments. This hypothesis could be confirmed during subsequent experiments.

The conditions with glucose in the media resulted in the formation of itaconate, ranging from 5 to 12 g L^{-1} itaconate. The highest itaconate titer was achieved by the combination of 50 g L^{-1} glucose and 10 g L^{-1} acetate producing 25.2 ± 0.9 g L^{-1} itaconate which equals a yield of 0.48 g g^{-1}. Corresponding to that, 50 g L^{-1} glucose, 10 g L^{-1} acetate and 2 g L^{-1} glyoxylate resulted in an itaconate production of 11.7 ± 0.2 g L^{-1} itaconate (corresponding to yield of 0.29 g g^{-1}). In summary, these results indicate a negative impact of glyoxylate on itaconate production, which is to be expected, as the glyoxylate shunt competes for cis-aconitate (*via* isocitrate) with itaconate synthesis. A possible strategy would be to aim for a 2-phasic culture, whereas biomass formation is realized with acetate and glyoxylate and afterwards itaconate is produced by feeding acetate only.

Investigating of acetate co-metabolization via ^{13}C-labeling

Previous experiments demonstrated a beneficial effect of acetate on itaconate production with *U. maydis*. The question raised was if acetate was used as carbon source for itaconate production. Fully ^{13}C-labeled acetate was used and the labeling pattern of itaconate was investigated. The incorporation of the acetate carbon atoms into itaconate is crucial for the CO_2 balance of the product. Samples were measured by gas chromatography in combination with a mass spectrometer (GC-MS) to determine the labeling patterns of the analytes. **Figure 30** shows the metabolism of *U. maydis* with the proposed acetate assimilation pathway [69], [107], [166], [213].

In order to evaluate incorporation of acetate into itaconate, the following culture conditions were determined. First, biomass formation of *U. maydis* was ensured by cultivation in MTM with 50 g L^{-1} glucose, 3 g L^{-1} acetate, and 0.8 g L^{-1} NH_4Cl for 48 h (30°C, 200 rpm). Thereby, an OD_{600} value of 10.87 ± 0.25 was reached after 48 h. The substrate composition of the second cultivation phase with labeled acetate was determined in preliminary experiments. Thereby, 2 g L^{-1} glucose and 2 g L^{-1} acetate achieved the highest itaconate yield. Results of the second cultivation phase are shown in **Figure 31** whereas no nitrogen was present in the medium. The data were obtained from the cultivation with $^{13}C_2$-acetate in the medium. Itaconate concentrations of 1.51 ± 0.07 g L^{-1} were already reached after 2 h. After 24 h, the itaconate achieved a value of 2.73 ± 0.12 g L^{-1}.

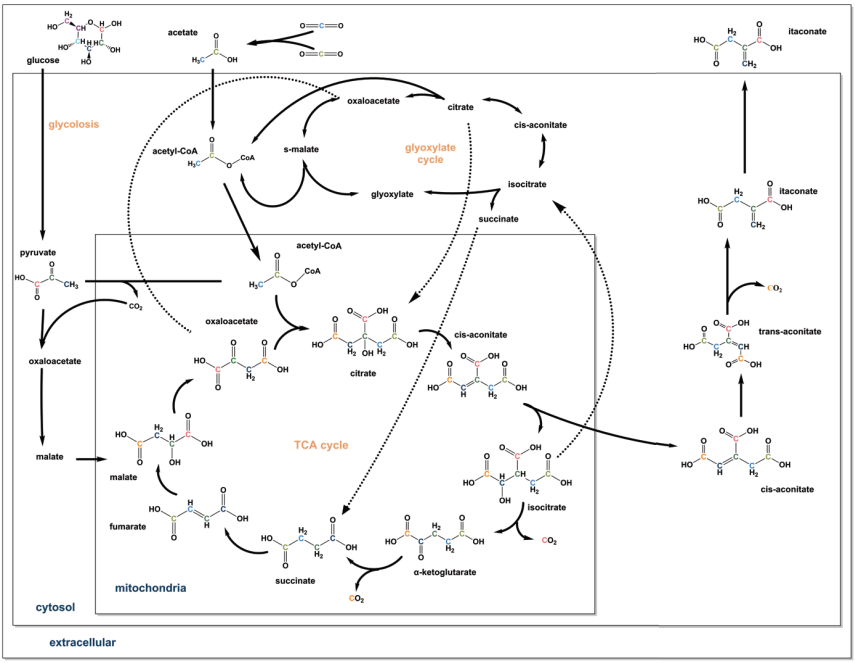

Figure 30: Simplified itaconic acid biosynthesis in *U. maydis* with a proposed acetate metabolism.
Pyruvate is generated from glucose through glycolysis taking place in the cytosol. Pyruvate is transported into the mitochondria, where it is converted to acetyl-CoA by the pyruvate dehydrogenase complex. Acetyl-CoA and OAA form citrate catalyzed by the citrate synthase during the TCA cycle. Citrate is dehydrated to *cis*-aconitate, which is transported from the mitochondria into the cytosol *via* the mitochondrial tricarboxylate transporter Mtt1. When citrate is converted to cis-aconitate, a double bond is formed. In the cytosol, *cis*-aconitate is converted to itaconate *via* the intermediate *trans*-aconitate. Modified from [69], [166]. Proposed acetate assimilation modified from [107], [109]. Data associated to this figure were modified from Philipp Kohl's Master Thesis [211].

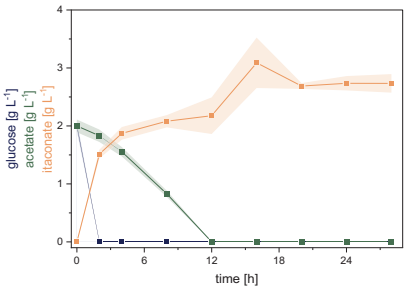

Figure 31: Co-substrate use of *U. maydis* – a labeling experiment.
U. maydis MB215 Δ*cyp3* Δ*fuz7* ΔUA ΔMEL $\Delta P_{ria1}::P_{etef}$ P_{etef}mttA was cultivated in MTM with 19.5 g L^{-1} MES-buffer without addition of NH_4Cl. 2 g L^{-1} unlabeled glucose and 2 g L^{-1} ^{13}C-acetate were used as substrates. The start OD_{600} was 11 obtained from a 48 h cultivation. First main culture was performed in MTM with 19.5 g L^{-1} MES-buffer, 50 g L^{-1} glucose, 3 g L^{-1} acetate and 0.8 NH_4Cl. Itaconate production is shown in orange (●), glucose consumption

in blue (●) and acetate consumption in green (●). Error bars depict the standard deviation of the mean (n = 3). Data associated to this figure were taken from Philipp Kohl's Master Thesis [211].

Itaconate was completely non-labeled, as indicated by the highly similar results of the GC-MS analysis between sample and reference (**Figure 32**).

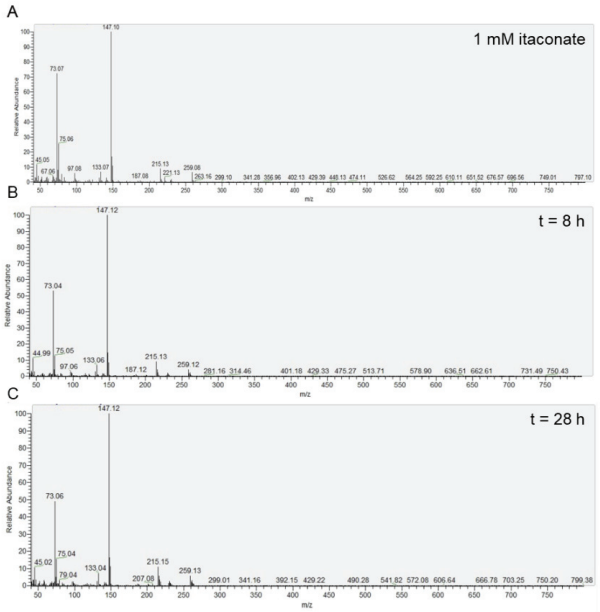

Figure 32: Extracellular metabolite identification *via* GC-MS.
Product ion scan for extracellular metabolite samples taken after 8 and 28 h (B, C) and their corresponding 1 mM itaconate standard (A). Extracellular metabolites in the supernatant formed by *U. maydis* MB215 Δ*cyp3* Δ*fuz7* ΔUA ΔMEL $\Delta P_{nia1}::P_{etef}$ P_{etef}mttA during cultivation in MTM medium (19.5 g L^{-1} MES, 30°C, 200 rpm). Data associated to this figure were taken from Philipp Kohl's Master Thesis [211].

Acetate as a co-substrate was not converted into itaconate by *U. maydis*. Therefore, other metabolic pathways are active for acetate consumption.

Firstly, cell maintenance and energy metabolism might be a sink for acetate. This is supported by cultivation data, where an equal concentration of itaconate was observed in cultivations with and without acetate, but a lower amount of biomass was formed in the approach with acetate, suggesting an additional energy source for the cell through the acetate. Because of the different metabolic pathways of glucose and acetate, there is no competition for enzymes, which means that it is advantageous for the cell, if acetate is available as a co-substrate in the medium. The results of the majority of cultivations with only acetate as substrate and glyoxylate as co-substrate showed a biomass production but no production of itaconate, hence, only cell maintenance was finanzed by acetate. Thereby, one exeption was observed for condition 10 g L^{-1} acetate and 2 g L^{-1} glyoxylate resulting in an itaconate production of 0.15 ± 0,10 g L^{-1}.

This indicates a potential lack of nitrogen limitation during cultivation experiments in combination with relatively low biomass formation due to lower carbon sources used during cultivations. During subsequent experiments, lower nitrogen concentrations than 0.8 g L^{-1} NH_4Cl could be tested to confirm the hypothesis.

Secondly, acetate is directly converted to CO_2. This possible respiration of acetate is part of the energy metabolism and hence of general cell respiration. This assumption was strengthened by the increased CO_2 emission in cultivations with acetate in. In preparations with 4 g L^{-1} glucose as substrate, maximum CO_2 values between 4.5 and 5.5 vol. % were measured in the shake flasks head space. In the preparation with the same C-molarity of the substrates as the 4 g L^{-1} glucose preparation, namely with 2 g L^{-1} glucose and 2 g L^{-1} acetate, higher CO_2 values were measured with a maximum of 6.5 and 7 vol. %.

Investigating acetate co-metabolization using metabolically engineered U. maydis

Previous work confirmed a beneficial effect of acetate co-metabolization on itaconate production by testing 72 different Ustilaginaceae wildtype strains [91]. Given the results, *U. maydis* MB215 was determined as the most promising strain metabolizing acetate with a 2.2-fold increase in itaconate titer (6.25 g L^{-1} acetate and 50 g L^{-1} glucose vs. 50 g L^{-1} glucose) [91]. Interestingly, the yield also increased 2.3-fold.

In contrast to the previous study, this study focused on the established genetically modified *U. maydis* MB215 Δ*cyp3* Δ*fuz7* ΔUA ΔMEL $\Delta P_{ria1}::P_{etef}$ P_{etef}mttA strain for acetate co-metabolization (**Figure 33**). During shake-flask cultivation equal amounts of glucose (108.8 g L^{-1}) and glucose (100 g L^{-1}) and in addition acetate (12 g L^{-1} acetate) were used. Both cultivation experiments showed a similar itaconate production reaching a maximum itaconate titer of 53.4 ± 9.1 g L^{-1} during sole glucose and 54.7 ± 0.3 g L^{-1} during acetate co-metabolization. Production parameters are summarized in **Table 12**. Thus, glucose was successfully substituted with acetate resulting in an equal itaconate production, validating the usability of metabolically engineered *U. maydis* strains for acetate co-metabolization toward a carbon-neutral itaconate production.

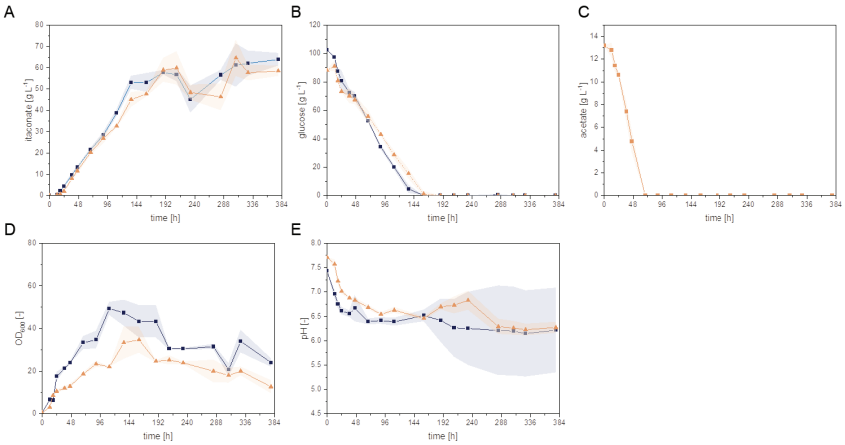

Figure 33: Acetate co-metabolization of metabolically engineered *U. maydis* MB215 Δ*cyp3* Δ*fuz7* ΔUA ΔMEL ΔP_{ria1}::P_{etef} P_{etef}mttA.
Itaconate production (A), glucose consumption (B), acetate consumption (C), growth *via* OD_{600} (D), pH (D) were monitored. Shake-flask cultivations were perfomed in MTM using 33 g L^{-1} $CaCO_3$, 0.8 g L^{-1} NH_4Cl with a 10% filling volume (30°C, 200 rpm). Cultivation using glucose (108.8 g L^{-1}) as a sole carbon source is shown in blue (■), whereas combined cultivation (100 g L^{-1} glucose, 12 g L^{-1} acetate) is highlighted in orange (▲). Error bars indicate the deviation from the mean (n= 3).

Table 12: Production parameter during acetate co-metabolization experiments.
Shake-flask cultivations were perfomed in MTM using 33 g L^{-1} $CaCO_3$, 0.8 g L^{-1} NH_4Cl with a 10 % filling volume (30°C, 200 rpm). Cultivation using glucose (108.8 g L^{-1}) as a sole carbon source is shown in blue (■), whereas combined cultivation (100 g L^{-1} glucose, 12 g L^{-1} acetate) is highlighted in orange (▲). Error bars indicate the deviation from the mean (n= 3).

Parameter	Glucose	Co-feed
OD_{600}	62.00 ± 3.42	52.00 ± 3.46
μ_{max} [h^{-1}]	1.66 ± 0.05 (18 - 24 h)	1.02 ± 0.01 (12 - 18 h)
pH_{min} [-]	6.27 ± 0.05	6.53 ± 0.05
$Titer_{max}$ [g L^{-1}]	53.40 ± 9.10	54.73 ± 0.32
$q_{P,max}$ [g L^{-1} h^{-1}]	0.54 ± 0.39 (193 - 216 h)	0.53 ± 0.01 (144 - 168 h)
$Y_{P/S,max}$ [mol mol^{-1}]	0.52 ± 0.01	0.53 ± 0.01
$Y_{P/S,max}$ [g g^{-1}]	0.49 ± 0.01	0.51 ± 0.01

As a next step, pulsed fed-batch experiments were performed to compare different feeding strategies using *U. maydis* MB215 Δ*cyp3* Δ*fuz7* ΔUA ΔMEL ΔP_{ria1}::P_{etef} P_{etef} mttA. Thereby, a sole glucose cultivation was compared to an acetate co-metabolization as well as to a sole acetate feed (**Figure 34**).

Differences between the cultures were observed in growth behavior. Presence of acetate in the medium negatively impacts growth rate of *U. maydis* as the sole carbon source, shows a

faster growth rate of 0.5 ± 0.02 h^{-1} compared to the other approaches (i.e., 0.43 ± 0.02 h^{-1} acetate only). Overall, a higher biomass formation was observed in the glucose feeding approach. The maximum OD_{600} value of 50.0 ± 7.8 was almost 2-fold higher than in the acetate feeding cultivation with 27.3 ± 0.9. This effect was already observed during previous experiments (**Figure 33**) and studies [91].

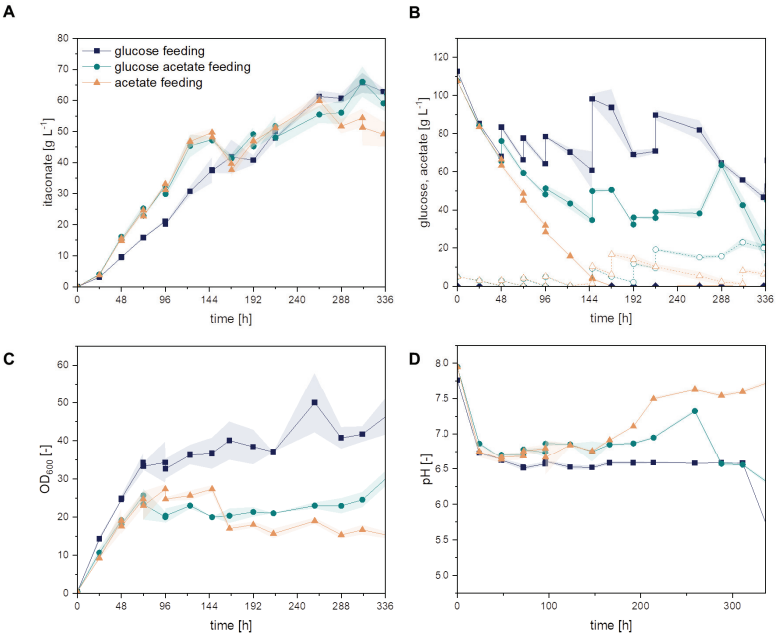

Figure 34: Pulsed fed-batch experiments of *U. maydis* MB215 Δcyp3 Δfuz7 ΔUA ΔMEL ΔP_{ria1}::P_{etef} P_{etef} mttA . *U. maydis MB215* Δcyp3 Δfuz7 ΔUA ΔMEL ΔP_{ria1}::P_{etef} P_{etef} mttA was cultivated in MTM with 33 g L^{-1} $CaCO_3$-buffer and 0.8 g L^{-1} NH_4Cl (10% filling volume, 30°C, 200 rpm). Itaconate production was displayed in (A), substrate consumption in (B), cell growth *via* OD_{600} (C) and pH (D). Glucose only cultivation was shown in blue (■), acetate co-feed in green (●) and acetate only culture in orange (▲). Feeding was added individually to keep the Glucose and acetate concentration at an equal c-molar level. Error bars depict the standard deviation of the mean (n = 3). Data associated to this figure were taken from Philipp Kohl's Master Thesis [211].

Similar to the previous cultivation experiment, culture with glucose and the mixed feed performed equally concerning itaconate production. Thereby, titers of 65.6 ± 3.2 g L^{-1} (glucose) and 66.0 ± 4.7 g L^{-1} itaconate (mixed feed) were reached respectively. In contrast, sole acetate feed resulted in a lower itaconate production of 59.9 ± 2.2 g L^{-1}. After glucose limitation in the acetate-feeding approach, no further increase in itaconate production was observed. Thus, it was not possible to confirm itaconate formation with acetate as the sole carbon source. This observation could be explained with the results obtained during ^{13}C-labeling experiments.

Thereby, no incorporated labeling was determined within the itaconate. Results once again emphasize the need for a suitable glucose and acetate co-feeding in order to boost itaconate production. During this cultivation a higher itaconate production rate was observed within the first 144 h upon glucose limitation. Acetate cultures showed a maximum production rate 0.43 g L^{-1} h^{-1}compared to of 0.28 g L^{-1} h^{-1} for sole glucose feed.

Modelling acetate co-metabolization via Design of Experiment (DoE)

In contrast to a one-factor-at-a-time (OFAT) optimization, a DoE approach allows to gain a deeper understanding of how different combinations of the following factors, i.e., glucose, sodium acetate and ammonium chloride, impact itaconate production. Itaconate production will be evaluated by the responses titer and yield. The importance of ammonium chloride for itaconate production was previously shown by Maassen *et al.* (2014), as *Ustilago* only produces itaconate under nitrogen limitation [62]. Low, medium, and high levels for each parameter (glucose, sodium acetate and ammonium chloride) included in the central composite (CCD) response surface design (RSD) are reported in **Table 13**.

Table 13: Factor levels for CCD during this study.

Factor	-1	0	+1
Glucose [g L^{-1}]	50	165	280
Sodium acetate [g L^{-1}]	3	10.5	18
Ammonium chloride [g L^{-1}]	0.8	2.4	4

The presented data (**Table 34**, appendix) display the input for the DoE models. The term 'model' represents the response, either yield or titer, as a function of glucose and acetate start concentration. Each response is based on its separate model, built with the same input data and design type, here a CCD. Thereby, the two acquired models were statistically evaluated with an ANOVA analysis (**Figure 74** and **Figure 75**, see appendix). The ANOVA analysis confirmed the calculated models to be significant, implied by the F- and R^2-values. Thereby, the established models show a R^2-value of 0.9985 for the titer and 0.9920 for yield model. **Fehler! Verweisquelle konnte nicht gefunden werden.** comprises the influence of acetate, glucose and ammonium chloride on the itaconate titer and yield visualized *via* 3D-surface diagrams (**Figure 35**).

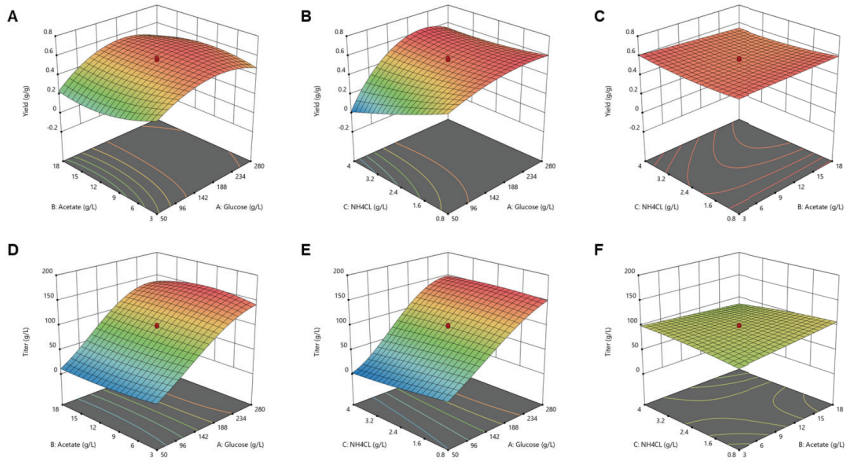

Figure 35: 3D-surface diagrams of the effect of glucose, sodium acetate and ammonium chloride on itaconate production.
A – C: itaconate yield, D-F: itaconate titer with an ammonium chloride concentration of 2.4 g L^{-1} (A, D), a sodium acetate concentration of 10.5 g L^{-1} (B, E) and a glucose concentration of 165 g L^{-1} (C, F). Red dots represent the design points of the model (filled above predicted value, transparent below predicted value). Models were established for *U. maydis* MB215 Δ*cyp3* Δ*fuz7* ΔUA ΔMEL ΔP_{ria1}::P_{etef} P_{etef}mttA. Color of the diagrams indicate predicted itaconate titer (g L^{-1} itaconate) and yield (g g^{-1}). Data associated to this figure were taken from Philipp Kohl's Master Thesis [211].

An increase in the glucose concentration is predicted to result in an increase of the itaconate titer and yield as indicated by the red color and increased area of the 3D-surface diagram. The models predicted increasing itaconate titers with rising C-source concentration which was also observed in previous work. An upper limit of glucose concentration, after which the titer drops again, was not determined within the given design space up to 280 g L^{-1} glucose and 18 g L^{-1} sodium acetate.

Further, interaction between the model factors is visualized in **Figure 36** for itaconate titer and yield. The effect of different glucose concentrations can be explained by the fact that all cultures need nitrogen limitation to induce itaconate production after an initial growth phase [62]. Microorganisms require a certain amount of glucose to build up biomass until further biomass production is impossible due to nitrogen limitation. The cultures with low glucose concentrations may have lost most of their accessible carbon into biomass resulting in only a marginal amount of remaining carbon available for itaconate production [214]. As far as the itaconate yield is concerned, the observations are similar, as low glucose concentrations equal low itaconate yields. However, the highest possible yields do not result in the highest possible glucose concentration of 280 g L^{-1}. Lower concentrations, in the range of 165 - 188 g L^{-1}, led to higher predicted yields of 0.67 g g^{-1} (predicted in combination with 2.4 g L^{-1} NH_4Cl,

Figure 36 B). In conclusion, highest itaconate titers are reached with highest glucose concentrations, but yields do not follow this trend. This optimum of glucose concentration for the yield could be attributed to higher biomass formation or increased osmotic stress. At least for batch cultivations, this sets a limit in efficiently achievable itaconate titers. Fermentations with a glucose feed could be an alternative for reaching high titers with yields above 0.6 $g_{itaconate}$ $g_{substrate}^{-1}$ avoiding osmotic stress at the beginning of the process.

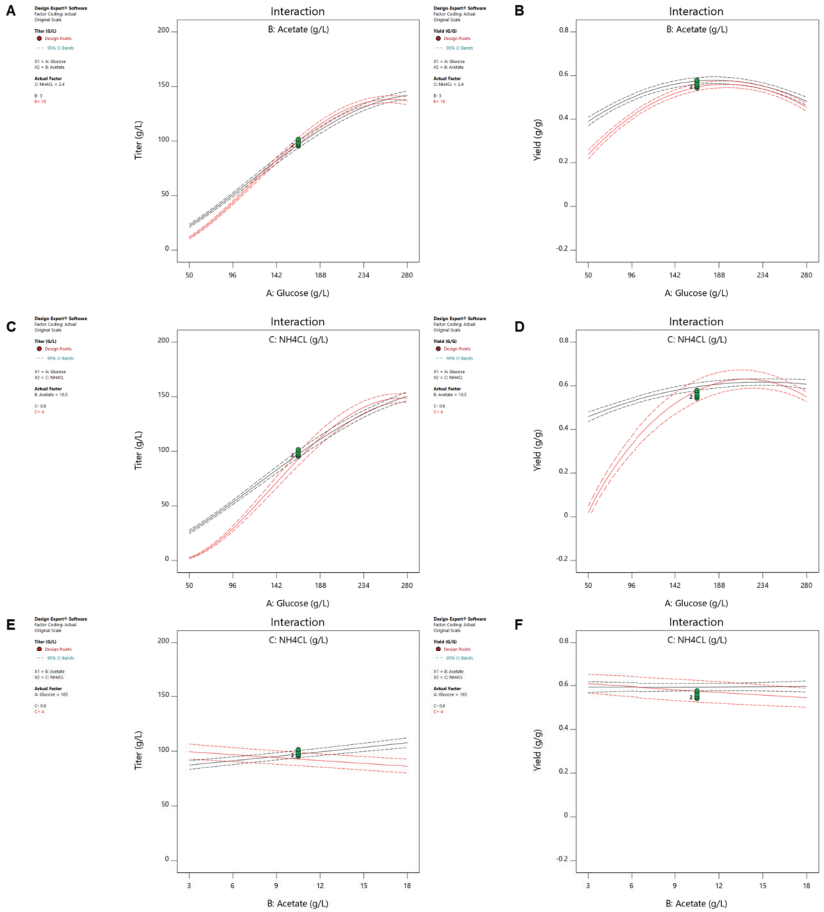

Figure 36: Interaction between glucose, sodium acetate and ammonium chloride on itaconate titer obtained *via* DoE approach.
A, B show interaction of glucose and sodium acetate for 2.4 g L^{-1} ammonium chloride. C, D show interaction of glucose and ammonium chloride for 10.5 g L^{-1} sodium acetate. E, F show interaction of ammonium chloride and sodium acetate for 165 g L^{-1} glucose condition. (A, C, E) correspond to itaconate titer model whereas (B, D, F) correspond to itaconate yield model. Data associated to this figure were taken from Philipp Kohl's Master Thesis [211].

Figure 36 E (itaconate titer model) and **F** (itaconate yield model) show the interaction of glucose and sodium acetate at an ammonium chloride concentration of 2.4 g L^{-1}. The established model predictions did not differ much within the tested range of 3 – 18 g L^{-1} acetate. This indicates that the influence of sodium acetate on itaconate production is not very prominent within the tested design space. Itaconate titers were not affected greatly by the addition of sodium acetate, possibly because the ratio glucose to sodium acetate is highly on the glucose side. Therefore, sodium acetate does not influence production greatly at comparably low concentrations (up to 18 g L^{-1}) in contrast to glucose concentrations up to 280 g L^{-1}. Nevertheless, its beneficial effect compared to sole glucose cultivations were demonstrated in previous studies and during this work in **Figure 33** [91]. Instead, the results outline that a feeding strategy may be beneficial for further investigation of acetate´s role as co-substrate.

Itaconate production gets induced upon ammonium limitation in *Ustilago*. With ammonium chloride being the sole ammonium supplier of these cultivations, it was expected that ammonium chloride concentration impacts itaconate production during DoE experiments [62]. Thereby, two different effects were observed concerning itaconate titer and yield. Itaconate titer and yield benefits from a lower ammonium chloride concentration (0.8 g L^{-1} NH_4Cl) when glucose concentrations were below 142 g L^{-1} **(Figure 36 C** and **D**). When higher glucose concentrations are applied, a concentration of 4 g L^{-1} NH_4Cl improves the predicted production compared to low ammonium chloride concentration of 0.8 g L^{-1}.

Within this work, empirical models were generated, predicting itaconate acid titers and yields within the tested design space with given starting concentrations of glucose, sodium acetate and ammonium chloride. The established models can be used to optimize the given parameters maximizing itaconate production.

Those predicted maximum production conditions were tested to verify the established models. Two numerical optimizations were performed resulting in two predictions. The best prediction for maximizing both responses, while keeping all factors in range, resulted in 280 g L^{-1} glucose, 10.3 g L^{-1} sodium acetate, 0.8 g L^{-1} ammonium chloride maximized both responses. In order to meet the approach toward a carbon reduced footprint of the process, glucose concentration was minimized for the next prediction resulting in the following conditions: 107 g L^{-1} glucose, 18 g L^{-1} sodium acetate and 0.8 g L^{-1} NH_4Cl.

The model predictions and actual values obtained during cultivation experiments are displayed in **Table 14**.

Table 14: Model validation experiments with *U. maydis* MB215 Δ*cyp3* Δ*fuz7* ΔUA ΔMEL ΔP$_{ria1}$::P$_{etef}$ P$_{etef}$mttA. ±values indicate the standard error of the mean (n = 3). Model predictions are highlighted in orange whereas the obtained parameter during cultivation experiments were displayed in black. *U. maydis* cultivations were performed in MTM with 66 g L^{-1} $CaCO_3$ buffer. Data associated to this table were taken from Philipp Kohl's Master Thesis [211].

Condition	Symbol	Titer$_{max}$ [g L^{-1}]	Y$_{P/S,max}$ [g g^{-1}]	q$_{p,max}$ [g L^{-1} h^{-1}]
280 g L^{-1} glucose 10.3 g L^{-1} acetate 0.8 g L^{-1} NH_4Cl	■	142.85 ± 4.33 145.9 ± 4.25	0.49 ± 0.01 0.61 ± 0.02	0.26
107 g L^{-1} glucose 18 g L^{-1} acetate 0.8 g L^{-1} NH_4Cl	▲	66.8 ± 0.84 72.44 ± 3.02	0.53 ± 0.01 0.57 ± 0.02	0.26

Figure 37 shows the conducted cultivation experiments for model validation.

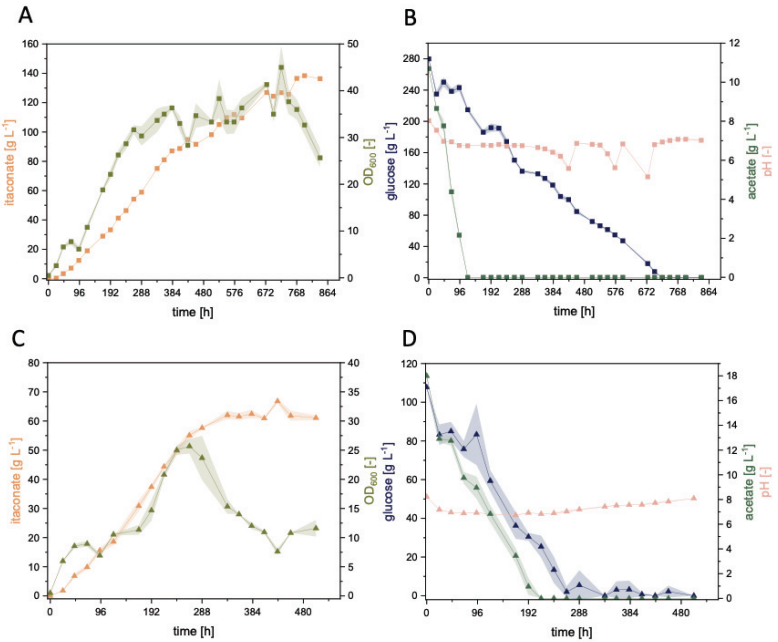

Figure 37: Model validation experiments.
Two validation conditions were tested using *U. maydis* MB215 Δ*cyp3* Δ*fuz7* ΔUA ΔMEL ΔP$_{ria1}$::P$_{etef}$ P$_{etef}$mttA in MTM with 66 g L^{-1} $CaCO_3$ as a buffer. Diagrams **a**, **b** display cultivation using 280 g L^{-1} glucose, 10.3 g L^{-1} acetate, 0.8 g L^{-1} NH_4Cl (■) whereas diagrams **c**, **d** show cultivation using 107 g L^{-1} glucose, 18 g L^{-1} acetate, 0.8 g L^{-1} NH_4Cl (▲). Color scheme is determined as the following: OD_{600} light green (●), itaconate production orange (●), glucose consumption blue (●), acetate consumption dark green (●) and pH pink (●). Error bars depict the standard deviation of the mean (n = 3). Data associated to this figure were taken from Philipp Kohl's Master Thesis [211].

Thereby, both cultivation experiments were successful for model validation as the itaconate titer and yield was obtained within the 95% confidence interval of the respective prediction. Furthermore, an itaconate titer of 142.85 ± 4.33 g L^{-1} which corresponds to a yield of 0.49 ± 0.01 g g^{-1} (68% of the theoretical maximum) was reached for the high factor concentration experiment. Both models were successfully validated during cultivation experiments. An itaconate titer of 66.8 ± 0.84 g L^{-1} and a yield of 0.53 ± 0.01 g g^{-1} (73% of theoretical maximum) was achieved with the lower substrate concentration condition. This condition showed a higher yield compared to the 280 g L^{-1} glucose approach (0.49 ± 0.01 g g^{-1}). This confirms the beneficial effect of lower initial substrate concentrations which was already observed during previous studies [65], [73], [91]. The lowered substrate concentrations reduced osmotic pressure for the cells in the beginning of the cultivation. This was evident in the production of by-products such as erythritol, malate, and succinate (**Figure 38**).

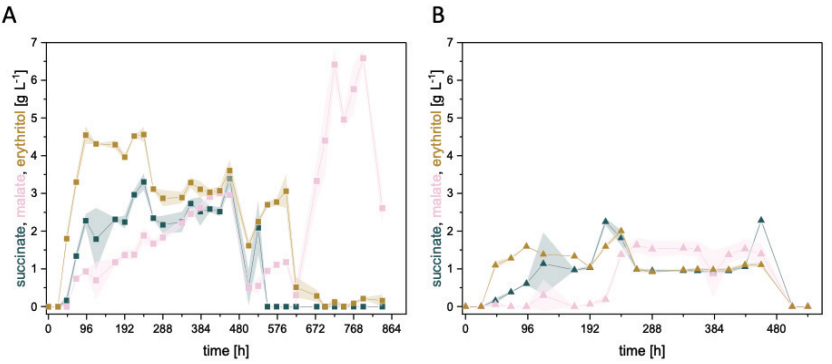

Figure 38: By-product formation during model validation experiments.
Two validation conditions were tested using *U. maydis* MB215 Δ*cyp3* Δ*fuz7* ΔUA ΔMEL ΔP_{ria1}::P_{etef} P_{etef} mttA in MTM with 66 g L^{-1} $CaCO_3$ buffer. Diagram **a** displays cultivation using 280 g L^{-1} glucose, 10.3 g L^{-1} sodium acetate, 0.8 g L^{-1} NH_4Cl (■) whereas diagram **b** shows cultivation using 107 g L^{-1} glucose, 18 g L^{-1} sodium acetate, 0.8 g L^{-1} NH_4Cl (▲). Color scheme is determined as succinate production (●), malate production (●), erythritol production (●). Error bars depict the standard deviation of the mean (n = 3). Data associated to this figure were taken from Philipp Kohl's Master Thesis [211].

The results showed clear differences of the by-product spectrum between the two tested validation conditions. Especially, erythritol is known to function as an osmotolerant. Further, it is known for Ustilaginaceae that higher glucose concentrations lead to a slower growth and osmotic stress [63]. Osmotic stress could be reduced using a lower glucose starting concentration in combination with a (continuous) fed-batch cultivation in order to further increase itaconate yield [64].

Implementing an external membrane module for itaconate production in U. maydis

Product inhibition of itaconate and toxic effects of acetate could be addressed in suitable feeding strategies and continuous process approaches within subsequent experiments focusing on process development. One approach overcoming product inhibition of itaconate demonstrates the *in-situ* precipitation using $CaCO_3$. Nevertheless, this method shows several disadvantages such as an increased viscosity during fermentation leading to a decreased oxygen supply for the cells. Alternatively, a continuous or semi-continuous process with cell recycling could help to avoid product toxicity as well, by extending the productive time of the biomass [61]. Hosseinpour Tehrani *et al.* (2019) demonstrated the advantages of a repeated batch approach with cell recycling of *U. cynodontis* [61]. This study showed that the cell recycling positively affected the product yield, which was stable across two repeated batches. However, significant lag phases and reductions in biomass and production rates indicate a high stress imposed by the centrifugation steps applied here for cell recycling.

To overcome these issues, during this work a membrane-based cell retention system was used. The general set-up of the process is shown in **Figure 39**. It represents a variation of a standard external loop layout used for processes with *Candida* [215] and *Azotobacter* [216]. Fermentation broth is pumped through the main loop, starting from the bioreactor vessel *via* the membrane and back into the vessel. Thereby, the membrane module separates cells from the soluble organic acid. A second exit on the upper right leads from the outer channel into the filtrate bottle.

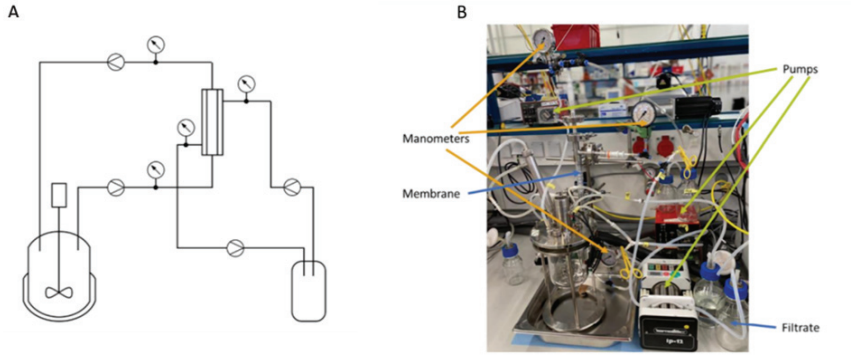

Figure 39: Membrane set-up
Schematic membrane set-up is shown in (A) with position of the pumps and manometers. The physical set-up in laboratory is visualized in (B).

Membrane was used during pulsed fed-batch bioreactor experiments shown in **Figure 40**. As starting conditions, 160 g L^{-1} glucose, 10 g L^{-1} sodium acetate and 4 g L^{-1} NH_4Cl in MTM in MES-buffer were used. A conventional pulsed fed-batch bioprocess was compared to a reactor

implementing external membrane for cell-retention and product removal. During proof-of-principle cultivation, membrane was used during certain timepoints during fermentation instead of a continuous operation (**Figure 40 A**). When removing product solution, fermenter was fed with MTM without NH_4Cl.

During reference fermentation 58.5 g L^{-1} itaconate was produced ($Y_{P/S}$ = 0.31 g g^{-1}), clearly demonstrating product inhibition in MTM without $CaCO_3$. Regardless of the excess substrate available for *U. maydis* from 200 h fermentation time, no further increase in itaconate production was observed. Due to product inhibition, a relatively low yield of 0.31 g g^{-1} was obtained (42 % theoretical maximum).

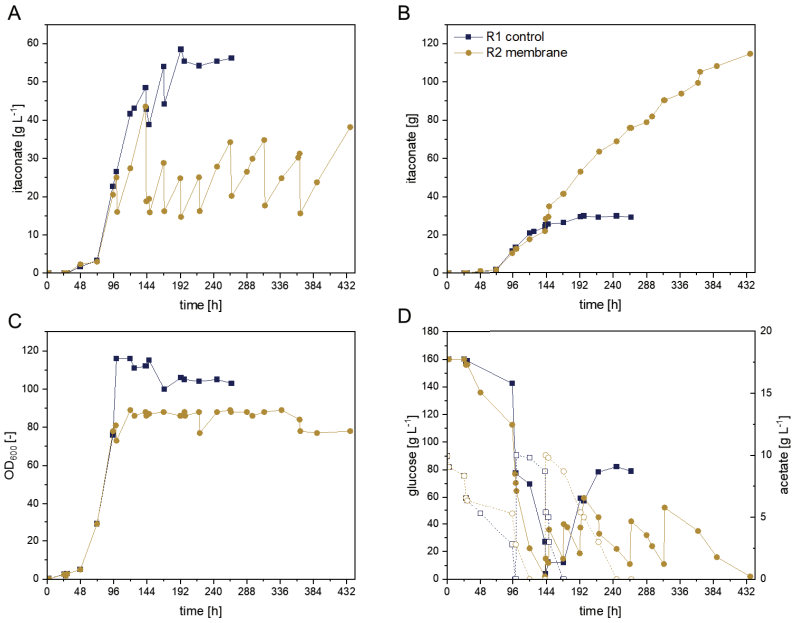

Figure 40: Pulsed fed-batch cultivation of *U. maydis* MB215 Δ*cyp3* Δ*fuz7* ΔUA ΔMEL $\Delta P_{ria1}::P_{etef}$ P_{etef} mttA incorporating external membrane module for cell retention.
Itaconate production [g L^{-1}] (A), itaconate production [g] (B), OD_{600} (C) and substrate consumption (D) a single representative fermentation in a bioreactor containing batch medium with 160 g L^{-1} glucose, 10 g L^{-1} sodium acetate, 4 g L^{-1} NH_4Cl at pH 6.5 titrated with 10 M NaOH and 1 M HCl. Color scheme is determined as reference reactor without membrane (blue, ■) whereas membrane set-up is shown in yellow (●). Acetate consumption is shown with dashed lines (D).

During bioreactor cultivation with the membrane set-up, product inhibition was avoided by removing product solution when reaching titers from 30 – 40 g L^{-1} itaconate. Thus, production of the two set-ups was compared by itaconate production in total grams. Both cultivations showed a similar production up to 144 h with a production rate of 0.31 g h^{-1}. Whereas reactor 1 (control) showed clear product inhibition, reactor 2 (membrane) further showed an increased

itaconate production with a constant production rate of 0.22 g itaconate per hour up to 357 h. Afterwards rate decrease toward 0.14 g h^{-1}. Comparing total itaconate production, bioreactor with membrane set-up produced 91.6 g itaconate, displaying a 2.9-fold increase in production. Comparing the maximum obtained OD_{600} values of both reactors, the control reactor showed a higher biomass formation. Thus, it indicates that membrane process impacts cell growth negatively.

Overall, the cell implemented membrane set-up enabling product removal and cell-retention increased the overall itaconate production as well as the product yield. However, reduction in biomass and production rates at later stages of the process indicate a high stress imposed by the repeated membrane process. To overcome these issues further optimization toward a continuous process is required.

3.2.4 Conclusion

This study demonstrates the applicability of the established metabolically engineered *U. maydis chassis* using CO_2-derived acetate co-feeding strategies toward a production process with the overall goal of a reduced carbon footprint. Within this work, a new marker-free chassis strain was developed focusing on the reduction of the *U. maydis* metabolite spectrum and simultaneously overexpressing itaconate production using CRISPR/Cas9 strategy. Acetate assimilation in *U. maydis* was investigated *via* off-gas analysis and ^{13}C-labeling.

Off-gas experiments verified that acetate as a sole carbon source did not support the growth of *U. maydis*. To test if a regulatory reason exists for the non-growth phenotype, glyoxylate was used as a co-substrate. Thereby, it was demonstrated that glyoxylate was beneficial for acetate co-metabolization. Further, itaconate production experiments indicate a positive effect of glyoxylate co-feed together with acetate as for condition 10 g L^{-1} acetate and 2 g L^{-1} glyoxylate and 0.8 gL^{-1} NH_4Cl an itaconate production of 0.15 ± 0,10 g L^{-1} was observed. The low itaconate production could be explained by the relatively high amount of nitrogen present in the medium. Thus subsequent experiments could verify the glyoxylate effect on itaconate production using acetate as a substrate for *U. maydis*. Further a triple feed of glucose, acetate and glyoxylate could be optimized during the following experiments.

^{13}C-labeling indicates that acetate will not be incorporated into itaconate production. Moreover, alternative routes have to be clarified, e.g., the use for respiration, cell maintenance, and/or energy metabolism. Subsequent experiments, e.g., using ^{13}C-labeling measuring amino acids or the use of off-gas sensors capturing ^{13}C-labeled CO_2 could contribute to that strategy.

Nevertheless, acetate showed beneficial effects on itaconate production booting *U. maydis* productivity when used as a co-feed. Higher itaconate production rates were obtained compared to sole glucose feed Further, using DoE approach acetate co-feeding strategy was optimized by establishing empirical models predicting itaconate titer and yield.

Further, economic evaluation of the process could be approached as the presented work lays the foundation for an improved itaconate production process with a potentially reduced carbon footprint.

Implementation of an external membrane module indicated high stability of the biomass, showing the potential to overcome product toxicity in a continuous itaconate production system with cell retention, especially if centrifugation steps can be avoided in the future and process parameters will be further optimized. Moreover, the membrane module could be extended with a purification step, such as adsorption chromatography, avoiding loss of substrate or other media components.

Chapter 3.3

Improved itaconate production with *U. cynodontis* via co-metabolism of CO_2-derived formate

Partially published as:

Ullmann, L., Guntermann, N., Kohl, P., Müsgens, A., Schröders, G., Franciò, G., Leitner, W., Blank, L. M. Improved Itaconate Production with *U. cynodontis via* Co-Metabolism of CO_2-Derived Formate. *J. Fungi* 2022, 8, 12. https://doi.org/10.3390/jof8121277

Contributions:

Lena Ullmann performed bioreactor cultivation experiments, analyzed the data, prepared figures, and wrote this chapter. Cultivation experiments for DoE approach were carried out by Philipp Kohl and Gereon Schröders coordinated by Lena Ullmann. Andreas Müsgens performed cultivation experiments testing alternative formate salts supervised by Lena Ullmann. Nils Guntermann performed hydrogenation experiments and provided formate product solutions used within this work. *U. cynodontis* strains were constructed by Hamed Hosseinpour Tehrani. Lars M. Blank advised on all experiments, analyzed and discussed data, and reviewed the chapter. Giancarlo Franciò and Nils Guntermann contributed to data discussion and review of this chapter.

3.3 Improved itaconate production with *U. cynodontis via* co-metabolism of CO_2-derived formate

3.3.1 Summary

In the last years, it was shown that itaconic acid can be produced from glucose with strains of the family *Ustilago* at up to maximum theoretical yield. The use of acetate and formate as co-feedstocks can boost the efficiency of itaconate production with Ustilaginaceae wild-type strains by reducing the glucose amount and thus the agricultural land required for the biotechnological production of this chemical compound.

Metabolically engineered strains (*U. cynodontis* Δ*fuz7* Δ*cyp3* $\Delta P_{ria1}::P_{etef}$ and *U. cynodontis* Δ*fuz7* Δ*cyp3* P_{etef}*mttA* $\Delta P_{ria1}::P_{etef}$) were tested for itaconate production obtaining a titer of 56.1 g L^{-1} and a yield of 0.55 $g_{itaconate}$ $g_{substrate}^{-1}$. Both improved titer (increase of 5.2 g L^{-1}) and yield (increase of 0.04) were achieved when using sodium formate as auxiliary substrate. By applying the design-of-experiments (DoE) methodology, cultivation parameters (glucose, formate and ammonium chloride concentrations) were optimized resulting in two empirical models predicting itaconate titer and yield for *U. cynodontis* Δ*fuz7* Δ*cyp3* P_{etef}*mttA* $\Delta P_{ria1}::P_{etef}$. Thereby, an almost doubled itaconate titer of 138 g L^{-1} was obtained and a yield of 0.62 $g_{itaconate}$ $g_{substrate}^{-1}$ was reached corresponding to 86% of the theoretical maximum. Further, the biphasic Ru-catalysed hydrogenation of CO_2 to formate could be integrated into the bioprocess directly using the obtained aqueous solution of formates as co-feedstock without any purification steps and demonstrating the (bio)compatibility of the two processes.

Metabolically engineered strains of *U. cynodontis* were used as host for itaconate production utilizing a solution of sodium formate obtained from CO_2 hydrogenation within a fully integrated biocompatible process as co-substrate. Optimization of the reaction conditions *via* DoE methodology allowed to improve the titer by 66 % from 83 to 138 g L^{-1} and the yield from 0.61 to 0.62 $g_{itaconate}$ $g_{substrate}^{-1}$ corresponding to 86 % of the theoretical maximum. This study outlines the great potential of *U. cynodontis* as a host for itaconate production.

3.3.2 Introduction

Itaconic acid is an attractive bio-based building-block that has the potential to act as a green substitute for many petroleum-based chemicals in the polymer industry [91]. It is an unsaturated dicarboxylic acid with two carboxy and one methylene group. The presence of these functional groups, along with a conjugated double bond, makes itaconic acid a versatile molecule with multiple applications such as styrene-butadiene rubbers, synthetic latexes, super absorbents, unsaturated polyester resins, plastics, coatings, chemical fibers, biofuels, and detergents [91].

For the last 70 years, itaconic acid is produced using *Aspergillus terreus*, reaching titers of max. 130 - 160 g L^{1} [39], [52], [217] . However, various drawbacks are associated with the use

of this native producer. For instance, it shows filamentous growth and its itaconate production is morphology-dependent. Further, it leads to comparably low yields (<0.50 $g_{itaconate}/g_{glucose}$, i.e. 69% of the maximum theoretical yield) in combination with long fermentation times (>150 h), it is sensitive to shear forces and interruption of oxygen supply [217]. All these factors limit the process efficiency and increase production costs. Indeed, the comparably high price of close to 2$ per kg holds back the broader commercial application of itaconic acid [169]. To circumvent these limitations Ustilaginaceae are sought as alternative itaconic acid production hosts with a special focus on *Ustilago maydis*. The non-filamentous native producer *U. maydis* could be suitable for industrial production as it shows the highest reported titer at laboratory scale so far (220 g L^{-1}). The increased titer was obtained through integrated metabolic and morphological engineering accompanied by process optimization and *in-situ* crystallization of itaconic acid as calcium itaconate [64]. Furthermore, the morphology of *Ustilago* can be controlled by deletion of the *fuz7* gene abolishing filamentous growth and stabilizing the yeast-like morphology [72].

During previous studies, significant improvements by strain- and process engineering were achieved and *Ustilago* strains are now available producing itaconic acid at almost maximum theoretical yield [65]. With the awareness that glucose and other carbohydrates compete for valuable resources of agricultural land, much effort has been dedicated to the search of co-feedstocks able to improve the overall process efficiency. Recently, C1 compounds got attention as microbial feedstocks as they can be readily produced out of widely available resources utilizing excess energy. Formate, in particular, can be generated effectively *via* photochemical or electrochemical reduction of carbon dioxide or by hydrogenation of CO_2 using transition metal catalysts [218]–[224]. Although formate is toxic for many organisms even in relatively small concentrations, this is not the case for *U. cynodontis*, which was found to be highly tolerant to the presence of formate in the cultivation medium [91]. Further, studies reported *U. cynodontis* as one of the best itaconate producing species in the family of the Ustilaginaceae showing relatively high *p*H tolerance in comparison to other smut fungi [4]. During previous studies, *U. cynodontis* NBRC 7530 even showed improved itaconate production with sodium formate as co-substrate in addition to glucose [91]. Sodium formate is believed to be an energy donor *via* formate dehydrogenase activity rather than a conventional carbon-source [114]. This indicates a putative role of formate as auxiliary substrate delivering energy to the organism rather than being converted into biomass or product(s) of interest [115]. Thereby, there are several different ways to order the substrates; e.g. according to the degree of reduction, the oxidation number, in respect to the available electrons and with regard to the combustion enthalpy [225]. Based on that, various substrates can be subdivided into energy-deficient and energy-excess substrates. Whereas e.g. methane, methanol and formic acid are considered as energy-excess substrates, glucose and acetic acid are energy-deficient [225]. Further, it was also shown in previous studies that the auxiliary substrate concept is suitable

to increase the biomass and/or secondary metabolite yield coefficients [114], [226]. Thus, it is assumed that formate as auxiliary substrate provide energy to the organism rather than being converted into biomass or product(s) of interest [24]. In contrast to acetate, which can directly be used as a carbon and energy source, formate co-consumption delivers extra electrons to the fungal metabolism [1].

While previous work on formate co-metabolism of Ustilaginaceae focused on wildtype strains [91], in this study we investigated several available metabolically engineered strains established by Hosseinpour Tehrani *et al.* (2019) for the itaconate production in the presence of formate [3]. By applying the design-of-experiments (DoE) methodology, cultivation parameters (glucose, sodium formate and ammonium chloride concentrations) were adjusted enabling further bioprocess optimization toward a continuous production process. Additionally, implementation of CO_2-derived formate *via* hydrogenation of CO_2 was established in this study by the direct use of the product solution as visualized in **Figure 41** [14]. Thus, using a biphasic catalytic approach [227]–[234],[235]. the tailored Ru-catalyst was “immobilized” in an apolar organic phase while the aqueous phase containing the formate salt could be used in the fermentation without any treatments. The biphasic approach not only contributes to the biocompatibility of the product solution, but also enables catalyst reusability, which is very much desirable for chemo-catalysis.

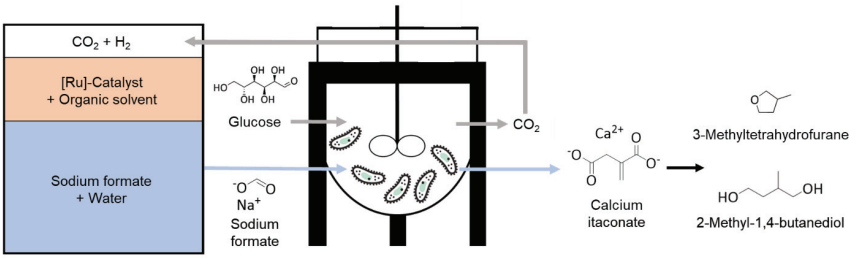

Figure 41: Schematic overview - implementing CO_2-derived formate from chemo-catalysis as co-substrate for itaconate production in biocatalysis.
Implementing CO_2-derived formate *via* hydrogenation into *Ustilago* bioprocess using glucose as a substrate. First, production of an aqueous solution of the respective formate salt in a multiphasic approach with separable and recyclable metal catalyst. The use of formate salts boosts efficiency of itaconate production by Ustilaginaceae. The obtained product solution from chemo-catalysis is directly applied as a substrate for biocatalysis. Produced itaconic acid can further be converted by chemo-catalysis e.g. into biofuels such as 3-methyl-tetrahydrofuran (3-MTHF) and 2-methyl-1,2-butanediol [136] [27].

3.3.3 Results and discussion

3.3.3.1 Investigating formate co-metabolization of metabolically engineered *U. cynodontis* strains

Previous experiments determined glucose, sodium formate and ammonium chloride (NH_4Cl) as significant factors impacting the itaconate production of *U. cynodontis* [62], [91]. Moreover, recent studies confirmed a beneficial effect of formate co-metabolization on itaconate production by testing 72 different Ustilaginaceae wildtype strains [91]. Among these, *U. cynodontis* #2705 was identified as the most promising strain metabolizing formate with 30% increase in itaconate titer (6.25 g L^{-1} sodium formate and 50 g L^{-1} glucose) in comparison to sole glucose as a carbon source [91]. In contrast to the previous work [91], this study focused on available genetically modified *U. cynodontis* strains (*U. cynodontis* Δ*fuz7* Δ*cyp3* $\Delta P_{ria1}::P_{etef}$ and *U. cynodontis* Δ*fuz7* Δ*cyp3* P_{etef}mttA $\Delta P_{ria1}::P_{etef}$) for formate co-metabolization (**Figure 42**). Thereby, the by Hosseinpour Tehrani et al (2019) metabolically engineered strain, *U. cynodontis* Δ*fuz7* Δ*cyp3* P_{etef}mttA $\Delta P_{ria1}::P_{etef}$ produced 6.5-fold more itaconate in shake flasks using glucose as a sole carbon source compared to the wildtype strain [3].

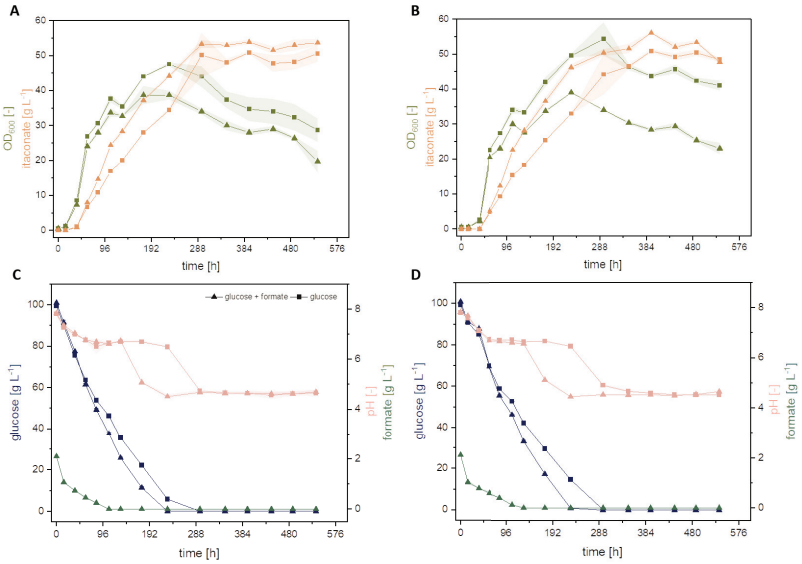

Figure 42: Formate co-metabolization of metabolically engineered *U. cynodontis* strains.
A, C display cultivation of *U. cynodontis* Δ*fuz7* Δ*cyp3* $\Delta P_{ria1}::P_{etef}$ and B, D of *U. cynodontis* Δ*fuz7* Δ*cyp3* P_{etef}mttA $\Delta P_{ria1}::P_{etef}$. Formate co-metabolization conditions are shown *via* ▲ and the respective glucose reference as ■. Color scheme is determined as OD_{600} (green), itaconate production (orange), glucose consumption (blue), sodium formate consumption (dark green), pH (light pink). Cultivations were carried out in shake flasks. MTM medium (33 g L^{-1} $CaCO_3$, 0.8 g L^{-1} NH_4Cl, 100 g L^{-1} glucose) with 0 g L^{-1} or 2 g L^{-1} sodium formate was used. Error bars depict the standard deviation of the mean (n = 3).

The addition of sodium formate had a significant impact on obtained itaconate titer and yields for both metabolically engineered strains compared to their respective glucose reference as already observed with *U. cynodontis* wildtype strains [91]. Both strains displayed 10% increase in itaconate titer during co-consumption of formate. *U. cynodontis* Δ*fuz7* Δ*cyp3* $\Delta P_{ria1}::P_{etef}$ reached a maximum itaconate titer of 50.9 ± 0.3 g L^{-1} during cultivation on glucose only and a titer of 53.9 ± 0.7 g L^{-1} with addition of sodium formate. A higher itaconate titer of 56.1 ± 0.2 g L^{-1} during sodium formate co-metabolization (2 g L^{-1}) was reached using *U. cynodontis* Δ*fuz7* Δ*cyp3* P_{etef}mttA $\Delta P_{ria1}::P_{etef}$ whereas the glucose control reached a titer of 50.9 ± 0.4 g L^{-1} itaconate. Despite the improved itaconate titers, the yield increases toward 0.55 $g_{itaconate}$ $g_{substrate}^{-1}$ (0.56 $g_{itaconate}$ $g_{glucose}^{-1}$ compared to 0.51 $g_{itaconate}$ $g_{glucose}^{-1}$).

Table 15: Itaconate production parameters during shake flask cultivations of metabolically engineered *U. cynodontis* strains.
Cultivations were carried out in shake flasks using MTM medium (33 g L^{-1} $CaCO_3$, 0.8 g L^{-1} NH_4Cl, 100 g L^{-1} glucose) with 0 g L^{-1} or 2 g L^{-1} sodium formate was applied. Error bars depict the standard deviation of the mean (n = 3). Statistically significant differences in itaconate production are indicated as * ($p < 0.05$) and ** ($p < 0.005$). Details of statistical analyses are displayed in **Table 31**, appendix.

Condition	Strain	$Titer_{max}$ [g L^{-1}]	$Y_{P/S,max}$ [g g^{-1}]	$q_{p,max}$ [g L^{-1} h^{-1}]
100 g L^{-1} glucose, 0 g L^{-1} formate, 0.8 g L^{-1} NH_4Cl	*U. cynodontis* Δ*fuz7* Δ*cyp3* $\uparrow P_{ria1}$	50.9 ± 0.3	0.51 ± 0.003	0.12
100 g L^{-1} glucose, 2 g L^{-1} formate, 0.8 g L^{-1} NH_4Cl		53.9 ± 0.7 *	0.52 ± 0.007	0.14
100 g L^{-1} glucose, 0 g L^{-1} formate, 0.8 g L^{-1} NH_4Cl	*U. cynodontis* Δ*fuz7* Δ*cyp3* P_{etef}*mttA* $\uparrow P_{ria1}$	50.9 ± 0.4	0.51 ± 0.004	0.12
100 g L^{-1} glucose, 2 g L^{-1} formate, 0.8 g L^{-1} NH_4Cl		56.1 ± 0.2 **	0.55 ± 0.001	0.14

The results indicate a beneficial effect of sodium formate on metabolically engineered strains similar to the wildtype strains tested in previous studies [91]. Nevertheless, the optimum feeding ratio of formate to glucose should be determined. Thus, a Design of Experiment (DoE) approach was used to establish regression fit models *via* response surface design to model itaconate titer and yield using the *U. cynodontis* Δ*fuz7* Δ*cyp3* P_{etef}mttA $\Delta P_{ria1}::P_{etef}$ hyper-producing strain to determine the optimum formate glucose feeding ratio potentially pushing itaconate production even further [61].

3.3.4 Optimization of formate co-metabolization *via* Design of Experiment (DoE) approach

In contrast to a one-factor-at-a-time (OFAT) optimization, a DoE approach allows to gain a deeper understanding of how different combinations of the following factors, i.e. glucose, formate and ammonium chloride, impact itaconate production. Itaconate production will be evaluated by the responses titer and yield. The importance of ammonium chloride for itaconate production was previously shown by Maassen *et al.* (2014), as *Ustilago* only produces itaconate under nitrogen limitation [62]. Based on previous studies by Hosseinpour Tehrani *et al.* (2019) and the performed shake flasks cultivation within this study, *U. cynodontis* Δ*fuz7* Δ*cyp3* P_{etef}mttA ΔP_{ria1}::P_{etef} was chosen for the following DoE experiments [72]. Low, medium, and high levels for each parameter (glucose, sodium formate and ammonium chloride) included in the central composite (CCD) response surface design (RSD) are reported in **Table 16**.

Table 16: Factor levels for CCD during this study.

Factor	-1	0	+1
Glucose [g L^{-1}]	50	165	280
Sodium formate [g L^{-1}]	2.5	8.8	15
Ammonium chloride [g L^{-1}]	0.8	2.4	4

The presented data (**Table 35**, appendix) display the input for the DoE models. The term 'model' represents the response, either yield or titer, as a function of glucose and formate start concentration. Each response is based on its separate model, built with the same input data and design type, here a CCD. Thereby, the two acquired models were statistically evaluated with an ANOVA analysis (**Figure 76**, see appendix). The ANOVA analysis confirmed the calculated models to be significant, implied by the F- and R^2-values. Thereby, the established models show a R^2-value of 0.9918 for the titer and 0.9845 for yield model. **Figure 43** comprises the influence of formate, glucose and ammonium chloride on the itaconate titer and yield visualized *via* 3D-surface diagrams.

Recently, a yield of 0.61 $g_{itaconate}$ $g_{glucose}^{-1}$ was reported displaying 84% of the theoretical maximum [64]. During DoE cultivation experiments, a yield of 0.62 $g_{itaconate}$ $g_{substrate}^{-1}$ was observed for 165 g L^{-1} glucose, 0.52 g L^{-1} sodium formate and 2.4 g L^{-1} NH_4Cl which equals 86% of the theoretical maximum.

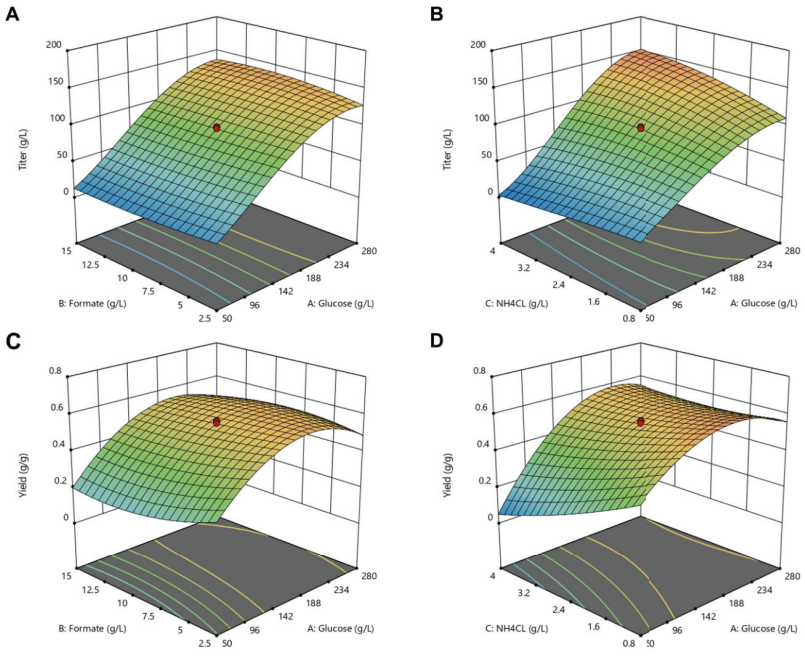

Figure 43: 3D-surface diagrams of the effect of glucose, formate and ammonium chloride on itaconate production.
A – B: itaconate titer, C-D: itaconate yield with a sodium formate concentration of 8.8 g L^{-1} (B, D) and an ammonium chloride concentration of 2.4 g L^{-1} (A, C). Red dots represent the design points of the model (filled above predicted value, transparent below predicted value). Models were established for *U. cynodontis* Δ*fuz7* Δ*cyp3* P_{etef}mttA ΔP_{ria1}::P_{etef}. Color of the diagrams indicate predicted itaconate titer (g L^{-1} itaconate) and yield (g g^{-1}).

An increase in the glucose concentration is predicted to result in an increase of the itaconate titer and yield as indicated by the red color in the heat-map and increased area of the 3D-surface diagram. The models predicted increasing itaconate titers with rising C-source concentration which was also observed in previous work (**Figure 43 A-B**). An upper limit of glucose concentration, after which the titer drops again, was not determined within the given design space up to 280 g L^{-1} glucose and 15 g L^{-1} sodium formate.

Further, interaction between the model factors is visualized in **Figure 44** and **Figure 45** for itaconate titer and yield. The effect of different glucose concentrations can be explained by the fact that all cultures need nitrogen limitation to induce itaconate production after an initial growth phase [236]. A certain amount of glucose is used to build up biomass until further biomass production is impossible due to nitrogen limitation. The cultures with low glucose concentrations may have lost most of their accessible carbon into biomass resulting in only a marginal amount of remaining carbon available for itaconate production [214].

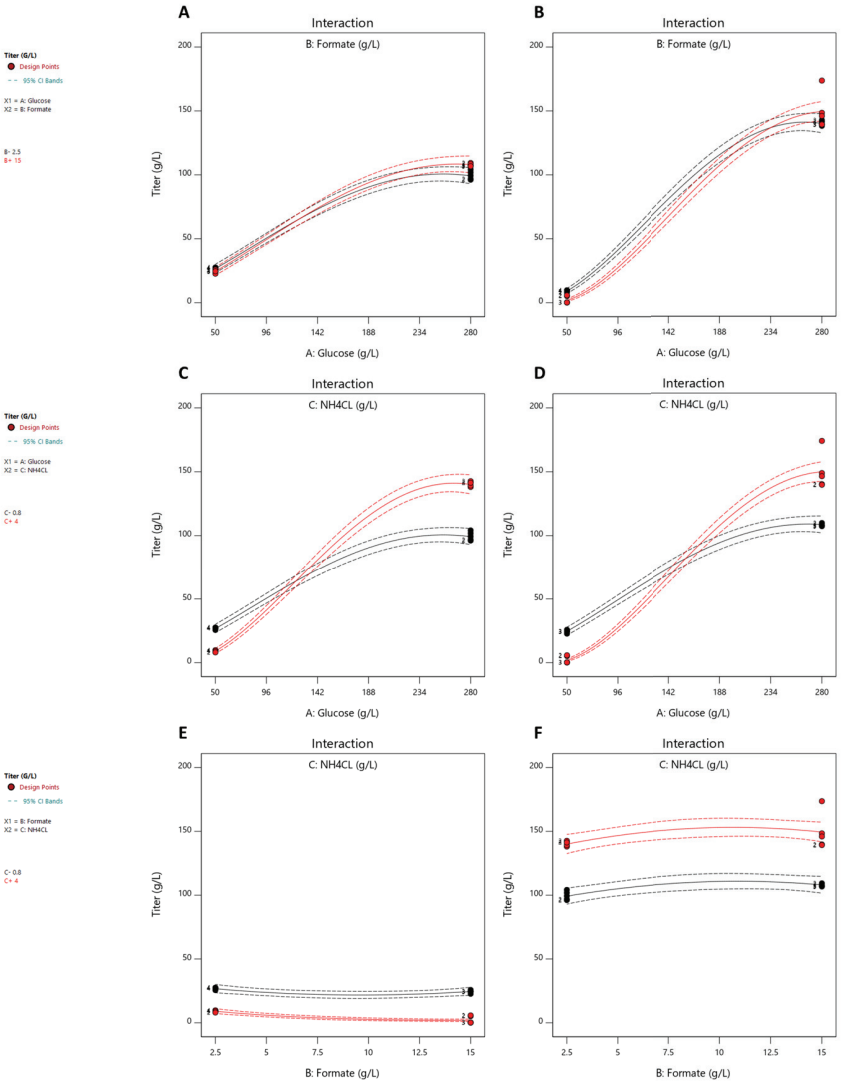

Figure 44: Interaction between glucose, formate and ammonium chloride on itaconate titer obtained *via* DoE approach.

A, B shows interaction of glucose and formate for A: 0.8 g L^{-1} and B: 4 g L^{-1} ammonium chloride concentrations. C, D shows interaction of glucose and ammonium chloride for C: 2.5 g L^{-1} and D: 15 g L^{-1} formate concentrations. E, F shows interaction of formate and ammonium chloride concentration for E: 50 g L^{-1} and F: 280 g L^{-1} glucose concentrations.

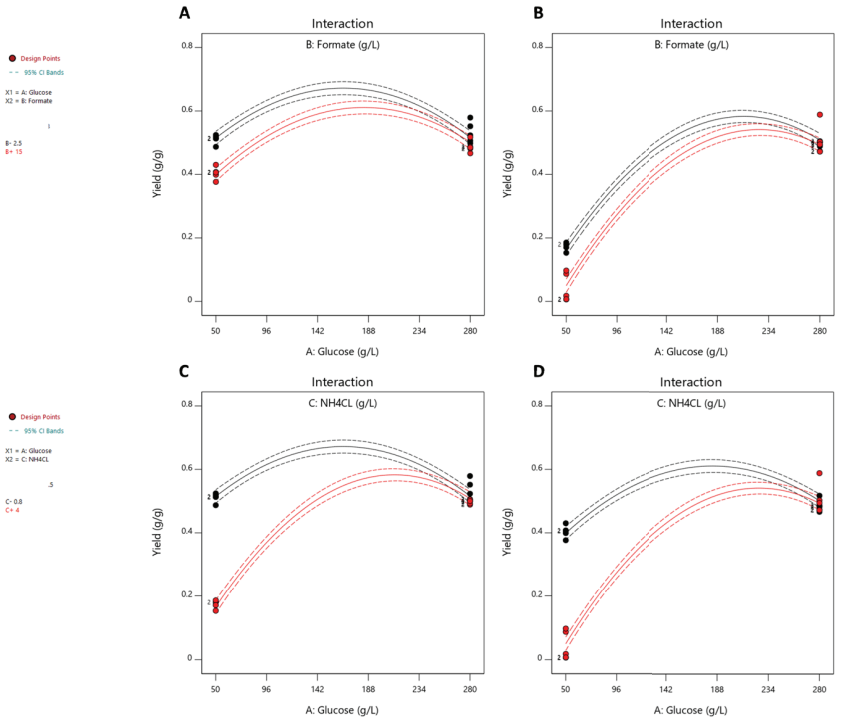

Figure 45: Interaction between glucose, formate and ammonium chloride on itaconate yield obtained *via* DoE approach.
A, B shows interaction of glucose and formate for A: 0.8 g L^{-1} and B: 4 g L^{-1} ammonium chloride concentrations. C, D shows interaction of glucose and ammonium chloride for C: 2.5 g L^{-1} and D: 15 g L^{-1} formate concentrations.

Thereby, the observations are similar for the yield, as low glucose concentrations equal low itaconate yields. However, the highest possible yields do not result in the highest possible glucose concentration of 280 g L^{-1}. Lower concentrations, in the range of 165 g L^{-1}, led to higher predicted yields of 0.67 g g^{-1} (predicted in combination with 2.5 g L^{-1} sodium formate and 0.8 g L^{-1} NH_4Cl, **Figure 46** and **Figure 47**). In conclusion, highest itaconate titers are reached with highest glucose concentrations, but yields do not follow this trend. This optimum of glucose concentration for the yield could be attributed to higher biomass formation or increased osmotic stress. At least for batch cultivations, this sets a limit in efficiently achievable itaconate titers. Fermentations with a glucose feed could be an alternative for reaching high titers with yields above 0.6 $g_{itaconate}$ $g_{substrate}^{-1}$ avoiding osmotic stress at the beginning of the process.

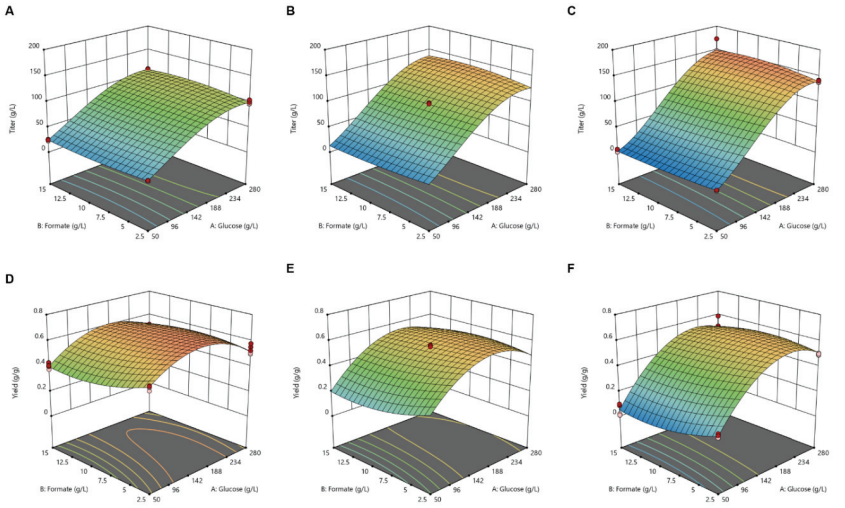

Figure 46: 3D-surface diagrams of the effect of glucose, formate and ammonium chloride on itaconate production.
A – C: itaconate titer, D-F: itaconate yield with varying ammonium chloride concentrations (A, D: 0.8 g L^{-1}; B, E: 2.4 g L^{-1}; E, F: 4 g L^{-1}). Red dots represent the design points of the model (filled above predicted value, transparent below predicted value). Models were established for *U. cynodontis* Δ*fuz7* Δ*cyp3* P_{etef}mttA ΔP_{ria1}::P_{etef}. Color of the diagrams indicate predicted itaconate titer (0.068 173.61 g L^{-1} itaconate) and yield (0.00354798 0.755284 g g^{-1}).

Figure 46 A and **B** show the interaction of glucose and sodium formate concentration for conditions of **A** i.e. 0.8 g L^{-1} and 4 g L^{-1} ammonium chloride. It can be observed that the established model for itaconate titer did not differ much between the tested range of 2.5 and 15 g L^{-1} formate, indicating that the influence of formate on itaconate titer is not very prominent within the tested design space. Itaconate titers were not affected greatly by the addition of sodium formate, possibly because the ratio glucose to sodium formate is highly on the glucose side. Therefore, sodium formate does not influence production greatly at comparably low concentrations (up to 15 g L^{-1}) in contrast to glucose concentrations up to 280 g L^{-1}.
Nevertheless, the darkest areas concerning itaconate titers are shown in a range between 5 to 15 g L^{-1} sodium formate (**Figure 47 B, C**). In contrast, in **Figure 46** and **Figure 47 D-F** it is shown that lower sodium formate concentrations are beneficial compared to higher concentrations concerning itaconate yield as darker areas can be found in this range. Within the tested design space, sodium formate did not show a great influence on itaconate production. Nevertheless, its beneficial effect compared to sole glucose cultivations were shown in **Figure 42** by a 10% increased itaconate titer. Instead, the results outline that a feeding strategy may be beneficial for further investigation of formate´s role as co-substrate.

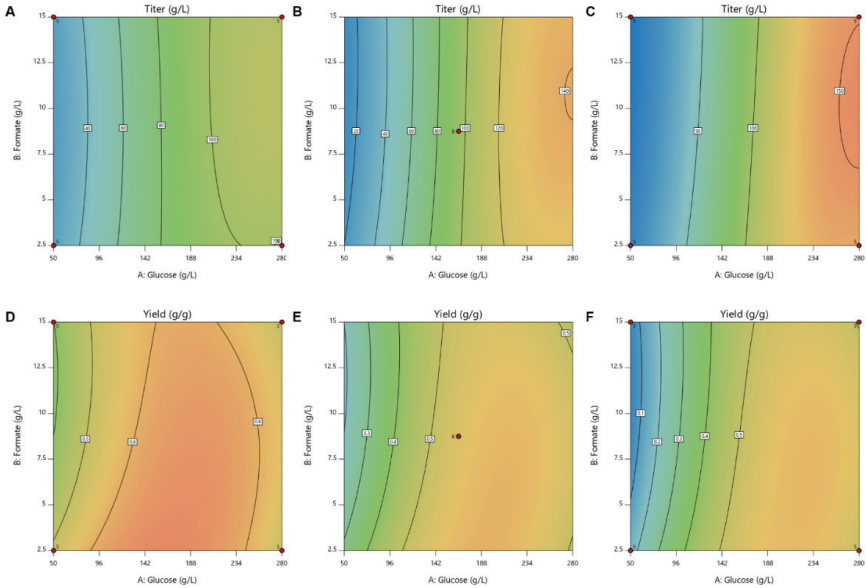

Figure 47: Heatmap diagrams of the effect of glucose, formate and ammonium chloride on itaconate production.
A – C: itaconate titer, D-F: itaconate yield with varying NH_4Cl concentrations (A, D: 0.8 g L^{-1}; B, E: 2.4 g L^{-1}; E, F: 4 g L^{-1}). Red dots represent the design points of the respective model. Models were established for *U. cynodontis* Δ*fuz7* Δ*cyp3* P_{etef}mttA ΔP_{ria1}::P_{etef}.

As itaconate production gets induced upon ammonium limitation and with ammonium chloride being the sole ammonium supplier of these cultivations, it was expected that ammonium chloride concentration impacts itaconate production during DoE experiments [62]. Thereby, two different effects were observed concerning itaconate titer and yield. Itaconate titer benefits from a lower ammonium chloride concentration (0.8 g L^{-1} NH_4Cl) when glucose concentrations were below 142 g L^{-1} (**Figure 44 C** & **D**). When higher glucose concentrations are applied, a concentration of 4 g L^{-1} NH_4Cl improves the predicted titers compared to low ammonium chloride concentration of 0.8 g L^{-1}. As far as the itaconate yield is concerned, lower ammonium chloride concentrations were beneficial for glucose concentrations higher than 234 g L^{-1} (**Figure 45**). In conclusion, low ammonium chloride concentrations are predicted to result in the highest possible itaconate titers for lower glucose concentrations and itaconate yields independent of the glucose level. However, one drawback of low ammonium chloride concentrations is the slow growth and therefore slow volumetric production rate [62].

To sum up, empirical models were generated, which can predict itaconate acid titers and yields within the tested design space with given starting concentrations of glucose, formate and ammonium chloride. During these experiments' different combinations of these three substrates were used to gain underlaying data so that the models can accurately predict titer

and yields for *U. cynodontis*. The established models can be used to optimize the given parameters maximizing itaconate production.

Those predicted maximum production conditions were tested to verify the established models. Two numerical optimizations were performed resulting in two predictions. The best prediction for maximizing both responses, while keeping all factors in range, resulted in 238.8 g L^{-1} glucose, 9.35 g L^{-1} sodium formate, 3.5 g L^{-1} ammonium chloride maximized both responses. In order to meet the approach toward a carbon reduced footprint of the process, glucose concentration was minimized for the next prediction resulting in the following conditions: 95.2 g L^{-1} glucose, 2.5 g L^{-1} sodium formate and 0.8 g L^{-1} NH_4Cl.

The model predictions and actual values obtained during cultivation experiments are displayed in **Table 17**. **Figure 48** shows the conducted cultivation experiments for model validation. Thereby, both cultivation experiments were successful for model validation as the itaconate titer and yield was obtained within the 95% confidence interval of the respective prediction. Furthermore, an itaconate titer of 138.2 ± 7.0 g L^{-1} was reached for the high factor concentration experiment, which displays the highest published titer for *U. cynodontis* so far [61]. The previously reported titer of 82.9 ± 0.8 g L^{-1} was improved upon DoE optimization (**Table 35**, see appendix) by implementing *in-situ* product removal of itaconate by calcium salt precipitation as previously shown by Hosseinpour Tehrani *et al.* (2019) [64]. During both validation experiments a yield of 0.55 ± 0.1 g g^{-1} was achieved, which is 76% of the theoretical maximum pathway yield [65]. Excluding sodium formate from the yield calculation under assumption of the auxiliary substrate concept a yield of 0.57 ± 0.1 $g_{itaconate}$ $g_{glucose}^{-1}$ was achieved.

Table 17: Model validation experiments with *U. cynodontis* Δ*fuz7* Δ*cyp3* P_{etef}mttA ΔP_{ria1}::P_{etef}.

Condition	Symbol	$Titer_{max,predicted}$ [g L^{-1}]	$Titer_{max}$ [g L^{-1}]	$Y_{P/S,max,predicted}$ [g g^{-1}]	$Y_{P/S,max}$ [g g^{-1}]	$q_{p,max}$ [g L^{-1} h^{-1}]
238,8 g L^{-1} glucose, 9.35 g L^{-1} formate, 3.5 g L^{-1} NH_4Cl	■	141.9 ± 8.6	138.2 ± 7.0	0.57 ± 0.1	0.55 ± 0.1	0.22
95.2 g L^{-1} glucose, 2.5 g L^{-1} formate, 0.8 g L^{-1} NH_4Cl	▲	50.1 ± 5.1	52 ± 3.3	0.56 ± 0.1	0.55 ± 0.1	0.11

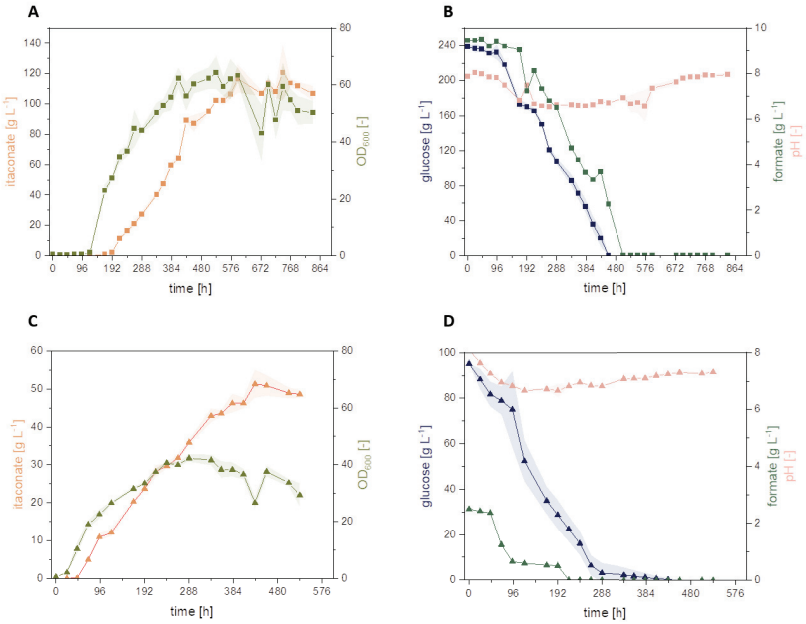

Figure 48: Model validation experiment.
Two validation conditions were tested in shake flask cultivation using *U. cynodontis* Δ*fuz7* Δ*cyp3* P_{etef}mttA ΔP_{ria1}::P_{etef}. A, B display cultivation using 238,8 g L^{-1} glucose, 9.35 g L^{-1} sodium formate, 3.5 g L^{-1} NH_4Cl (■) whereas C, D show cultivation using 95.2 g L^{-1} glucose, 2.5 g L^{-1} sodium formate, 0.8 g L^{-1} NH_4Cl (▲). Color scheme is determined as OD_{600} (light green), itaconate production (orange), glucose consumption (blue), sodium formate consumption (dark green), pH (light pink). Cultivations were carried out in shake flasks following (section 4.1). MTM medium with 66 g L^{-1} $CaCO_3$ was used. Error bars depict the standard deviation of the mean (n = 3).

3.3.5 Implementing CO_2-derived formate

The implementation of CO_2-derived formate obtained *via* catalytic hydrogenation into the existing bioprocess was investigated. As a formate salt and not “free” formic acid is used in fermentation and a base is needed to shift the endergonic hydrogenation of CO_2 to formic acid, the combination of these two processes represents a win-win situation. Thereby a biphasic catalytic system was envisaged, with a homogeneous Ru-catalyst residing preferentially in an apolar organic phase. The aqueous solution containing the formate should be used directly in the fermentation preferably without any purification steps. Moreover, this approach allows facile reusability of the metal catalyst.

During a first step, six different formate salts were tested to find the one with the best initial biocompatibility and highest itaconate production. The bases show a beneficial effect on carbon capture strategies to produce formate in a CO_2 hydrogenation process [160]. Therefore,

the following bases were tested as equimolar solutions of base and formic acid during this work: diethanolamine (DEA), methyl diethanolamine (MDEA), ethanolamine, triethylamine, arginine and ammonia. Sodium formate, which was used in all previous experiments, served as a reference [91].

First, tolerance of *U. cynondontis* #2705 wild-type strain was determined in a range from 9-18 g L^{1} (200 – 400 mM) of the respective base-formate salt (**Figure 49**).

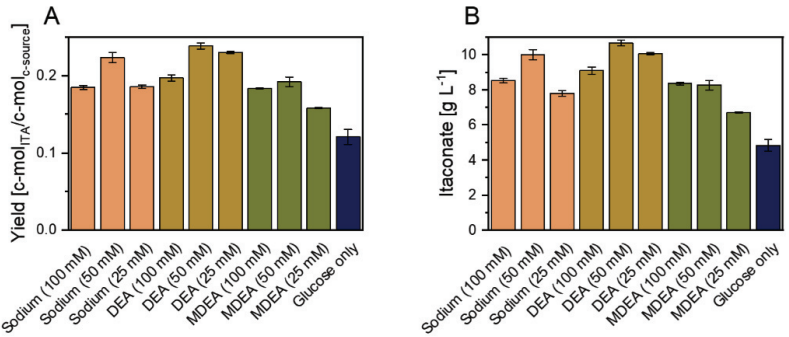

Figure 49: Itaconate production using alternative formate salts.
Itaconate yield [C-mol$_{Itaconate}$/C-mol$_{c\text{-}source}$], (B) titer [g L^{-1}] during itaconate production experiments. Experiments were performed using *U. cynodontis* #2705 wild-type strain in the Growth Profiler (30 °C, 225 rpm, 50 mm throw, start OD 0.5) in 24-well plates filled with 1.5 mL MTM (100 mM MES pH 6.5, 50 g L^{-1} glucose, 0.8 g L^{-1} NH_4Cl). Sodium formate (orange), DEA formate (yellow) or MDEA formate (green) were added in concentrations of 100 mM, 50 mM or 25 mM. A glucose-only (blue) condition was included for reference. Error bars indicate the standard deviation of the mean (n = 2).

The highest tolerance was observed for MDEA, DEA, ammonium and sodium formate. Formate salts with a negative impact on fungal growth were excluded for subsequent experiments on itaconate production (**Figure 50**).

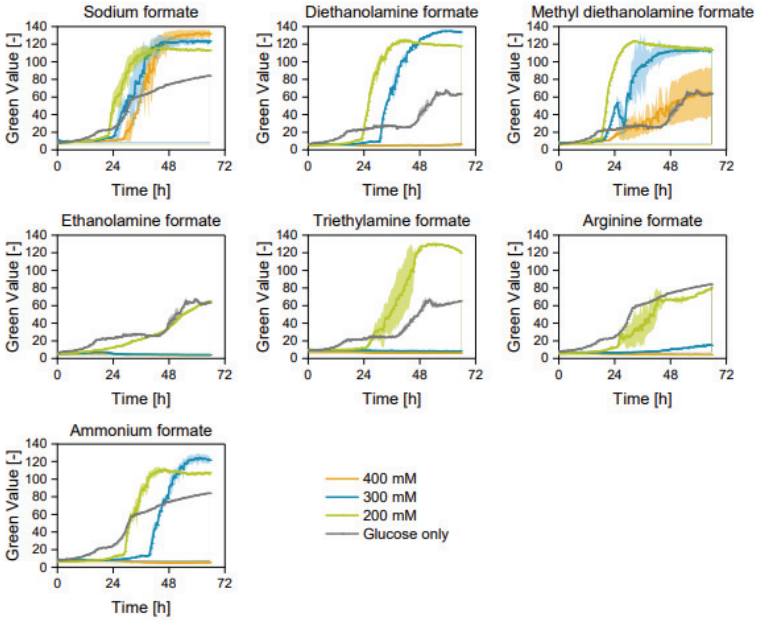

Figure 50: Overview of growth experiments of *U. cynodontis* #2705 using alternative formate sources. Summary of Growth Profiler cultivations of *U. cynodontis* NBRC 7530 (#2705) in the presence of seven different formate sources. Experiments were performed in 24-well plates filled with 1.5 mL MTM (100 mM MES pH 6.5, 50 g L^{-1} glucose, 0.8 g L^{-1} NH_4Cl) testing formate concentrations of 400 mM (orange), 300 mM (blue) and 200 mM (green). As a reference 50 g L^{-1} glucose-only is shown in grey. Cultivations were performed at 30°C (225 rpm, 50 mm throw) with a start OD_{600} of 0.5. Error bars indicate the standard deviation of the mean (n = 2).

Obtained growth curves are shown in **Figure 51** whereby no substantial differences between the tested conditions were observed regarding growth behavior. Itaconate production is displayed in **Figure 49** with further production parameters such as pH, OD_{600} and by-product formation being visualized in **Figure 52**. Addition of 50 mM DEA and sodium showed highest itaconate production whereas all conditions performed better compared to the glucose reference. Cultivation with 50 mM DEA formate showed maximum titer of 10.7 ± 0.2 g L^{-1} and a yield of 0.24 ± 0.00 C-$mol_{itaconate}$/C-$mol_{c\text{-}source}$. In comparison to the glucose-only control, yields and titers were doubled.

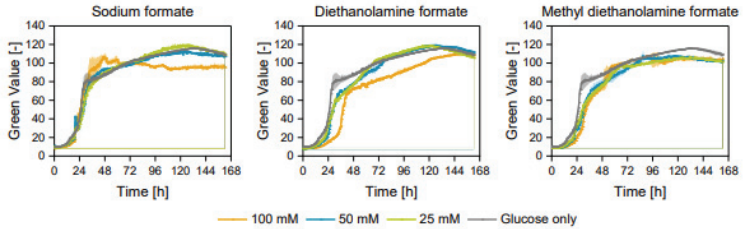

Figure 51: Growth behavior of *U. cynodontis* #2705 during itaconate production test.
The growth curves for the itaconate productions tests for three different formate salts are shown during Growth Profiler cultivation (start OD_{600} 0.5, 24-well format, 1.5 mL per well, 225 rpm, 50 mm throw). The formate salts were added to MTM (100 mM MES pH 6.5, 50 g L^{-1} glucose, 0.8 g L^{-1} NH4Cl) in concentrations of 100 mM (orange), 50 mM (blue), 25 mM (green). A glucose-only (grey) condition was included for reference. Error bars indicate the standard deviation of the mean (n = 2).

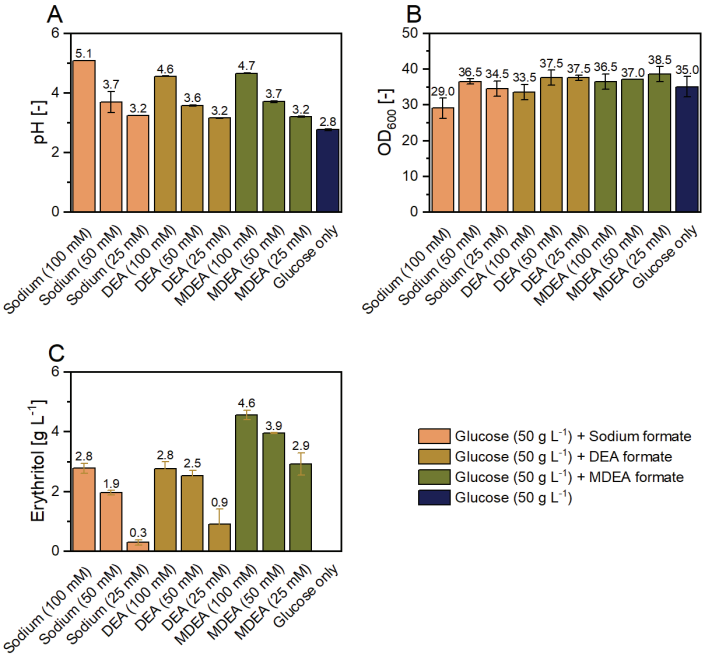

Figure 52: Itaconate production using different formate salts.
(A) Minimum pH [-], (B) maximum optical density (OD_{600} [-]), and (C) maximum erythritol levels [g L^{-1}] during itaconate production tests. Experiments were performed in the Growth Profiler (30 °C, 225 rpm, 50 mm throw, start OD 0.5) in 24-well plates filled with 1.5 mL MTM (100 mM MES pH 6.5, 50 g L^{-1} glucose, 0.8 g L^{-1} NH_4Cl). Sodium formate (orange), DEA formate (yellow) or MDEA formate (green) were added in concentrations of 100 mM, 50 mM or 25 mM. A glucose-only (blue) condition was included for reference. Error bars indicate the standard deviation of the mean (n = 2).

To sum up, this production test showed that DEA formate is suitable to replace sodium formate without adverse effects on itaconic acid production. Nevertheless, DEA shows toxicological

and ecotoxicological properties, harming for example aquatic species [237] Since there was only a minor improvement compared to the sodium salt, all further experiments were done utilizing the sodium salt as a formate source.

To enable implementation, the biocompatibility of various organic solvents with *U. cynodontis* cultivation experiments was verified, whereby the toxicity in combination with the cross-solubility in water is the major issue. Aqueous solutions saturated with nine different solvents (anisole, ethylacetate, 2-MTHF, *n*-dodecanol, *n*-octanol, *n*-tetradecane, *n*-hexanol, octylacetate, toluene) were tested for growth using the *U. cynodontis #2705* wild-type strain in hungate tubes (**Figure 53**).

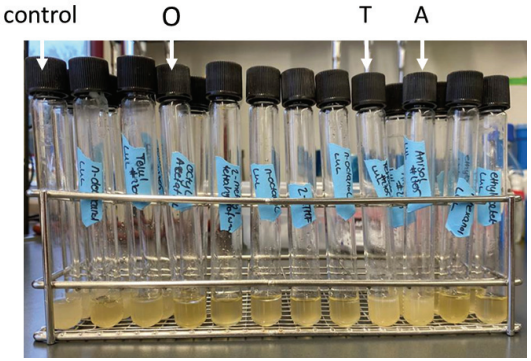

Figure 53: Organic solvent tolerance test in *U. cynodontis* #2705.
Experiment was performed using 2 ml YEP-medium, 4 gL-1 glucose in addition of 100 µl solvent (n=2). Control without addition of solvent is displayed on the left. Growth was evaluated based on cultures turbidity. Thereby, ocytlacetate (O), anisol (A) and tetradecane (T) were selected for subsequent experiments.

Thereby, octylacetate, anisole and tetradecane were selected for subsequent experiments as these three solvents showed the strongest growth based on cultures turbidity, very comparably with the growth observed in a solvent free reference solution.

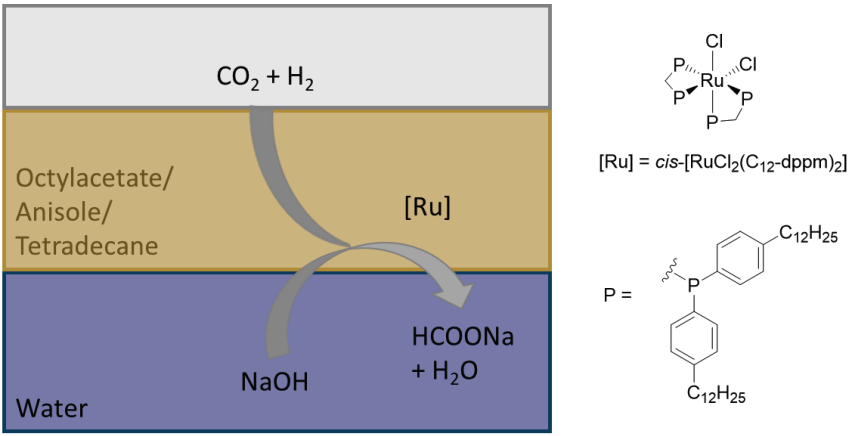

Figure 54: Schematic depiction of the biocompatible, multiphasic system for catalytic conversion of CO_2 and H_2 to sodium formate.

The complex *cis*-[$RuCl_2dppm_2$] (dppm = bis-diphenylphosphino methane) is a well-established catalyst promoting the CO_2 hydrogenation to formate [238]. To ensure good solubility and high retention of the Ru-catalyst in the selected very apolar organic phase, a lipophilic variant of the dppm ligand, the bis(bis(4-dodecylphenyl)phosphanyl)methane (C_{12}-dppm), tagged with apolar C_{12} alkyl chains at the phenyl rings was used [229].With sodium formate chosen as formate source and the three mentioned solvents as candidates for the catalyst phase, in the next step real product solutions from catalytic hydrogenation of CO_2 were generated as described in the experimental section and depicted in **Figure 54**. The 1 M NaOH solution in water was saturated with CO_2 simulating gas-scrubbing. The pressure was then released, H_2 was added and the dissolved CO_2 was converted to 0.78-0.81 M solutions of sodium formate corresponding to 53-55 g L^{-1}as determined by quantitative ^{1}H-NMR. The progress of the reaction was observed through the recorded pressure drop curves (**Figure 55**). As gaseous H_2 is consumed and converted into the dissolved formate, the pressure decreases and a constant pressure indicates completion. Furthermore, the reusability of the catalyst phase was demonstrated for tetradecane, anisole and octylacetate (**Figure 55**).

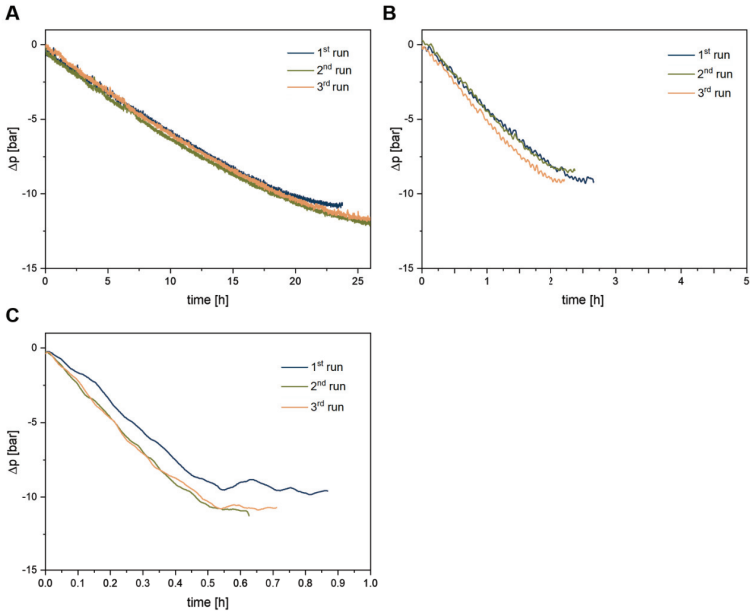

Figure 55: Pressure-drop curve of with A: tetradecane, B: octylacetate and C: anisole as catalyst phase. Reaction conditions: 3 mL of 1 M NaOH solution saturated with CO_2, 60 bar H_2, 1 µmol [Ru] in 2 mL solvent, 70 °C.

Consistent amounts of sodium formate were obtained, also indicated by a similar total pressure drop of 10 bar. However, the reaction velocity differs strongly depending on the used solvent with completion for anisole after 0.5 h, for octylacetate after 2 h and for tetradecane after 25 h. Thus, the choice of the solvent not only influences biocompatibility, but also the speed of the chemical reaction and hence its efficiency. Still, the major goal was to find a biocompatible product solution, which was examined next.

In a subsequent shake-flask cultivation experiment with direct implementation of the product solutions the itaconate production was investigated using the metabolically engineered *U. cynodontis* Δ*fuz7* Δ*cyp3* P_{etef}mttA ΔP_{ria1}::P_{etef} strain displayed in **Figure 56** and **Table 18**. Based on previous cultivations, the product solutions were adjusted to a final formate concentration of 2 g L^{-1} in the cultivation medium and 50 g L^{-1} glucose was used as a substrate. A prolonged lag phase compared to the previous conditions was observed. This effect could be avoided by adding them to the respective pre-culture. The highest itaconate titer of 36.7 ± 0.1 g L^{-1} and 34.3 ± 0.1 g L^{-1} were achieved with addition of a product formate solution obtained with tetradecane and anisole as catalyst phase, respectively. Thus, the direct use of product solutions originated from the devised biphasic CO_2 hydrogenation did not result in a decreased itaconate production confirming the biocompatibility of the overall process. No significant impact was observed on cell growth (**Figure 56 B**).

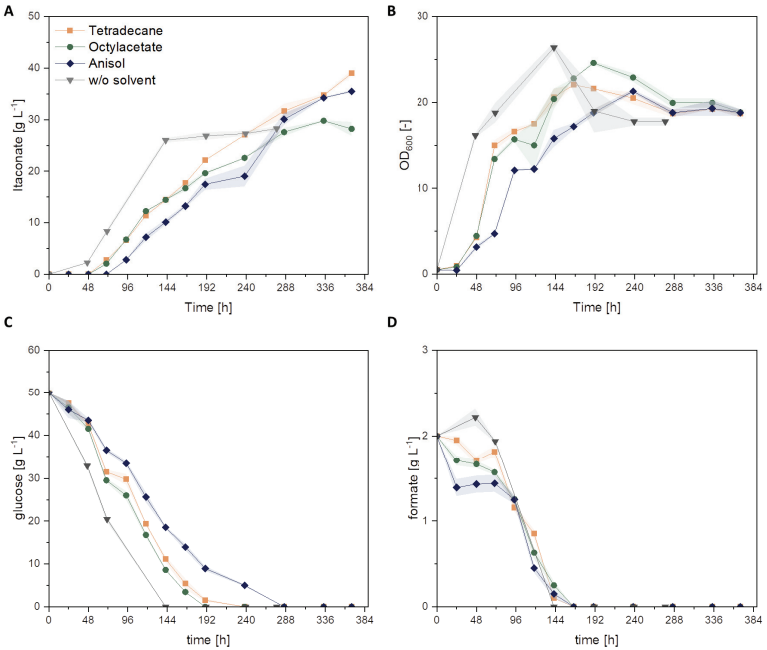

Figure 56: Tolerance of *U. cynodontis* Δ*fuz7* Δ*cyp3* P_{etef}mttA ΔP_{ria1}::P_{etef} toward solvent contamination. (A) itaconate production, (B) growth *via* OD_{600}, (C) glucose consumption and (D) formate concentration. Cultivation was performed with 10% filling volume (50 mL) in addition of 1 mL organic solvent using MTM medium with 50 g L^{-1} glucose, 2 g L^{-1} formate, 0.8 g L^{-1} NH_4Cl. Solvents: tetradecane (■ yellow), octylacetate (● green), anisole (♦ blue) and reference (no solvent, (▼grey). Cultivations were carried out in shake flasks following (section 4.1). 33 g L^{-1} $CaCO_3$ was used as buffer system. Error bars depict the standard deviation of the mean (n = 3).

Based on shake-flask cultivation experiments, utilization of sodium formate produced in the catalytic hydrogenation with tetradecane as catalyst phase was further examined during a controlled fed-batch bioreactor experiment (**Figure 57**). Thereby, culture starting conditions were optimized using the established model. This led to similar itaconate production (**Figure 57 A**) of 63.3 g L^{-1} with commercial sodium formate and 64.2 g L^{-1} itaconate with CO_2-derived formate with tetradecane as catalyst phase in fed-batch experiments. Surprisingly, the latter cultivations showed a higher yield of 0.66 $g_{itaconate}$ $g_{substrate}^{-1}$ compared to 0.57 g g^{-1} using commercially available sodium formate.

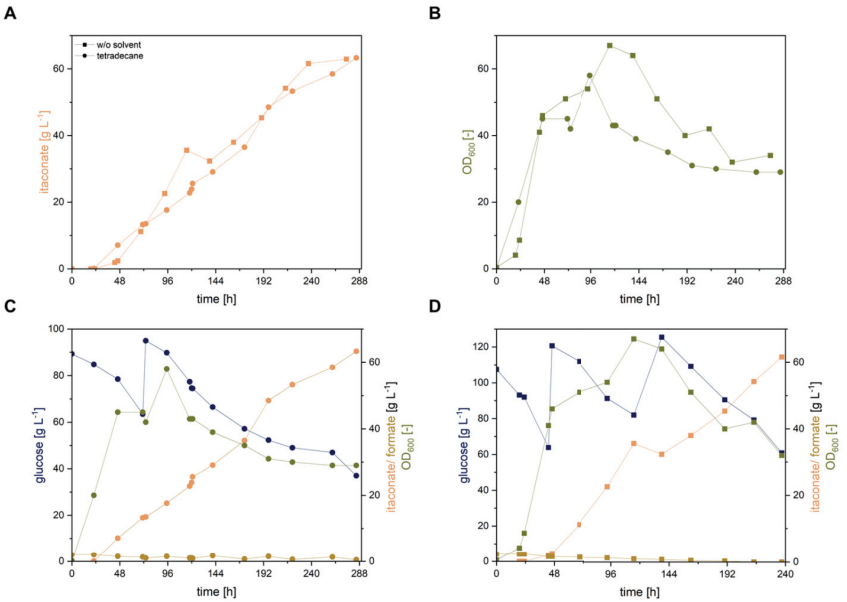

Figure 57: Itaconate production in pulsed fed-batch bioreactor using commercially available sodium formate and formate solutions obtained from biphasic CO_2 hydrogenation (catalyst phase: tetradecane). *U. cynodontis* Δ*fuz7* Δ*cyp3* P_{etef}mttA ΔP_{ria1}::P_{etef} was used in these experiments. (A) itaconate production, (B) growth *via* OD_{600}, (C) process parameters of cultivation with catalytic product (●) and (D) cultivation with commercial sodium formate (■). Cultivation was performed with a controlled bioreactor set-up (500 mL filling volume) using MTM medium with 100 g L^{-1} glucose, 4 g L^{-1} sodium formate, 3.5 g L^{-1} NH_4Cl and MES buffer. pH was controlled at 6.5 *via* addition of NaOH and HCl (30°C, 80% DO, n = 1). Color scheme is determined as itaconate (orange), OD_{600} (green), glucose (blue) and formate concentration (yellow).

Table 18: Itaconate production with formate solutions from CO_2-hydrogenation experiments.
Strain *U. cynodontis* Δ*fuz7* Δ*cyp3* $\Delta P_{ria1}::P_{etef}$ + mttA ± Values indicate the standard error of the mean (n = 3). Symbols refer to conditions shown in **Figure 56** and **Figure 57**.

Condition	Solvent	Symbol	$Titer_{max}$ [g L^{-1}]	$Y_{P/S,max}$ [g_{ITA} g_{sub}^{-1}] [g_{ITA} g_{glu}^{-1}]	$q_{p,max}$ [g L^{-1} h^{-1}]
50 g L^{-1} glucose, 2 g L^{-1} sodium formate, 0.8 g L^{-1} NH_4Cl	w/o solvent + commercial HCOONa	▼	28.4 ± 0.5	0.54 ± 0.1 0.56 ± 0.1	0.10
	catalyst in tetradecane	■	36.7 ± 0.1	0.69 ± 0.1 0.71 ± 0.1	0.10
	catalyst in octylacetate	●	29.8 ± 0.1	0.57 ± 0.1 0.59 ± 0.1	0.10
	catalyst in anisole	♦	34.3 ± 0.1	0.66 ± 0.1 0.68 ± 0.1	0.10
100 g L^{-1} glucose, 4 g L^{-1} sodium formate, 3.5 g L^{-1} NH_4Cl	w/o solvent + commercial HCOONa	■	63.3	0.57 0.59	0.22
	catalyst in tetradecane	●	64.2	0.66 0.68	0.22

3.3.6 Conclusion and outlook

This study demonstrates the use of the pH tolerant and non-filamentous *U. cynodontis* as an alternative itaconate production host in formate co-metabolization experiments. Thereby, an improvement of itaconate production was achieved for metabolically engineered *U. cynodontis* Δ*fuz7* Δ*cyp3* $\Delta P_{ria1}::P_{etef}$ and *U. cynodontis* Δ*fuz7* Δ*cyp3* $\Delta P_{ria1}::P_{etef}$ + mttA by the use of sodium formate as energy co-substrate boosting production titer (up to 10 % increase) and yield (up to 7 %).

Furthermore, formate co-metabolization was optimized using DoE approach reaching an itaconate titer of 138.2 ± 7.0 g L^{-1} corresponding to an increase in maximum titer of 66%, which displays the highest published titer for *U. cynodontis* so far [31]. Thereby, empirical models were generated, which can predict itaconate titers and yields within the tested design space with given starting concentrations of glucose, formate and ammonium chloride.

The bioprocess could be successfully combined with biphasic catalytic hydrogenation of CO_2 directly delivering the aqueous sodium formate solutions and enabling catalyst recycling. Tetradecane as catalyst phase yields a biocompatible sodium formate solution performing as good as commercial sodium formate. This productivity of *U. cynodontis* compared to the current industrially used production host using *A. terreus*. Within this study, yield up to 0.62 $g_{itaconate}\ g_{substrate}^{-1}$ were achieved which equals 86% of the theoretical maximum.

Product inhibition of itaconate and toxic effects of formate could be addressed in suitable feeding strategies and continuous process approaches within subsequent experiments, e.g. implementing an external membrane enabling cell retention system as repeated batch-cultivations with *U. cynodontis* showed high potential.

Further, economic evaluation, e.g. *via* life-cycle assessment (LCA) of the process could be approached as the presented work lays the foundation for an improved itaconate production process with a potentially reduced carbon footprint.

The proposed role of formate as an energy source for the cell is just assumed here. By conducting ^{13}C-labeling experiments with formate this hypothesis could be confirmed or falsified and new insights on the potential formate carbon flux in *U. cynodontis* could be gained.

Chapter 3.4

Seventeen Ustilaginaceae high-quality genome sequences allow phylogenomic analysis and provide insights into secondary metabolite synthesis

Partially published as:

Ullmann, L., Wibberg, D., Busche, T., Rückert, C., Müsgens, A., Kalinowski, J., Blank, L.M. Seventeen Ustilaginaceae High-Quality Genome Sequences Allow Phylogenomic Analysis and Provide Insights into Secondary Metabolite Synthesis. *J. Fungi* 2022, 8, 269. https://doi.org/10.3390/jof8030269

Contributions:

Lena Ullmann performed experiments concerning genomic DNA isolation with the help of Andreas Müsgens, analyzed the data, prepared figures, and wrote this chapter. Experiments concerning genome sequencing were performed by Tobias Busche and Christian Rückert as well as the respective software analysis. Daniel Wibberg and Jörn Kalinowski discussed the data and critically revised the chapter. Lars M. Blank conceived the study, advised on all experiments, discussed data, and reviewed this chapter.

3.4 Seventeen Ustilaginaceae high-quality genome sequences allow phylogenomic analysis and provide insights into secondary metabolite synthesis

3.4.1 Summary

The family of Ustilaginaceae belongs to the order of Basidiomycetes. Despite their plant pathogenicity causing, e.g., corn smut disease, they are also known as natural producers of value-added chemicals such as extracellular glycolipids, organic acids, and polyols. Here, we present 17 high-quality draft genome sequences (N50 > 1 Mb) combining third-generation nanopore and second-generation Illumina sequencing. The data were analyzed with taxonomical genome-based bioinformatics methods such as Percentage of Conserved Proteins (POCP), Average Nucleotide Identity (ANI), and Average Amino Acid Identity (AAI) analyses indicating that a reclassification of the Ustilaginaceae family might be required. Further, conserved core genes were determined to calculate a phylogenomic core genome tree of the Ustilaginaceae that also supported the results of the other phylogenomic analysis. In addition, to genomic comparisons, secondary metabolite clusters (e.g., itaconic acid, mannosylerythritol lipids, and ustilagic acid) of biotechnological interest were analyzed, whereas the sheer number of clusters did not differ much between species.

3.4.2 Introduction

The family of Ustilaginaceae belongs to the order of Ustilaginomycetes. It consists of 14 genera, including *Ustilago*, *Sporisorium*, and *Macalpinomyces* [75]. The taxonomy of the Ustilaginaceae, which is still a matter of debate, was focused on during several studies resulting in several taxonomic revisions [239]. For instance, Kirk *et al.* (2008) proposed that the Ustilaginaceae family comprises 17 genera comprising 607 species [76]. The ever-increasing genomic data should settle the discussion at one point. Ustilaginaceae are known for their plant pathogenicity and the capability to infect economically essential crops, including barley, sugarcane, wheat, and oats [76]. Even though these plant diseases cause crop loss, smut fungi attracted particular attention in the field of industrial biotechnology.

Ustilaginaceae show a versatile product spectrum including organic acids (e.g., itaconate, malate, succinate), polyols (e.g., erythritol, mannitol), and extracellular glycolipids, which are considered value-added chemicals with potential applications in the pharmaceutical, food, and chemical industries [43], [83]. For instance, mannosylerythritol lipids (MELs) are surface-active glycolipids secreted by various fungi, including *U. maydis*. MELs can be used as biosurfactants, displaying the much-asked biodegradability resource for the production of detergents or pharmaceuticals [86]. The various organic acids produced by Ustilaginaceae are

known as platform chemicals, which have the potential to contribute to the transition from a fossil- to a bio-based economy [78].

U. maydis does not only show a broad product spectrum, but also metabolizes a range of renewable carbon sources, which, apart from sugars, also include the monomers acetate, galacturonic acid, glycerol, and xylose, as well as the polymers cellulose, pectin, lignin, and xylan [62], [165], [186], [240], [241]. Among the Ustilaginaceae, *U. maydis* is the best-studied species in plant pathogenicity and biotechnology, and is a model organism in cell biology [167]. A broad range of molecular, genetic, bioinformatics, and cell biological techniques have been developed over the past years [69], [166], [168]. This, along with their yeast-like growth, makes Ustilaginaceae attractive for biotechnological applications.

Recent studies have advanced our understanding of the smut fungi by elucidating complete genome sequences of *U. maydis* and other members of the Ustilaginaceae family [87]. With a particular interest in itaconate producers, Geiser *et al.* (2016) compared nine different strains and observed that the synteny of the itaconate cluster is preserved in the investigated Ustilaginaceae [242]. Furthermore, the sequencing revealed genome sizes between 19 and 25 Mb of the investigated Ustilaginaceae *via* Illumina short-read sequencing.

Technological progress and the development of third-generation sequencing methods, e.g., nanopore sequencing, allow for the rapid and cost-efficient high-throughput generation of complete genome sequences with long reads [153]. Thus, next-generation sequencing displays a valuable tool for the investigation of phylogenomic and population genomic relationships, e.g., as shown previously in the investigation of Hypoxylaceae by Wibberg *et al.* (2021) [159].

In this study, 17 strains of the Ustilaginaceae were genomically analyzed by establishing high-quality draft genomes (N50 > 1 Mb) combining Oxford Nanopore and Illumina sequencing. Various comparative genomics methods, including Average Amino Acid Identity (AAI), Average Nucleotide Identity (ANI), and Percentage of Conserved Proteins (POCP), were used to estimate the similarity of the selected isolates and to compute a phylogenomic core genome tree of the Ustilaginaceae. In more detailed analyses, the presence of secondary metabolite gene clusters was investigated for potential biotechnological exploitation. With these high-quality draft genomes, a data set was established, enabling the investigation of Ustilaginaceae biodiversity, as well as contributing to biotechnological applications, e.g., metabolic engineering of secondary metabolite production.

3.4.3 Results

3.4.3.1 Genomic data

Within this work, 17 different Ustilaginaceae strains from 14 species were chosen for genome sequencing by application of third-generation Oxford Nanopore sequencing in combination with second-generation Illumina sequencing. Long-read nanopore sequencing was combined

with the short-read Illumina sequencing method to improve base accuracy and thus significantly reduce error rates in the final genomes. The strain selection was based on previous work, including relevant species such as *U. cynodontis* [72], *U. trichophora* [186], *U. vetiveriae* [165], and *U. maydis* [64], [65], [86]. Several *U. maydis* isolates were included as previous studies determined differences in the secondary metabolite profiles. Apart from the named *Ustilago* species, a broad species selection was aimed for, including *Macalspinomyces* [243], *Pseudozyma* [44], *Sporisorium* [243], and *Ustanciosporium*.

The amount of obtained reads by Nanopore sequencing ranged from 175,216 to 621,889 with an average read count of 350,192, whereas the mean read length shows an average of 13,253 bp (8214–17,321 bp). Assemblies polished by Illumina short reads resulted in an average contig number of 66 (22–316) with a 72-fold average coverage (45.8–95.3 fold). Established genome sequences range in size from 18 to 36 Mb and feature GC contents around 54%, which is common for eukaryotes as they barely reach GC values above 60%. **Table 19** shows the assembly results in more detail, incorporating genome size, contig numbers, GC-content, and the number of annotated genes.

Table 19: Details of the genome sequences of the selected Ustilaginaceae.
[a] as identified *via* GeneMark tool, * diploid/ + additional fungi.

No.	Organism	Strain	Genome Size (bp)	Contigs	Largest Contig	N50 (bp)	GC (%)	Annotated Genes [a]
#2814	*Macalpinomyces mackinlayi*	BRIP 52549a	20,011,713	79	2,517,462	778,176	55.2	6780
#2816	*Macalpinomyces ordensis*	BRIP 26904a	21,488,978	42	1,934,029	92,1621	54.4	7166
#1946	*Pseudozyma antarctica*	NRRLY 7808	18,256,718	27	2,397,276	72,913	60.8	6532
#2212	*Sporisorium exsertum*	RK 033	19,675,720	41	1,762,232	1,163,924	56.7	6772
#2213	*Sporisorium scitamineum*	UMa698	20,280,126	51	1,999,406	881,538	54.9	6757
#2214	*Sporisorium walkeri*	RK 031	18,415,360	22	2,584,725	1,158,577	53.9	6584
#2215	*Ustanciosporium gigantosporum* *	UMa706	26,778,318	86	3,628,339	1,232,426	55.3	8712
#2215	*Ustanciosporum gigantosporum*	UMa706	20,177,783	36	3,087,333	1,238,668	52.0	6690
#2821	*Ustilago curta*	BRIP 26929a	18,446,555	39	1,762,630	682,062	55.2	6420
#2706	*Ustilago cynodontis*	NBRC 9727	23,130,474	48	2,786,107	1,026,819	52.1	7322
#2826	*Ustilago lituana*	BRIP 46795a	25,770,532	69	1,993,860	819,494	54.3	7741
#2136	*Ustilago maydis*	No. 198	21,122,121	107	2,522,778	660,941	53.8	6807
#2169	*Ustilago maydis*	No. 482	20,585,367	46	3,568,257	876,01	54.0	6827
#2169	*Ustilago maydis*	No. 482	20,591,394	68	2,499,251	674,905	53.9	6833
#2172	*Ustilago maydis*	No. 485	20,582,581	43	2,514,809	743,668	53.9	6777
#2701	*Ustilago trichophora*	NBRC 100157	20,713,809	48	1,974,389	794,480	53.8	6585
#2220	*Ustilago vetiveriae*	RK 075	18,373,116	37	2,393,662	780,848	54.8	6347
#2836	*Ustilago xerochloae* *	BRIP 60876a	36,081,614	315	4,586,684	648,688	54.8	11,418

A previous study presented draft genome sequences from nine different Ustilaginaceae that are known for itaconic acid production [242]. Nevertheless, so far, no study has focused on a broader spectrum of Ustilaginaceae isolates for whole-genome sequencing, including genomic and phylogenomic analyses.

In summary, the combinatorial approach of Illumina and nanopore sequencing resulted in 17 high-quality and state-of-the-art fungal draft genome sequences that can be used for further analysis.

3.4.3.2 Phylogenomic analysis

To deduce the phylogeny of the Ustilaginaceae isolates, the comparative genomics platform EDGAR 3.0 was applied. Based on all core genes determined for the 14 species - in total 2370 genes - a phylogenetic tree was computed and shown in **Figure 58**. In the case of two strains - *U. maydis* No. 482 and *U. gigantosporum* Uma 706 - two isolates were sequenced. Thus, they were labeled with -1 and -2, respectively. The tree consists of six different clusters. In total, two outgroups are visible representing *Pseudozyma* antartica NRRL Y7808 and *U. gigantosporum* UMa706 (group 1, highlighted in blue), as well as *M. ordensis* BRIP 26904 a (group 2), followed by two clusters consisting of two different *Ustilago* species. The largest cluster consists of all *U. maydis* isolates (highlighted in orange), *U. vetiveriae,* and *M. mackinlayi*. The last cluster includes all Sporisorium isolates and *U. curta*.

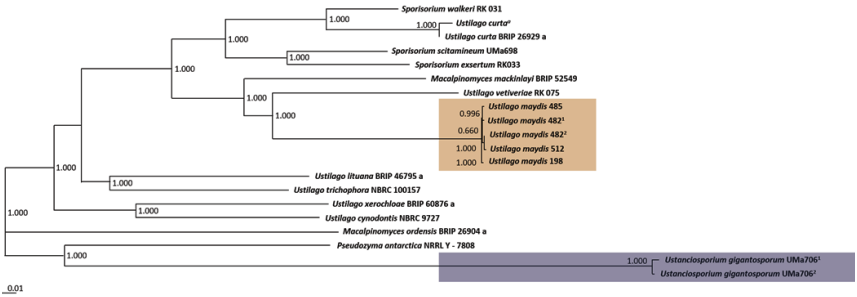

Figure 58: Phylogenetic tree of the investigated Ustilaginaceae strains.
The phylogenetic tree is based on the core genes (2370 genes) of the selected strains. The SH-like local support values were computed using FASTtree within the comparative genomics tool EDGAR 3.0 [244]. [1,2] Two isolates were sequenced. [a] Additional strain isolated from sample #2836* (**Table 19**).

Previous comparative studies on genomes of smut fungi have indicated that *U. maydis* is more closely related to other taxa than to species of *Ustilago* [75]. Other systematic studies confirmed this fact and further showed that *U. maydis* is closely related to species of *Sporisorium* and *Anthracocystis* [245], [246]. The close relationship can be explained by similarities in their hostplant infection mechanism. McTaggart *et al.* (2016) recovered *U. maydis* in a clade, among others, with M. mackinlayi, which all form hypertrophied sori in inflorescences of their hosts [75]. Furthermore, the authors considered that localized, host-derived, hypertrophied sori were an apomorphy for this group [75]. During our phylogenomic analysis based on the core genes of the selected strains, the close relationship between *U. maydis*, *M. mackinlayi*, and *Sporisorium* species was also observed, confirming previous

studies. The question remains if *U. maydis* or the other *Ustilago* species require a reclassification.

3.4.3.3 Comparative genomics

In order to determine the similarities within the Ustilaginaceae species, comparative genomic tools such as Percentage of Conserved Proteins (POCP, **Figure 59**), Average Nucleotide Identity (ANI, **Figure 60**), and Average Amino Acid Identity (AAI, **Figure 61**) were applied to the whole genome sequences.

Pairwise Percentage of Conserved Proteins

The POCP analysis has been proposed as a novel method to define genus boundaries in prokaryotes [152]. In prokaryotic studies, POCP analysis revealed that all pairwise comparisons of species from different families resulted in values lower than 50%, the proposed threshold for a genus boundary. A recent study by Wibberg *et al.* (2021) proposed that this threshold cannot be directly applied to fungal genomes [159]. Since fungal genes are much more conserved than prokaryotic genes, the threshold was proposed to be set at 70% separating family and non-family members [159]. POCP analysis can be used to compare two strains to estimate their evolutionary and phenotypic distance. Thereby, the quality of POCP analysis depends on the reliability of the applied gene prediction models. Wibberg *et al.* (2021) showed that protein sequences derived from GeneMark delivered an adequate coverage of the gene content, which is comparable to RNA-Seq-based prediction pipelines [159].

The POCP identities determined in this study ranged from 52–99% (**Figure 59**). Thereby, the observed identities of <70% could be explained by the impurity of another fungus in samples of *U. gigantosporium* and *U. xerochloae*. Excluding this artifact, the observed identities are comparable to the previously published ones showing POCP identities from 70–99% between the tested family members [159]. The different *U. maydis* strains within one species even share 96–99% identity. The remaining species show identities up to 95%. Nevertheless, *U. maydis* displays the only species that contained several strains within the obtained analysis. In order to verify a potential species threshold, various additional isolates should be genome sequenced. Differentiation of interspecific and intergeneric identities between the different Ustilaginaceae isolates was not possible, which was also observed in previous studies due to overlapping identities [159]. Thus, our results combined with the phylogenomic analysis indicate that a reclassification of the Ustilaginaceae family might be required.

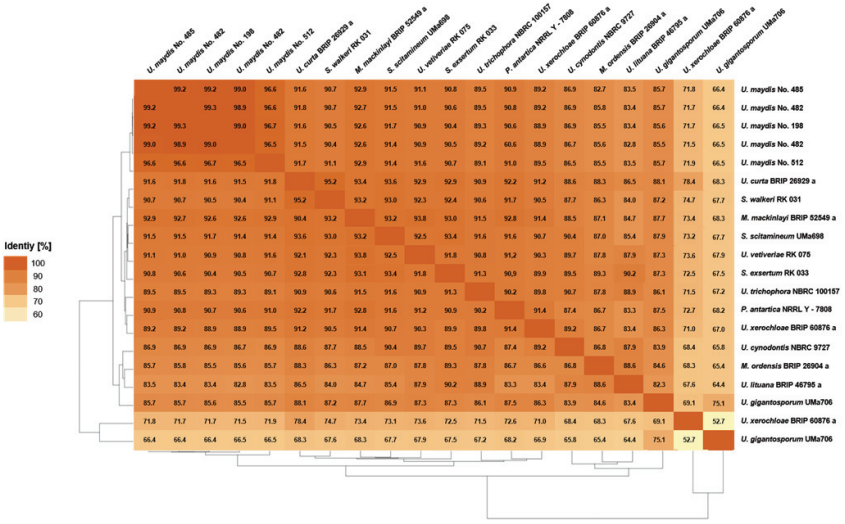

Figure 59: Pairwise Percentage of Conserved Proteins (POCP) analysis for members of the Ustilaginaceae family.
The conserved proteins between a pair of genomes were determined by aligning all the protein sequences of one genome (query genome) with all the protein sequences of another genome using the BLASTP program [152]. Proteins from the query genome were considered conserved when they had a BLAST match with an E-value of less than 1 × 10−5, a sequence identity of more than 40%, and an alignable region of the query protein sequence of more than 50% [152]. Two isolates were sequenced in case of *U. maydis* No. 482 and *U. gigantosporum* UMa706.

Average Nucleotide Identity

Apart from POCP, ANI (**Figure 60**) was performed to determine the nucleotide-level genomic similarity between two genomes. The obtained ANI values range from 76.6 to 99.9% identity. Again, the highest identities and similarities were observed for the *U. maydis* isolates ranging from 96.7 to 99.9%. Further, the other comparisons showed a maximum identity of 99.8% for *U. curta* and *U. xerochloae*. Thus, a clear boundary between inter- and intraspecies comparison is not feasible for our obtained data set using ANI analysis only. Furthermore, differentiation of interspecific and intergeneric identities was impossible due to overlapping identities similar to POCP. Wibberg *et al.* (2021) observed that members of the Hypoxylaceae share at least 70% of their nucleotide content [159]. The different Ustilaginaceae isolates compared during this study showed at least 77% nucleotide content, which is comparable to the previous data received from other fungal families. This threshold is identical to the one estimated for the POCP analysis.

For prokaryotic genome data sets, ANI analyses have been widely used to identify genomic variations and, thus, define species boundaries [247]. Concerning fungal data sets, studies are available for comparably small taxon selections [248]. For selected *Rhizoctonia solani* isolates,

an approximate sequence identity of 80% was shown. In a recent study of a larger data set on Hypoxylaceae, a sequence identity within the family of 73.2–93.3% was demonstrated [159]. Moreover, in a study on *Arthrodermataceae*-related species, identities of 76.4–90.0% were observed, which are comparable to the other studies and our obtained identities (76.6 to 99.9%) [159], [249]. When comparing the ANI and POCP between species pairs in the family of Ustilaginaceae, it can be seen that POCP values are overall higher. Comparing U. curta BRIP 2629a with *U. maydis* isolates, POCP identities of 91.5–91.8 were obtained. ANIs for the comparison resulted in values of 79.5%. A similar phenomenon, higher conservation of protein sequence, was observed for the family of Hypoxylaceae, confirming the obtained results during this study [159].

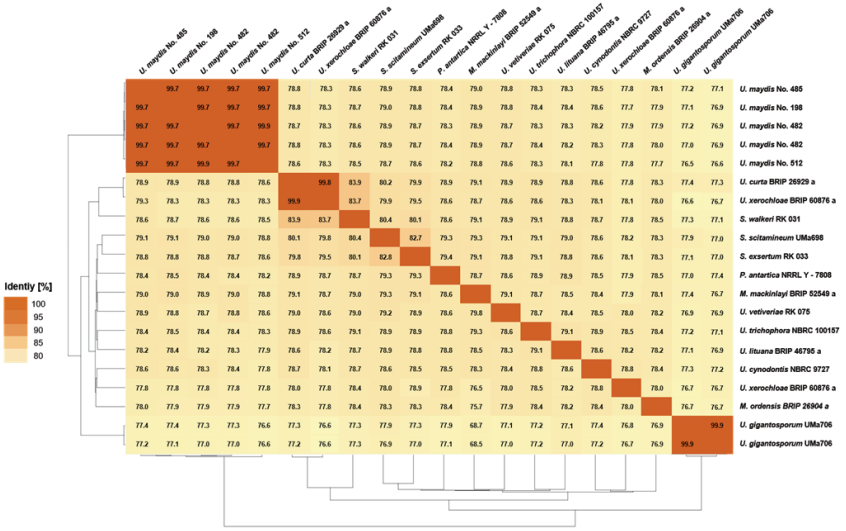

Figure 60: Pairwise Average Nucleotide Identity (ANI) analysis between genome-sequenced Ustilaginaceae. The ANI between the query genome and the reference genome was calculated as the mean identity of all BLASTN matches [157]. Two isolates were sequenced in the case of *U. maydis* No. 482 and *U. gigantosporum* Uma706.

Average Amino Acid Identity

AAI (**Figure 61**) measures the genomic difference of the investigated strains based on orthologous proteins [159]. The AAI identities of the different Ustilaginaceae range from 67.7–99.9%, indicating that the strains share at least two-thirds of the presented protein-coding genes. Excluding *U. gigantosporium* and *U. xerochloae* with a contaminated or diploid genome, the identities increase to 74.6–99.9%. The different sequenced *U. maydis* isolates show AAIs ranging from 99–100%. Comparing isolates from different genera, AAIs up to 91.2% were observed, e.g., comparing *U. curta* BRIP 26929 and *S. walkeri* RK031. Comparing the different *U. maydis* isolates and *S. walkeri* RK031 results in AAIs of 80%. *U. xerochloae* BRIP 2629a and *U. maydis* isolates showed identities of 78%. During a previous study, Wibberg

et al. (2021) proposed an intergeneric and interfamilial threshold value of 75% for the tested Hypoxylaceae [159]. This study focused on one fungal Ustilaginaceae family only. Nevertheless, AAIs above 74.6% were observed, supporting the findings of the previous study. In comparison to ANI, the AAIs were higher, which can be explained by the degenerated genetic code as nucleotide sequence changes do not necessarily result in an amino acid change [250].

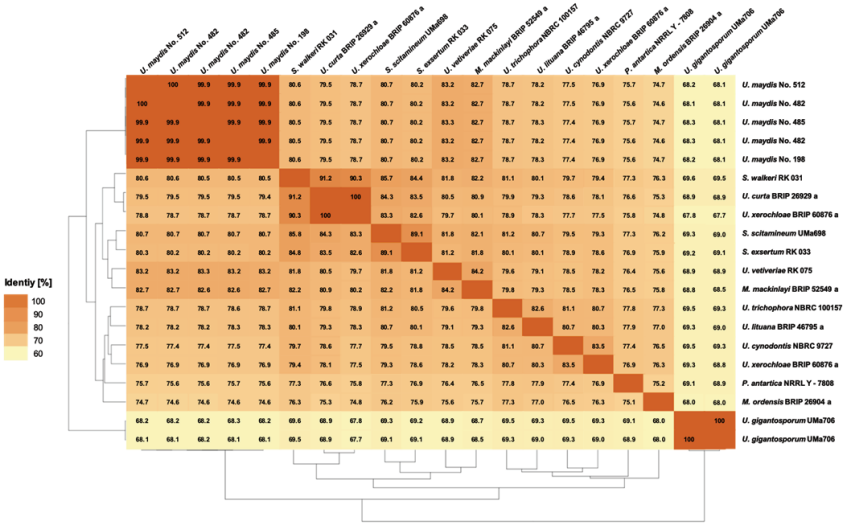

Figure 61: Pairwise Average Amino Acid Identity (AAI) analysis between genome-sequenced Ustilaginaceae.
The AAI between the query genome and the reference genome was calculated as the mean identity of all BLASTN matches [157]. Two isolates were sequenced in the case of *U. maydis* No. 482 and *U. gigantosporum* Uma706.

Gene-based comparison

Results of the genomic comparison by analyzing the number of core and individual genes between different *U. maydis* and *Sporisorium isolates*, respectively, are displayed in **Figure 62**. Similar to the POCP, the numbers strongly depend on the accuracy of gene prediction and hence cannot be considered as exact measurements. Nevertheless, it gives insights into the distribution of orthologous genes between related and unrelated species.

U. maydis isolates (**Figure 62 A**) share 6245 core genes and contain between 136 (*U. maydis* No. 385) to 396 singleton genes (*U. maydis* No. 512). The number of common genes between the individual pairs varied in the range of 6305 (*U. maydis* No. 512 and 198) to 6578 (*U. maydis* No. 485 and 482).

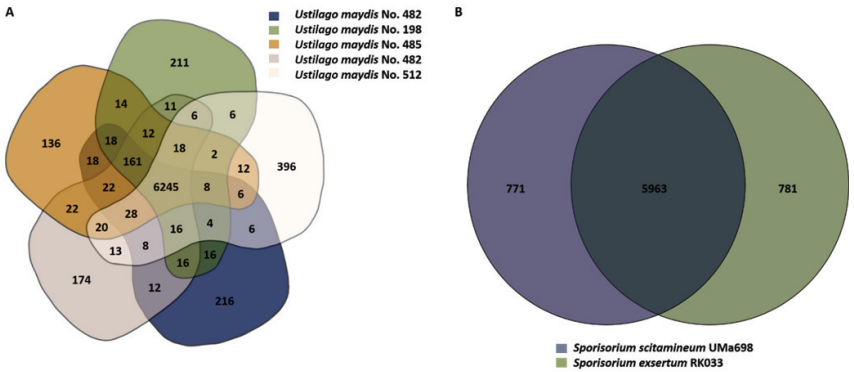

Figure 62: Gene-based comparison of Ustilaginaceae.
Venn diagrams of (A): *U. maydis* and (B): *Sporisorium* isolates obtained from the comparative genomics tool EDGAR 3.0 [244]. Two isolates were sequenced in the case of *U. maydis* No. 482.

In addition to the core genome, the regions involved in secondary metabolite synthesis for the different Ustilaginaceae isolates were analyzed and compared (**Table 20**). In general, these fungi include - also in comparison with other basidomycota, e.g., *R. solani* [159] - only a few secondary metabolite synthesis genes and gene clusters, which agrees with previous reports [194]. The number ranges between 10 and 15 regions per genome. Here, the differences between species are not very pronounced. Most of the predicted regions belong to the core genome of the isolates. However, also unique regions were predicted, e.g., the RIPP region in *U. gigantosporum* Uma706 or a second T1PKs region in *M. mackinlayi* BRIP 52549a. Here, additional experiments are needed, such as RNA sequencing experiments to predict the function of the metabolites and to predict if it is involved in the pathogenic interaction with the host plant. Differences between the two respective isolates of *U. maydis* No. 482 and *U. gigantosporum* Uma706 can be explained by separate cultivation and isolation experiment. In the case of eukaryotes, such genetic differences are a common phenomenon. In general, the presented results solely display a prediction on the chosen enzyme families and do not cover all potential secondary metabolites. In the case of polyketide synthases (PKSs), antiSMASH predicts one type 1 PKS, whereas it is known that *U. maydis* has three polyketide synthases (pks3, pks4, and pks5) for the production of the pigment melanin [192]. Indeed, antiSMASH updates are announced to further improve the predictions of secondary metabolite synthesis gene clusters in varying organisms [251]. Another example of missed secondary metabolites are isoprenoids derived from carotenoids - for example, the plant hormone abscisic acid, of which its synthesis was reported for *U. maydis* [59]. The largest class of genes encoding enzymes involved in secondary metabolite synthesis identified here are NRPSs (**Table 20**). A prominent example of a Ustilaginaceae product requiring NRPS enzymes is the metal chelator ferrichrome [252].

Table 20: Investigation of secondary metabolite synthesis *via* antiSMASH analysis [251].
[1,2] Two isolates were sequenced, contains * diploid/ + additional fungi.

Organism	Strain	NRPS	Terpene	T1PKS	RIPP	Total
Ustilago maydis	No. 485	11	2	1	0	14
Ustilago maydis	No. 482 [1]	11	2	1	0	14
Ustilago maydis	No. 482 [2]	13	2	1	0	15
Ustilago vetiveriae	RK 075	7	2	1	0	10
Ustilago curta	BRIP 26929a	7	3	1	0	11
Macalpinomyces ordensis	BRIP 26904a	6	3	1	0	10
Ustilago trichophora	NBRC 100157	7	2	1	0	10
Sporisorium exsertum	RK 033	8	3	1	0	12
Ustanciosporium gigantosporum	UMa706 [1]	7	4	1	1	13
Sporisorium scitamineum	UMa698	9	3	1	0	13
Ustilago xerochloae	BRIP 60876a *	8	2	1	0	11
Ustilago xerochloae	BRIP 60876a *	5	2	0	0	7
Macalpinomyces mackinlayi	BRIP 52549a	7	3	2	0	12
Ustanciosporium gigantosporum	UMa706 [2]	7	2	1	0	10
Sporisorium walkeri	RK 031	6	3	1	0	10
Ustilago maydis	No. 198	11	2	1	0	14
Ustilago cynodontis	NBRC 9727	9	2	1	0	12
Ustilago lituana	BRIP 46795a	6	3	1	0	10

Itaconate cluster identification

Based on the obtained genomes, secondary metabolite clusters were investigated in order to verify genetic similarities and differences between the Ustilaginaceae. During previous empirical studies, differences in itaconic acid production were observed for various Ustilaginaceae strains [43]. Thus, the itaconate gene cluster was compared at first (**Figure 63**). The complete itaconate cluster was identified in six isolates: *U. maydis* No. 198, 485, 482, and 512, as well as in *U. vetiveriae* RK075 and *U. cynodontis*. *M. mackinlayi* BRIP 52549a did not contain *mtt1* and *ria1*, which encode a mitochon-drial tricarboxylate transporter and the regulator of itaconic acid biosynthesis, respectively [69]. Thus, itaconate production was tested during a cultivation experiment (**Figure 64**). An itaconate production of 2.2 ± 0.01 g L^{-1} after 48 h was observed, indicating a functional itaconic acid synthesis cluster that is also reacting to nitrogen starvation as previously reported for the other *Ustilago* itaconate producer [62]. Previous studies focused on the role of different itaconate cluster genes as, e.g., a deletion of *mtt1* in *U. maydis* MB215 (No. 512) led to a strong decrease in itaconate production, but its production was not completely abolished [69]. This transporter is known as the rate-limiting step in itaconate biosynthesis in *U. maydis* [253]. Most likely in *M. mackinlayi* BRIP 52549a, different less specialized, and therefore less efficient, transport proteins substitute the dedicated itaconic acid transporter, as most eukaryotic mitochondrial transporters have a diverse substrate spectrum with different affinities [70].

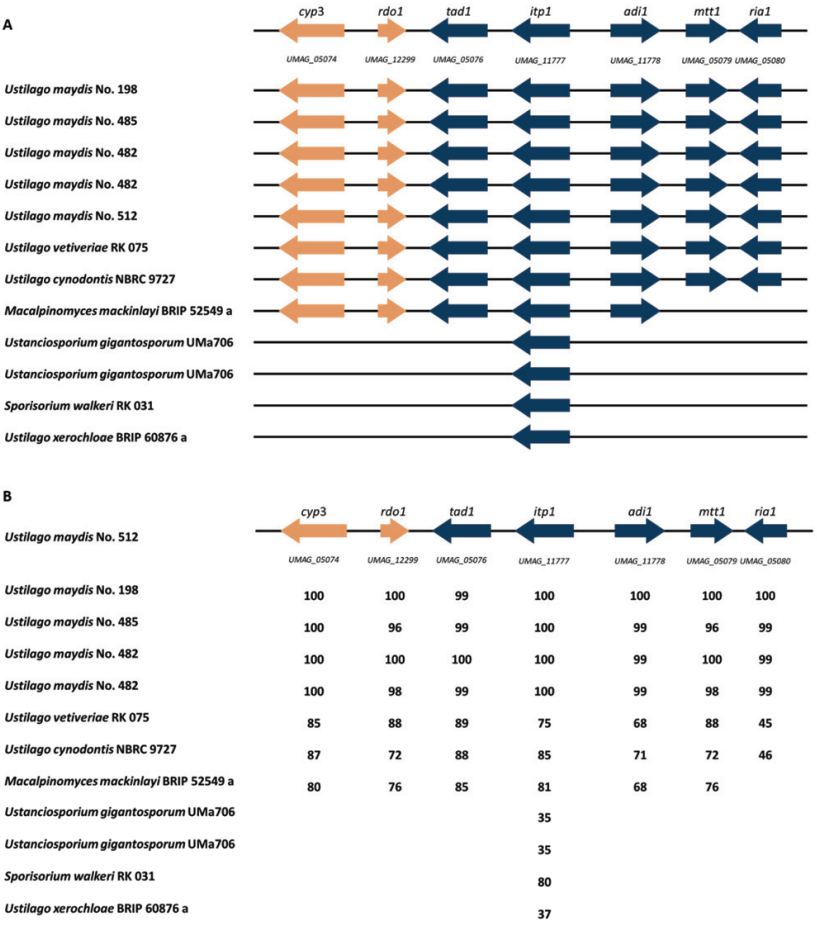

Figure 63: Schematic overview of the itaconate biosynthesis gene cluster in *U. maydis*.
Modified from [208] (A): Organization of the cluster genes is compared to the sequenced Ustilaginaceae isolates. Blue color indicates genes directly involved in itaconate production and transport [166]. Orange-colored genes are involved in itaconic acid conversion into its derivates [69]. *Cyp3* (P450 monooxygenase), *rdo1* (glyoxalase domain-containing protein RDO1), *tad1* (trans-aconitate decarboxylase 1) *itp1* (itaconate transport protein), *adi1* (aconitate-delta-isomerase 1), *mtt1* (mitochondrial tricarbox-ylate transporter 1), *ria1* (regulator of itaconic acid biosynthesis). (B): Itaconate cluster comparison of selected Ustilaginaceae. Numbers given show amino acid sequence identity as percentage compared to the reference strain *U. maydis* No. 512 using antiSMASH 6.0 [251]. Two isolates were sequenced in the case of *U. maydis* No. 482 and *U. gigantosporum* UMa706.

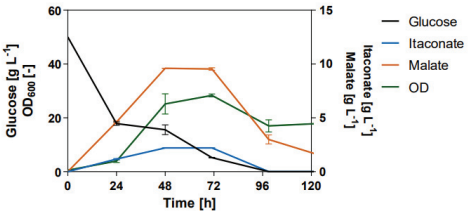

Figure 64: Shake flask cultivation experiment of *M. mackinlayi* BRIP 52549a.
Growth *via* OD_{600} measurement (green line), glucose concentration (black line), malate production (orange line) and itaconate production (blue line) are visualized during small scale (50 ml) cultivation experiment using MTM medium and 50 g L^{-1} glucose and 0.8 g L^{-1} NH_4Cl. Error bars indicate the deviation from the mean for n=3.

Four isolates, *U. gigantosporum* UMa706, *S. walkeri* RK031, and *U. xerochloae* BRIP 60876a, only harbor *itp1*, encoding the itaconate transport protein lacking the remaining itaconic acid cluster genes. This transporter secretes itaconic acid, itatartarate, and 2-hydroxyparaconate from the cytosol to the exterior of the cell [70]. As itaconate reduction was observed in some long-lasting experiments (**Figure 65**), itaconate import might be facilitated by *Itp1*. Indeed, the degradation of itaconate might be important in some niches due to the antimicrobial properties of itaconic acid [254], [255]. Geiser *et al.* (2016) [242] presented draft genome sequences of itaconate-producing Ustilaginaceae, including *S. iseilematis-ciliati* BRIP 60887a, *P. tsukubaensis* NBRC 1940, *P. hubeiensis* NBRC 105055, as well as *U. maydis* and *U. vetiveriae* strains. All strains showed the complete itaconate cluster except for *P. tsukubaensis* NBRC 1940. Available genome sequences of investigated Ustilaginaceae strains could be included in the obtained data, which helps facilitate further research on the biology of Ustilaginaceae and increase the list of tools for metabolic engineering of itaconate production by Ustilaginaceae.

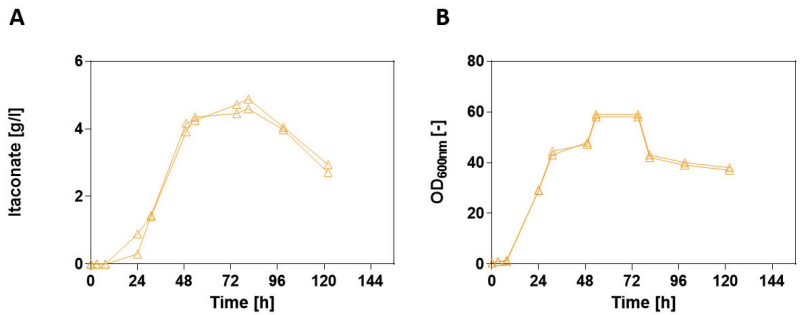

Figure 65: Controlled-batch fermentation of *U. maydis* No. 512.
A: Itaconate production and B: growth *via* OD_{600} measurement on in a bioreactor containing MTM medium using 50 g L^{-1} glucose, 6.25 g L^{-1}, 0.8 g L^{-1} NH4Cl, 80% DOT, at pH 6.5 [91].

To further investigate the itaconic acid cluster genes, amino acid sequence identities were compared (**Figure 63 B**). Each enzyme shares amino acid sequence identities with the

corresponding enzymes in *U. maydis* No. 512, with identities ranging from 35 - 100%. Among those, the highest identities were found for the different *U. maydis* isolates ranging from 96 - 100%. The lowest identity of 96% is obtained comparing *U. maydis* No. 485 and No. 512 for genes *rdo1* and *mtt1*. *Mtt1* is directly involved in itaconic acid biosynthesis as it encodes a mitochondrial tricarboxylate transporter. *Rdo1* is not directly involved in the itaconic acid synthesis, but it is proposed to encode an enzyme converting (S)-2-hydroxyparaconate to itatartarate [70]. An empirical study by Geiser *et al.* (2014) confirmed a lower itaconate production of *U. maydis* 485, which might result from genetic differences within the itaconic acid gene cluster [43]. Comparing the different genes, *cyp3* encoding a cytochrome P450 monooxygenase and *itp1* encoding an itaconate transport protein are highly conserved, showing amino acid identities of 100% between the tested *U. maydis* isolates.

For *U. cynodontis* and *U. vetiveriae*, the sequence identity of proteins encoded by the itaconate biosynthesis genes is mostly conserved in a range of 68 - 89% compared to the *U. maydis* No. 512 sequence. The most divergent protein of the itaconate cluster is Ria1, showing identities from 45 - 46% for *U. vetiveriae* and *U. cynodontis*, respectively. Geiser *et al.* (2018) observed a similar identity of 43 % between *U. maydis* and *U. vetiveriae* even though they are phylogenetically closely related [166]. Further, Geiser *et al.* (2018) were able to activate silent itaconate clusters by overexpression of Ria1 originating from related species, although the amino acid sequences of Ria1 regulators are less conserved than the enzymes involved in itaconic acid synthesis [166]. Additionally, the authors could enhance itaconate production in weak producers up to 4-fold [166]. Thus, it was shown that activation of silent secondary metabolite clusters could be achieved in a range of related species with reduced genetic engineering efforts.

To conclude, this study confirmed a highly conserved itaconate cluster of the in-vestigated *U. maydis* strains (96 - 100% identity), even though there are differences in itaconate production and by-product formation such as (S)-2-hydroxyparaconate, which were observed during previous empirical studies. Thus, the obtained results can be used to further increase the list of tools for metabolic engineering of itaconate production by Ustilaginaceae.

MEL cluster identification

Mannosylerythritol lipids (MELs) are glycolipid biosurfactants produced by vari-ous basidiomycetous yeasts belonging to the genera *Ustilago*, *Pseudozyma*, *Moesziomyces*, and *Sporisorium* [256]. Apart from their interfacial activity, MELs are known to repair damaged human skin and hair. Thus, they have been commercialized in the cosmetics industry for more than a decade [256]. Hewald *et al.* (2006) [84] identified the gene cluster involved in MEL biosynthesis and outlined the pathway for MEL biosynthesis in *U. maydis*. The cluster consists of four enzymes and a transporter: erythritol/mannose transferase (*emt1*), two acyltransferases (*mac1* and *mac2*), acetyltransferase (*mat1*), and the putative transporter (*mmf1*) (**Figure 66**).

The identification of gene clusters *via* whole-genome sequencing is essential for the modification of the MEL biosynthesis pathway. Recently, the gene clusters in-volved in MEL biosynthesis in various Pseudozyma strains have been identified by genomic sequencing [86]. The cluster genes were also identified in Ustilaginaceae strains, including *S. graminicola* and *U. hordei*, during recent work [257]. Within this study, 14 isolates exhibited the whole MEL cluster. *S. scitamenium* exhibited all genes except mac2, encoding an acyl transferase. Based on the identification of the MEL cluster, new potential MEL producers were reported within this work: *U. curta*, *U. lituana*, *U. trichophora*, *U. xerochloae*, *M. ordensis*, and *M. mackinlayi*. Nevertheless, production levels could differ due to regulation of the secondary metabolite clusters as observed for itaconate production. MEL production of strains *U. cynodontis* and *S. exsertum* was already observed during cultivation experiments [86], [257]. Geiser *et al.* (2014) identified *M. eriachnes* as a natural MEL producer [43]. No MEL cluster genes were identified in *U. gigantosporum*, *U. vetiveriae*, and *S. walkeri*, asking for further analyses into the function of MELs.

Further, amino acid identities between the different MEL cluster genes were compared between *U. maydis* No. 512 and the different Ustilaginaceae strains. Amino acid identities ranging from 52 - 100% compared to *U. maydis* No. 512 were computed. A study from Saika *et al.* (2018) reported similar identities of 54 - 82% comparing different *Pseudozyma* strains to *U. maydis* No. 512 [86]. The data set obtained during this study extends the existing set with several *U. maydis* strains enabling the interspecies comparison of the different isolates. MEL cluster genes are highly conserved, showing identities ranging from 99 - 100% for the different *U. maydis* strains. Comparing other *Ustilago* species (such as *U. curta*, *U. cynodontis*, *U. xerochloae*, *U. lituana* and *U. trichophora*) to *U. maydis* No. 512 identities ranging from 55 - 80% were observed. Comparing the different analyzed Pseudozyma strains by Saika *et al.* (2018), identities from 55 – 82% were obtained, confirming our intraspecies (intergeneric) observations [86]. Nevertheless, no clear amino acid identity boundary can be set comparing different genera such as M*acalpinomyces*, *Pseudozyma*, and *Sporisorium*.

The obtained genomic and gene cluster data can be used for modifications in MEL production, e.g., *via* metabolic engineering. Previous studies identified *mac1* and *mac2* as essential genes encoding two acyltransferases for MEL production in *U. maydis* as the deletion strains Δmac1 and Δ*mac2* lacked any MEL synthesis [86]. Furthermore, gained knowledge about MEL cluster genes can be used to tailor MEL production in Ustilaginaceae, exploiting more strains than the existing model organisms.

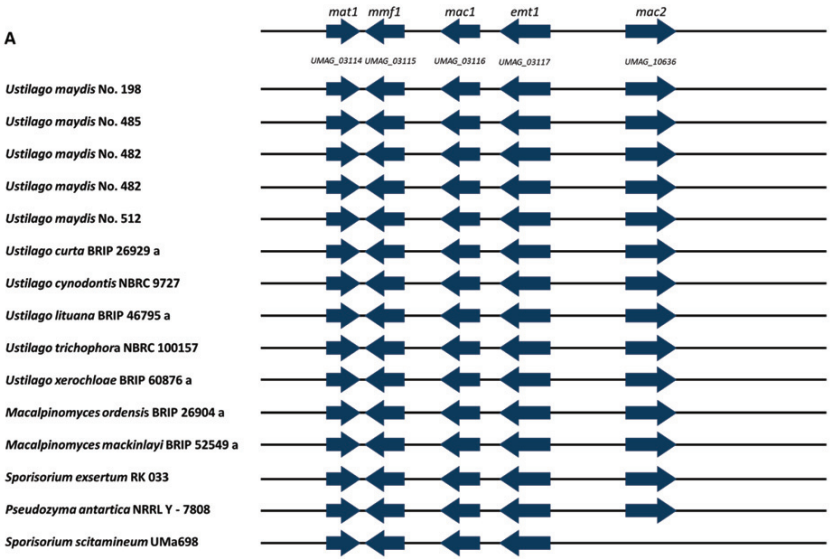

B

	mat1	mmf1	mac1	emt1	mac2
	UMAG_03114	UMAG_03115	UMAG_03116	UMAG_03117	UMAG_10636
Ustilago maydis No. 512					
Ustilago maydis No. 198	99	99	99	100	99
Ustilago maydis No. 485	99	100	99	100	100
Ustilago maydis No. 482	100	100	100	100	100
Ustilago maydis No. 482	99	99	99	100	99
Ustilago curta BRIP 26929 a	57	74	69	77	63
Ustilago cynodontis NBRC 9727	59	72	59	80	65
Ustilago lituana BRIP 46795 a	58	70	59	69	65
Ustilago trichophora NBRC 100157	55	82	62	76	61
Ustilago xerochloae BRIP 60876 a	55	71	60	80	64
Macalpinomyces ordensis BRIP 26904 a	53	74	59	67	60
Macalpinomyces mackinlayi BRIP 52549 a	60	79	74	81	68
Sporisorium exsertum RK 033	57	72	65	81	65
Pseudozyma antartica NRRL Y - 7808*	53	77	59	75	53
Sporisorium scitamineum UMa698	52	72	65	81	

Figure 66: Schematic organization of the MEL synthesis gene cluster (modified from [208]**).**
(A): Organization of the gene cluster is compared to the sequenced Ustilaginaceae. *Emt1* (erythritol/mannose transferase), *mac1* and *mac2* (acyl transferases), *mat1* (acetyl transferase), *mmf1* (putative trans-porter). (B): MEL gene cluster comparison of selected Ustilaginaceae. Numbers given represent amino acid sequence identity as percentage compared to the reference strain *U. maydis* No. 512 using antiSMASH 6.0 [251]. Two isolates were sequenced in case of *U. maydis* No. 482.

During this study, 14 out of 17 isolates, i.e., 82%, exhibited genes responsible for MEL production. In general, MEL improves the accessibility of hydrophobic nutrients and enhances attachment to nonpolar surfaces. In addition to these more general functions, some biosurfactants also bind heavy metals, display antimicrobial activity, or play an important role in pathogenic development or biofilm formation [258]. The findings in our study display a valuable genomic data set facilitating further understanding of MEL production in different Ustilaginaceae strains.

Ustilagic acid cluster identification

The phytopathogenic basidiomycetous fungus *U. maydis* secretes, under conditions of nitrogen starvation, large amounts of the biosurfactant ustilagic acid (UA). Further, UA displays antibiotic activity [193].

The genes responsible for UA in *U. maydis* No. 512 production are displayed in **Figure 67**, which also includes the gene cluster comparison to the other isolates. Based on the given data set, only the reference genome of *U. maydis* No. 512 shows all genes responsible for ustilagic acid production. The remaining *U. maydis* isolates *U. maydis* No. 482, 198, and 485 lack *uat2* encoding an acetyltransferase. Furthermore, another group was identified consisting of *U. xerochloae*, *M. ordensis*, *M. mackinlayi*, and *S. scitamineum* showing all UA cluster genes except *orf2*, which encodes an ustilagic acid biosynthesis cluster protein with a so far unknown function [208]. To conclude, 9 out of 17 isolates (52%) show UA cluster genes. Thereby, this study shows similar findings compared to Geiser *et al.* (2014), confirming *U. maydis*, *S. scitamenieum*, *S. walkeri*, and *M. eriachnes* as UA-producing strains during cultivation experiments [43]. Furthermore, smut fungi such as *U. cynodontis*, *U. vetiveriae*, and *S. exertum* did not show UA production during the experiments [43]. Our genomic comparison revealed that this could be explained by the complete lack of the UA cluster. *U. xerocholoae* was identified as a potential novel UA producer as its UA production was not observed during previous studies.

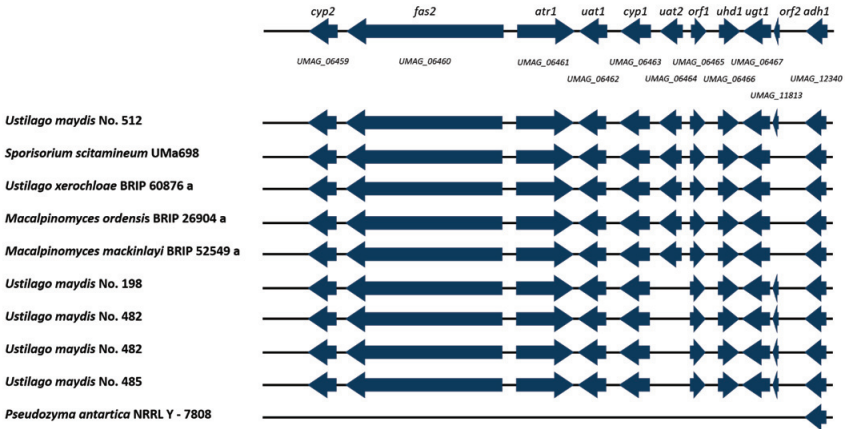

Figure 67: Schematic organization of the ustilagic acid (UA) synthesis gene cluster in *U. maydis* (modified from [208]**).**
Organization of the gene cluster is compared to the here sequenced Ustilaginaceae. *Cyp2* (P450 monooxygenase), *fas2* (fatty acid synthase 2), *atr1* (ABC-type transporter), *uat1* (acyltransferase), *cyp1* (P450 monooxygenase), *uat2* (acetyltransferase), *orf1* (alcohol acetyltrans-ferase), *uhd1* (fatty acid hydroxylase), *ugt1* (glycosyltransferase), *orf2* (ustilagic acid biosynthesis cluster protein), *adh1* (alcohol dehydrogenase I). Gene cluster analysis *via* antiSMASH 6.0 [251]. Two isolates were sequenced in case of *U. maydis* No. 482.

Macro syntenyplot of U. maydis isolates

Genomic synteny of the tested *U. maydis* isolates was compared to *U. maydis* No. 512, the reference strain in biotechnology (**Figure 68**). When comparing the different isolates, a high genomic synteny can be observed between the respective organism pairs. The chromosomes structure of the *U. maydis* strains is highly conserved. As stated previously, in the case of two strains - *U. maydis* No. 482 and *U. gigantosporum* Uma 706 - two isolates were sequenced. Thus, they were labeled with -1 and -2, respectively. Only the two isolates of *U. maydis* No. 482 show different rearrangements of the second chromosome. Differences between the two isolates might result from separate cultivation, assembly errors, or different read length in the respective region. Nevertheless, the two isolates show rearrangements in the same region of the second chromosome which indicates a difference to chromosomes of *U. maydis* No. 512. To conclude, the highly conserved chromosome structures of the *U. maydis* strains confirm the high identities obtained from POCP, AAI, and ANI resulted in high identities between the different strains.

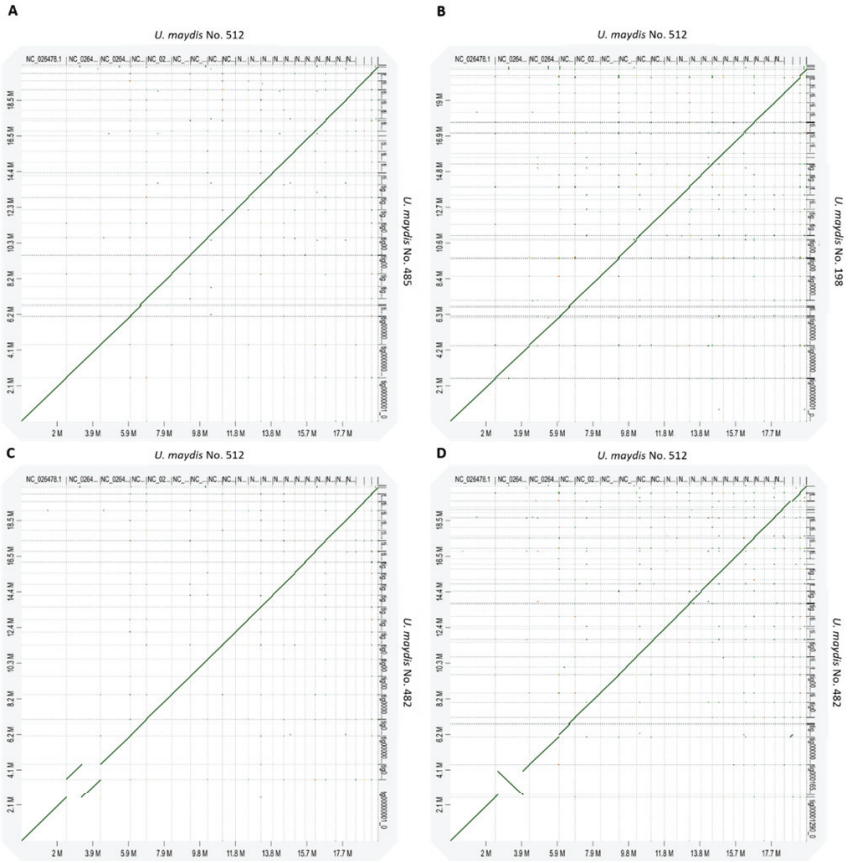

Figure 68: Whole genome macro synteny plot between the different *U. maydis* isolates compared to *U. maydis* No. 512.
(A): *U. maydis* No. 485 and (B): *U. maydis* No. 198. (C,D): Two isolates were sequenced in case of *U. maydis* No. 482 and therefore are visualized separately.

3.4.4 Conclusion

Here, we reported high-quality genomes of 17 Ustilaginaceae strains covering 14 species combining nanopore and Illumina sequencing. A broad strain selection for genomic investigation was aimed for based on previous work on relevant Ustilaginaceae species (i.e., *U. cynodontis* [72], *U. trichophora* [259], *U. vetiveriae* [165], *U. maydis* [64], [65], [73]). By phylogenomic comparison and the application of taxonomical genome-based bioinformatics methods such as POCP, ANI, and AAI analyses on a larger set of related fungal species, we gained insights into their relationships and were able to deduce taxonomic hierarchies. The obtained results indicate that a reclassification of the Ustilaginaceae family might be required.

In addition to genomic comparisons, secondary metabolite cluster analysis was performed. The numbers of identified secondary metabolite clusters did not differ much between species and ranged between 10 and 15 regions per genome. Here, the differences between the different isolates were not very pronounced. Notably, few of the identified regions could be associated with the secondary metabolite synthesized, asking for additional experiments such as RNA sequencing to predict the function of the metabolite and to predict if it is involved in the pathogenic interaction with the host plant.

With the presented high-quality draft genomes (N50 > 1 Mb), the investigation of Ustilaginaceae biodiversity is enabled, as well as metabolic engineering of secondary metabolites production (e.g., MELs, UA, itaconic acid) is fostered. The generated genomic data set enhances our toolbox for investigating and engineering the fungal Ustilaginaceae family.

Chapter 4

General discussion and outlook

Contributions:

This chapter was written by Lena Ullmann and reviewed by Lars M. Blank.

4 General discussion and outlook

This thesis evaluates the potential of Ustilaginaceae strains as itaconate producers from CO_2-derived co-substrates such as acetate and formate are evaluated. The overarching goal is a carbon-neutral or ideally carbon-negative production process. Some general aspects of establishing sustainable bio-based production processes at an industrial scale are discussed in this chapter.

4.1 Process optimization

The prospect of consolidating and expanding itaconic acid as a commercially competitive product lies in improving three technological bottlenecks: cheap carbon source, fermentation with high performance parameters (TRY: titer, rate, and yield), and low downstream costs.

Current biotechnological processes for itaconic acid production with *A. terreus* and *U. maydis* are based on carbohydrates, such as arabinose, glucose, molasses, and xylose [19], [170]. Furthermore, glycerol from biodiesel production is an alternative feedstock for itaconate synthesis by *U. vetiveriae* [165]. Starch is considered one of the best alternatives to glucose, given its high purity, low cost, and source stability [260]. Corn starch has already been reported as a substrate for *A. terreus,* achieving a product titer of 60 g L^{-1} [260]. Nevertheless, glucose and starch compete with food and feed when used as a substrate in biotechnology.

An alternative substrate concerning agricultural and forestal residues, was reported for *U. maydis*: pretreated cellulose in seawater or the hydrolyzed hemicellulose fraction of pretreated beech wood [30]. Additionally, pretreated wood hydrolyzates were established as carbon source for itaconate production by *A. terreus* [260]. However, these applications could not be established due to significant growth deficits caused by inhibitory compounds present in the medium [23], [30].

The usage of refined sugar is more expensive during the upstreaming process but also enables a cheap downstream processing. The abovementioned carbon-providing waste streams are comparably cheap, but they lead to side products that are generated during the process, which leads to higher purification costs [37]. Thus, several factors impact the substrate choice during biotechnological production processes.

The itaconate production of *Ustilago* was optimized regarding TRY [61], [64], [65], [72]. Integrated strain and bioprocess optimization enabled a maximum itaconate titer of 220 g L^{-1} using a metabolically engineered strain, *U. maydis* MB215 Δ*cyp3* $\Delta P_{ria1}::P_{etef}$ Δ*fuz7* P_{etef}mttA strain [64]. These strain modifications enabled the development of an efficient fermentation process with *in-situ* product crystallization with $CaCO_3$. Another study focused on combining genetic modifications to push itaconic acid production toward theoretical maximal yield, which was achieved by a fed-batch fermentation process with a continuous glucose feed [65].

Nevertheless, additional aspects must be considered to improve the process and enhance its biotechnological relevance. For example, producing itaconic acid at low pH values is a primary objective. Low pH values are preferred for organic acid production since this reduces base consumption, enhances sterility, and benefits downstream processing later [37]. The possibility to execute low-pH fermentations strongly depends on the host organism's tolerance toward low pH values and ability to produce the desired product under these conditions. Unlike *U. maydis*, *U. cynodontis* has a high tolerance toward low pH, significantly benefiting itaconate production. For *U. cynodontis*, Hosseinpour Tehrani *et al.* (2019) reported an optimal pH value for itaconate production [61]. The production parameters achieved with a constant pH of 3.6 were comparable to those achieved with *U. maydis* at pH > 6 [61]. Further, Demir *et al.* (2021) studied itaconate production at low pH by *U. maydis* [261]. During several bioreactor experiments, extracellular pH was decreased from 6 to 3.5. Despite the gradual decrease in itaconic acid levels with decreasing pH (~ 50% decrease in itaconic acid concentration at pH 3.5, compared to pH 6), significant itaconate production is still observed at pH 4 (63 g L^{-1}) [261]. To sum up, these results powerfully illustrate the potential of engineered *Ustilago sp.* for itaconate production at commercial levels.

Other factors impacting itaconate productivity are product toxicity and weak organic acid stress caused by increasing itaconic acid titers, which are common challenges in organic acid fermentations [262]. Production at higher pH values reduces acid stress for the production host. One strategy to avoid product toxicity is *in-situ* product removal (ISPR) *via* $CaCO_3$. In this thesis, cultivation experiments were performed using $CaCO_3$ as a potent buffering agent. Using $CaCO_3$ as a buffer can also be considered as integrated initial step of the downstream process. This procedure was previously used for several Ustilaginaceae strains such as *U. maydis* [64] and *U. cynodontis* [61], and for *U. trichophora* during malic acid production [186]. Nevertheless, the main drawbacks of this technique display the high viscosity, handling during $CaCO_3$ feeding and sedimentation during fermentation. Alternatively, an external membrane module enabling cell retention and simultaneous product removal was established in this thesis. This work was based on Hosseinpour Tehrani *et al.* (2019) who already demonstrated the advantages of a repeated batch approach with cell recycling of *U. cynodontis* [61]. Implementation of an external ceramic membrane module demonstrated high stability of the biomass until 500 h process duration and a constant itaconate production rate. Moreover, the membrane module could be extended with a DSP purification step, avoiding the loss of substrate or other media components.

Bioprocess development does not end after upstreaming, but downstream processing (DSP) considerations need to be implemented in the early stages of biotechnological approaches. The separation of itaconic acid from cultivation broth considerably impacts the total cost of production, about 30 to 40 % [263]. The search for high-efficiency and low-cost processes for organic acid recovery is one of the critical steps for replacing petrochemical-based products.

Although biotechnological production of itaconic acid is already industrially established with *A. terreus* as the production host, there is significant research on improving fermentative and recovery steps. A recent study from Gausmann *et al.* (2021) demonstrated a new DSP approach. A joint development of a bio-based production route for itaconic acid featuring low pH value fermentation, reactive extraction, and electrochemical product recovery was presented [264]. By implementing an electrochemical pH-T-swing separation process, itaconic acid with a purity of over 99% was recovered in the crystalline form from the fermentation broth [264]. Based on the measured liquid-liquid and solid-liquid equilibrium, a viable overall yield of >90% for itaconic acid recovery was calculated for the proposed downstream process [264]. The authors stated that implementing a process setup with *in-situ* product removal is the next step to fully exploit synergies [264]. This again highlights the potential of simultaneous bioprocess and DSP development with the overall goal of an economically feasible production process for itaconic acid.

4.2 CO_2-derived substrates

The raw materials significantly impact on the total costs of biotechnological processes. Hence, attempts are made to reduce costs by using cheap and renewable substrates. Here simultaneously improving the sustainability of the itaconate production process by a new co-substrate approach was followed using potential CO_2-derived C1 and C2 compounds such as acetate and formate.

As a first step during this work, 72 different Ustilaginaceae strains from 36 species were investigated for their ability to (co-)consume acetate and formate. *U. maydis* MB215 was identified as promising candidate for acetate metabolization whereas *U. cynodontis* NBRC 7530 was identified as a potential production host using formate as a co-substrate enhancing its itaconate production. This section will first discuss the potential of acetate as a co-substrate, followed by formate.

This work not only demonstrated the applicability of *U. maydis* wildtype but also the use of metabolically engineered strains for acetate co-feeding strategies. Thereby, a beneficial effect of acetate co-metabolization of *U. maydis* MB215 wildtype strain on itaconate production was confirmed showing a 2.2-fold increase in itaconate titer and a 2.3-fold increase in itaconate yield [91]. To understand the mechanism of the increased production, acetate assimilation in *U. maydis* was investigated *via* ^{13}C-labeling indicating that acetate was not directly incorporated into itaconate. Our approach focused on measuring extracellular metabolites (i.e., itaconic acid, citric acid, malic acid) and tracking potential labeling patterns. This methodology lacks information about the use of acetate for biomass formation or more specific metabolically pathways besides secondary metabolite formation. Further, a metabolically engineered strain was used for that purpose, showing a reduced by-product spectrum. Thus, only analysis of the itaconate labeling pattern was feasible. Repeating the experiment with *U. maydis* MB215

wildtype strain could contribute to a better understanding of acetate assimilation. Moreover, alternative biosynthesis pathways must be clarified, i.e., the use for respiration, cell maintenance, and/or energy metabolism. Further research could focus on, e.g., using ^{13}C-labeling to analyze proteinogenic amino acids, as demonstrated by Schmitz *et al.* (2015) [265]. Measuring proteinogenic amino acids also provides information about pathways that produce intracellular metabolites and biomass. To investigate if acetate might be used for CO_2 formation during cultivation, using off-gas sensors capturing ^{13}C-labeled CO_2 could contribute to that investigation. During this approach, it was not confirmed if 50% of itaconates carbon during production could be derived from CO_2 as proposed by co-feeding acetate (**Figure 6**). Nevertheless, the carbon footprint of the production process can be reduced by verifying an improved itaconate production. By co-feeding CO_2-derived acetate the proportion of glucose could be subsequently reduced impacting the carbon footprint of the process.

Within this work, commercially available sodium acetate was used for co-feeding. For the use of CO_2-derived formate, the proof-of-principle for its use as a direct and unpurified product solution after hydrogenation reaction was demonstrated in chapter 3.3 for *U. cynodontis*. As far as CO_2-derived acetate is concerned, a new study by Jürling-Will *et al.* (2022) published a novel route to acetic acid production *via* palladium-catalyzed isomerization of methyl formate [106]. To investigate the applicability of this material for *U. maydis*, biocompatibility must be tested with particular interest on remaining side products in the product solution such as solvents (acetone), methyl formate or the palladium catalyst, which is not recyclable yet [106]. Besides the demonstrated acetate production route, other processes, e.g. production with acetogens could be focused on during further research [174].

This study focused on *U. cynodontis* as an itaconate production host using formate as a co-substrate. Thereby, the addition of formate significantly impacted itaconate titers and yields for both wildtype (1.3-fold increase) and metabolically engineered strains (10 % increase) compared to their respective glucose reference. Improvement of the itaconate production during formate co-metabolization indicates a benefit other than just a higher amount of available carbon in the culture. As no formic acid fixation pathway is known in smut fungi, the results suggest a role of formate as an auxiliary substrate delivering energy to the organism rather than being converted into biomass or product(s) of interest [114], [115]. The proposed role of formate as an energy source for the cell is just assumed here. By conducting ^{13}C-labeling experiments with formate this hypothesis could be confirmed or falsified and new insights on the potential formate carbon flux in *U. cynodontis* could be gained.

This work illustrated the inhibitory effects of acetate and fomate on Ustilaginaceae were demonstrated, while the exact mechanism of toxicity remains unknown [93]. Adaptive Laboratory Evolution (ALE) displays a valuable tool to enhance substrate tolerance and utilization for an improved biocatalyst. However, for ALE to be effective in generating strains with increased productivity, the product-of-interest needs to be coupled with cellular growth or

survival. Selective pressure is a crucial factor for the success of an ALE approach to achieve mutants with the desired traits. Moreover, due to relatively new technologies, including next-generation DNA sequencing (NGS), phenotype-genotype correlations can be easily obtained by whole genome resequencing [153]. *Via* reverse engineering potential targets can be tested with the aim of chassis strain development *via* metabolic engineering. Zambanini *et al.* (2017) already established enhanced glycerol consumption of *U. vetiveriae via* ALE [165]. Becker *et al.* (2019) focused on improving the growth and itaconate production of *U. maydis* at acidic pH, whereas selection parameters did not lead to the desired goal [208]. One disadvantage of ALE experiments is that they display the duration with ideally hundreds of generations. *Ustilago* ALE experiments are time-consuming, with a relatively slow growth rate of $\mu = 0.05\ h^{-1}$. Establishing automation protocols (i.e., online growth determination and automated inoculation of the cells) could simplify the process.

Results obtained during this study indicate the beneficial effects of actetate and formate on the itaconate production of several Ustilaginaceae strains [91]. Further, valuable empirical models were established using DoE methodology predicting itaconate production (titer, yield). Those findings could be combined in a subsequent DoE approach, using glucose, acetate, and formate potentially further pushing itaconate production. Thereby, glucose and acetate could function as C-sources whereas formate boosts productivity as an energy donor [114].

Especially, the economic evaluation (i.e., *via* LCA) of the demonstrated process using acetate and formate as a co-substrate could be approached as the presented work lays the foundation for an improved itaconate production process with a potentially reduced carbon footprint.

4.3 Optimization *via* metabolic engineering

In the biotechnological field, metabolic engineering aims to modify an organism's endogenous metabolic network to improve the production of a value-added compound. This goal can either be achieved by the deletion or overexpression of genes involved in the responsible pathway for a determined product. Additionally, natural or synthetic pathways from other organisms can be introduced into the biotechnological host of choice to increase efficiency or to broaden the product spectrum further [266].

The identification and annotation of the itaconate cluster during previous studies, which is accessible for several Ustilaginaceae laid the foundation for metabolic engineering approaches focused on during this work. Based on a previous study from Becker *et al.* (2020) [73], the CRISPR/Cas9 [208], [267] and FLP/FRT system [268] were used for genome editing . Becker *et al.* (2020) focused on increasing the metabolic flux into the targeted itaconate biosynthesis pathway by overexpressing the itaconate gene cluster regulator Ria1 and preventing side product formation (2-HP, ustilagic acid, MELs and diacylglycerol lipids [73]. It was demonstrated by combining metabolic engineering and process engineering that itaconic acid

can be produced from glucose with metabolically and morphology-engineered *U. maydis* strains at up to maximum theoretical yield and with an improved itaconate titer of 220 g L^{-1} [64]. However, it was observed that the neutral lipid knockout Δ*dgat*, caused a decline in fitness. Therefore, this study established a new chassis strain combining a reduced by-product spectrum and itaconic acid overexpression while maintaining the TAG biosynthesis in *U. maydis* – a compromise between by-product formation and fitness of the cells.

Nevertheless, further upregulation strategies could help to increase itaconate production further. As already shown by Geiser *et al.* (2016), overexpression of the gene cluster regulator *ria1* was an essential step to generate an itaconate hyper producer strain. In combination with the deletion of 2-HP synthesis pathway (Δ*cyp3*), the engineered strain produced up to 4.5-fold more itaconate in comparison to the wildtype [63]. Subsequent metabolic engineering strategies could focus on engineering the remaining itaconic acid cluster genes such as *tad1* (trans-aconitate decarboxylase 1, *itp1* (itaconate transport protein), and *adi1* (aconitate-delta-isomerase 1). In this context, several challenges can be named. For *Ustilago*, only a limited number of available constitutive promotors are known (P_{etef}, P_{oma}) [236]. In contrast, several inducible promotors such as P_{nar1} (nitrogen-regulated) or P_{crg1} (arabinose-inducable), P_{hsp70} (heat-inducable), P_{rbf1} (nitrate-inducable) and P_{clp1} (arabinose-inducable) are available for *U. maydis* [269]. Several options could be tested for generating overexpression constructs with the aim of a hyperproducing strain incorporating several genetically overexpressed itaconate cluster genes.

As numerous genes are included in this strategy, the CRISPR/Cas9 technology should be improved in the future since the genome editing lacked efficiency and the efforts to find the correct transformants were very high in this study. The long duration of mutant generation usually constitutes a time delay factor. The initial CRISPR/Cas9 protocol was substantially improved by Zuo *et al.* (2019), who applied the high-fidelity endonuclease Cas9HF1 which minimizes off-target effects [270]. Further complementary cloning techniques are available for *Ustilago,* such as Golden Gate and FLP/FRT system with marker recycling [268], [271]. Resistance marker recycling allows for reusing available resistance cassettes and generating marker-free strains with multiple genetic modifications, as only a limited number of resistance markers is available for *Ustilago* [271]–[273]. The development, improvement, and implementation of existinv and new cloning strategies and techniques are necessary to enable efficient metabolic engineering in Ustilaginaceae.

Additionally, identifiying the physiological role of itaconate in its natural producers such as *A. terreus* or Ustilaginaceae, will help to understand cellular mechanisms and identifiy new targets for optimizing the production process. Further improvements, especially on the regulation of its formation, would be possible. It is assumed that itaconate synthesis in fungi is used as a defense strategy against other fungi and bacteria in their environment [34].

Nevertheless, further research is required to understand the exact mechanisms of both itaconate producer, *Ustilago* and *Aspergillus*.

Besides itaconate production, metabolic engineering approaches could also enhance substrate utilization and spectrum. This work focused on the CO_2-derived substrates acetate and formate. Whereas acetate assimilation in *Ustilago* remains unclear for the most part, formate is used as an auxiliary substrate.

The efficiency of formate metabolization could be improved by introducing synthetic formic acid assimilation pathways in *Ustilago* [274], [275]. Native C1-fixing microorganisms, able to assimilate methanol, methane, formate or formaldehyde, differ in the assimilation pathway, fixation product and efficiency, i.e., consumption of energy and redox equivalents per carbon atom fixed [275]. In general, there are two main strategies for microorganisms to utilize formate:

On the one hand, the dissimilatory route involves the complete oxidation of formate to CO_2, reducing the carbon fixation power. On the other hand, the assimilatory route involves the condensation of formate with other metabolic intermediates [276]. Thereby, formate is oxidized to generate CO_2 and reducing equivalents, which are then used for carbon assimilation and as an energy source for sustaining cellular growth (e.g., *via* the Calvin-Benson Bassham cycle) [276]. In the other strategy, not all formate molecules are oxidized into CO_2. However, a part is used as a carbon source to generate reducing equivalents and energy, while another part is directly assimilated *via* the central metabolism. This strategy entails hydrolyzing ATP to convert formate into formyl-tetrahydrofolate (THF), which is then reduced to the active intermediatemethylene-THF. This strategy includes the serine cycle, the reductive acetyl-coA, the reductive glycine, the xylulose 5-phosphate, and the ribulose-monophosphate pathways. All these native pathways underlie complex metabolic mechanisms [276]. Because the natural formate assimilation pathways have certain drawbacks such as low efficiency, attempts have been made to design artificial formate metabolism pathways rationally [276]. This can not only increase the efficiency of formate assimilation but can also be used to adapt the microorganisms to the culture conditions better and increase substrate or target product concentrations.

Artificial formate-assimilation pathways can form the basis for producing high-value-added chemicals in industrially relevant model organisms. Gonzalez de la Cruz *et al.* (2019) demonstrated the modification of *Saccharomyces cerevisiae* introducing native enzymes for the synthetic reductive glycine pathway and demonstrating growth on formate [277]. As reported for *S. cerevisiae* and the glycine pathway, there are potential pathways that can be targeted for a synthetic formate assimilation in *Ustilago* with the overall goal of a carbon-neutral, or ideally, -negative itaconate production process. By enabling growth on CO_2-derived formate, the overall footprint of the itaconate production process could be reduced by at least partially replacing glucose as a carbon source, especially when additionally combined with

CO_2-derived acetate. Nevertheless, many of these microbes can grow on formate are biochemically not well studied and genetically intractable imposing a high initial activation energy for metabolic engineering projects.

Moreover, alternative acetate assimilation routes have to be clarified, i.e., the use for respiration, cell maintenance and/or energy metabolism. Further metabolic engineering approaches could focus on incorporating respective genes and enabling acetate assimilation *via* the glyoxylate shunt and the TCA cycle to efficiently generate the desired product itaconate from CO_2-derived substrate [201]. As stated by Kiefer *et al.* (2021) microbial growth on acetate generally requires the following steps: acetate uptake into the cell, acetate activation to acetyl-CoA, and acetate assimilation *via* the glyoxylate and TCA cycle [201]. Besides introducing genes into *U. maydis* to improve acetate assimilation, other potential targets could be the acetate transport mechanism or conversion into acetyl-CoA, e.g., improving acetate uptake rates. By using and further improving the recently established genome-scale model of *U. maydis*, potential targets for metabolic engineering could be identified [278].

4.4 Concluding remarks and outlook

This thesis demonstrated itaconate production by various Ustilaginaceae strainsfrom co-utilization of the CO_2-derived substrates acetate and formate. While acetate and formate co-utilization was successfully presented, the challenge of low co-substrate uses remains. A fed-batch mode with *in-situ* sensing of the organic acid concentration might help to overcome the toxicity of these short, weak organic acids. To uphold *Ustilago* as an industrial itaconate producer, transfer to larger production scales in combination with a cost-effective and suitable downstream processing strategy of itaconate is required.

The results presented here contribute to the sustainable production of itaconic acid with the overall goal of reducing the carbon footprint. This is inevitable as climate change is progressing through the steady rise in using fossil resources. Combining the single disciplines of chassis engineering, bioprocess engineering, and the use of CO_2-derived substrates will further improve the economic feasibility of biotechnological processes.

Appendix

4.5 Appendix

4.5.1 Supplementary tables

Table 21: Maximum optical densities (OD [-]) of all 72 strains obtained during biodiversity screening. Whole set of growth screening results using the Growth Profiler device by Enzyscreen with different acetate and formate concentrations as co-substrates in combination with with 20 g L^{-1} glucose (n=2).

Strain	Glucose	2.5 g/l Acetate	5 g/l Acetate	10 g/l Acetate	2.5 g/l Formate	5 g/l Formate	10 g/l Formate
#1946	46.8 ± 0.6	55.9 ± 1.5	47.4 ± 0.3	46.4 ± 0.1	50.0 ± 0.7	42.5 ± 0.1	35.1 ± 0.2
#1947	37.0 ± 1.1	45.0 ± 0.1	42.5 ± 0.0	33.2 ± 0.6	40.8 ± 0.1	34.3 ± 1.5	27.8 ± 0.1
#1949	44.4 ± 0.5	55.5 ± 1.0	35.2 ± 0.1	52.9 ± 0.3	19.2 ± 0.2	21.2 ± 0.1	4.1 ± 0.5
#1951	34.3 ± 1.4	52.3 ± 1.6	43.8 ± 0.1	49.1 ± 0.3	21.4 ± 0.4	19.3 ± 0.1	17.5 ± 1.9
#2134	32.4 ± 0.3	27.3 ± 0.6	22.8 ± 0.6	38.8 ± 2.3	24.5 ± 2.7	22.6 ± 0.3	23.5 ± 2.2
#2135	19.7 ± 2.8	37.2 ± 0.8	38.2 ± 0.2	49.5 ± 0.4	13.3 ± 1.3	15.3 ± 1.6	18.2 ± 0.9
#2136	29.9 ± 0.1	41.9 ± 1.7	44.6 ± 0.1	51.4 ± 1.5	18.0 ± 0.9	19.4 ± 0.4	18.8 ± 0.5
#2144	33.4 ± 1.1	36.8 ± 1.5	41.6 ± 1.3	42.8 ± 0.9	26.9 ± 0.8	21.5 ± 1.3	24.5 ± 0.9
#2152	34.0 ± 2.8	36.8 ± 1.1	43.2 ± 0.1	10.2 ± 0.3	27.4 ± 0.1	15.9 ± 1.0	23.9 ± 1.1
#2158	41.9 ± 0.3	28.6 ± 1.1	25.0 ± 0.1	50.0 ± 0.6	28.6 ± 0.6	23.2 ± 0.4	22.8 ± 0.2
#2162	27.9 ± 0.4	35.9 ± 0.3	35.4 ± 0.1	30.3 ± 0.2	29.1 ± 3.6	11.2 ± 3.4	21.5 ± 2.1
#2167	37.1 ± 0.1	48.3 ± 0.5	33.6 ± 1.1	44.2 ± 0.3	41.1 ± 0.5	38.8 ± 0.7	30.4 ± 0.8
#2169	25.9 ± 0.5	34.1 ± 0.9	26.8 ± 1.0	27.8 ± 0.1	34.0 ± 1.1	28.8 ± 2.5	23.5 ± 0.4
#2172	26.4 ± 0.2	37.0 ± 0.2	28.7 ± 0.2	33.4 ± 0.2	34.2 ± 0.2	15.8 ± 0.3	25.8 ± 0.5
#2177	29.0 ± 1.2	37.6 ± 0.1	19.8 ± 0.1	40.6 ± 0.1	42.0 ± 1.1	21.4 ± 0.4	19.9 ± 0.1
#2178	24.9 ± 0.1	35.7 ± 0.4	37.9 ± 1.3	0.1 ± 0.0	20.3 ± 1.3	17.2 ± 0.1	2.0 ± 0.1
#2179	27.4 ± 0.1	33.8 ± 0.7	18.8 ± 0.1	28.6 ± 0.1	39.0 ± 0.1	17.9 ± 1.3	20.6 ± 0.4
#2196	36.3 ± 1.5	48.5 ± 1.0	32.6 ± 0.2	38.1 ± 0.2	42.3 ± 1.1	35.0 ± 0.0	30.5 ± 0.4
#2197	29.0 ± 1.3	36.6 ± 1.3	31.0 ± 0.0	30.7 ± 2.0	29.8 ± 1.0	30.9 ± 1.3	27.6 ± 0.1
#2199	36.0 ± 0.6	34.1 ± 1.1	37.4 ± 1.7	41.6 ± 0.6	29.6 ± 0.7	22.8 ± 2.0	24.8 ± 0.6
#2205	19.1 ± 3.0	24.2 ± 2.2	22.6 ± 0.7	4.8 ± 0.5	24.2 ± 2.2	8.2 ± 2.1	10.0 ± 3.6
#2208	18.4 ± 0.5	26.5 ± 0.1	20.6 ± 0.7	3.7 ± 0.2	17.2 ± 0.0	19.6 ± 0.2	13.0 ± 0.4
#2209	31.3 ± 1.1	28.6 ± 0.1	24.2 ± 1.2	6.6 ± 0.1	26.4 ± 0.3	16.2 ± 0.5	16.8 ± 0.1
#2210	35.8 ± 0.5	14.1 ± 0.4	37.4 ± 0.5	2.7 ± 0.2	3.6 ± 0.1	33.3 ± 0.7	23.3 ± 0.0
#2211	16.9 ± 0.5	23.6 ± 0.1	19.7 ± 0.4	32.0 ± 1.0	17.3 ± 0.3	12.1 ± 0.0	30.3 ± 0.6
#2212	38.1 ± 0.6	49.7 ± 0.1	39.3 ± 1.5	18.5 ± 3.0	35.5 ± 2.6	11.0 ± 2.6	23.2 ± 2.2
#2213	32.3 ± 0.3	35.6 ± 0.0	17.3 ± 0.1	0.24 ± 0.0	29.5 ± 0.9	13.3 ± 0.6	18.6 ± 0.4
#2214	38.8 ± 1.3	48.8 ± 1.8	19.7 ± 0.1	8.8 ± 1.0	33.2 ± 0.0	18.4 ± 0.4	34.2 ± 4.3
#2215	47.2 ± 0.6	42.2 ± 0.1	50.8 ± 0.2	18.6 ± 2.5	37.7 ± 2.8	30.2 ± 0.0	33.9 ± 0.2
#2218	30.6 ± 0.6	38.6 ± 2.2	17.5 ± 0.4	0.6 ± 0.3	30.6 ± 0.5	15.9 ± 0.3	12.0 ± 0.0
#2219	38.2 ± 0.0	35.3 ± 0.0	15.2 ± 1.6	25.3 ± 4.5	39.5 ± 0.0	16.1 ± 2.0	26.4 ± 0.2
#2220	41.3 ± 0.9	49.9 ± 0.1	27.3 ± 0.1	26.3 ± 1.1	34.7 ± 0.1	14.6 ± 0.7	1.1 ± 0.6
#2221	37.7 ± 0.3	42.0 ± 1.6	19.6 ± 0.3	12.4 ± 1.8	30.7 ± 0.4	14.0 ± 0.3	33.0 ± 0.0
#2229	33.2 ± 0.4	33.3 ± 0.0	18.2 ± 1.1	29.9 ± 1.3	28.2 ± 0.4	12.5 ± 1.3	32.6 ± 0.5
#2696	51.7 ± 1.8	59.7 ± 0.1	28.3 ± 0.4	49.2 ± 2.0	47.7 ± 0.0	20.7 ± 0.7	49.2 ± 0.9
#2697	37.0 ± 1.0	53.4 ± 0.1	38.6 ± 0.8	43.5 ± 0.2	56.6 ± 0.8	39.6 ± 0.7	45.2 ± 0.1
#2698	62.2 ± 1.8	72.9 ± 2.2	33.5 ± 0.3	51.8 ± 1.9	61.2 ±1.5	26.0 ± 0.3	49.1 ± 1.0
#2699	22.7 ± 0.8	27.3 ± 1.4	20.7 ± 0.5	30.8 ± 0.4	40.2 ± 0.2	23.6 ± 0.4	22.1 ± 0.0
#2700	28.4 ± 0.0	26.8 ± 3.2	21.3 ± 2.3	36.3 ± 4.9	34.7 ± 4.2	25.1 ± 2.9	22.8 ± 2.7
#2701	35.5 ± 0.5	38.1 ± 0.2	27.1 ± 0.9	47.5 ± 0.1	41.4 ± 3.0	25.8 ± 0.5	25.5 ± 0.2
#2702	22.2 ± 0.9	23.4 ± 0.4	15.7 ± 0.0	34.0 ± 1.1	30.0 ± 0.0	17.4 ± 0.1	16.5 ± 0.8
#2703	47.8 ± 1.3	50.2 ± 0.3	60.2 ± 0.3	62.1 ± 0.1	47.1 ± 0.1	25.4 ± 0.2	37.6 ± 0.1
#2704	49.8 ± 0.1	52.1 ± 1.5	57.9 ± 2.1	67.0 ± 0.7	52.4 ± 0.9	25.6 ± 0.1	38.4 ± 0.0
#2705	27.5 ± 0.2	36.4 ± 3.6	22.6 ± 3.2	36.6 ± 4.9	40.3 ± 3.9	24.1 ± 2.2	25.1 ± 2.7
#2706	31.6 ± 1.4	44.0 ± 0.1	30.0 ± 0.1	33.5 ± 2.7	50.0 ± 0.5	30.5 ± 0.6	27.2 ± 0.1
#2707	40.7 ± 0.3	53.7 ± 0.7	45.9 ± 0.1	44.4 ± 0.4	21.9 ± 1.1	18.6 ± 1.0	29.7 ± 0.8
#2708	38.1 ± 0.1	48.2 ± 1.8	35.2 ± 0.1	23.8 ± 0.6	56.6 ± 0.1	35.4 ± 0.1	26.9 ± 1.3
#2710	18.3 ± 1.4	17.4 ± 1.5	15.4 ± 1.8	18.1 ± 2.0	20.7 ± 1.5	17.4 ± 1.9	22.0 ± 1.4
#2813	40.7 ± 0.3	63.7 ± 0.3	61.6 ± 0.1	53.7 ± 0.7	21.1 ± 1.1	22.1 ± 0.7	37.3 ± 0.7
#2814	23.8 ± 0.6	44.1 ± 0.6	41.0 ± 0.1	17.8 ± 0.2	23.6 ± 0.6	27.2 ± 0.7	36.0 ± 5.0
#2815	40.4 ± 2.0	58.3 ± 2.0	38.9 ± 4.1	0.2 ± 0.1	37.2 ± 1.2	35.6 ± 0.6	5.0 ± 0.6
#2816	27.1 ± 0.7	41.8 ± 0.8	37.2 ± 0.7	34.6 ± 1.7	33.9 ± 1.3	32.4 ± 0.1	31.1 ± 0.6
#2817	23.4 ± 0.5	29.4 ± 5.3	31.5 ± 0.0	31.5 ± 3.7	14.6 ± 1.7	15.9 ± 1.5	17.1 ± 1.8
#2818	52.7 ± 0.4	44.1 ± 0.1	11.1 ± 1.6	0.7 ± 0.1	48.6 ± 0.4	20.5 ± 0.5	18.2 ± 1.9
#2819	26.6 ± 0.1	29.5 ± 0.9	34.7 ± 1.7	53.6 ± 0.0	25.6 ± 2.0	26.8 ± 0.8	33.4 ± 2.2
#2820	45.2 ± 0.3	67.2 ± 0.0	103.9 ± 6.5	4.2 ± 0.6	50.7 ± 0.3	47.3 ± 2.3	78.2 ± 4.0
#2821	31.1 ± 0.3	40.8 ± 0.0	25.8 ± 0.4	1.1 ± 0.2	32.0 ± 0.0	13.8 ± 1.6	1.2 ± 0.1
#2822	48.1 ± 1.3	27.3 ± 1.5	23.6 ± 0.8	47.5 ± 5.7	67.6 ± 0.3	25.8 ± 0.1	26.2 ± 2.7
#2823	38.1 ± 5.2	47.7 ± 0.0	40.9 ± 4.8	29.9 ± 4.2	35.9 ± 3.5	33.5 ± 3.5	41.4 ± 8.6
#2824	39.1 ± 0.2	54.7 ± 1.8	56.8 ± 0.1	47.9 ± 1.3	33.4 ± 0.7	27.6 ± 0.1	29.9 ± 0.2
#2825	18.5 ± 6.5	53.5 ± 0.2	52.8 ± 0.7	19.1 ± 1.4	35.4 ± 1.3	30.7 ± 4.6	30.8 ± 1.3
#2826	70.6 ± 0.1	67.4 ± 0.7	84.4 ± 2.4	11.5 ± 0.4	63.2 ± 0.0	13.9 ± 0.1	21.1 ± 0.0
#2832	28.1 ± 0.7	37.2 ± 0.7	32.4 ± 0.3	30.8 ± 3.0	28.3 ± 2.8	27.9 ± 0.1	14.6 ± 1.7
#2833	28.9 ± 0.1	32.9 ± 0.8	31.3 ± 1.1	23.5 ± 0.4	27.1 ± 2.2	23.9 ± 1.6	11.7 ± 0.5
#2834	34.1 ± 1.5	35.9 ± 1.4	32.1 ± 1.3	36.1 ± 2.2	35.5 ± 2.9	26.2 ± 3.0	26.7 ± 0.9
#2835	32.6 ± 1.4	42.0 ± 0.7	42.1 ± 1.2	43.6 ± 5.7	21.6 ± 1.4	17.5 ± 0.4	16.3 ± 1.7
#2836	35.7 ± 0.1	39.5 ± 1.7	33.3 ± 2.6	38.1 ± 2.6	28.4 ± 0.1	20.7 ± 0.2	26.8 ± 1.9
#2838	33.1 ± 2.0	35.7 ± 1.8	29.1 ± 1.3	38.5 ± 2.1	32.6 ± 0.1	28.5 ± 0.8	33.8 ± 1.3
#2841	30.6 ± 0.6	40.2 ± 0.1	38.2 ± 0.0	41.8 ± 0.8	24.6 ± 0.5	22.2 ± 0.4	23.9 ± 0.2
#2842	30.38 ± 0.0	35.2 ± 1.4	35.9 ± 0.4	17.5 ± 2.2	15.8 ± 1.4	15.6 ± 0.1	17.4 ± 2.0
#2850	41.4 ± 0.6	45.1 ± 0.5	40.8 ± 5.4	29.3 ± 3.2	37.4 ± 0.9	26.3 ± 0.2	19.3 ± 1.9
#3600	27.7 ± 0.2	24.4 ± 3.3	17.5 ± 2.3	25.6 ± 2.6	31.9 ± 3.4	24.2 ± 2.8	24.1 ± 2.4

Table 22: Maximum growth rates (μmax [h^{-1}]) of all 72 strains obtained during biodiversity screening.
Whole set of growth screening results using the Growth Profiler device by Enzyscreen with different acetate and formate concentrations as co-substrates in combination with 20 g L^{-1} glucose (n=2).

Strain	Glucose	2.5 g/l Acetate	5 g/l Acetate	10 g/l Acetate	2.5 g/l Formate	5 g/l Formate	10 g/l Formate
#1946	0.33 ± 0.01	0.29 ± 0.02	0.26 ± 0.03	0.25 ± 0.01	0.29 ± 0.00	0.32 ± 0.01	0.30 ± 0.02
#1947	0.26 ± 0.02	0.30 ± 0.00	0.25 ± 0.00	0.23 ± 0.01	0.28 ± 0.00	0.29 ± 0.00	0.41 ± 0.00
#1949	0.17 ± 0.03	0.12 ± 0.00	0.12 ± 0.00	0.11 ± 0.00	0.09 ± 0.01	0.10 ± 0.02	0.04 ± 0.00
#1951	0.30 ± 0.01	0.23 ± 0.01	0.25 ± 0.00	0.21 ± 0.02	0.27 ± 0.00	0.25 ± 0.01	0.22 ± 0.02
#2134	0.32 ± 0.04	0.26 ± 0.00	0.22 ± 0.01	0.20 ± 0.01	0.31 ± 0.00	0.23 ± 0.02	0.22 ± 0.01
#2135	0.30 ± 0.02	0.29 ± 0.02	0.29 ± 0.00	0.25 ± 0.00	0.31 ± 0.01	0.27 ± 0.01	0.19 ± 0.00
#2136	0.40 ± 0.00	0.33 ± 0.02	0.25 ± 0.00	0.23 ± 0.00	0.26 ± 0.01	0.27 ± 0.00	0.18 ± 0.00
#2144	0.28 ± 0.00	0.29 ± 0.00	0.26 ± 0.00	0.20 ± 0.00	0.30 ± 0.00	0.23 ± 0.01	0.29 ± 0.00
#2152	0.29 ± 0.01	0.30 ± 0.01	0.26 ± 0.02	0.17 ± 0.00	0.31 ± 0.00	0.25 ± 0.01	0.20 ± 0.00
#2158	0.26 ± 0.01	0.29 ± 0.00	0.24 ± 0.01	0.25 ± 0.01	0.27 ± 0.01	0.22 ± 0.00	0.22 ± 0.00
#2162	0.26 ± 0.05	0.25 ± 0.00	0.24 ± 0.01	0.20 ± 0.00	0.21 ± 0.01	0.21 ± 0.03	0.17 ± 0.02
#2167	0.34 ± 0.02	0.31 ± 0.00	0.28 ± 0.00	0.25 ± 0.01	0.27 ± 0.01	0.26 ± 0.00	0.21 ± 0.01
#2169	0.25 ± 0.02	0.28 ± 0.00	0.26 ± 0.01	0.19 ± 0.02	0.27 ± 0.00	0.31 ± 0.01	0.20 ± 0.00
#2172	0.22 ± 0.00	0.29 ± 0.00	0.28 ± 0.00	0.21 ± 0.00	0.22 ± 0.00	0.19 ± 0.00	0.19 ± 0.00
#2177	0.25 ± 0.01	0.32 ± 0.00	0.26 ± 0.01	0.20 ± 0.00	0.27 ± 0.02	0.24 ± 0.00	0.18 ± 0.00
#2178	0.37 ± 0.02	0.24 ± 0.03	0.21 ± 0.01	0.00 ± 0.00	0.27 ± 0.01	0.28 ± 0.00	0.05 ± 0.00
#2179	0.22 ± 0.01	0.29 ± 0.01	0.27 ± 0.01	0.17 ± 0.01	0.24 ± 0.03	0.23 ± 0.00	0.22 ± 0.00
#2196	0.33 ± 0.02	0.28 ± 0.01	0.29 ± 0.00	0.22 ± 0.02	0.26 ± 0.00	0.29 ± 0.00	0.22 ± 0.00
#2197	0.28 ± 0.02	0.27 ± 0.00	0.29 ± 0.01	0.15 ± 0.01	0.21 ± 0.00	0.30 ± 0.02	0.20 ± 0.01
#2199	0.25 ± 0.00	0.28 ± 0.00	0.25 ± 0.01	0.21 ± 0.01	0.28 ± 0.01	0.20 ± 0.01	0.25 ± 0.00
#2205	0.15 ± 0.00	0.21 ± 0.02	0.19 ± 0.01	0.07 ± 0.00	0.17 ± 0.00	0.00 ± 0.00	0.14 ± 0.01
#2208	0.21 ± 0.01	0.20 ± 0.00	0.19 ± 0.00	0.15 ± 0.03	0.16 ± 0.01	0.20 ± 0.00	0.17 ± 0.02
#2209	0.22 ± 0.00	0.24 ± 0.01	0.20 ± 0.00	0.14 ± 0.02	0.23 ± 0.00	0.19 ± 0.01	0.18 ± 0.00
#2210	0.16 ± 0.00	0.14 ± 0.01	0.19 ± 0.00	0.00 ± 0.00	0.06 ± 0.01	0.14 ± 0.00	0.14 ± 0.00
#2211	0.24 ± 0.01	0.14 ± 0.01	0.14 ± 0.02	0.24 ± 0.01	0.16 ± 0.02	0.20 ± 0.00	0.20 ± 0.0
#2212	0.26 ± 0.04	0.19 ± 0.01	0.23 ± 0.00	0.12 ± 0.00	0.13 ± 0.00	0.12 ± 0.02	0.20 ± 0.02
#2213	0.20 ± 0.00	0.21 ± 0.02	0.18 ± 0.00	0.00 ± 0.00	0.17 ± 0.01	0.18 ± 0.00	0.20 ± 0.01
#2214	0.25 ± 0.02	0.25 ± 0.00	0.17 ± 0.00	0.12 ± 0.01	0.25 ± 0.01	0.19 ± 0.01	0.11 ± 0.01
#2215	0.29 ± 0.01	0.24 ± 0.00	0.20 ± 0.02	0.10 ± 0.02	0.24 ± 0.00	0.21 ± 0.00	0.15 ± 0.01
#2218	0.29 ± 0.02	0.32 ± 0.00	0.27 ± 0.01	0.00 ± 0.00	0.30 ± 0.01	0.30 ± 0.00	0.08 ± 0.00
#2219	0.18 ± 0.00	0.29 ± 0.00	0.20 ± 0.03	0.19 ± 0.00	0.21 ± 0.01	0.15 ± 0.01	0.23 ± 0.00
#2220	0.25 ± 0.01	0.25 ± 0.01	0.16 ± 0.00	0.21 ± 0.01	0.20 ± 0.01	0.19 ± 0.00	0.01 ± 0.01
#2221	0.28 ± 0.01	0.37 ± 0.00	0.25 ± 0.00	0.13 ± 0.00	0.28 ± 0.01	0.25 ± 0.00	0.12 ± 0.00
#2229	0.24 ± 0.01	0.32 ± 0.00	0.21 ± 0.02	0.18 ± 0.00	0.24 ± 0.00	0.24 ± 0.00	0.20 ± 0.02
#2696	0.30 ± 0.01	0.26 ± 0.00	0.19 ± 0.01	0.25 ± 0.03	0.26 ± 0.00	0.24 ± 0.00	0.21 ± 0.01
#2697	0.26 ± 0.01	0.21 ± 0.00	0.29 ± 0.00	0.17 ± 0.01	0.17 ± 0.01	0.23 ± 0.00	0.22 ± 0.00
#2698	0.26 ± 0.01	0.28 ± 0.00	0.27 ± 0.01	0.18 ± 0.01	0.26 ± 0.03	0.24 ± 0.04	0.21 ± 0.02
#2699	0.23 ± 0.01	0.31 ± 0.01	0.29 ± 0.00	0.22 ± 0.02	0.25 ± 0.00	0.25 ± 0.00	0.25 ± 0.00
#2700	0.27 ± 0.00	0.31 ± 0.01	0.26 ± 0.03	0.20 ± 0.01	0.26 ± 0.01	0.27 ± 0.00	0.22 ± 0.00
#2701	0.33 ± 0.03	0.33 ± 0.02	0.33 ± 0.01	0.24 ± 0.01	0.28 ± 0.01	0.29 ± 0.01	0.25 ± 0.00
#2702	0.28 ± 0.01	0.34 ± 0.01	0.31 ± 0.01	0.21 ± 0.01	0.27 ± 0.01	0.29 ± 0.00	0.25 ± 0.00
#2703	0.36 ± 0.01	0.37 ± 0.00	0.34 ± 0.00	0.27 ± 0.00	0.32 ± 0.00	0.27 ± 0.00	0.28 ± 0.00
#2704	0.32 ± 0.01	0.32 ± 0.00	0.28 ± 0.00	0.24 ± 0.00	0.29 ± 0.00	0.27 ± 0.00	0.29 ± 0.01
#2705	0.19 ± 0.03	0.23 ± 0.02	0.18 ± 0.04	0.12 ± 0.00	0.18 ± 0.00	0.19 ± 0.01	0.14 ± 0.00
#2706	0.19 ± 0.00	0.17 ± 0.01	0.17 ± 0.01	0.10 ± 0.00	0.12 ± 0.00	0.17 ± 0.00	0.15 ± 0.00
#2707	0.24 ± 0.01	0.25 ± 0.00	0.19 ± 0.00	0.19 ± 0.00	0.18 ± 0.00	0.18 ± 0.00	0.18 ± 0.00
#2708	0.15 ± 0.01	0.20 ± 0.00	0.15 ± 0.01	0.09 ± 0.00	0.14 ± 0.01	0.17 ± 0.00	0.14 ± 0.00
#2710	0.18 ± 0.02	0.24 ± 0.00	0.22 ± 0.01	0.11 ± 0.00	0.18 ± 0.01	0.22 ± 0.00	0.17 ± 0.02
#2813	0.20 ± 0.01	0.21 ± 0.02	0.20 ± 0.01	0.16 ± 0.00	0.17 ± 0.02	0.16 ± 0.02	0.19 ± 0.01
#2814	0.35 ± 0.00	0.19 ± 0.00	0.19 ± 0.00	0.17 ± 0.00	0.27 ± 0.00	0.22 ± 0.02	0.21 ± 0.01
#2815	0.28 ± 0.00	0.16 ± 0.01	0.08 ± 0.01	0.02 ± 0.02	0.14 ± 0.01	0.13 ± 0.01	0.08 ± 0.00
#2816	0.30 ± 0.01	0.17 ± 0.01	0.15 ± 0.00	0.18 ± 0.00	0.24 ± 0.02	0.22 ± 0.02	0.22 ± 0.01
#2817	0.26 ± 0.00	0.18 ± 0.00	0.19 ± 0.02	0.19 ± 0.01	0.20 ± 0.02	0.15 ± 0.02	0.12 ± 0.01
#2818	0.12 ± 0.00	0.13 ± 0.00	0.10 ± 0.00	0.00 ± 0.00	0.16 ± 0.00	0.06 ± 0.00	0.08 ± 0.00
#2819	0.34 ± 0.03	0.28 ± 0.03	0.23 ± 0.01	0.25 ± 0.01	0.22 ± 0.00	0.24 ± 0.01	0.22 ± 0.01
#2820	0.32 ± 0.03	0.16 ± 0.02	0.29 ± 0.02	0.60 ± 0.02	0.18 ± 0.00	0.17 ± 0.02	0.46 ± 0.00
#2821	0.26 ± 0.00	0.25 ± 0.00	0.18 ± 0.01	0.00 ± 0.00	0.22 ± 0.00	0.21 ± 0.00	0.00 ± 0.00
#2822	0.32 ± 0.00	0.24 ± 0.00	0.23 ± 0.01	0.25 ± 0.03	0.37 ± 0.01	0.24 ± 0.02	0.26 ± 0.00
#2823	0.53 ± 0.04	0.27 ± 0.01	0.27 ± 0.04	0.37 ± 0.03	0.33 ± 0.01	0.31 ± 0.01	0.25 ± 0.06
#2824	0.22 ± 0.00	0.20 ± 0.00	0.19 ± 0.00	0.20 ± 0.00	0.16 ± 0.01	0.18 ± 0.00	0.17 ± 0.00
#2825	0.22 ± 0.02	0.18 ± 0.00	0.17 ± 0.03	0.27 ± 0.01	0.17 ± 0.01	0.08 ± 0.01	0.23 ± 0.02
#2826	0.24 ± 0.00	0.23 ± 0.00	0.22 ± 0.01	0.12 ± 0.00	0.24 ± 0.00	0.00 ± 0.00	0.13 ± 0.00
#2832	0.31 ± 0.00	0.22 ± 0.00	0.20 ± 0.01	0.21 ± 0.00	0.23 ± 0.00	0.21 ± 0.00	0.21 ± 0.03
#2833	0.34 ± 0.02	0.26 ± 0.01	0.20 ± 0.00	0.19 ± 0.03	0.21 ± 0.01	0.22 ± 0.01	0.11 ± 0.01
#2834	0.25 ± 0.07	0.24 ± 0.00	0.20 ± 0.00	0.23 ± 0.01	0.28 ± 0.01	0.23 ± 0.03	0.19 ± 0.00
#2835	0.37 ± 0.02	0.27 ± 0.02	0.24 ± 0.00	0.21 ± 0.00	0.27 ± 0.00	0.25 ± 0.00	0.18 ± 0.00
#2836	0.35 ± 0.02	0.25 ± 0.02	0.19 ± 0.01	0.26 ± 0.01	0.29 ± 0.07	0.41 ± 0.02	0.18 ± 0.01
#2838	0.32 ± 0.00	0.23 ± 0.00	0.19 ± 0.01	0.28 ± 0.08	0.21 ± 0.00	0.22 ± 0.00	0.24 ± 0.00
#2841	0.39 ± 0.11	0.22 ± 0.00	0.21 ± 0.00	0.30 ± 0.01	0.37 ± 0.05	0.33 ± 0.00	0.22 ± 0.00
#2842	0.42 ± 0.01	0.33 ± 0.02	0.26 ± 0.00	0.26 ± 0.01	0.23 ± 0.00	0.31 ± 0.00	0.21 ± 0.03
#2850	0.28 ± 0.01	0.16 ± 0.00	0.17 ± 0.00	0.24 ± 0.00	0.14 ± 0.00	0.10 ± 0.00	0.17 ± 0.00
#3600	0.23 ± 0.00	0.27 ± 0.01	0.25 ± 0.00	0.15 ± 0.00	0.22 ± 0.01	0.30 ± 0.03	0.16 ± 0.05

Table 23: pH [-] values of all 72 strains obtained during biodiversity screening.
Whole set of growth screening results using the Growth Profiler device by Enzyscreen with different acetate and formate concentrations as co-substrates in combination with 20 g L^{-1} glucose (n=2).

Strain	Glucose	2.5 g/l Acetate	5 g/l Acetate	10 g/l Acetate	2.5 g/l Formate	5 g/l Formate	10 g/l Formate
#1946	5.51 ± 0.02	6.20 ± 0.00	6.70 ± 0.01	8.84 ± 0.05	6.42 ± 0.00	7.46 ± 0.00	8.89 ± 0.00
#1947	5.64 ± 0.00	6.22 ± 0.00	6.77 ± 0.01	8.89 ± 0.03	6.42 ± 0.00	7.50 ± 0.00	8.95 ± 0.00
#1949	5.37 ± 0.01	5.90 ± 0.00	6.46 ± 0.01	8.22 ± 0.01	6.40 ± 0.02	6.96 ± 0.00	7.99 ± 0.01
#1951	5.70 ± 0.00	6.19 ± 0.01	6.35 ± 0.01	8.51 ± 0.00	6.74 ± 0.00	7.80 ± 0.30	7.52 ± 0.00
#2134	5.92 ± 0.01	6.56 ± 0.02	7.36 ± 0.01	9.03 ± 0.03	6.87 ± 0.00	7.75 ± 0.01	7.39 ± 0.00
#2135	5.78 ± 0.02	6.33 ± 0.00	6.89 ± 0.03	8.60 ± 0.00	6.88 ± 0.00	7.37 ± 0.00	7.91 ± 0.00
#2136	5.85 ± 0.01	6.35 ± 0.00	6.83 ± 0.00	8.62 ± 0.02	6.89 ± 0.00	7.54 ± 0.01	7.86 ± 0.02
#2144	5.87 ± 0.01	6.43 ± 0.00	7.30 ± 0.02	8.97 ± 0.00	6.78 ± 0.01	8.01 ± 0.01	8.28 ± 0.00
#2152	5.89 ± 0.00	6.43 ± 0.00	6.98 ± 0.01	8.43 ± 0.06	6.86 ± 0.01	7.82 ± 0.01	8.49 ± 0.01
#2158	5.85 ± 0.01	6.40 ± 0.00	7.30 ± 0.16	9.08 ± 0.01	6.69 ± 0.01	7.96 ± 0.00	8.31 ± 0.00
#2162	5.64 ± 0.00	6.16 ± 0.00	6.68 ± 0.00	8.82 ± 0.03	6.25 ± 0.00	6.26 ± 0.00	6.95 ± 0.01
#2167	5.56 ± 0.00	6.10 ± 0.00	6.59 ± 0.01	8.90 ± 0.01	6.55 ± 0.00	6.41 ± 0.00	7.66 ± 0.06
#2169	5.46 ± 0.00	6.05 ± 0.00	6.54 ± 0.00	8.80 ± 0.07	6.36 ± 0.01	6.41 ± 0.00	8.04 ± 0.00
#2172	5.52 ± 0.00	6.09 ± 0.00	6.57 ± 0.00	8.87 ± 0.00	6.39 ± 0.00	6.54 ± 0.00	7.72 ± 0.01
#2177	5.68 ± 0.00	6.22 ± 0.00	6.73 ± 0.01	8.38 ± 0.00	6.74 ± 0.00	7.72 ± 0.01	7.70 ± 0.02
#2178	5.72 ± 0.00	6.17 ± 0.00	6.80 ± 0.00	6.61 ± 0.01	6.60 ± 0.03	8.20 ± 0.01	7.11 ± 0.05
#2179	5.63 ± 0.00	6.24 ± 0.00	6.74 ± 0.00	8.33 ± 0.00	6.79 ± 0.00	7.00 ± 0.00	7.30 ± 0.03
#2196	5.55 ± 0.00	6.07 ± 0.00	6.57 ± 0.01	8.69 ± 0.00	6.53 ± 0.00	6.43 ± 0.01	7.54 ± 0.02
#2197	5.66 ± 0.00	6.18 ± 0.00	6.73 ± 0.02	8.95 ± 0.03	5.98 ± 0.02	6.23 ± 0.07	7.76 ± 0.00
#2199	5.73 ± 0.01	6.30 ± 0.00	6.95 ± 0.04	8.88 ± 0.00	6.73 ± 0.01	7.97 ± 0.02	8.31 ± 0.00
#2205	5.63 ± 0.00	6.17 ± 0.00	6.65 ± 0.00	7.57 ± 0.06	6.44 ± 0.00	6.97 ± 0.01	8.09 ± 0.09
#2208	5.58 ± 0.00	6.15 ± 0.00	6.62 ± 0.01	7.58 ± 0.02	6.44 ± 0.00	6.44 ± 0.00	7.83 ± 0.02
#2209	5.66 ± 0.01	6.23 ± 0.01	6.92 ± 0.03	7.89 ± 0.05	6.69 ± 0.01	7.89 ± 0.00	7.94 ± 0.01
#2210	5.52 ± 0.00	6.50 ± 0.01	6.92 ± 0.01	8.04 ± 0.02	5.84 ± 0.00	5.97 ± 0.00	8.07 ± 0.05
#2211	5.86 ± 0.01	6.26 ± 0.00	6.44 ± 0.01	8.70 ± 0.03	6.48 ± 0.10	6.71 ± 0.01	8.64 ± 0.01
#2212	5.64 ± 0.00	6.21 ± 0.00	6.58 ± 0.04	8.73 ± 0.04	6.06 ± 0.00	6.25 ± 0.00	6.54 ± 0.01
#2213	5.64 ± 0.00	6.19 ± 0.01	7.28 ± 0.00	6.46 ± 0.00	6.50 ± 0.00	7.52 ± 0.17	6.65 ± 0.01
#2214	6.00 ± 0.00	6.48 ± 0.00	7.30 ± 0.04	8.19 ± 0.05	6.27 ± 0.00	6.29 ± 0.00	7.84 ± 0.04
#2215	5.68 ± 0.00	6.21 ± 0.00	7.03 ± 0.03	8.67 ± 0.03	6.00 ± 0.00	6.02 ± 0.00	8.67 ± 0.06
#2218	5.72 ± 0.00	6.20 ± 0.00	7.65 ± 0.03	6.46 ± 0.00	6.41 ± 0.00	7.69 ± 0.01	6.92 ± 0.01
#2219	5.72 ± 0.00	6.22 ± 0.00	7.65 ± 0.03	8.77 ± 0.00	6.37 ± 0.00	8.04 ± 0.01	8.31 ± 0.03
#2220	5.66 ± 0.00	6.20 ± 0.00	7.61 ± 0.01	8.61 ± 0.04	6.35 ± 0.01	6.38 ± 0.01	6.52 ± 0.02
#2221	5.81 ± 0.00	6.32 ± 0.00	7.67 ± 0.00	8.15 ± 0.00	6.62 ± 0.00	6.49 ± 0.00	6.16 ± 0.00
#2229	5.80 ± 0.00	6.27 ± 0.00	7.71 ± 0.00	8.88 ± 0.02	6.63 ± 0.00	6.47 ± 0.00	7.71 ± 0.89
#2696	5.77 ± 0.00	6.34 ± 0.00	7.71 ± 0.04	8.74 ± 0.02	6.51 ± 0.00	7.77 ± 0.00	8.98 ± 0.00
#2697	5.81 ± 0.00	6.32 ± 0.01	6.99 ± 0.02	8.50 ± 0.00	6.52 ± 0.02	7.82 ± 0.03	8.93 ± 0.00
#2698	5.53 ± 0.00	6.11 ± 0.01	7.68 ± 0.03	8.73 ± 0.01	6.27 ± 0.00	7.93 ± 0.02	8.71 ± 0.02
#2699	5.61 ± 0.01	6.22 ± 0.00	6.78 ± 0.01	8.47 ± 0.01	8.37 ± 0.00	7.81 ± 0.00	8.35 ± 0.02
#2700	5.38 ± 0.30	6.28 ± 0.01	6.96 ± 0.01	8.31 ± 0.00	6.69 ± 0.00	7.78 ± 0.02	8.21 ± 0.01
#2701	5.73 ± 0.01	6.34 ± 0.01	7.01 ± 0.02	8.27 ± 0.01	6.70 ± 0.01	7.82 ± 0.01	8.31 ± 0.02
#2702	6.03 ± 0.01	6.48 ± 0.00	7.20 ± 0.00	8.33 ± 0.00	6.77 ± 0.00	7.84 ± 0.01	8.06 ± 0.01
#2703	5.68 ± 0.02	6.37 ± 0.00	7.25 ± 0.01	8.76 ± 0.00	6.62 ± 0.00	7.70 ± 0.05	8.61 ± 0.01
#2704	5.71 ± 0.00	6.35 ± 0.00	7.24 ± 0.00	8.78 ± 0.00	6.55 ± 0.00	7.93 ± 0.20	8.55 ± 0.01
#2705	5.65 ± 0.01	6.51 ± 0.00	7.11 ± 0.02	8.14 ± 0.00	6.82 ± 0.02	7.16 ± 0.01	7.14 ± 0.00
#2706	5.90 ± 0.02	6.51 ± 0.00	7.12 ± 0.04	8.25 ± 0.07	6.80 ± 0.01	7.67 ± 0.00	6.56 ± 0.04
#2707	6.06 ± 0.04	6.49 ± 0.06	7.20 ± 0.10	8.55 ± 0.01	6.73 ± 0.01	6.68 ± 0.03	6.18 ± 0.00
#2708	5.97 ± 0.02	6.55 ± 0.00	7.24 ± 0.02	8.11 ± 0.00	6.81 ± 0.00	7.74 ± 0.13	6.64 ± 0.01
#2710	6.23 ± 0.00	6.69 ± 0.00	7.33 ± 0.00	8.41 ± 0.03	6.91 ± 0.00	8.08 ± 0.00	8.07 ± 0.04
#2813	5.98 ± 0.02	6.46 ± 0.02	7.21 ± 0.00	8.25 ± 0.01	6.62 ± 0.00	6.17 ± 0.00	7.88 ± 0.04
#2814	5.81 ± 0.01	6.19 ± 0.01	6.85 ± 0.02	8.14 ± 0.00	6.27 ± 0.00	7.90 ± 0.00	8.51 ± 0.01
#2815	5.70 ± 0.07	6.23 ± 0.01	6.85 ± 0.02	6.48 ± 0.00	6.56 ± 0.02	7.76 ± 0.00	8.48 ± 0.02
#2816	5.97 ± 0.00	6.23 ± 0.01	6.96 ± 0.00	8.61 ± 0.01	6.44 ± 0.00	7.98 ± 0.00	8.22 ± 0.01
#2817	5.78 ± 0.01	6.43 ± 0.00	6.82 ± 0.00	8.51 ± 0.00	6.20 ± 0.00	6.21 ± 0.02	6.39 ± 0.02
#2818	5.76 ± 0.01	6.22 ± 0.02	6.40 ± 0.01	6.50 ± 0.01	6.43 ± 0.01	6.42 ± 0.09	6.46 ± 0.06
#2819	6.04 ± 0.00	6.25 ± 0.00	7.16 ± 0.02	8.23 ± 0.01	6.57 ± 0.00	7.85 ± 0.00	8.43 ± 0.02
#2820	5.95 ± 0.00	6.56 ± 0.00	7.11 ± 0.01	7.96 ± 0.01	6.57 ± 0.00	7.98 ± 0.01	8.52 ± 0.00
#2821	5.78 ± 0.01	6.33 ± 0.00	7.67 ± 0.00	6.50 ± 0.04	6.62 ± 0.00	7.98 ± 0.01	7.93 ± 0.01
#2822	4.18 ± 0.03	6.46 ± 0.00	4.89 ± 0.02	8.92 ± 0.04	6.19 ± 0.01	7.97 ± 0.06	8.54 ± 0.02
#2823	5.79 ± 0.05	4.34 ± 0.01	6.85 ± 0.00	8.28 ± 0.01	6.49 ± 0.00	7.83 ± 0.00	8.78 ± 0.00
#2824	6.01 ± 0.01	6.29 ± 0.00	7.16 ± 0.02	8.35 ± 0.01	6.82 ± 0.00	7.85 ± 0.01	6.92 ± 0.00
#2825	5.82 ± 0.08	6.45 ± 0.01	6.94 ± 0.01	8.08 ± 0.01	6.72 ± 0.00	7.65 ± 0.03	8.12 ± 0.00
#2826	5.66 ± 0.01	6.38 ± 0.15	6.86 ± 0.01	8.24 ± 0.04	6.38 ± 0.01	7.13 ± 0.63	6.21 ± 0.01
#2832	5.85 ± 0.01	6.19 ± 0.02	7.09 ± 0.01	8.71 ± 0.01	6.56 ± 0.00	7.74 ± 0.01	8.22 ± 0.00
#2833	5.60 ± 0.01	6.47 ± 0.00	6.81 ± 0.02	6.96 ± 0.01	6.45 ± 0.00	7.85 ± 0.02	7.91 ± 0.04
#2834	5.78 ± 0.00	6.17 ± 0.01	7.09 ± 0.01	8.52 ± 0.03	6.59 ± 0.02	7.91 ± 0.01	8.60 ± 0.03
#2835	5.75 ± 0.00	6.31 ± 0.00	7.04 ± 0.01	8.56 ± 0.00	6.65 ± 0.00	8.03 ± 0.01	8.49 ± 0.00
#2836	5.69 ± 0.01	6.52 ± 0.00	7.31 ± 0.00	8.60 ± 0.00	6.58 ± 0.00	7.94 ± 0.02	8.76 ± 0.02
#2838	5.59 ± 0.00	6.23 ± 0.00	7.06 ± 0.00	8.63 ± 0.01	6.48 ± 0.00	7.76 ± 0.00	8.74 ± 0.00
#2841	5.63 ± 0.00	6.22 ± 0.00	6.87 ± 0.00	8.55 ± 0.01	6.56 ± 0.00	7.79 ± 0.00	8.70 ± 0.02
#2842	5.77 ± 0.00	6.27 ± 0.00	6.97 ± 0.00	8.59 ± 0.02	6.82 ± 0.00	8.09 ± 0.00	8.44 ± 0.02
#2850	5.64 ± 0.06	6.21 ± 0.00	6.56 ± 0.02	8.61 ± 0.03	6.32 ± 0.03	7.06 ± 0.08	8.35 ± 0.02
#3600	5.77 ± 0.00	6.28 ± 0.00	6.75 ± 0.00	8.54 ± 0.02	6.66 ± 0.00	6.90 ± 0.01	6.72 ± 0.01

Table 24: Production parameters of biodiversity screening for acetate co-utilization.

Strain	C-source	Max. OD_{600nm} [-]	$Y_{OD/S}$ [max. $OD_{600nm}/g_{c\text{-}source}$]	$Y_{OD/S}$ [max. OD_{600nm}/c-$mol_{c\text{-}source}$]
U. maydis #1946	Glucose	46.8	2.34	69.9
		48.3	2.42	72.1
	Glucose + Acetate	55.9	2.48	77.6
		56.5	2.51	78.5
U. cynodontis #2707	Glucose	40.7	2.03	60.7
		41.3	2.07	61.7
	Glucose + Acetate	53.7	2.38	74.5
		54.0	2.40	75.0
U. maydis #2136	Glucose	29.9	1.40	44.6
		19.9	1.00	29.8
	Glucose + Acetate	51.4	1.71	56.5
		52.8	1.76	58.1
U. maydis #2135	Glucose	19.7	0.99	29.4
		22.5	1.13	33.6
	Glucose + Acetate	49.5	1.65	54.4
		49.8	1.66	54.8
U. rabenhorstiana #2708	Glucose	38.0	1.90	56.8
		38.2	1.91	57.0
	Glucose + Acetate	48.3	2.14	67.0
		50.0	2.22	69.5

Table 25: Production parameters of biodiversity screening for formate co-utilization.

Strain	C-source	Max. OD_{600nm} [-]	$Y_{OD/S}$ [max. $OD_{600nm}/g_{c\text{-}source}$]	$Y_{OD/S}$ [max. OD_{600nm}/c-$mol_{c\text{-}source}$]
U. rabenhorstiana #2708	Glucose	38.0	1.90	56.8
		38.2	1.91	57.0
	Glucose + Formate	56.6	2.52	80.9
		56.7	2.52	81.0
U. cynodontis #2707	Glucose	31.6	1.58	47.2
		33.0	1.65	49.3
	Glucose + Formate	50.0	2.22	71.5
		50.5	2.25	72.2
U. maydis #2177	Glucose	29.0	1.45	43.3
		30.2	1.51	45.0
	Glucose + Formate	42.0	1.86	59.9
		43.1	1.91	61.5
U. cynodontis #2706	Glucose	27.5	1.37	41.0
		27.7	1.38	41.3
	Glucose + Formate	40.4	1.70	57.6
		44.2	1.93	63.1
U. maydis #2196	Glucose	36.3	1.82	54.2
		37.8	1.89	56.4
	Glucose + Formate	42.3	1.88	60.4
		43.4	1.93	62.0

Table 26: Production parameters of System Duetz cultivation for acetate co-utilization in MES buffer.

Strain	C-source	$Titer_{max}$ [g L^{-1}]	$Y_{P/S}$ [$g_{ITA}/g_{c\text{-}source}$]	$Y_{P/S}$ [$c\text{-}mol_{ITA}/c\text{-}mol_{c\text{-}source}$]	Max. OD [-]
U. maydis #2229	Glucose	2.99	0.060	0.069	39
		3.38	0.068	0.078	33
	Glucose + Acetate	7.20	0.144	0.152	49
		7.60	0.152	0.161	48
U. rabenhorstiana #2708	Glucose	4.30	0.086	0.099	39
		4.31	0.101	0.099	40
	Glucose + Acetate	6.88	0.136	0.144	41
		6.80	0.138	0.145	45
U. cynodontis #2707	Glucose	2.24	0.045	0.052	53
		2.05	0.041	0.047	52
	Glucose + Acetate	2.88	0.056	0.060	50
		2.88	0.058	0.061	53
U. maydis #2135	Glucose	2.40	0.048	0.055	46
		2.42	0.048	0.056	47
	Glucose + Acetate	2.97	0.071	0.075	54
		2.35	0.059	0.063	58
U. maydis #2136	Glucose	2.36	0.047	0.054	50
		2.28	0.046	0.053	51
	Glucose + Acetate	2.32	0.046	0.049	49
		2.22	0.044	0.047	50
U. maydis #1946	Glucose	0.09	0.002	0.002	71
		0.06	0.001	0.001	73
	Glucose + Acetate	0.01	0.000	0.00	72
		0.01	0.000	0.00	66

Table 27: Production parameters of System Duetz cultivation for acetate co-utilization in $CaCO_3$ buffer.

Strain	C-source	$Titer_{max}$ [g L^{-1}]	$Y_{P/S}$ [$g_{ITA}/g_{c\text{-}source}$]	$Y_{P/S}$ [$c\text{-}mol_{ITA}/c\text{-}mol_{c\text{-}source}$]	Max. OD [-]
U. maydis #2229	Glucose	4.08	0.082	0.087	39
		4.47	0.089	0.095	40
	Glucose + Acetate	5.62	0.100	0.119	56
		5.16	0.092	0.110	58
U. rabenhorstiana #2708	Glucose	3.26	0.065	0.069	60
		3.09	0.062	0.066	62
	Glucose + Acetate	3.10	0.055	0.066	60
		3.23	0.057	0.069	59
U. cynodontis #2707	Glucose	6.33	0.127	0.134	62
		6.22	0.124	0.132	65
	Glucose + Acetate	5.30	0.094	0.113	55
		5.78	0.103	0.123	60
U. maydis #2135	Glucose	3.13	0.063	0.066	54
		3.27	0.065	0.070	53
	Glucose + Acetate	3.40	0.060	0.072	56
		3.78	0.067	0.080	60
U. maydis #2136	Glucose	3.80	0.076	0.081	56
		3.95	0.079	0.084	53
	Glucose + Acetate	3.82	0.068	0.081	50
		3.56	0.063	0.076	51
U. maydis #1946	Glucose	0.08	0.002	0.002	67
		0.05	0.001	0.000	68
	Glucose + Acetate	0.01	0.000	0.000	72
		0.01	0.000	0.000	73

Table 28: Production parameters of System Duetz cultivation for formate co-utilization in MES buffer.

Strain	C-source	$Titer_{max}$ [g L^{-1}]	$Y_{P/S}$ [$g_{ITA}/g_{c\text{-}source}$]	$Y_{P/S}$ [$c\text{-}mol_{ITA}/c\text{-}mol_{c\text{-}source}$]	Max. OD [-]
U. cynodontis #2706	Glucose	6,64	0.133	0.153	51
		6,90	0.138	0.159	50
	Glucose + Formate	6,90	0.123	0.151	38
		5,81	0.103	0.127	36
U. cynodontis #2705	Glucose	6,18	0.124	0.143	52
		6,32	0.126	0.146	57
	Glucose + Formate	9,04	0.161	0.198	50
		8,20	0.146	0.179	54
U. rabenhorstiana #2708	Glucose	4,16	0,083	0.096	48
		4,35	0,087	0.100	50
	Glucose + Formate	3,98	0.071	0.087	35
		2,64	0.047	0.058	37
U. maydis #2229	Glucose	2,61	0,052	0.060	50
		2,87	0,057	0.066	54
	Glucose + Formate	0,30	0.005	0.007	37
		0,31	0.004	0.007	36
U. maydis #2177	Glucose	2,78	0.056	0.064	66
		2,60	0.052	0.060	65
	Glucose + Formate	0,43	0.008	0.009	65
		0,49	0.009	0.011	66
U. maydis #2196	Glucose	0,66	0,013	0.015	79
		0,55	0,011	0.013	80
	Glucose + Formate	0,04	0.001	0.001	60
		0,04	0.001	0.001	57

Table 29: Production parameters of System Duetz cultivation for formate co-utilization in $CaCO_3$ buffer.

Strain	C-source	$Titer_{max}$ [g L^{-1}]	$Y_{P/S}$ [$g_{ITA}/g_{c\text{-}source}$]	$Y_{P/S}$ [$c\text{-}mol_{ITA}/c\text{-}mol_{c\text{-}source}$]	Max. OD [-]
U. cynodontis #2706	Glucose	11.09	0.222	0.256	28
		8.94	0.179	0.206	25
	Glucose + Formate	8.09	0.144	0.177	26
		11.55	0.205	0.253	25
U. cynodontis #2705	Glucose	4.88	0.098	0.113	25
		4.85	0.097	0.112	24
	Glucose + Formate	6.29	0.112	0.138	24
		5.41	0.096	0.118	22
U. rabenhorstiana #2708	Glucose	1.85	0.037	0.043	47
		1.89	0.040	0.046	46
	Glucose + Formate	0.92	0.016	0.020	34
		1.02	0.018	0.022	35
U. maydis #2229	Glucose	4.08	0.082	0.094	34
		3.68	0.074	0.085	35
	Glucose + Formate	0.87	0.015	0.019	32
		1.41	0.025	0.031	30
U. maydis #2177	Glucose	1.94	0.039	0.045	47
		1.73	0.035	0.040	46
	Glucose + Formate	0.91	0.016	0.020	47
		0.88	0.016	0.019	50
U. maydis #2196	Glucose	1.73	0.035	0.045	50
		1.55	0.036	0.036	51
	Glucose + Formate	0.91	0.016	0.020	43
		1.01	0.018	0.022	44

Table 30: pH values during System Duetz cultivation for formate and acetate co-utilization.

Strain	Buffer	C-source	Min. pH [-]	End pH [-]	Strain	Buffer	C-source	Min. pH [-]	End pH [-]
U. maydis #2229	MES	Glucose	4.98	5.76	*U. cynodontis* #2706	MES	Glucose	3.04	3.07
			4.96	5.80				3.03	3.01
		Glucose + Acetate	5.49	5.78			Glucose + Formate	4.96	4.96
			5.48	5.80				4.94	4.94
	CaCO3	Glucose	6.01	6.77		CaCO3	Glucose	5.21	5.47
			6.26	6.80				5.33	5.46
		Glucose + Acetate	6.68	7.18			Glucose + Formate	6.16	7.94
			6.58	7.22				6.07	8.12
U. rabenhorstiana #2708	MES	Glucose	2.51	2.86	*U. cynodontis* #2705	MES	Glucose	2.86	2.86
			2.47	2.85				2.83	2.83
		Glucose + Acetate	3.11	3.36			Glucose + Formate	4.26	4.26
			3.13	3.37				4.34	4.34
	CaCO3	Glucose	6.54	7.10		CaCO3	Glucose	5.72	5.81
			6.51	7.34				5.64	6.79
		Glucose + Acetate	6.83	7.61			Glucose + Formate	6.40	8.03
			6.82	7.65				6.62	8.25
U. cynodontis #2707	MES	Glucose	3.37	3.44	*U. rabenhorstiana* #2708	MES	Glucose	3.80	3.95
			3.44	3.45				3.76	3.84
		Glucose + Acetate	3.79	3.79			Glucose + Formate	5.08	5.08
			3.78	3.78				5.11	5.11
	CaCO3	Glucose	6.55	7.18		CaCO3	Glucose	6.21	7.63
			6.57	7.19				6.04	7.62
		Glucose + Acetate	6.91	7.15			Glucose + Formate	6.59	6.59
			6.94	7.11				6.63	7.94
U. maydis #2135	MES	Glucose	4.64	5.68	*U. maydis* #2229	MES	Glucose	4.85	5.87
			4.70	5.71				4.87	5.88
		Glucose + Acetate	5.07	5.85			Glucose + Formate	5.54	6.05
			5.09	5.80				5.56	6.06
	CaCO3	Glucose	6.50	7.71		CaCO3	Glucose	5.13	5.57
			6.53	7.72				5.30	5.65
		Glucose + Acetate	6.72	7.63			Glucose + Formate	5.77	8.13
			6.88	7.82				5.86	8.02
U. maydis #2136	MES	Glucose	5.02	5.72	*U. maydis* #2177	MES	Glucose	5.11	5.60
			5.03	5.74				5.10	5.56
		Glucose + Acetate	5.36	5.78			Glucose + Formate	5.64	6.57
			5.38	5.79				5.65	6.56
	CaCO3	Glucose	6.65	7.46		CaCO3	Glucose	6.50	8.42
			6.67	7.59				6.48	8.48
		Glucose + Acetate	6.89	7.81			Glucose + Formate	6.50	8.92
			6.84	7.71				6.48	8.96
U. maydis #1946	MES	Glucose	5.61	5.63	*U. maydis* #2196	MES	Glucose	5.93	5.98
			5.64	5.70				5.93	5.99
		Glucose + Acetate	6.34	6.43			Glucose + Formate	5.87	7.27
			6.32	6.42				5.87	7.26
	CaCO3	Glucose	6.66	7.63		CaCO3	Glucose	6.71	7.80
			6.56	7.72				6.75	7.09
		Glucose + Acetate	6.88	8.39			Glucose + Formate	6.66	7.69
			6.94	8.40				6.70	7.79

Table 31: Welch t-test result for shake flask cultivations of metabolically engineered *U. cynodontis* strains. *#4852: U. cynodontis Δfuz7 Δcyp3 ↑P_{ria1}* (highlighted in yellow) and *#4853: U. cynodontis Δfuz7 Δcyp3 P_{etef}mttA ↑P_{ria1}* (highlighted in blue). Cultivations were carried out following (section 4.1). MTM medium (33 g · L^{-1} CaCO3, 0.8 g L^{-1} NH_4Cl, 100 g · L^{-1} glucose) with 0 g · L^{-1} or 2 g · L^{-1} formate was used.

t-test: two-sample assuming unequal variances		
#4853 maximum titer	shake flasks	
	Glc	*Glc + Form*
Mean	50.866	56.0923333
Variance	0.277263	0.04606233
Observations	3	3
Hypothesized Mean Difference	0	
df	3	
t Stat	-15.9198095	
P(T<=t) one-tail	0.00026946	
t Critical one-tail	2.35336343	
P(T<=t) two-tail	0.00053892	
t Critical two-tail	3.18244631	

t-test: two-sample assuming unequal variances		
#4853 maximum yield	shake flasks	
	Glc	*Glc + Form*
Mean	0.51234375	0.55606885
Variance	2.8129E-05	4.5268E-06
Observations	3	3
Hypothesized Mean Difference	0	
df	3	
t Stat	-13.2528308	
P(T<=t) one-tail	0.00046418	
t Critical one-tail	2.35336343	
P(T<=t) two-tail	0.0009283	
t Critical two-tail	3.18244631	

t-test: two-sample assuming unequal variances		
#4852 maximum titer	shake flasks	
	Glc	*Glc + Form*
Mean	50.859	53.875
Variance	0.170443	0.674719
Observations	3	3
Hypothesized Mean Difference	0	
df	3	
t Stat	-5.68227154	
P(T<=t) one-tail	0.00540075	
t Critical one-tail	2.35336343	
P(T<=t) two-tail	0.0108015	
t Critical two-tail	3.18244631	

t-test: two-sample assuming unequal variances		
#4852 maximum yield	shake flasks	
	Glc	*Glc + Form*
Mean	0.51227324	0.53408742
Variance	1.7292E-05	6.6309E-05
Observations	3	3
Hypothesized Mean Difference	0	
df	3	
t Stat	-4.13231314	
P(T<=t) one-tail	0.01285643	
t Critical one-tail	2.35336343	
P(T<=t) two-tail	0.02571287	
t Critical two-tail	3.18244631	

Table 32: Tested DoE conditions and responses during this study investigating acetate co-metabolization for *U. maydis* MB215 wildtype strain.

No.	Run	Glucose [g L^{-1}]	Acetate [g L^{-1}]	Buffer [-]	Yield [c-mol c-mol^{-1}][a]	Titer [g L^{-1}]
32	1	100	2	$CaCO_3$	0.11	9.64
41	2	25.6	7	$CaCO_3$	0.09	2.56
12	3	100	12	MES	0.08	7.52
8	4	30	12	MES	0.05	1.76
26	5	65	7	MES	0.06	2.90
9	6	30	12	MES	0.05	3.52
17	7	65	1.4	MES	0.05	2.41
27	8	65	7	MES	0.06	7.53
30	9	30	2	$CaCO_3$	0.08	2.41
47	10	65	12.6	$CaCO_3$	0.11	7.53
36	11	30	12	$CaCO_3$	0.09	2.93
22	12	65	7	MES	0.06	3.87
10	13	100	12	MES	0.09	8.15
52	14	65	7	$CaCO_3$	0.10	6.37
45	15	65	1.4	$CaCO_3$	0.95	5.44
54	16	65	7	$CaCO_3$	0.12	7.30
50	17	65	7	$CaCO_3$	0.12	7.78
2	18	30	2	MES	0.54	1.49
35	19	30	12	$CaCO_3$	0.08	2.79
42	20	25.9	7	$CaCO_3$	0.09	2.54
53	21	65	7	$CaCO_3$	0.11	6.74
44	22	104	7	$CaCO_3$	0.14	13.18
18	23	65	1.4	MES	0.04	2.77
23	24	100	7	MES	0.06	3.68
33	25	100	2	$CaCO_3$	0.11	9.86
34	26	30	2	$CaCO_3$	0.11	9.89
1	27	65	2	MES	0.06	1.64
49	28	65	7	$CaCO_3$	0.11	7.13
38	29	100	12	$CaCO_3$	0.13	12.86
55	30	65	7	$CaCO_3$	0.12	7.60
5	31	100	2	MES	0.04	3.42
15	32	104	7	MES	0.07	6.96
56	33	65	7	$CaCO_3$	0.12	7.33
48	34	65	12.6	$CaCO_3$	0.11	7.55
4	35	100	2	MES	0.04	3.48
51	36	65	7	$CaCO_3$	0.11	7.20
16	37	104	7	MES	0.07	6.80
21	38	65	7	MES	0.09	5.57
19	39	65	12	MES	0.09	5.82
43	40	104	6	$CaCO_3$	0.13	13.1
20	41	65	12.6	MES	0.09	5.50
11	42	100	12	MES	0.08	7.62
37	43	30	12	$CaCO_3$	0.08	2.70
24	44	65	7	MES	0.08	5.01
28	45	65	7	MES	0.08	5.14
39	46	100	12	$CaCO_3$	0.13	12.41
29	47	30	2	$CaCO_3$	0.09	2.43
7	48	30	12	MES	0.06	2.11
6	49	100	2	MES	0.05	4.07
14	50	26	7	MES	0.09	2.33
25	51	65	7	MES	0.09	5.22
3	52	30	2	MES	0.05	1.28
13	53	26	7	MES	0.08	2.20
46	54	65	1.4	$CaCO_3$	0.10	5.66
40	55	100	12	$CaCO_3$	0.14	13.45
31	56	30	2	$CaCO_3$	0.09	2.45

Table 33: Tested DoE conditions and responses during this study investigating acetate co-metabolization for *U. rabenhorstiana* #2708 wildtype strain.

No.	Run	Glucose [g L^{-1}]	Acetate [g L^{-1}]	Buffer [-]	Yield [c-mol c-mol^{-1}][a]	Titer [g L^{-1}]
21	1	65	7	$CaCO_3$	0.07	4.06
19	2	65	12.6	$CaCO_3$	0.07	4.67
11	3	100	12	$CaCO_3$	0.09	8.35
28	4	65	7	$CaCO_3$	0.07	4.02
12	5	100	12	$CaCO_3$	0.09	8.77
8	6	30	12	$CaCO_3$	0.02	0.66
10	7	100	12	$CaCO_3$	0.09	9.31
9	8	104	12	$CaCO_3$	0.02	0.62
15	9	30	7	$CaCO_3$	0.10	10.21
1	10	104	2	$CaCO_3$	0.04	1.21
16	11	65	7	$CaCO_3$	0.11	10.73
27	12	100	7	$CaCO_3$	0.07	4.05
6	13	30	2	$CaCO_3$	0.10	9.27
2	14	30	2	$CaCO_3$	0.04	1.23
3	15	100	2	$CaCO_3$	0.04	1.08
5	16	26	2	$CaCO_3$	0.12	10.6
14	17	30	7	$CaCO_3$	0.04	1.11
7	18	65	12	$CaCO_3$	0.02	0.51
24	19	65	7	$CaCO_3$	0.09	5.33
18	20	26	1.4	$CaCO_3$	0.07	3.92
13	21	65	7	$CaCO_3$	0.04	1.09
17	22	65	1.4	$CaCO_3$	0.07	4.05
22	23	65	7	$CaCO_3$	0.13	8.11
25	24	65	7	$CaCO_3$	0.13	8.10
26	25	100	7	$CaCO_3$	0.12	7.86
4	26	65	2	$CaCO_3$	0.11	10.12
23	27	65	7	$CaCO_3$	0.12	7.86
20	28	65	12.6	$CaCO_3$	0.06	3.85

Table 34: Tested DoE conditions and responses during this study investigating acetate co-metabolization for *U. maydis* MB215 Δ*cyp3* Δ*fuz7* ΔUA ΔMEL ΔP_{ria1}::P_{etef} P_{etef} .

Different combinations of glucose, sodium acetate and ammonium chloride in MTM using $CaCO_3$ buffer [63]. [a]yield calculation incl. sodium acetate.

No.	Run	Glucose [g L^{-1}]	Acetate [g L^{-1}]	NH_4Cl [g L^{-1}]	Yield [g g^{-1}][a]	Titer [g L^{-1}]
27	7	13.65	10.5	2.4	0.01	0.31
26	13	13.65	10.5	2.4	0.01	0.26
25	33	13.65	10.5	2.4	0.02	0.42
21	4	50	18	4	0.01	0.32
15	9	50	3	4	0.26	13.96
2	11	50	3	0.8	0.58	30.73
20	12	50	18	4	0.01	0.33
3	18	50	3	0.8	0.59	31.52
1	19	50	3	0.8	0.60	31.89
13	26	50	3	4	0.20	10.40
19	30	50	18	4	0.01	0.28
14	31	50	3	4	0.24	12.75
9	37	50	18	0.8	0.49	33.24
8	39	50	18	0.8	0.50	33.70
7	44	50	18	0.8	0.50	33.93
45	2	165	10.5	2.4	0.55	96.56
38*	3	165	10.5	0.3	0.62	96.55
42	5	165	10.5	4.5	0.40	97.32
43	8	165	10.5	2.4	0.54	95.27
34	10	165	20.4	2.4	0.56	103.98
36	15	165	20.4	2.4	0.56	104.59
33	16	165	0.6	2.4	0.56	92.18
32	17	165	0.6	2.4	0.58	96.61
37*	21	165	10.5	0.3	0.61	94.21
39*	22	165	10.5	0.3	0.62	96.24

31	23	165	0.6	2.4	0.60	99.21
46	24	165	10.5	2.4	0.55	96.95
35	27	165	20.4	2.4	0.50	92.95
40	29	165	10.5	4.5	0.41	98.69
44	36	280	10.5	2.4	0.57	100.3
47	43	280	10.5	2.4	0.56	98.56
41	47	280	10.5	4.5	0.42	103.50
48	48	280	10.5	2.4	0.58	101.53
5*	6	280	3	0.8	0.53	138.85
11*	14	280	18	0.8	0.52	135.30
17	20	280	3	4	0.48	136.23
16	25	280	3	4	0.49	137.59
6*	28	280	3	0.8	0.51	135.51
18	32	280	3	4	0.51	143.18
23	34	280	18	4	0.42	124.97
24	35	280	18	4	0.43	126.95
12*	38	280	18	0.8	0.55	142.45
4*	41	280	3	0.8	0.54	137.14
10*	42	280	18	0.8	0.50	128.85
22	46	280	18	4	0.47	139.70
30	1	316.4	10.5	2.4	0.48	150.30
28	40	316.4	10.5	2.4	0.47	154.82
29	45	316.4	10.5	2.4	0.48	152.00

Table 35: Tested DoE conditions and responses during this study investigating formtate co-metabolization for *U. cynodontis* Δ*fuz7* Δ*cyp3* ↑P_{etef}mttA ↑P_{ria1}.

Different combinations of glucose, formate and ammonium chloride in MTM using $CaCO_3$ buffer [63]. [a]yield calculation incl. formate, [b]yield calculation excluding formate.

No.	Run	Glucose [g L^{-}	Formate [g	NH_4Cl [g L^{-}	Yield [g g^{-}	Yield [g g^{-}	Titer [g L^{-1}]
44	10	13.65	8.75	2.4	0.01	0.01	0.07
42	14	13.65	8.75	2.4	0.02	0.03	0.42
43	68	13.65	8.75	2.4	0.01	0.01	0.14
41	72	13.65	8.75	2.4	0.02	0.02	0.34
1	9	50	2.5	0.8	0.49	0.51	25.58
25	25	50	2.5	4	0.16	0.16	8.04
3	32	50	2.5	0.8	0.51	0.53	26.93
22	39	50	2.5	4	0.18	0.18	9.42
4	54	50	2.5	0.8	0.51	0.55	27.25
5	56	50	2.5	0.8	0.01	0.53	26.98
24	60	50	2.5	4	0.17	0.18	8.94
2	64	50	2.5	0.8	0.52	0.55	27.53
21	66	50	2.5	4	0.17	0.18	9.43
23	70	50	2.5	4	0.18	0.19	9.74
14	16*	50	15	0.8	0.37	0.45	22.67
13	18*	50	15	0.8	0.39	0.48	24.17
32	21*	50	15	4	0.02	0.01	0.10
31	31*	50	15	4	0.01	0.01	0.25
12	33*	50	15	0.8	0.40	0.49	24.58
33	34*	50	15	4	0.10	0.10	5.18
34	41*	50	15	4	0.10	0.11	5.76
35	47*	50	15	4	0.01	0.01	0.13
15	51*	50	15	0.8	0.40	0.49	24.54
11	65	50	15	0.8	0.43	0.51	25.76
50	29	165	0.52	2.4	0.62	0.62	103.38
51	37	165	0.52	2.4	0.58	0.58	96.74
49	42	165	0.52	2.4	0.59	0.59	98.05
52	57	165	0.52	2.4	0.56	0.56	92.80
66	1	165	8.75	2.4	0.57	0.59	98.75
62	5	165	8.75	4.5	0.52	0.54	90.29
72	19	165	8.75	2.4	0.52	0.58	96.03
63	24	165	8.75	4.5	0.51	0.53	87.81
57	26*	165	8.75	0.29	0.65	0.65	101.10
71	27	165	8.75	2.4	0.56	0.59	98.01

70	28	165	8.75	2.4	0.52	0.55	90.57
67	30	165	8.75	2.4	0.56	0.59	97.38
64	36	165	8.75	4.5	0.48	0.51	84.20
59	38*	165	8.75	0.29	0.65	0.66	66.35
69	40	165	8.75	2.4	0.56	0.59	97.88
65	43	165	8.75	2.4	0.57	0.60	98.31
68	46	165	8.75	2.4	0.53	0.56	93.22
58	59*	165	8.75	0.29	0.65	0.65	65.66
60	61*	165	8.75	0.29	0.66	0.43	71.95
61	62	165	8.75	4.5	0.52	0.54	90.56
54	2	165	16.98	2.4	0.52	0.57	94.67
53	7	165	16.98	2.4	0.52	0.57	93.86
55	52	165	16.98	2.4	0.51	0.56	92.120
56	63	165	16.98	2.4	0.53	0.58	95.78
9	3*	280	2.5	0.8	0.58	0.58	104.16
28	12	280	2.5	4	0.49	0.49	139.21
29	13	280	2.5	4	0.50	0.50	142.67
10	17*	280	2.5	0.8	0.51	0.51	96.84
8	22*	280	2.5	0.8	0.50	0.50	96.16
27	44	280	2.5	4	0.49	0.49	138.14
7	50*	280	2.5	0.8	0.52	0.53	99.37
30	53	280	2.5	4	0.50	0.50	141.36
26	55	280	2.5	4	0.49	0.50	141.64
6	71*	280	2.5	0.8	0.55	0.55	101.9
37	4	280	15	4	0.47	0.49	139.25
36	8	280	15	4	0.47	0.50	139.67
16	15	280	15	0.8	0.52	0.55	109.29
20	20*	280	15	0.8	0.48	0.49	106.72
39	23	280	15	4	0.50	0.53	148.39
18	35*	280	15	0.8	0.48	0.38	107.08
19	45*	280	15	0.8	0.48	0.51	108.4
38	48	280	15	4	0.59	0.62	173.61
40	67	280	15	4	0.49	0.52	145.95
17	69*	280	15	0.8	0.49	0.49	107.3
48	6*	316.35	8.75	2.4	0.43	0.43	128.31
46	11*	316.35	8.75	2.4	0.42	0.42	132.67
47	49*	316.35	8.75	2.4	0.47	0.48	139.35
45	58*	316.35	.75	2.4	0.46	0.47	136.12

Table 36: Results from the catalytic conversion of CO_2 for formate.
Reaction conditions: 3 mL of 1 M NaOH solution saturated with CO_2, 60 bar H_2, 1 µmol [Ru] in 2 mL solvent, 70 °C. Multiple runs resemble re-use of the same catalyst phase.

No.	Run	Solvent	Time [h]	c(Formate) [M]	c(Formate) [g L^{-1}]
1	1	Tetradecane	23.7	0.783	53.2
2	2	Tetradecane	26.0	0.788	53.6
3	3	Tetradecane	26.0	0.720	49.0
4	1	Octylacetate	2.7	0.783	53.3
5	2	Octylacetate	2.4	0.793	54.0
6	3	Octylacetate	2.2	0.779	53.0
7	1	Anisole	0.6	0.772	52.5
8	2	Anisole	0.5	0.688	46.8
9	3	Anisole	0.5	0.770	52.40

4.5.2 Supplementary figures

Figure 69: ANOVA analysis for the itaconate titer model for acetate co-metabolization of *U. maydis* MB215. (A) ANOVA analysis table regarding itaconate c-mol yield, (B) ANOVA analysis table regarding itaconate titer.

A

Source	p-value	
Model	< 0.0001	significant
A-Glucose	< 0.0001	
B-Acetate	< 0.0001	
C-Buffer	< 0.0001	
AB	< 0.0001	
AC	< 0.0001	
BC	0.0276	
A^2	0.1319	
B^2	< 0.0001	
Lack of Fit	0.0540	not significant
R^2= 0.9285		

B

Source	p-value	
Model	< 0.0001	significant
A-Glucose	< 0.0001	
B-Acetate	< 0.0001	
C-Buffer	< 0.0001	
AB	< 0.0001	
AC	< 0.0001	
BC	0.0931	
A^2	0.5299	
B^2	< 0.0001	
Lack of Fit	0.0555	not significant
R^2= 0.9808		

Figure 70: Prediction vs. actual plot for *U. maydis* MB215.
The actual reached titers (a) and yields (b) are compared against the model prediction. Generated using the software Design Expert

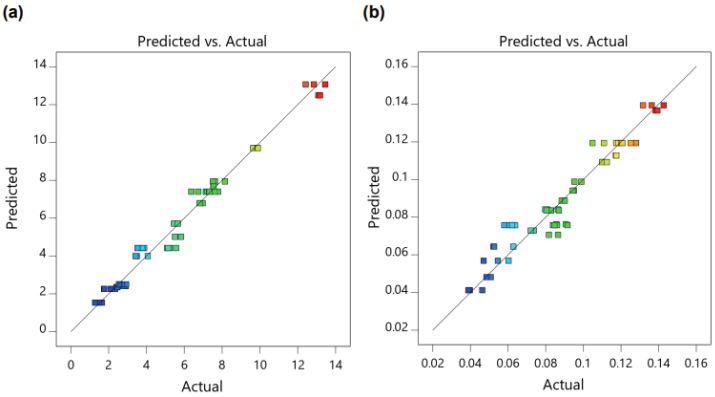

Figure 71: ANOVA analysis for the itaconate titer model for acetate co-metabolization of *U. rabenhorstiana* #2708.
(A) ANOVA analysis table regarding itaconate titer, (B) ANOVA analysis table regarding itaconate c-mol yield.

A

Source	p-value	
Model	< 0.0001	significant
A-Glucose	< 0.0001	
B-Acetate	0.0285	
AB	0.0545	
A^2	< 0.0001	
B^2	0.0024	
Lack of Fit	0.1109	not significant
R^2= 0.9552		

B

Source	p-value	
Model	< 0.0001	significant
A-Glucose	< 0.0001	
B-Acetate	0.0025	
AB	0.0204	
A^2	0.0022	
B^2	0.0027	
Lack of Fit	0.0799	not significant
R^2= 0.8746		

Figure 72: Prediction vs. actual plot for *U. rabenhorstiana* #2708.
The actual reached titers (a) and yields (b) are compared against the model prediction. Generated using the software Design Expert

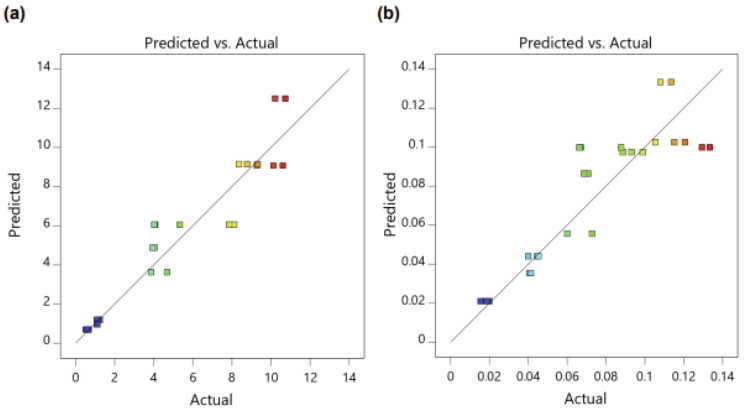

Figure 73: ANOVA analysis for the itaconate titer model for acetate co-metabolization of *U. maydis* MB215 Δ*cyp3* Δ*fuz7* ΔUA ΔMEL ΔP_{ria1}::P_{etef} P_{etef} mttA.
(A) ANOVA analysis table, (B) fit statistics, (C) predicted vs. actual plot.

A ANOVA

Response 2: Titer
Transform: Square Root
Constant: 0.5

Source	Sum of Squares	df	Mean Square	F-value	p-value	
Model	951.01	13	73.15	538.27	< 0.0001	significant
A-Glucose	230.84	1	230.84	1698.50	< 0.0001	
B-Formate	0.0674	1	0.0674	0.4957	0.4842	
C-NH4CL	0.9594	1	0.9594	7.06	0.0102	
AB	4.33	1	4.33	31.88	< 0.0001	
AC	54.62	1	54.62	401.91	< 0.0001	
BC	1.28	1	1.28	9.44	0.0032	
A^2	98.14	1	98.14	722.14	< 0.0001	
B^2	0.0338	1	0.0338	0.2487	0.6199	
C^2	3.67	1	3.67	26.97	< 0.0001	
ABC	1.13	1	1.13	8.34	0.0054	
A^2B	0.0531	1	0.0531	0.3906	0.5344	
A^2C	2.65	1	2.65	19.49	< 0.0001	
AB^2	1.36	1	1.36	9.98	0.0025	
Residual	7.88	58	0.1359			
Lack of Fit	0.0563	1	0.0563	0.4103	0.5244	not significant
Pure Error	7.83	57	0.1373			
Cor Total	958.89	71				

B Fit Statistics

Std. Dev.	0.3687	**R^2**	0.9918
Mean	8.00	**Adjusted R^2**	0.9899
C.V. %	4.61	**Predicted R^2**	0.9869
		Adeq Precision	69.6685

C

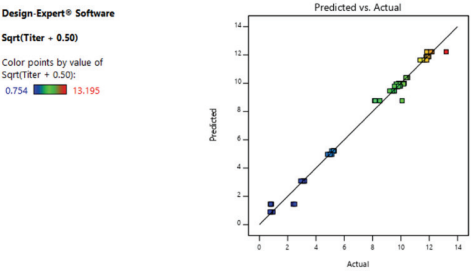

Figure 74: ANOVA analysis for the itaconate yield model for acetate co-metabolization of *U. maydis* MB215 Δ*cyp3* Δ*fuz7* ΔUA ΔMEL ΔP_{ria1}::P_{etef} P_{etef} mttA.
(A) ANOVA analysis table, (B) fit statistics, (C) predicted vs. actual plot.

A ANOVA

Response 1: Yield

Source	Sum of Squares	df	Mean Square	F-value	p-value	
Model	3.33	13	0.2565	282.91	< 0.0001	significant
A-Glucose	0.5079	1	0.5079	560.30	< 0.0001	
B-Formate	0.0013	1	0.0013	1.43	0.2372	
C-NH4CL	0.0075	1	0.0075	8.31	0.0055	
AB	0.0572	1	0.0572	63.14	< 0.0001	
AC	0.5783	1	0.5783	637.90	< 0.0001	
BC	0.0000	1	0.0000	0.0141	0.9058	
A^2	0.6212	1	0.6212	685.22	< 0.0001	
B^2	0.0000	1	0.0000	0.0256	0.8735	
C^2	0.0026	1	0.0026	2.90	0.0940	
A^2B	0.0085	1	0.0085	9.33	0.0034	
A^2C	0.1236	1	0.1236	136.38	< 0.0001	
AB^2	0.0785	1	0.0785	86.57	< 0.0001	
A^2B^2	0.0204	1	0.0204	22.48	< 0.0001	
Residual	0.0526	58	0.0009			
Lack of Fit	0.0026	1	0.0026	2.93	0.0924	not significant
Pure Error	0.0500	57	0.0009			
Cor Total	3.39	71				

B Fit Statistics

Std. Dev.	0.0301	**R^2**	0.9845
Mean	0.5279	**Adjusted R^2**	0.9810
C.V. %	5.70	**Predicted R^2**	0.9758
		Adeq Precision	52.3154

C

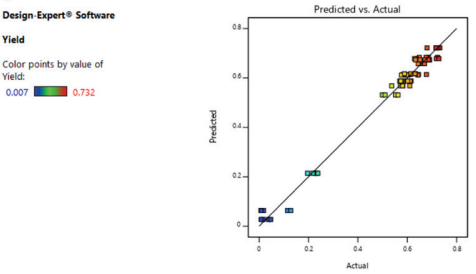

Figure 75: ANOVA analysis for the itaconate titer model for formate co-metabolism of *U. cynodontis* Δ*cyp3* Δ*fuz7* ΔP_{ria1}::P_{etef} P_{etef}*mttA*.
(A) ANOVA analysis table, (B) fit statistics, (C) predicted vs. actual plot

A ANOVA

Response 2: Titer
Transform: Square Root
Constant: 0.5

Source	Sum of Squares	df	Mean Square	F-value	p-value	
Model	951.01	13	73.15	538.27	< 0.0001	significant
A-Glucose	230.84	1	230.84	1698.50	< 0.0001	
B-Formate	0.0674	1	0.0674	0.4957	0.4842	
C-NH4CL	0.9594	1	0.9594	7.06	0.0102	
AB	4.33	1	4.33	31.88	< 0.0001	
AC	54.62	1	54.62	401.91	< 0.0001	
BC	1.28	1	1.28	9.44	0.0032	
A^2	98.14	1	98.14	722.14	< 0.0001	
B^2	0.0338	1	0.0338	0.2487	0.6199	
C^2	3.67	1	3.67	26.97	< 0.0001	
ABC	1.13	1	1.13	8.34	0.0054	
A^2B	0.0531	1	0.0531	0.3906	0.5344	
A^2C	2.65	1	2.65	19.49	< 0.0001	
AB^2	1.36	1	1.36	9.98	0.0025	
Residual	7.88	58	0.1359			
Lack of Fit	0.0563	1	0.0563	0.4103	0.5244	not significant
Pure Error	7.83	57	0.1373			
Cor Total	958.89	71				

B Fit Statistics

Std. Dev.	0.3687	R^2	0.9918
Mean	8.00	**Adjusted R^2**	0.9899
C.V. %	4.61	**Predicted R^2**	0.9869
		Adeq Precision	69.6685

C

Figure 76: ANOVA analysis for the itaconate yield model for formate co-metabolism of *U. cynodontis* Δ*cyp3* Δ*fuz7* ΔP_{ria1}::P_{etef} P_{etef}*mttA*.
(A) ANOVA analysis table, (B) fit statistics, (C) predicted vs. actual plot.

A ANOVA

Response 1: Yield

Source	Sum of Squares	df	Mean Square	F-value	p-value	
Model	3.33	13	0.2565	282.91	< 0.0001	significant
A-Glucose	0.5079	1	0.5079	560.30	< 0.0001	
B-Formate	0.0013	1	0.0013	1.43	0.2372	
C-NH4CL	0.0075	1	0.0075	8.31	0.0055	
AB	0.0572	1	0.0572	63.14	< 0.0001	
AC	0.5783	1	0.5783	637.90	< 0.0001	
BC	0.0000	1	0.0000	0.0141	0.9058	
A^2	0.6212	1	0.6212	685.22	< 0.0001	
B^2	0.0000	1	0.0000	0.0256	0.8735	
C^2	0.0026	1	0.0026	2.90	0.0940	
A^2B	0.0085	1	0.0085	9.33	0.0034	
A^2C	0.1236	1	0.1236	136.38	< 0.0001	
AB^2	0.0785	1	0.0785	86.57	< 0.0001	
A^2B^2	0.0204	1	0.0204	22.48	< 0.0001	
Residual	0.0526	58	0.0009			
Lack of Fit	0.0026	1	0.0026	2.93	0.0924	not significant
Pure Error	0.0500	57	0.0009			
Cor Total	3.39	71				

B Fit Statistics

Std. Dev.	0.0301	R^2	0.9845
Mean	0.5279	**Adjusted R^2**	0.9810
C.V. %	5.70	**Predicted R^2**	0.9758
		Adeq Precision	52.3154

C

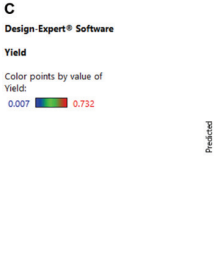

References

References

[1] O.-O. E. Roser M, “World population growth,” 2022. https://ourworldindata.org/world-population-growth (accessed Jun. 23, 2022).

[2] M. Antar, D. Lyu, M. Nazari, A. Shah, X. Zhou, and D. L. Smith, “Biomass for a sustainable bioeconomy: An overview of world biomass production and utilization,” *Renewable and Sustainable Energy Reviews*, vol. 139, no. January, p. 110691, 2021, doi: 10.1016/j.rser.2020.110691.

[3] A. Demirbaş, “Biomass resource facilities and biomass conversion processing for fuels and chemicals,” *Energy Convers Manag*, vol. 42, no. 11, pp. 1357–1378, 2001, doi: 10.1016/S0196-8904(00)00137-0.

[4] K. M. K. Yu, I. Curcic, J. Gabriel, and S. C. E. Tsang, “Recent advances in CO_2 capture and utilization.,” *ChemSusChem*, vol. 1, no. 11, pp. 893–899, 2008, doi: 10.1002/cssc.200800169.

[5] D. Nagarajan, D. J. Lee, and J. S. Chang, Circular Bioeconomy: An Introduction. Elsevier Inc., 2021. doi: 10.1016/B978-0-12-821878-5.00006-4.

[6] “European Commission Bioeconomy.” https://ec.europa.eu/info/research-and-innovation/research-area/environment/bioeconomy_en

[7] R. Hatti-Kaul, U. Törnvall, L. Gustafsson, and P. Börjesson, “Industrial biotechnology for the production of bio-based chemicals - a cradle-to-grave perspective,” *Trends Biotechnol*, vol. 25, no. 3, pp. 119–124, 2007, doi: 10.1016/j.tibtech.2007.01.001.

[8] I. Bator and Apprimus Verlag, 2020, Deep genome editing of *Pseudomonas putida* for rhamnolipid production using non-conventional substrates.

[9] D. G. Christian, “Biomass for Renewable Energy, Fuels, and Chemicals,” *J Environ Qual*, vol. 29, no. 2, pp. 662–663, 2000, doi: 10.2134/jeq2000.00472425002900020040x.

[10] R. A. Lee and J. M. Lavoie, “From first- to third-generation biofuels: Challenges of producing a commodity from a biomass of increasing complexity,” *Animal Frontiers*, vol. 3, no. 2, pp. 6–11, 2013, doi: 10.2527/af.2013-0010.

[11] Julia. Helliwell. Richard. Tomei, “Food versus fuel? Going beyond biofuels,” *Land use policy*, 2015.

[12] V. F. Wendisch *et al.*, “The flexible feedstock concept in Industrial Biotechnology: Metabolic engineering of *Escherichia coli, Corynebacterium glutamicum, Pseudomonas, Bacillus* and yeast strains for access to alternative carbon sources,” *J Biotechnol*, vol. 234, pp. 139–157, 2016, doi: 10.1016/j.jbiotec.2016.07.022.

[13] T. Werpy and G. Petersen, “Top Value Added Chemicals from Biomass: Volume I -- Results of Screening for Potential Candidates from Sugars and Synthesis Gas. Office of Scientific and Technical Information (OSTI),” *Office of Scientific and Technical*

Information, vol. 1, no. May 2014, p. 69, 2004, [Online]. Available: http://oai.dtic.mil/oai/oai?verb=getRecord&metadataPrefix=html&identifier=ADA436528

[14] O. Rosales-Calderon and V. Arantes, A review on commercial-scale high-value products that can be produced alongside cellulosic ethanol, vol. 12, no. 1. BioMed Central, 2019. doi: 10.1186/s13068-019-1529-1.

[15] L. M. Blank, T. Narancic, J. Mampel, T. Tiso, and K. O'Connor, "Biotechnological upcycling of plastic waste and other non-conventional feedstocks in a circular economy," *Curr Opin Biotechnol*, vol. 62, pp. 212–219, 2020, doi: 10.1016/j.copbio.2019.11.011.

[16] L. Brennan and P. Owende, "Biofuels from microalgae-A review of technologies for production, processing, and extractions of biofuels and co-products," *Renewable and Sustainable Energy Reviews*, vol. 14, no. 2, pp. 557–577, 2010, doi: 10.1016/j.rser.2009.10.009.

[17] M. J. Griffiths and S. T. L. Harrison, "Lipid productivity as a key characteristic for choosing algal species for biodiesel production," *J Appl Phycol*, vol. 21, no. 5, pp. 493–507, 2009, doi: 10.1007/s10811-008-9392-7.

[18] T. J. Farmer, "Platform Molecules for the Manufacture Pharmaceuticals Dr Thomas Farmer Green Chemistry Centre of Excellence University of York 29 th April 2015," no. October, 2015.

[19] A. Kuenz and S. Krull, "Biotechnological production of itaconic acid—things you have to know," *Appl Microbiol Biotechnol*, vol. 102, no. 9, pp. 3901–3914, 2018, doi: 10.1007/s00253-018-8895-7.

[20] S. Baup, "Ueber eine neue Pyrogen-Citronensäure, und über Benennung der Pyrogen-Säuren überhaupt," *Annalen der Pharmacie*, vol. 19, no. 1, pp. 29–38, 1836, doi: 10.1002/jlac.18360190107.

[21] J. H. Kane, G. City, A. C. Finlay, L. I. City, P. F. Amann, and C. Pfizer, "Production of itaconic acid. Patent US 2 385 283," 1945.

[22] T. Willke and K. D. Vorlop, "Biotechnological production of itaconic acid," *Appl Microbiol Biotechnol*, vol. 56, no. 3–4, pp. 289–295, 2001, doi: 10.1007/s002530100685.

[23] T. Klement and J. Büchs, "Itaconic acid - A biotechnological process in change," *Bioresour Technol*, vol. 135, pp. 422–431, 2013, doi: 10.1016/j.biortech.2012.11.141.

[24] M. G. Steiger, M. L. Blumhoff, D. Mattanovich, and M. Sauer, "Biochemistry of microbial itaconic acid production," *Front Microbiol*, vol. 4, no. FEB, pp. 1–5, 2013, doi: 10.3389/fmicb.2013.00023.

[25] A. Kuenz, Y. Gallenmüller, T. Willke, and K. D. Vorlop, "Microbial production of itaconic acid: Developing a stable platform for high product concentrations," *Appl Microbiol Biotechnol*, vol. 96, no. 5, pp. 1209–1216, 2012, doi: 10.1007/s00253-012-4221-y.

[26] K. Satoh, D. H. Lee, K. Nagai, and M. Kamigaito, “Precision synthesis of Bio-based acrylic thermoplastic elastomer by RAFT polymerization of itaconic acid derivatives,” *Macromol Rapid Commun*, vol. 35, no. 2, pp. 161–167, 2014, doi: 10.1002/marc.201300638.

[27] M. Okabe, D. Lies, S. Kanamasa, and E. Y. Park, “Biotechnological production of itaconic acid and its biosynthesis in *Aspergillus terreus*,” *Appl Microbiol Biotechnol*, vol. 84, no. 4, pp. 597–606, 2009, doi: 10.1007/s00253-009-2132-3.

[28] A. S. Puranik, L. P. Pao, V. M. White, and N. A. Peppas, “Synthesis and characterization of pH-responsive nanoscale hydrogels for oral delivery of hydrophobic therapeutics,” *European Journal of Pharmaceutics and Biopharmaceutics*, vol. 108, pp. 196–213, 2016, doi: 10.1016/j.ejpb.2016.09.007.

[29] F. M. A. Geilen, B. Engendahl, A. Harwardt, W. Marquardt, J. Klankermayer, and W. Leitner, “Selective and flexible transformation of biomass-derived platform chemicals by a multifunctional catalytic system,” *Angewandte Chemie - International Edition*, vol. 49, no. 32, pp. 5510–5514, 2010, doi: 10.1002/anie.201002060.

[30] T. Klement, S. Milker, G. Jäger, P. M. Grande, P. Domínguez de María, and J. Büchs, “Biomass pretreatment affects *Ustilago maydis* in producing itaconic acid,” *Microb Cell Fact*, vol. 11, Apr. 2012, doi: 10.1186/1475-2859-11-43.

[31] A. Michelucci *et al.*, “Immune-responsive gene 1 protein links metabolism to immunity by catalyzing itaconic acid production,” *Proc Natl Acad Sci U S A*, vol. 110, no. 19, pp. 7820–7825, 2013, doi: 10.1073/pnas.1218599110.

[32] T. Cordes, A. Michelucci, and K. Hiller, “Itaconic Acid: The Surprising Role of an Industrial Compound as a Mammalian Antimicrobial Metabolite,” *Annu Rev Nutr*, vol. 35, no. 1, pp. 451–473, 2015, doi: 10.1146/annurev-nutr-071714-034243.

[33] M. Sugimoto *et al.*, “Non-targeted metabolite profiling in activated macrophage secretion,” *Metabolomics*, vol. 8, no. 4, pp. 624–633, 2012, doi: 10.1007/s11306-011-0353-9.

[34] L. Karaffa and C. P. Kubicek, “Citric acid and itaconic acid accumulation: variations of the same story?,” *Appl Microbiol Biotechnol*, vol. 103, no. 7, pp. 2889–2902, 2019, doi: 10.1007/s00253-018-09607-9.

[35] Weastra, “Determination of market potential for selected platform chemicals: Itaconic acid, Succinic acid, 2,5-Furandicarboxylic acid,” *BioConSepT*, pp. 1–173, 2011, [Online]. Available: http://www.bioconsept.eu/wp-content/uploads/BioConSepT_Market-potential-for-selected-platform-chemicals_report1.pdf

[36] “Itaconic acid market size, growth and trends (2022-2027).” https://www.marketdataforecast.com/market-reports/itaconic-acid-market

[37] M. Sauer, D. Porro, D. Mattanovich, and P. Branduardi, “Microbial production of organic acids: expanding the markets,” *Trends Biotechnol*, vol. 26, no. 2, pp. 100–108, 2008, doi: 10.1016/j.tibtech.2007.11.006.

[38] M. Sriariyanun, J. H. Heitz, P. Yasurin, S. Asavasanti, and P. Tantayotai, “Itaconic acid: A promising and sustainable platform chemical?,” *Applied Science and Engineering Progress*, vol. 12, no. 2, pp. 75–82, 2019, doi: 10.14416/j.asep.2019.05.002.

[39] S. Krull, A. Hevekerl, A. Kuenz, and U. Prüße, “Process development of itaconic acid production by a natural wild type strain of *Aspergillus terreus* to reach industrially relevant final titers,” *Appl Microbiol Biotechnol*, vol. 101, no. 10, pp. 4063–4072, 2017, doi: 10.1007/s00253-017-8192-x.

[40] A. Hevekerl, A. Kuenz, and K. D. Vorlop, “Influence of the pH on the itaconic acid production with *Aspergillus terreus*,” *Appl Microbiol Biotechnol*, vol. 98, no. 24, pp. 10005–10012, 2014, doi: 10.1007/s00253-014-6047-2.

[41] and G.-T. C. Shin, Woo-Shik, Dohoon Lee, Sangyong Kim, Yong-Seob Jeong, “Application of Scale-Up Criterion of Constant Oxygen Mass Transfer Coefficient (k,” *J. Microbiol. Biotechnol*, vol. 23, no. 10, pp. 1445–1453, 2013.

[42] G. Qian, L. Jie, and L. Liming, “Relationship between morphology and itaconic acid production by *Aspergillus terreus*,” *J Microbiol Biotechnol*, vol. 24, no. 2, pp. 168–176, 2014, doi: 10.4014/jmb.1303.03093.

[43] E. Geiser, V. Wiebach, N. Wierckx, and L. M. Blank, “Prospecting the biodiversity of the fungal family Ustilaginaceae for the production of value-added chemicals,” *Fungal Biol Biotechnol*, vol. 1, no. 1, Dec. 2014, doi: 10.1186/s40694-014-0002-y.

[44] W. E. Levinson, C. P. Kurtzman, and T. M. Kuo, “Production of itaconic acid by *Pseudozyma antarctica* NRRL Y-7808 under nitrogen-limited growth conditions,” *Enzyme Microb Technol*, vol. 39, no. 4, pp. 824–827, 2006, doi: 10.1016/j.enzmictec.2006.01.005.

[45] T. Tabuchi, T. Sugisawa, T. Ishidori, T. Nakahara, and J. Sugiyama, “Itaconic Acid Fermentation by a Yeast Belonging to the Genus Candida,” *Agric Biol Chem*, vol. 45, no. 2, pp. 475–479, 1981, doi: 10.1271/bbb1961.45.475.

[46] A. Sayama, K. Kobayashi, and A. Ogoshi, “Morphological and physiological comparisons of Helicobasidium mompa and H. purpureum,” *Mycoscience*, vol. 35, no. 1, pp. 15–20, 1994, doi: 10.1007/BF02268523.

[47] J. Cunha da Cruz, A. Machado de Castro, and E. F. Camporese Sérvulo, “World market and biotechnological production of itaconic acid,” *3 Biotech*, vol. 8, no. 3, pp. 0–15, 2018, doi: 10.1007/s13205-018-1151-0.

[48] J. Becker, U. W. Liebal, A. N. Phan, L. Ullmann, and L. M. Blank, “Renewable carbon sources to biochemicals and -fuels: contributions of the smut fungi Ustilaginaceae,” *Curr Opin Biotechnol*, vol. 79, p. 102849, 2023, doi: 10.1016/J.COPBIO.2022.102849.

[49] M. L. Heilig, “United States Patent Office,” *ACM SIGGRAPH Computer Graphics*, vol. 28, no. 2, pp. 131–134, 1994, doi: 10.1145/178951.178972.

[50] M. L. Heilig, “United States Patent Office,” *ACM SIGGRAPH Computer Graphics*, vol. 28, no. 2, pp. 131–134, 1994, doi: 10.1145/178951.178972.

[51] H. Kautola, M. Vahvaselkä, Y. Y. Linko, and P. Linko, “Itaconic acid production by immobilized *Aspergillus terreus* from xylose and glucose,” *Biotechnol Lett*, vol. 7, no. 3, pp. 167–172, 1985, doi: 10.1007/BF01027812.

[52] L. Karaffa, R. Díaz, B. Papp, E. Fekete, E. Sándor, and C. P. Kubicek, “A deficiency of manganese ions in the presence of high sugar concentrations is the critical parameter for achieving high yields of itaconic acid by *Aspergillus terreus*,” *Appl Microbiol Biotechnol*, vol. 99, no. 19, pp. 7937–7944, 2015, doi: 10.1007/s00253-015-6735-6.

[53] C. S. K. Reddy and R. P. Singh, “Enhanced production of itaconic acid from corn starch and market refuse fruits by genetically manipulated *Aspergillus terreus* SKR10,” *Bioresour Technol*, vol. 85, no. 1, pp. 69–71, 2002, doi: 10.1016/S0960-8524(02)00075-5.

[54] L. Dwiarti, M. Otsuka, S. Miura, M. Yaguchi, and M. Okabe, “Itaconic acid production using sago starch hydrolysate by *Aspergillus terreus* TN484-M1,” *Bioresour Technol*, vol. 98, no. 17, pp. 3329–3337, 2007, doi: 10.1016/j.biortech.2006.03.016.

[55] V. Nikolay, M. Almudena, M. Gilberto, G. Antonia, M. Vanessa, and V. Maria, “Solubilization of animal bonechar by a filamentous fungus employed in solid state fermentation,” *Ecol Eng*, vol. 58, pp. 165–169, 2013, doi: 10.1016/j.ecoleng.2013.06.029.

[56] Y. C. Tsai, Huang M.C., L. S.F., and Su Y.C., “Method for the Production of Itaconic acid using *Aspergillus Terreus* Solid State Fermentation,” *Control Engineering*, vol. 53, no. 9, pp. 12–15, 2001.

[57] M. L. Blumhoff, M. G. Steiger, D. Mattanovich, and M. Sauer, “Targeting enzymes to the right compartment: Metabolic engineering for itaconic acid production by *Aspergillus niger*,” *Metab Eng*, vol. 19, pp. 26–32, 2013, doi: 10.1016/j.ymben.2013.05.003.

[58] B. J. Harder, K. Bettenbrock, and S. Klamt, “Model-based metabolic engineering enables high yield itaconic acid production by *Escherichia coli*,” *Metab Eng*, vol. 38, pp. 29–37, 2016, doi: 10.1016/j.ymben.2016.05.008.

[59] R. Nl and N. van Luijk, “(12) United States Patent,” vol. 2, no. 12, 2013.

[60] H. Hosseinpour Tehrani, Engineering the morphology and metabolism of *Ustilago* to expand the process window for itaconic acid production, vol. 13. 2019. [Online]. Available: http://publications.rwth-aachen.de/record/765515

[61] H. Hosseinpour Tehrani, K. Saur, A. Tharmasothirajan, L. M. Blank, and N. Wierckx, “Process engineering of pH tolerant *Ustilago cynodontis* for efficient itaconic acid

production," *Microb Cell Fact*, vol. 18, no. 1, pp. 1–12, 2019, doi: 10.1186/s12934-019-1266-y.

[62] N. Maassen *et al.*, "Influence of carbon and nitrogen concentration on itaconic acid production by the smut fungus *Ustilago maydis*," *Eng Life Sci*, vol. 14, no. 2, pp. 129–134, 2014, doi: 10.1002/elsc.201300043.

[63] E. Geiser *et al.*, "Genetic and biochemical insights into the itaconate pathway of *Ustilago maydis* enable enhanced production," *Metab Eng*, vol. 38, no. August, pp. 427–435, 2016, doi: 10.1016/j.ymben.2016.10.006.

[64] H. Hosseinpour Tehrani *et al.*, "Integrated strain- And process design enable production of 220 g L-1 itaconic acid with *Ustilago maydis*," *Biotechnol Biofuels*, vol. 12, no. 1, Nov. 2019, doi: 10.1186/s13068-019-1605-6.

[65] J. Becker, H. H. Tehrani, P. Ernst, L. M. Blank, and N. Wierckx, "An optimized *Ustilago maydis* for itaconic acid production at maximal theoretical yield," *Journal of Fungi*, vol. 7, no. 1, pp. 1–14, 2021, doi: 10.3390/jof7010020.

[66] S. Krull, M. Lünsmann, U. Prüße, and A. Kuenz, "*Ustilago rabenhorstiana*—An alternative natural itaconic acid producer," *Fermentation*, vol. 6, no. 1, 2020, doi: 10.3390/fermentation6010004.

[67] J. Blazeck, A. Hill, M. Jamoussi, A. Pan, J. Miller, and H. S. Alper, "Metabolic engineering of *Yarrowia lipolytica* for itaconic acid production," *Metab Eng*, vol. 32, pp. 66–73, 2015, doi: 10.1016/j.ymben.2015.09.005.

[68] H. Hosseinpour Tehrani *et al.*, "The interplay between transport and metabolism in fungal itaconic acid production," *Fungal Genetics and Biology*, vol. 125, no. October 2018, pp. 45–52, 2019, doi: 10.1016/j.fgb.2019.01.011.

[69] E. Geiser *et al.*, "*Ustilago maydis* produces itaconic acid via the unusual intermediate trans-aconitate," *Microb Biotechnol*, vol. 9, no. 1, pp. 116–126, 2016, doi: 10.1111/1751-7915.12329.

[70] N. Wierckx, G. Agrimi, P. S. Lübeck, M. G. Steiger, N. P. Mira, and P. J. Punt, "Metabolic specialization in itaconic acid production: a tale of two fungi," *Curr Opin Biotechnol*, vol. 62, pp. 153–159, 2020, doi: 10.1016/j.copbio.2019.09.014.

[71] A. Li, N. van Luijk, M. ter Beek, M. Caspers, P. Punt, and M. van der Werf, "A clone-based transcriptomics approach for the identification of genes relevant for itaconic acid production in Aspergillus," *Fungal Genetics and Biology*, vol. 48, no. 6, pp. 602–611, 2011, doi: 10.1016/j.fgb.2011.01.013.

[72] H. Hosseinpour Tehrani, A. Tharmasothirajan, E. Track, L. M. Blank, and N. Wierckx, "Engineering the morphology and metabolism of pH tolerant *Ustilago cynodontis* for efficient itaconic acid production," *Metab Eng*, vol. 54, no. April, pp. 293–300, 2019, doi: 10.1016/j.ymben.2019.05.004.

[73] J. Becker, H. Hosseinpour Tehrani, M. Gauert, J. Mampel, L. M. Blank, and N. Wierckx, "An *Ustilago maydis* chassis for itaconic acid production without by-products," *Microb Biotechnol*, vol. 13, no. 2, pp. 350–362, Mar. 2020, doi: 10.1111/1751-7915.13525.

[74] Q. Wang *et al.*, "Studies in Mycology," *Stud Mycol*, vol. 81, pp. 55–83, 2016, doi: 10.1016/j.simyco.2015.10.004.

[75] A. R. McTaggart *et al.*, "Mycosarcoma (Ustilaginaceae), a resurrected generic name for corn smut (*Ustilago maydis*) and its close relatives with hypertrophied, tubular sori," *IMA Fungus*, vol. 7, no. 2, pp. 309–315, 2016, doi: 10.5598/imafungus.2016.07.02.10.

[76] G. Bakkeren, J. Kämper, and J. Schirawski, "Sex in smut fungi: Structure, function and evolution of mating-type complexes," *Fungal Genetics and Biology*, vol. 45, no. SUPPL. 1. Aug. 2008. doi: 10.1016/j.fgb.2008.04.005.

[77] T. Zambanini, J. M. Buescher, G. Meurer, N. Wierckx, and L. M. Blank, "Malic Acid Producer," vol. 4, no. 4, pp. 10–11, 2016, doi: 10.1128/genomeA.00749-16.Copyright.

[78] E. D. Guevarra and T. Tabuchi, "Accumulation of itaconic, 2-hydroxyparaconic, itatartaric, and malic acids by strains of the genus *Ustilago*," *Agric Biol Chem*, vol. 54, no. 9, pp. 2353–2358, 1990, doi: 10.1271/bbb1961.54.2353.

[79] J. G. Zeikus, M. K. Jain, and P. Elankovan, "Biotechnology of succinic acid production and markets for derived industrial products," *Appl Microbiol Biotechnol*, vol. 51, no. 5, May 1999, doi: 10.1007/s002530051431.

[80] B. N. Paulino *et al.*, "Biotechnological production of value-added compounds by ustilaginomycetous yeasts," *Appl Microbiol Biotechnol*, vol. 101, no. 21, pp. 7789–7809, 2017, doi: 10.1007/s00253-017-8516-x.

[81] H.-J. Moon, M. Jeya, I.-W. Kim, and J.-K. Lee, "Biotechnological production of erythritol and its applications," *Appl Microbiol Biotechnol*, vol. 86, no. 4, Apr. 2010, doi: 10.1007/s00253-010-2496-4.

[82] V. Castañeda de León *et al.*, "Productivity and flavor of diverse genotypes of *Ustilago maydis* 'cuitlacoche' for human consumption," *Fungal Biol*, vol. 123, no. 6, pp. 481–488, 2019, doi: 10.1016/j.funbio.2019.04.003.

[83] B. C. Saha, "Emerging biotechnologies for production of itaconic acid and its applications as a platform chemical," *J Ind Microbiol Biotechnol*, vol. 44, no. 2, pp. 303–315, 2017, doi: 10.1007/s10295-016-1878-8.

[84] S. Hewald, K. Josephs, and M. Bölker, "Genetic analysis of biosurfactant production in *Ustilago maydis," Appl Environ Microbiol*, vol. 71, no. 6, pp. 3033–3040, 2005, doi: 10.1128/AEM.71.6.3033-3040.2005.

[85] S. Hewald, U. Linne, M. Scherer, M. A. Marahiel, J. Kämper, and M. Bölker, "Identification of a gene cluster for biosynthesis of mannosylerythritol lipids in the basidiomycetous fungus *Ustilago maydis*," *Appl Environ Microbiol*, vol. 72, no. 8, pp. 5469–5477, 2006, doi: 10.1128/AEM.00506-06.

[86] A. Saika, H. Koike, T. Fukuoka, and T. Morita, “Tailor-made mannosylerythritol lipids: current state and perspectives,” *Appl Microbiol Biotechnol*, vol. 102, no. 16, pp. 6877–6884, 2018, doi: 10.1007/s00253-018-9160-9.

[87] J. Kämper *et al.*, “Insights from the genome of the biotrophic fungal plant pathogen *Ustilago maydis*,” *Nature*, vol. 444, no. 7115, pp. 97–101, 2006, doi: 10.1038/nature05248.

[88] N. Wierckx, K. Miebach, N. Ihling, K. P. Hussnaetter, J. Büchs, and K. Schipper, “Perspectives for the application of Ustilaginaceae as biotech cell factories,” *Essays Biochem*, vol. 65, no. 2, p. 365, 2021, doi: 10.1042/EBC20200141.

[89] I. Schlembach *et al.*, “Consolidated bioprocessing of cellulose to itaconic acid by a co-culture of Trichoderma reesei and *Ustilago maydis*,” *Biotechnol Biofuels*, vol. 13, no. 1, pp. 1–18, 2020, doi: 10.1186/s13068-020-01835-4.

[90] L. Regestein *et al.*, “From beech wood to itaconic acid: Case study on biorefinery process integration,” *Biotechnol Biofuels*, vol. 11, no. 1, pp. 1–11, 2018, doi: 10.1186/s13068-018-1273-y.

[91] L. Ullmann *et al.*, “Ustilaginaceae Biocatalyst for Co-Metabolism of CO_2-Derived Substrates toward Carbon-Neutral Itaconate Production Citation: Ullmann,” 2021, doi: 10.3390/jof.

[92] E. Geiser *et al.*, “*Ustilago maydis* produces itaconic acid via the unusual intermediate trans-aconitate,” *Microb Biotechnol*, vol. 9, no. 1, pp. 116–126, 2016, doi: 10.1111/1751-7915.12329.

[93] Y. Kim, S. Lama, D. Agrawal, V. Kumar, and S. Park, “Acetate as a potential feedstock for the production of value-added chemicals: Metabolism and applications,” *Biotechnol Adv*, vol. 49, no. February, p. 107736, 2021, doi: 10.1016/j.biotechadv.2021.107736.

[94] G. Merli, A. Becci, A. Amato, and F. Beolchini, “Acetic acid bioproduction: The technological innovation change,” *Science of the Total Environment*, vol. 798, p. 149292, 2021, doi: 10.1016/j.scitotenv.2021.149292.

[95] A. Vidra and Á. Németh, “Bio-produced acetic acid: A review,” *Periodica Polytechnica Chemical Engineering*, vol. 62, no. 3, pp. 245–256, 2018, doi: 10.3311/PPch.11004.

[96] M. Ehsanipour, A. V. Suko, and R. Bura, “Fermentation of lignocellulosic sugars to acetic acid by *Moorella thermoacetica*,” *J Ind Microbiol Biotechnol*, vol. 43, no. 6, pp. 807–816, 2016, doi: 10.1007/s10295-016-1756-4.

[97] M. Gullo, G. Zanichelli, E. Verzelloni, F. Lemmetti, and P. Giudici, “Feasible acetic acid fermentations of alcoholic and sugary substrates in combined operation mode,” *Process Biochemistry*, vol. 51, no. 9, pp. 1129–1139, 2016, doi: 10.1016/j.procbio.2016.05.018.

[98] Y. Li, D. He, D. Niu, and Y. Zhao, “Acetic acid production from food wastes using yeast and acetic acid bacteria micro-aerobic fermentation,” *Bioprocess Biosyst Eng*, vol. 38, no. 5, pp. 863–869, 2015, doi: 10.1007/s00449-014-1329-8.

[99] K. Novak and S. Pflügl, “Towards biobased industry: Acetate as a promising feedstock to enhance the potential of microbial cell factories,” *FEMS Microbiol Lett*, vol. 365, no. 20, pp. 1–5, 2018, doi: 10.1093/femsle/fny226.

[100] H. Younesi, G. Najafpour, and A. R. Mohamed, “Ethanol and acetate production from synthesis gas via fermentation processes using anaerobic bacterium, *Clostridium ljungdahlii*,” *Biochem Eng J*, vol. 27, no. 2, pp. 110–119, 2005, doi: 10.1016/j.bej.2005.08.015.

[101] J. Daniell, M. Köpke, and S. D. Simpson, Commercial biomass syngas fermentation, vol. 5, no. 12. 2012. doi: 10.3390/en5125372.

[102] M. Köpke *et al.*, “*Clostridium ljungdahlii* represents a microbial production platform based on syngas,” *Proc Natl Acad Sci U S A*, vol. 107, no. 29, pp. 13087–13092, 2010, doi: 10.1073/pnas.1004716107.

[103] M. Köpke and S. D. Simpson, “Pollution to products: recycling of ‘above ground’ carbon by gas fermentation,” *Curr Opin Biotechnol*, vol. 65, pp. 180–189, 2020, doi: 10.1016/j.copbio.2020.02.017.

[104] S. Gadkari, B. H. Mirza Beigi, N. Aryal, and J. Sadhukhan, “Microbial electrosynthesis: is it sustainable for bioproduction of acetic acid?,” *RSC Adv*, vol. 11, no. 17, pp. 9921–9932, 2021, doi: 10.1039/d1ra00920f.

[105] S. Das, L. Diels, D. Pant, S. A. Patil, and M. M. Ghangrekar, “Review—Microbial Electrosynthesis: A Way Towards The Production of Electro-Commodities Through Carbon Sequestration with Microbes as Biocatalysts,” *J Electrochem Soc*, vol. 167, no. 15, p. 155510, 2020, doi: 10.1149/1945-7111/abb836.

[106] P. Jürling-Will, T. Botz, G. Franciò, and W. Leitner, “A ‘Power-to-X’ Route to Acetic Acid via Palladium-Catalyzed Isomerization of Methyl Formate,” *ChemSusChem*, vol. 202201006, pp. 1–8, 2022, doi: 10.1002/cssc.202201006.

[107] J. Nielsen, “Synthetic biology for engineering acetyl coenzyme a metabolism in yeast,” *mBio*, vol. 5, no. 6, pp. 14–16, 2014, doi: 10.1128/mBio.02153-14.

[108] M. Mollapour and P. W. Piper, “Hog1 Mitogen-Activated Protein Kinase Phosphorylation Targets the Yeast Fps1 Aquaglyceroporin for Endocytosis, Thereby Rendering Cells Resistant to Acetic Acid,” *Mol Cell Biol*, vol. 27, no. 18, pp. 6446–6456, 2007, doi: 10.1128/mcb.02205-06.

[109] M. Kretschmer, S. Lambie, D. Croll, and J. W. Kronstad, “Acetate provokes mitochondrial stress and cell death in *Ustilago maydis*,” *Mol Microbiol*, vol. 107, no. 4, pp. 488–507, 2018, doi: 10.1111/mmi.13894.

[110] J. A. Hargreaves and G. Turner, “Isolation of the Acetyl-CoA Synthase Gene from the Corn Smut Pathogen, *Ustilago maydis*,” *Microbiology (N Y)*, vol. 135, no. 10, pp. 2675–2678, 1989, doi: 10.1099/00221287-135-10-2675.

[111] Y. Chen, V. Siewers, and J. Nielsen, “Profiling of cytosolic and peroxisomal acetyl-CoA metabolism in *Saccharomyces cerevisiae*,” *PLoS One*, vol. 7, no. 8, 2012, doi: 10.1371/journal.pone.0042475.

[112] L. M. Blank, T. Narancic, J. Mampel, T. Tiso, and K. O’Connor, “Biotechnological upcycling of plastic waste and other non-conventional feedstocks in a circular economy,” *Curr Opin Biotechnol*, vol. 62, pp. 212–219, 2020, doi: 10.1016/j.copbio.2019.11.011.

[113] C. A. Cotton, N. J. Claassens, S. Benito-Vaquerizo, and A. Bar-Even, “Renewable methanol and formate as microbial feedstocks,” *Curr Opin Biotechnol*, vol. 62, pp. 168–180, 2020, doi: 10.1016/j.copbio.2019.10.002.

[114] W. Babel, “The Auxiliary Substrate Concept: From simple considerations to heuristically valuable knowledge,” *Eng Life Sci*, vol. 9, no. 4, pp. 285–290, 2009, doi: 10.1002/elsc.200900027.

[115] W. Babel, R. H. Müller, and K. D. Markuske, “Improvement of growth yield of yeast on glucose to the maximum by using an additional energy source,” *Arch Microbiol*, vol. 136, no. 3, pp. 203–208, 1983, doi: 10.1007/BF00409845.

[116] J. B. Siegel *et al.*, Computational protein design enables a novel one-carbon assimilation pathway, vol. 112, no. 12. 2015. doi: 10.1073/pnas.1500545112.

[117] H. Li *et al.*, “Integrated electromicrobial conversion of CO_2 to higher alcohols,” *AIChE Annual Meeting, Conference Proceedings*, vol. 335, no. March, p. 2012, 2012.

[118] O. Yishai, S. N. Lindner, J. Gonzalez de la Cruz, H. Tenenboim, and A. Bar-Even, “The formate bio-economy,” *Curr Opin Chem Biol*, vol. 35, pp. 1–9, 2016, doi: 10.1016/j.cbpa.2016.07.005.

[119] H. Yang, J. J. Kaczur, S. D. Sajjad, and R. I. Masel, “Electrochemical conversion of CO_2 to formic acid utilizing Sustainion^{TM} membranes,” *Journal of CO2 Utilization*, vol. 20, no. April, pp. 208–217, 2017, doi: 10.1016/j.jcou.2017.04.011.

[120] D. Kopljar, A. Inan, P. Vindayer, N. Wagner, and E. Klemm, “Electrochemical reduction of CO2 to formate at high current density using gas diffusion electrodes,” *J Appl Electrochem*, vol. 44, no. 10, pp. 1107–1116, 2014, doi: 10.1007/s10800-014-0731-x.

[121] W. H. Wang, Y. Himeda, J. T. Muckerman, G. F. Manbeck, and E. Fujita, “CO_2 Hydrogenation to Formate and Methanol as an Alternative to Photo- and Electrochemical CO_2 Reduction,” *Chem Rev*, vol. 115, no. 23, pp. 12936–12973, 2015, doi: 10.1021/acs.chemrev.5b00197.

[122] K. Rohmann, J. Kothe, M. W. Haenel, U. Englert, M. Hölscher, and W. Leitner, “Hydrogenation of CO_2 to Formic Acid with a Highly Active Ruthenium Acriphos Complex in DMSO and DMSO/Water,” *Angewandte Chemie - International Edition*, vol. 55, no. 31, pp. 8966–8969, 2016, doi: 10.1002/anie.201603878.

[123] Y. Tamaki, T. Morimoto, K. Koike, and O. Ishitani, “Photocatalytic CO_2 reduction with high turnover frequency and selectivity of formic acid formation using Ru(II) multinuclear

complexes," *Proc Natl Acad Sci U S A*, vol. 109, no. 39, pp. 15673–15678, 2012, doi: 10.1073/pnas.1118336109.

[124] A. B. Sorokin, E. v. Kudrik, L. X. Alvarez, P. Afanasiev, J. M. M. Millet, and D. Bouchu, "Oxidation of methane and ethylene in water at ambient conditions," *Catal Today*, vol. 157, no. 1–4, pp. 149–154, 2010, doi: 10.1016/j.cattod.2010.02.007.

[125] J. Albert, D. Lüders, A. Bösmann, D. M. Guldi, and P. Wasserscheid, "Spectroscopic and electrochemical characterization of heteropoly acids for their optimized application in selective biomass oxidation to formic acid," *Green Chemistry*, vol. 16, no. 1, pp. 226–237, 2014, doi: 10.1039/c3gc41320a.

[126] R. S. Shukla, S. D. Bhatt, R. B. Thorat, and R. v. Jasra, "A novel effective hydration of carbon monoxide in liquid phase by a water-soluble ruthenium complex catalyst at moderate pressures in aqueous medium," *Appl Catal A Gen*, vol. 294, no. 1, pp. 111–118, 2005, doi: 10.1016/j.apcata.2005.07.034.

[127] J. Gonzalez De La Cruz, F. Machens, K. Messerschmidt, and A. Bar-Even, "Core Catalysis of the Reductive Glycine Pathway Demonstrated in Yeast," *ACS Synth Biol*, vol. 8, no. 5, pp. 911–917, 2019, doi: 10.1021/acssynbio.8b00464.

[128] V. I. Tishkov and V. O. Popov, "Catalytic mechanism and application of formate dehydrogenase," *Biochemistry (Moscow)*, vol. 69, no. 11, pp. 1252–1267, 2004, doi: 10.1007/s10541-005-0071-x.

[129] K. M. Overkamp *et al.*, "Functional analysis of structural genes for NAD+ -dependent formate dehydrogenase in *Saccharomyces cerevisiae*," *Yeast*, vol. 19, no. 6, pp. 509–520, 2002, doi: 10.1002/yea.856.

[130] V. der and D.-B. Bernd Leuchtle aus, "Mikrobiologische Kontamination von Heizöl-Ursachen und Auswirkungen auf Brennstoff und Tank."

[131] Kellner and Ronny, "Der Einfluss sexueller Reproduktion und Virulenz auf die Evolution und Speziation der biotrophen Brandpilzfamilie Ustilaginaceae = Evolutionary impact of sexual reproduction and virulence on speciation in the plant-biotrophic grass smut family Ustilaginaceae," 2011.

[132] R. B. Willis, M. E. Montgomery, and P. R. Allen, "Improved method for manual, colorimetric determination of total kjeldahl nitrogen using salicylate," *J Agric Food Chem*, vol. 44, no. 7, pp. 1804–1807, 1996, doi: 10.1021/jf950522b.

[133] Y. Djoumbou-Feunang *et al.*, "Cfm-id 3.0: Significantly improved esi-ms/ms prediction and compound identification," *Metabolites*, vol. 9, no. 4, pp. 1–23, 2019, doi: 10.3390/metabo9040072.

[134] J. Hemmerich, W. Wiechert, and M. Oldiges, "Automated growth rate determination in high-throughput microbioreactor systems," *BMC Res Notes*, vol. 10, no. 1, pp. 1–7, 2017, doi: 10.1186/s13104-017-2945-6.

[135] D. Wibberg *et al.*, “Genome analysis of the sugar beet pathogen *Rhizoctonia solani* AG2-2IIIB revealed high numbers in secreted proteins and cell wall degrading enzymes,” *BMC Genomics*, vol. 17, no. 1, pp. 1–12, 2016, doi: 10.1186/s12864-016-2561-1.

[136] R. H. Rqzbndalt, “Geometry parameters for musculoskeletal modeling of the shoulder JB1992_Helm.pdf,” *bioRxiv*, vol. 25, no. 2, pp. 1–2, 2016, doi: 10.1101/gr.215087.116.Freely.

[137] B. J. Walker *et al.*, “Pilon: An integrated tool for comprehensive microbial variant detection and genome assembly improvement,” *PLoS One*, vol. 9, no. 11, 2014, doi: 10.1371/journal.pone.0112963.

[138] H. Li, “Aligning sequence reads, clone sequences and assembly contigs with BWA-MEM,” vol. 00, no. 00, pp. 1–3, 2013, [Online]. Available: http://arxiv.org/abs/1303.3997

[139] B. Langmead and S. L. Salzberg, “Fast gapped-read alignment with Bowtie 2,” *Nat Methods*, vol. 9, no. 4, pp. 357–359, 2012, doi: 10.1038/nmeth.1923.

[140] V. Ter-Hovhannisyan, A. Lomsadze, Y. O. Chernoff, and M. Borodovsky, “Gene prediction in novel fungal genomes using an ab initio algorithm with unsupervised training,” *Genome Res*, vol. 18, no. 12, pp. 1979–1990, 2008, doi: 10.1101/gr.081612.108.

[141] F. Meyer *et al.*, “GenDB - An open source genome annotation system for prokaryote genomes,” *Nucleic Acids Res*, vol. 31, no. 8, pp. 2187–2195, 2003, doi: 10.1093/nar/gkg312.

[142] T. Takahara, T. Minamoto, H. Yamanaka, H. Doi, and Z. Kawabata, “Estimation of fish biomass using environmental DNA,” *PLoS One*, vol. 7, no. 4, pp. 3–10, 2012, doi: 10.1371/journal.pone.0035868.

[143] R. L. Tatusov *et al.*, “The COG database: An updated vesion includes eukaryotes,” *BMC Bioinformatics*, vol. 4, pp. 1–14, 2003, doi: 10.1186/1471-2105-4-41.

[144] M. Kanehisa, S. Goto, S. Kawashima, Y. Okuno, and M. Hattori, “The KEGG resource for deciphering the genome,” *Nucleic Acids Res*, vol. 32, no. DATABASE ISS., 2004, doi: 10.1093/nar/gkh063.

[145] B. Boeckmann *et al.*, “The SWISS-PROT protein knowledgebase and its supplement TrEMBL in 2003,” *Nucleic Acids Res*, vol. 31, no. 1, pp. 365–370, 2003, doi: 10.1093/nar/gkg095.

[146] T. M. Lowe and S. R. Eddy, “TRNAscan-SE: A program for improved detection of transfer RNA genes in genomic sequence,” *Nucleic Acids Res*, vol. 25, no. 5, pp. 955–964, 1996, doi: 10.1093/nar/25.5.0955.

[147] F. A. Simão, R. M. Waterhouse, P. Ioannidis, E. v. Kriventseva, and E. M. Zdobnov, “BUSCO: Assessing genome assembly and annotation completeness with single-copy

orthologs," *Bioinformatics*, vol. 31, no. 19, pp. 3210–3212, 2015, doi: 10.1093/bioinformatics/btv351.

[148] J. Blom *et al.*, "EDGAR: A software framework for the comparative analysis of prokaryotic genomes," *BMC Bioinformatics*, vol. 10, 2009, doi: 10.1186/1471-2105-10-154.

[149] J. Blom *et al.*, "EDGAR 2.0: an enhanced software platform for comparative gene content analyses," *Nucleic Acids Res*, vol. 44, no. W1, pp. W22–W28, 2016, doi: 10.1093/nar/gkw255.

[150] D. Wibberg *et al.*, "Development of a *Rhizoctonia solani* AG1-IB Specific Gene Model Enables Comparative Genome Analyses between Phytopathogenic R. solani AG1-IA, AG1-IB, AG3 and AG8 Isolates," *PLoS One*, vol. 10, no. 12, pp. 1–14, 2015, doi: 10.1371/journal.pone.0144769.

[151] R. C. Edgar, "MUSCLE: Multiple sequence alignment with high accuracy and high throughput," *Nucleic Acids Res*, vol. 32, no. 5, pp. 1792–1797, 2004, doi: 10.1093/nar/gkh340.

[152] Q. L. Qin *et al.*, "A proposed genus boundary for the prokaryotes based on genomic insights," *J Bacteriol*, vol. 196, no. 12, pp. 2210–2215, 2014, doi: 10.1128/JB.01688-14.

[153] S. Goodwin, J. D. McPherson, and W. R. McCombie, "Coming of age: Ten years of next-generation sequencing technologies," *Nat Rev Genet*, vol. 17, no. 6, pp. 333–351, 2016, doi: 10.1038/nrg.2016.49.

[154] M. Adamek *et al.*, "Comparative genomics reveals phylogenetic distribution patterns of secondary metabolites in *Amycolatopsis* species," *BMC Genomics*, vol. 19, no. 1, pp. 1–15, 2018, doi: 10.1186/s12864-018-4809-4.

[155] G. Margos *et al.*, "The genus Borrelia reloaded," *PLoS One*, vol. 13, no. 12, pp. 1–14, 2018, doi: 10.1371/journal.pone.0208432.

[156] C. Camacho *et al.*, "BLAST+: Architecture and applications," *BMC Bioinformatics*, vol. 10, pp. 1–9, 2009, doi: 10.1186/1471-2105-10-421.

[157] J. Goris, K. T. Konstantinidis, J. A. Klappenbach, T. Coenye, P. Vandamme, and J. M. Tiedje, "DNA-DNA hybridization values and their relationship to whole-genome sequence similarities," *Int J Syst Evol Microbiol*, vol. 57, no. 1, pp. 81–91, 2007, doi: 10.1099/ijs.0.64483-0.

[158] D. Wibberg *et al.*, "Improved genome sequence of the phytopathogenic fungus *Rhizoctonia solani* AG1-IB 7/3/14 as established by deep mate-pair sequencing on the MiSeq (Illumina) system," *J Biotechnol*, vol. 203, pp. 19–21, 2015, doi: 10.1016/j.jbiotec.2015.03.005.

[159] D. Wibberg *et al.*, "High quality genome sequences of thirteen Hypoxylaceae (Ascomycota) strengthen the phylogenetic family backbone and enable the discovery of

new taxa," *Fungal Divers*, vol. 106, no. 1, pp. 7–28, 2021, doi: 10.1007/s13225-020-00447-5.

[160] M. Scott *et al.*, "Methylformate from CO_2: An integrated process combining catalytic hydrogenation and reactive distillation," *Green Chemistry*, vol. 21, no. 23, pp. 6307–6317, 2019, doi: 10.1039/c9gc03006a.

[161] T. Robert and S. Friebel, "Itaconic acid-a versatile building block for renewable polyesters with enhanced functionality," *Green Chemistry*, vol. 18, no. 10, pp. 2922–2934, 2016, doi: 10.1039/c6gc00605a.

[162] M. G. Steiger, N. Wierckx, L. M. Blank, D. Mattanovich, and M. Sauer, "Itaconic acid - An emerging building block," *Industrial Biotechnology: Products and Processes*, pp. 453–472, 2016, doi: 10.1002/9783527807833.

[163] M. Gyamerah, "Factors affecting the growth form of *Aspergillus terreus* NRRL 1960 in relation to itaconic acid fermentation," *Appl Microbiol Biotechnol*, vol. 44, no. 3–4, pp. 356–361, 1995, doi: 10.1007/BF00169929.

[164] E. D. Guevarra and T. Tabuchi, "Accumulation of itaconic, 2-hydroxyparaconic, itatartaric, and malic acids by strains of the genus *Ustilago*," *Agric Biol Chem*, vol. 54, no. 9, pp. 2353–2358, 1990, doi: 10.1080/00021369.1990.10870333.

[165] T. Zambanini *et al.*, "Efficient itaconic acid production from glycerol with *Ustilago vetiveriae TZ1*," *Biotechnol Biofuels*, vol. 10, no. 1, 2017, doi: 10.1186/s13068-017-0809-x.

[166] E. Geiser, H. H. Tehrani, S. Meyer, L. M. Blank, and N. Wierckx, "Evolutionary freedom in the regulation of the conserved itaconate cluster by *ria1* in related Ustilaginaceae," *Fungal Biol Biotechnol*, vol. 5, no. 1, pp. 1–15, 2018, doi: 10.1186/s40694-018-0058-1.

[167] G. Steinberg and J. Perez-Martin, "*Ustilago maydis*, a new fungal model system for cell biology," *Trends Cell Biol*, vol. 18, no. 2, pp. 61–67, 2008, doi: 10.1016/j.tcb.2007.11.008.

[168] E. Vollmeister, K. Schipper, and M. Feldbrügge, "Microtubule-dependent mRNA transport in the model microorganism *Ustilago maydis*," *RNA Biol*, vol. 9, no. 3, pp. 261–268, 2012, doi: 10.4161/rna.19432.

[169] R. Bafana and R. A. Pandey, "New approaches for itaconic acid production: bottlenecks and possible remedies," *Crit Rev Biotechnol*, vol. 38, no. 1, pp. 68–82, 2018, doi: 10.1080/07388551.2017.1312268.

[170] I. S. Kolláth *et al.*, "Manganese deficiency is required for high itaconic acid production from D-xylose in *Aspergillus terreus*," *Front Microbiol*, vol. 10, no. JULY, 2019, doi: 10.3389/fmicb.2019.01589.

[171] A. W. Westbrook, D. Miscevic, S. Kilpatrick, M. R. Bruder, M. Moo-Young, and C. P. Chou, "Strain engineering for microbial production of value-added chemicals and fuels

from glycerol," *Biotechnol Adv*, vol. 37, no. 4, pp. 538–568, 2019, doi: 10.1016/j.biotechadv.2018.10.006.

[172] K. Rohmann, J. Kothe, M. W. Haenel, U. Englert, M. Hölscher, and W. Leitner, "Hydrogenation of CO_2 to Formic Acid with a Highly Active Ruthenium Acriphos Complex in DMSO and DMSO/Water," *Angewandte Chemie - International Edition*, vol. 55, no. 31, pp. 8966–8969, 2016, doi: 10.1002/anie.201603878.

[173] A. Groher and D. Weuster-Botz, "Comparative reaction engineering analysis of different acetogenic bacteria for gas fermentation," *J Biotechnol*, vol. 228, pp. 82–94, 2016, doi: 10.1016/j.jbiotec.2016.04.032.

[174] J. O. Park *et al.*, "Synergistic substrate cofeeding stimulates reductive metabolism," *Nat Metab*, vol. 1, no. 6, pp. 643–651, Jun. 2019, doi: 10.1038/s42255-019-0077-0.

[175] S. Gildemyn, K. Verbeeck, R. Slabbinck, S. J. Andersen, A. Prévoteau, and K. Rabaey, "Integrated production, extraction, and concentration of acetic acid from CO_2 through microbial electrosynthesis," *Environ Sci Technol Lett*, vol. 2, no. 11, pp. 325–328, 2015, doi: 10.1021/acs.estlett.5b00212.

[176] B. Turcotte, X. B. Liang, F. Robert, and N. Soontorngun, "Transcriptional regulation of nonfermentable carbon utilization in budding yeast," *FEMS Yeast Res*, vol. 10, no. 1, pp. 2–13, 2010, doi: 10.1111/j.1567-1364.2009.00555.x.

[177] A. Vilela-Moura *et al.*, "The impact of acetate metabolism on yeast fermentative performance and wine quality: Reduction of volatile acidity of grape musts and wines," *Appl Microbiol Biotechnol*, vol. 89, no. 2, pp. 271–280, 2011, doi: 10.1007/s00253-010-2898-3.

[178] J. Gonzalez De La Cruz, F. Machens, K. Messerschmidt, and A. Bar-Even, "Core Catalysis of the Reductive Glycine Pathway Demonstrated in Yeast," *ACS Synth Biol*, vol. 8, no. 5, pp. 911–917, 2019, doi: 10.1021/acssynbio.8b00464.

[179] C. A. Cotton, N. J. Claassens, S. Benito-Vaquerizo, and A. Bar-Even, "Renewable methanol and formate as microbial feedstocks," *Curr Opin Biotechnol*, vol. 62, pp. 168–180, 2020, doi: 10.1016/j.copbio.2019.10.002.

[180] A. J. Roe, D. McLaggan, I. Davidson, C. O'Byrne, and I. R. Booth, "Perturbation of anion balance during inhibition of growth of *Escherichia coli* by weak acids," *J Bacteriol*, vol. 180, no. 4, pp. 767–772, 1998, doi: 10.1128/jb.180.4.767-772.1998.

[181] B. Enjalbert, P. Millard, M. Dinclaux, J. C. Portais, and F. Létisse, "Acetate fluxes in *Escherichia coli* are determined by the thermodynamic control of the Pta-AckA pathway," *Sci Rep*, vol. 7, no. October 2016, pp. 1–11, 2017, doi: 10.1038/srep42135.

[182] J. B. Russell and F. Diez-Gonzalez, "The effects of fermentation acids on bacterial growth," *Adv Microb Physiol*, vol. 39, pp. 228–234, 1998, doi: 10.1016/s0065-2911(08)60017-x.

[183] D. Kaplan, "Bachelor thesis Biocatalyst development for itaconic acid," no. May, 2020.

[184] C. v. Salmond, R. G. Kroll, and I. R. Booth, “The effect of food preservatives on pH homeostasis in *Escherichia coli*,” *J Gen Microbiol*, vol. 130, no. 11, pp. 2845–2850, 1984, doi: 10.1099/00221287-130-11-2845.

[185] E. Lastauskiene, A. Zinkevičiene, I. Girkontaite, A. Kaunietis, and V. Kvedariene, “Formic acid and acetic acid induce a programmed cell death in pathogenic *Candida* species,” *Curr Microbiol*, vol. 69, no. 3, pp. 303–310, 2014, doi: 10.1007/s00284-014-0585-9.

[186] T. Zambanini *et al.*, “Efficient malic acid production from glycerol with *Ustilago trichophora* TZ1,” *Biotechnol Biofuels*, vol. 9, no. 1, pp. 1–8, 2016, doi: 10.1186/s13068-016-0483-4.

[187] M. Feldbrügge, R. Kellner, and K. Schipper, “The biotechnological use and potential of plant pathogenic smut fungi,” *Applied Microbiology and Biotechnology*, vol. 97, no. 8. pp. 3253–3265, Apr. 2013. doi: 10.1007/s00253-013-4777-1.

[188] M. Jeya *et al.*, “Isolation of a novel high erythritol-producing *Pseudozyma tsukubaensis* and scale-up of erythritol fermentation to industrial level,” *Appl Microbiol Biotechnol*, vol. 83, no. 2, pp. 225–231, 2009, doi: 10.1007/s00253-009-1871-5.

[189] A. N. T. Phan and L. M. Blank, “GC-MS-Based Metabolomics for the Smut Fungus *Ustilago maydis*: A Comprehensive Method Optimization to Quantify Intracellular Metabolites,” *Front Mol Biosci*, vol. 7, no. August, pp. 1–10, 2020, doi: 10.3389/fmolb.2020.00211.

[190] K. Stein, “Institute of Applied Microbiology Master thesis Establishing a co-feeding strategy of CO_2-derived acetate towards a carbon-neutral itaconate production,” 2021.

[191] P. Stegmann, M. Londo, and M. Junginger, “The circular bioeconomy: Its elements and role in European bioeconomy clusters,” *Resources, Conservation and Recycling: X*, vol. 6, no. January, p. 100029, 2020, doi: 10.1016/j.rcrx.2019.100029.

[192] E. Z. Reyes-Fernández, Y. M. Shi, P. Grün, H. B. Bode, and M. Bölker, “An Unconventional Melanin Biosynthesis Pathway in *Ustilago maydis*,” *Appl Environ Microbiol*, vol. 87, no. 3, pp. 1–16, 2020, doi: 10.1128/AEM.01510-20.

[193] R. H. Haskins and J. A. Thorn, “Biochemistry of the Ustilaginales: Vii. Antibiotic Activity of Ustilagic Acid,” *Canadian Journal of Botany*, vol. 29, no. 6, pp. 585–592, 1951, doi: 10.1139/b51-046.

[194] M. Bölker, C. W. Basse, and J. Schirawski, “*Ustilago maydis* secondary metabolism-From genomics to biochemistry,” *Fungal Genetics and Biology*, vol. 45, no. SUPPL. 1, pp. 88–93, 2008, doi: 10.1016/j.fgb.2008.05.007.

[195] B. N. Paulino *et al.*, “Biotechnological production of value-added compounds by ustilaginomycetous yeasts,” *Appl Microbiol Biotechnol*, vol. 101, no. 21, pp. 7789–7809, 2017, doi: 10.1007/s00253-017-8516-x.

[196] A. Matei and G. Doehlemann, “Cell biology of corn smut disease — *Ustilago maydis* as a model for biotrophic interactions,” *Curr Opin Microbiol*, vol. 34, pp. 60–66, 2016, doi: 10.1016/j.mib.2016.07.020.

[197] D. Lanver *et al.*, “*Ustilago maydis* effectors and their impact on virulence,” *Nat Rev Microbiol*, vol. 15, no. 7, pp. 409–421, 2017, doi: 10.1038/nrmicro.2017.33.

[198] J. Béthune, R. P. Jansen, M. Feldbrügge, and K. Zarnack, “Membrane-Associated RNA-Binding Proteins Orchestrate Organelle-Coupled Translation,” *Trends Cell Biol*, vol. 29, no. 2, pp. 178–188, 2019, doi: 10.1016/j.tcb.2018.10.005.

[199] M. Reindl, S. Hänsch, S. Weidtkamp-Peters, and K. Schipper, “A potential lock-type mechanism for unconventional secretion in fungi,” *Int J Mol Sci*, vol. 20, no. 3, 2019, doi: 10.3390/ijms20030460.

[200] E. Saavedra, L. E. Ramos-Casillas, A. Marín-Hernández, R. Moreno-Sánchez, and G. Guerra-Sánchez, “Glycolysis in *Ustilago maydis*,” *FEMS Yeast Res*, vol. 8, no. 8, pp. 1313–1323, 2008, doi: 10.1111/j.1567-1364.2008.00437.x.

[201] D. Kiefer, M. Merkel, L. Lilge, M. Henkel, and R. Hausmann, “From Acetate to Bio-Based Products: Underexploited Potential for Industrial Biotechnology,” *Trends Biotechnol*, vol. 39, no. 4, pp. 397–411, 2021, doi: 10.1016/j.tibtech.2020.09.004.

[202] H. G. Lim, J. H. Lee, M. H. Noh, and G. Y. Jung, “Rediscovering Acetate Metabolism: Its Potential Sources and Utilization for Biobased Transformation into Value-Added Chemicals,” *J Agric Food Chem*, vol. 66, no. 16, pp. 3998–4006, 2018, doi: 10.1021/acs.jafc.8b00458.

[203] Y. Li, B. Huang, H. Wu, Z. Li, Q. Ye, and Y. H. P. Zhang, Production of Succinate from Acetate by Metabolically Engineered *Escherichia coli*, vol. 5, no. 11. 2016. doi: 10.1021/acssynbio.6b00052.

[204] K. T. Klasson, M. D. Ackerson, E. C. Clausen, and J. L. Gaddy, “Bioconversion of synthesis gas into liquid or gaseous fuels,” *Enzyme Microb Technol*, vol. 14, no. 8, pp. 602–608, 1992, doi: 10.1016/0141-0229(92)90033-K.

[205] J. Bertsch and V. Müller, “CO metabolism in the acetogen *Acetobacterium woodii*,” *Appl Environ Microbiol*, vol. 81, no. 17, pp. 5949–5956, 2015, doi: 10.1128/AEM.01772-15.

[206] T. Botz and W. Leitner, “Accepted article,” *J Subst Abuse Treat*, vol. 13, no. 3, pp. 287–288, 1996, doi: 10.1016/s0740-5472(96)90021-5.

[207] S. M. Wege, K. Gejer, F. Becker, M. Bölker, J. Freitag, and B. Sandrock, “Versatile CRISPR/Cas9 systems for genome editing in *Ustilago maydis*,” *Journal of Fungi*, vol. 7, no. 2, pp. 1–11, 2021, doi: 10.3390/jof7020149.

[208] J. Loevenich, “Optimization of itaconic acid production by *U. maydis* through metabolic engineering & adaptive laboratory evolution,” vol. 14, 2019.

[209] M. Casal, S. Paiva, O. Queirós, and I. Soares-Silva, “Transport of carboxylic acids in yeasts,” *FEMS Microbiol Rev*, vol. 32, no. 6, pp. 974–994, 2008, doi: 10.1111/j.1574-6976.2008.00128.x.

[210] S. Paiva, F. Devaux, S. Barbosa, C. Jacq, and M. Casal, “Ady2p is essential for the acetate permease activity in the yeast *Saccharomyces cerevisiae*,” *Yeast*, vol. 21, no. 3, pp. 201–210, 2004, doi: 10.1002/yea.1056.

[211] M. Thesis, “Master Thesis Bioprocess optimization of *Ustilago maydis* by establishing an acetate co-feeding strategy towards a carbon neutral itaconate production,” no. July, 2022.

[212] L. Palmieri *et al.*, “The mitochondrial dicarboxylate carrier is essential for the growth of *Saccharomyces cerevisiae* on ethanol or acetate as the sole carbon source,” *Mol Microbiol*, vol. 31, no. 2, pp. 569–577, 1999, doi: 10.1046/j.1365-2958.1999.01197.x.

[213] M. Kretschmer, J. Klose, and J. W. Kronstad, “Defects in mitochondrial and peroxisomal β-oxidation influence virulence in the maize pathogen *Ustilago maydis*,” *Eukaryot Cell*, vol. 11, no. 8, pp. 1055–1066, 2012, doi: 10.1128/EC.00129-12.

[214] L. Karaffa and C. P. Kubicek, “Production of organic acids by Fungi,” *Encyclopedia of Mycology*, pp. 406–419, 2021, doi: 10.1016/B978-0-12-809633-8.21066-2.

[215] M. K. H. Liew, A. G. Fane, and P. L. Rogers, “Applicability of continuous membrane bioreactor in production of phenylacetylcarbinol,” *Journal of Chemical Technology & Biotechnology*, vol. 64, no. 2, pp. 200–206, 1995, doi: 10.1002/jctb.280640214.

[216] N. Saude *et al.*, “Alginate production by *Azotobacter vinelandii* in a membrane bioreactor,” *Process Biochemistry*, vol. 38, no. 2, pp. 273–278, 2002, doi: 10.1016/S0032-9592(02)00090-0.

[217] D. Gopaliya, V. Kumar, and S. K. Khare, “Recent advances in itaconic acid production from microbial cell factories,” *Biocatal Agric Biotechnol*, vol. 36, no. July, p. 102130, 2021, doi: 10.1016/j.bcab.2021.102130.

[218] J. Wu, Y. Huang, W. Ye, and Y. Li, “CO_2 Reduction: From the Electrochemical to Photochemical Approach,” *Advanced Science*, vol. 4, no. 11, pp. 1–29, 2017, doi: 10.1002/advs.201700194.

[219] X. Liu, S. Inagaki, and J. Gong, “Heterogeneous Molecular Systems for Photocatalytic CO_2 Reduction with Water Oxidation,” *Angewandte Chemie - International Edition*, vol. 55, no. 48, pp. 14924–14950, 2016, doi: 10.1002/anie.201600395.

[220] R. Cauwenbergh and S. Das, “Photochemical reduction of carbon dioxide to formic acid,” *Green Chemistry*, vol. 23, no. 7, pp. 2553–2574, 2021, doi: 10.1039/d0gc04040a.

[221] N. W. Kinzel, C. Werlé, and W. Leitner, “Transition Metal Complexes as Catalysts for the Electroconversion of CO_2: An Organometallic Perspective,” *Angewandte Chemie - International Edition*, vol. 60, no. 21, pp. 11628–11686, 2021, doi: 10.1002/anie.202006988.

[222] R. Francke, B. Schille, and M. Roemelt, “Homogeneously Catalyzed Electroreduction of Carbon Dioxide - Methods, Mechanisms, and Catalysts,” *Chem Rev*, vol. 118, no. 9, pp. 4631–4701, 2018, doi: 10.1021/acs.chemrev.7b00459.

[223] J. Artz *et al.*, “Sustainable Conversion of Carbon Dioxide: An Integrated Review of Catalysis and Life Cycle Assessment,” *Chem Rev*, vol. 118, no. 2, pp. 434–504, 2018, doi: 10.1021/acs.chemrev.7b00435.

[224] J. Klankermayer, S. Wesselbaum, K. Beydoun, and W. Leitner, “Selective Catalytic Synthesis Using the Combination of Carbon Dioxide and Hydrogen: Catalytic Chess at the Interface of Energy and Chemistry,” *Angewandte Chemie - International Edition*, vol. 55, no. 26, pp. 7296–7343, 2016, doi: 10.1002/anie.201507458.

[225] W. Babel, U. Brinkmann, and R. H. Müller, “The auxiliary substrate concept — an approach for overcoming limits of microbial performances,” *Acta Biotechnol*, vol. 13, no. 3, pp. 211–242, 1993, doi: 10.1002/abio.370130302.

[226] D. M. Harris, Z. A. van der Krogt, W. M. van Gulik, J. P. van Dijken, and J. T. Pronk, “Formate as an auxiliary substrate for glucose-limited cultivation of *Penicillium chrysogenum*: Impact on penicillin G production and biomass yield,” *Appl Environ Microbiol*, vol. 73, no. 15, pp. 5020–5025, 2007, doi: 10.1128/AEM.00093-07.

[227] D. Preti, C. Resta, S. Squarcialupi, and G. Fachinetti, “Carbon Dioxide Hydrogenation to Formic Acid by Using a Heterogeneous Gold Catalyst,” *Angewandte Chemie*, vol. 123, no. 52, pp. 12759–12762, 2011, doi: 10.1002/ange.201105481.

[228] A. Behr, P. Ebbinghaus, and F. Naendrup, “Process concepts for the transition metal catalyzed syntheses of formic acid and dimethylformamide based on carbon dioxide,” *Chem Eng Technol*, vol. 27, no. 5, pp. 495–501, 2004, doi: 10.1002/ceat.200403221.

[229] M. Scott, B. Blas Molinos, C. Westhues, G. Franciò, and W. Leitner, “Aqueous Biphasic Systems for the Synthesis of Formates by Catalytic CO_2 Hydrogenation: Integrated Reaction and Catalyst Separation for CO_2-Scrubbing Solutions,” *ChemSusChem*, vol. 10, no. 6, pp. 1085–1093, 2017, doi: 10.1002/cssc.201601814.

[230] C. A. Ohlin and G. Laurenczy, “Carbon dioxide reduction in biphasic aqueous-ionic liquid systems by pressurized hydrogen,” *High Press Res*, vol. 23, no. 3 SPEC. ISS., pp. 239–242, 2003, doi: 10.1080/0895795032000102405.

[231] W. Leitner *et al.*, “Carbon2Polymer – Chemical Utilization of CO_2 in the Production of Isocyanates,” *Chem Ing Tech*, vol. 90, no. 10, pp. 1504–1512, 2018, doi: 10.1002/cite.201800040.

[232] S. Wesselbaum *et al.*, “Hydrogenation of carbon dioxide to methanol using a homogeneous ruthenium-Triphos catalyst: From mechanistic investigations to multiphase catalysis,” *Chem Sci*, vol. 6, no. 1, pp. 693–704, 2015, doi: 10.1039/c4sc02087a.

[233] J. Kothandaraman, A. Goeppert, M. Czaun, G. A. Olah, and G. K. Surya Prakash, “CO2 capture by amines in aqueous media and its subsequent conversion to formate with reusable ruthenium and iron catalysts,” *Green Chemistry*, vol. 18, no. 21, pp. 5831–5838, 2016, doi: 10.1039/c6gc01165a.

[234] S. Kar, R. Sen, A. Goeppert, and G. K. S. Prakash, “Integrative CO_2 capture and hydrogenation to methanol with reusable catalyst and amine: Toward a carbon neutral methanol economy,” *J Am Chem Soc*, vol. 140, no. 5, pp. 1580–1583, 2018, doi: 10.1021/jacs.7b12183.

[235] N. Guntermann, H. G. Mengers, G. Franciò, L. M. Blank, and W. Leitner, “Bio-energy conversion with carbon capture and utilization (BECCU): Integrated biomass fermentation and chemo-catalytic CO_2 hydrogenation for bioethanol and formic acid co-production,” *Green Chemistry*, vol. 23, no. 24, pp. 9860–9864, 2021, doi: 10.1039/d1gc02915k.

[236] T. Zambanini *et al.*, “Promoters from the itaconate cluster of *Ustilago maydis* are induced by nitrogen depletion,” *Fungal Biol Biotechnol*, vol. 4, no. 1, pp. 1–9, 2017, doi: 10.1186/s40694-017-0040-3.

[237] G. Libralato, A. Volpi Ghirardini, and F. Avezzù, “Seawater ecotoxicity of monoethanolamine, diethanolamine and triethanolamine,” *J Hazard Mater*, vol. 176, no. 1–3, pp. 535–539, 2010, doi: 10.1016/j.jhazmat.2009.11.062.

[238] W. Leitner *et al.*, “Carbon2Polymer – Chemical Utilization of CO_2 in the Production of Isocyanates,” *Chem Ing Tech*, vol. 90, no. 10, pp. 1504–1512, 2018, doi: 10.1002/cite.201800040.

[239] K. Vánky and M. Lutz, “Tubisorus, a new genus of smut fungi (Ustilaginomycetes) for *Sorosporium pachycarpum*,” *Mycol Balc*, vol. 8, no. 2, pp. 129–135, 2011.

[240] Y. Liu, C. M. J. Koh, and L. Ji, “Bioconversion of crude glycerol to glycolipids in *Ustilago maydis*,” *Bioresour Technol*, vol. 102, no. 4, pp. 3927–3933, Feb. 2011, doi: 10.1016/J.BIORTECH.2010.11.115.

[241] L. Ullmann, A. N. T. Phan, D. K. P. Kaplan, and L. M. Blank, “Ustilaginaceae biocatalyst for co-metabolism of CO_2-derived substrates toward carbon-neutral itaconate production,” *Journal of Fungi*, vol. 7, no. 2, pp. 1–19, 2021, doi: 10.3390/jof7020098.

[242] E. Geiser, F. Ludwig, T. Zambanini, N. Wierckx, and L. M. Blank, “Draft genome sequences of itaconate-producing Ustilaginaceae,” *Genome Announc*, vol. 4, no. 6, pp. 4–5, 2016, doi: 10.1128/genomeA.01291-16.

[243] A. R. McTaggart, R. G. Shivas, A. D. W. Geering, B. Callaghan, K. Vánky, and T. Scharaschkin, “Soral synapomorphies are significant for the systematics of the *Ustilago-Sporisorium*-Macalpinomyces complex (Ustilaginaceae),” *Persoonia: Molecular Phylogeny and Evolution of Fungi*, vol. 29, pp. 63–77, 2012, doi: 10.3767/003158512X660562.

[244] C. Hudec *et al.*, “Comparative Genomics of Potato Common Scab-Causing *Streptomyces* spp. Displaying Varying Virulence,” *Front Microbiol*, vol. 12, no. August, 2021, doi: 10.3389/fmicb.2021.716522.

[245] M. Piepenbring, M. Stoll, and F. Oberwinkler, “The generic position of *Ustilago maydis*, *Ustilago scitaminea*, and *Ustilago esculenta* (Ustilaginales),” *Mycol Prog*, vol. 1, no. 1, pp. 71–80, 2002, doi: 10.1007/s11557-006-0006-y.

[246] M. Stoll, D. Begerow, and F. Oberwinkler, “Molecular phylogeny of *Ustilago, Sporisorium*, and related taxa based on combined analyses of rDNA sequences,” *Mycol Res*, vol. 109, no. 3, pp. 342–356, 2005, doi: 10.1017/S0953756204002229.

[247] C. Jain, L. M. Rodriguez-R, A. M. Phillippy, K. T. Konstantinidis, and S. Aluru, “High throughput ANI analysis of 90K prokaryotic genomes reveals clear species boundaries,” *Nat Commun*, vol. 9, no. 1, pp. 1–8, 2018, doi: 10.1038/s41467-018-07641-9.

[248] A. Isolate *et al.*, “Genome Analyses of the Less Aggressive *Rhizoctonia solani*,” pp. 1–12, 2021.

[249] M. M. Alshahni *et al.*, “Insight into the draft whole-genome sequence of the dermatophyte *Arthroderma vanbreuseghemii,” Sci Rep*, vol. 8, no. 1, pp. 6–11, 2018, doi: 10.1038/s41598-018-33505-9.

[250] F. Castro-Chavez, “The rules of variation: amino acid exchange according to the rotating circular genetic code,” *J Theor Biol*, vol. 264, no. 3, p. 711—721, Jun. 2010, doi: 10.1016/j.jtbi.2010.03.046.

[251] K. Blin *et al.*, “AntiSMASH 6.0: Improving cluster detection and comparison capabilities,” *Nucleic Acids Res*, vol. 49, no. W1, pp. W29–W35, 2021, doi: 10.1093/nar/gkab335.

[252] B. Winterberg *et al.*, “Elucidation of the complete ferrichrome a biosynthetic pathway in *Ustilago maydis*,” *Mol Microbiol*, vol. 75, no. 5, pp. 1260–1271, 2010, doi: 10.1111/j.1365-2958.2010.07048.x.

[253] E. Geiser, *Ph.D dissertation:* Itaconic Acid Production by *Ustilago maydis*. 2015.

[254] X. Zhu, Y. Guo, Z. Liu, J. Yang, H. Tang, and Y. Wang, “Itaconic acid exerts anti-inflammatory and antibacterial effects via promoting pentose phosphate pathway to produce ROS,” *Sci Rep*, vol. 11, no. 1, pp. 1–9, 2021, doi: 10.1038/s41598-021-97352-x.

[255] T. van Nguyen, A. C. Alfaro, T. Young, S. Green, E. Zarate, and F. Merien, “Itaconic acid inhibits growth of a pathogenic marine Vibrio strain: A metabolomics approach,” *Sci Rep*, vol. 9, no. 1, pp. 1–9, 2019, doi: 10.1038/s41598-019-42315-6.

[256] A. Saika *et al.*, “A putative transporter gene PtMMF1-deleted strain produces mono-acylated mannosylerythritol lipids in *Pseudozyma tsukubaensis*,” *Appl Microbiol Biotechnol*, vol. 104, no. 23, pp. 10105–10117, 2020, doi: 10.1007/s00253-020-10961-w.

[257] T. Morita, M. Konishi, T. Fukuoka, T. Imura, and D. Kitamoto, “Identification of *Ustilago cynodontis* as a new producer of glycolipid biosurfactants, mannosylerythritol lipids, based on ribosomal DNA sequences,” *J Oleo Sci*, vol. 57, no. 10, pp. 549–556, 2008, doi: 10.5650/jos.57.549.

[258] E. Z. Ron and E. Rosenberg, “Natural roles of biosurfactants,” *Environ Microbiol*, vol. 3, no. 4, pp. 229–236, 2001, doi: 10.1046/j.1462-2920.2001.00190.x.

[259] T. Zambanini *et al.*, “Metabolic engineering of *Ustilago trichophora* TZ1 for improved malic acid production,” *Metab Eng Commun*, vol. 4, no. January, pp. 12–21, 2017, doi: 10.1016/j.meteno.2017.01.002.

[260] J. Yang *et al.*, “Production of Itaconic Acid Through Microbiological Fermentation of Inexpensive Materials,” *Journal of Bioresources and Bioproducts*, vol. 4, no. 3, pp. 135–142, 2019, doi: 10.12162/jbb.v4i3.001.

[261] H. T. Demir *et al.*, “High level production of itaconic acid at low pH by *Ustilago maydis* with fed-batch fermentation,” *Bioprocess Biosyst Eng*, vol. 44, no. 4, pp. 749–758, 2021, doi: 10.1007/s00449-020-02483-6.

[262] H. Takagi and H. Kitagaki, “Stress biology of yeasts and Fungi: Applications for industrial brewing and fermentation,”pp. 1–218, 2015, doi: 10.1007/978-4-431-55248-2.

[263] A. I. Magalhães, J. C. de Carvalho, J. F. Thoms, J. D. C. Medina, and C. R. Soccol, “Techno-economic analysis of downstream processes in itaconic acid production from fermentation broth,” *J Clean Prod*, vol. 206, pp. 336–348, 2019, doi: 10.1016/j.jclepro.2018.09.204.

[264] M. Gausmann, C. Kocks, J. Pastoors, J. Büchs, N. Wierckx, and A. Jupke, “Electrochemical pH-T-Swing Separation of Itaconic Acid for Zero Salt Waste Downstream Processing,” *ACS Sustain Chem Eng*, vol. 9, no. 28, pp. 9336–9347, 2021, doi: 10.1021/acssuschemeng.1c02194.

[265] A. Schmitz, B. E. Ebert, and L. M. Blank, “GC-MS-Based Determination of Mass Isotopomer Distributions for 13C-Based Metabolic Flux Analysis,” pp. 223–243, 2015, doi: 10.1007/8623_2015_78.

[266] T. J. Erb, P. R. Jones, and A. Bar-even, “Synthetic metabolism : Metabolic engineering meets enzyme design,” pp. 56–62, 2021, doi: 10.1016/j.cbpa.2016.12.023.Synthetic.

[267] M. Schuster, G. Schweizer, S. Reissmann, and R. Kahmann, “Genome editing in *Ustilago maydis* using the CRISPR-Cas system,” *Fungal Genetics and Biology*, vol. 89, pp. 3–9, Apr. 2016, doi: 10.1016/j.fgb.2015.09.001.

[268] Y. Khrunyk, K. Münch, K. Schipper, A. N. Lupas, and R. Kahmann, “The use of FLP-mediated recombination for the functional analysis of an effector gene family in the biotrophic smut fungus *Ustilago maydis*,” *New Phytologist*, vol. 187, no. 4, pp. 957–968, Sep. 2010, doi: 10.1111/j.1469-8137.2010.03413.x.

[269] C. W. Basse and J. W. Farfsing, “Promoters and their regulation in *Ustilago maydis* and other phytopathogenic fungi,” *FEMS Microbiol Lett*, vol. 254, no. 2, pp. 208–216, 2006, doi: 10.1111/j.1574-6968.2005.00046.x.

[270] W. Zuo, J. R. Depotter, and G. Doehlemann, “Cas9HF1 enhanced specificity in *Ustilago maydis*,” *Fungal Biol*, vol. 124, no. 3–4, pp. 228–234, 2020, doi: 10.1016/j.funbio.2020.02.006.

[271] M. Terfrüchte *et al.*, “Establishing a versatile Golden Gate cloning system for genetic engineering in fungi,” *Fungal Genetics and Biology*, vol. 62, pp. 1–10, 2014, doi: 10.1016/j.fgb.2013.10.012.

[272] P. Sarkari *et al.*, “Improved expression of single-chain antibodies in *Ustilago maydis*,” *J Biotechnol*, vol. 191, pp. 165–175, 2014, doi: 10.1016/j.jbiotec.2014.06.028.

[273] M. Terfrüchte *et al.*, “Tackling destructive proteolysis of unconventionally secreted heterologous proteins in *Ustilago maydis*,” *J Biotechnol*, vol. 284, pp. 37–51, 2018, doi: 10.1016/j.jbiotec.2018.07.035.

[274] O. Yishai, L. Goldbach, H. Tenenboim, S. N. Lindner, and A. Bar-Even, “Engineered Assimilation of Exogenous and Endogenous Formate in *Escherichia coli*,” *ACS Synth Biol*, vol. 6, no. 9, pp. 1722–1731, 2017, doi: 10.1021/acssynbio.7b00086.

[275] A. Bar-Even, “Formate Assimilation: The Metabolic Architecture of Natural and Synthetic Pathways,” *Biochemistry*, vol. 55, no. 28, pp. 3851–3863, 2016, doi: 10.1021/acs.biochem.6b00495.

[276] W. Mao, Q. Yuan, H. Qi, Z. Wang, H. Ma, and T. Chen, “Recent progress in metabolic engineering of microbial formate assimilation,” *Appl Microbiol Biotechnol*, vol. 104, no. 16, pp. 6905–6917, 2020, doi: 10.1007/s00253-020-10725-6.

[277] J. Gonzalez De La Cruz, F. Machens, K. Messerschmidt, and A. Bar-Even, “Core Catalysis of the Reductive Glycine Pathway Demonstrated in Yeast,” *ACS Synth Biol*, vol. 8, no. 5, pp. 911–917, 2019, doi: 10.1021/acssynbio.8b00464.

[278] U. W. Liebal *et al.*, “*Ustilago maydis* Metabolic Characterization and Growth Quantification with a Genome-Scale Metabolic Model,” *Journal of Fungi*, vol. 8, no. 5, p. 524, 2022, doi: 10.3390/jof8050524.

Curriculum vitae

Personal Data

Name	Lena Ullmann
Born	August 25th, 1991, in Elmshorn, Germany
Nationality	German
Email	lena.ullmann@rwth-aachen.de

Education

2019 - 2022	PhD student at the Institute of Applied Microbiology, RWTH Aachen University, Aachen, Germany
2015 - 2017	Studies: Master of Science in Molecular and Applied Biotechnology at RWTH Aachen University, Aachen, Germany Master thesis “Mixed cultures of Pseudomonas aeruginosa PA14 and 2,3- butanediol-fermenter for current generation in bio electrochemical systems (BES)” at Institute of Applied Microbiology, RWTH Aachen University, Aachen, Germany
2011 - 2015	Studies: Bachelor of Science in Biotechnology and Process Engineering at the Flensburg University of Applied Sciences, Flensburg, Germany Bachelor thesis “Predicting hair lightening performance by establishing an empirical model” at Procter & Gamble (Wella), Schwalbach am Taunus, Germany
2011	Abitur (qualification for university entrance) at Auguste-Viktoria-Schule Flensburg, Germany

Work Experience

2019 - 2022	Scientific employee at the Institute of Applied Microbiology, RWTH Aachen University, Aachen, Germany
2018 - 2019	Team member, Research and Development, Recombinant proteins, at Miltenyi Biotec GmbH, Bergisch Gladbach, Germany

Publications

Liebal, U., **Ullmann, L.**, Lieven C., Kohl, P., Wibberg, D., Zambanini, T., Blank, L. M. Ustilago maydis Metabolic Characterization and Growth Quantification with a Genome-Scale Metabolic Model. J. Fungi 2022, 8, 5. https://doi.org/10.3390/jof8050524

Ullmann, L., Wibberg, D., Busche, T., Rückert, C., Müsgens, A., Kalinowski, J., Blank, L. M. Seventeen Ustilaginaceae High-Quality Genome Sequences Allow Phylogenomic Analysis and Provide Insights into Secondary Metabolite Synthesis. J. Fungi 2022, 8, 269. https://doi.org/10.3390/jof8030269

Ullmann, L., Phan, A. N. T., Kaplan, D. K. P., Blank, L. M. Ustilaginaceae Biocatalyst for Co-Metabolism of CO_2-Derived Substrates toward Carbon-Neutral Itaconate Production. J. Fungi 2021, 7, 98. https://doi.org/10.3390/jof7020098

Poster presentations

Ullmann, L., Guntermann, N., Franciò, G., Leitner, W., Blank, L. M. (May 10-12, 2022) Co-metabolism of CO_2-derived formate for carbon-neutral itaconate production with *U. cynodontis*. 10th International Conference Fuel Science: From Production to Propulsion. Aachen, Germany

Ullmann, L., Müsgens, A., Stein, K., Blank, L. M. (September 21-23, 2021) Ustilaginaceae biocatalyst development for co-metabolism of CO_2-derived substrates for carbon-neutral itaconate production. 13th European Congress of Chemical Engineering and 6th European Congress of Applied Biotechnology. Germany

Ullmann, L., Müsgens, A., Stein, K., Blank, L. M. (June 22-24, 2021) Ustilaginaceae biocatalyst development for co-metabolism of CO_2-derived substrates for carbon-neutral itaconate production. 9th International Conference Fuel Science: From Production to Propulsion. Aachen, Germany

Ullmann, L., Blank, L. M. (June 23-25, 2020) Ustilaginaceae biocatalyst development for CO_2-negative production of itaconate. 8th International Conference Fuel Science: From Production to Propulsion. Aachen, Germany

Ullmann, L., Loevenich, J., Wierckx, N., Blank, L. M. (September 19-21, 2019) Optimization of itaconic acid production by *Ustilago maydis*. 13th Symposium of the VAAM Special Group, Göttingen, Germany